UNIVERSITY OF SALFORD

Active Noise Control in a Luxury Vehicle

by

Nikos Zafeiropoulos

A thesis submitted in partial fulfillment for the
degree of Doctor of Philosophy

in the
College of Science and Technology
School of Computer Science and Engineering

December 2015

UNIVERSITY OF SALFORD

ABSTRACT

COLLEGE OF SCIENCE AND TECHNOLOGY
SCHOOL OF COMPUTING SCIENCE AND ENGINEERING

Doctor of Philosophy

ACTIVE NOISE CONTROL IN A LUXURY VEHICLE

by Nikos Zafeiropoulos

Structure-borne road noise is a critical sound attribute for the overall Noise Vibration & Harshness (NVH) performance of modern luxury vehicles. Current passive NVH solutions require structural design modifications, in order to control low frequency sources that cause structure-borne noise. Active Road Noise Control (ARNC) has been demonstrated to several commercial vehicles as an alternative solution that does not compromise other performances of the car, especially vehicle dynamics. Automotive manufacturers of luxury vehicles, such as Bentley Motors Limited, are expected to build cars that meet high standards of driving performance and refinement levels. This thesis focuses on the development of an active sound technology for road noise with the use of NVH analysis methods, which are a common practice in the vehicle development process. Modern NVH methods of road noise analysis reveal the locations of the most predominant structure-borne noise sources. There are significant advantages in using NVH analysis techniques for the design of ARNC systems, since they offer integrated solutions to the automotive industry in terms of time and cost reduction. A method for defining the accelerometer sensors number and their locations on the axles has been developed as an alternative to existing methodologies, which are applied from the early stages of the NVH development. A physical road noise simulator was developed for replicating road noise. Four random uncorrelated forces were applied on the tyres for analysing and evaluating ARNC systems. In terms of feedforward control, a computer model of a causal adaptive feedforward system was used to investigate the relationship between the locations, DoF and the performance of the control system.

An adaptive system was installed on a Bentley vehicle for conducting the ARNC measurements. The adaptive ARNC system was tested on the physical road noise simulator. The vehicle's tyres were excited by broadband random forces and maximum 10 dB(A) reduction at the centre frequency of the tyre cavity resonance was achieved. When the control was focused on the road rumble, then overall 3 dB(A) up to 500 Hz were removed from the noise levels measured at the rear headrests. In terms of road noise testing, a portable multichannel controller was integrated with the vehicle electrical system for road noise data acquisition and real-time ARNC. Finally, the performance of the portable controller is predicted based on data acquired by the same multichannel system and therefore highlight the potential use of this system as an ARNC controller.

Contents

List of Figures

List of Tables

Glossary

Abbreviations

ADC	**A**nalog to **D**igital **C**onversion
ANC	**A**ctive **N**oise **C**ontrol/**C**ancellation
ARNC	**A**ctive **R**oad **N**oise **C**ontrol
AVC	**A**ctive **V**ibration **C**ontrol/**C**ancellation
DAC	**D**igital to **A**nalog **C**onversion
DAQ	**D**ata **A**cquisition **S**ystem
DSP	**D**igital **S**ignal **P**rocessing
DoF	**D**egrees **o**f **F**reedom
EOC	**E**ngine **O**rder **C**ontrol
FIR	**F**inite **I**mpulse **R**esponse
FPAA	**F**ield **P**rogramme **A**nalog **A**rrays
FRF	**F**requency **R**esponse **F**unction
IRF	**I**mpulse **R**esponse **F**unction
LHF	**L**eft **H**and **F**ront
LHR	**L**eft **H**and **R**ear
LMS	**L**east **M**ean **S**quare
MIMO	**M**ultiple **I**nput **M**ultiple **O**utput
MISO	**M**ultiple **I**nput **S**ingle **O**utput
SISO	**S**ingle **I**nput **S**ingle **O**utput
NTF	**N**oise **T**ransfer **F**unction
PCA	**P**rincipal **C**omponent **A**nalysis
RHF	**R**ight **H**and **F**ront
RHR	**R**ight **H**and **R**ight
SVD	**S**ingular **V**alue **D**ecomposition

Signal Conventions

$d(n)$	desired, disturbance signal
$e(n)$	error signal

$v(n)$	white noise signal
T_s	Sampling period
T_{FFT}	Time period of an FFT
f_s	Sampling frequency
$F(k)$	Spectral factor
$x(n)$	reference signal
$X(z)$	z-transform of $x(n)$
$X(k)$	Discrete Fourier Transform of $x(n)$
$r(n)$	filtered reference signal
$R(z)$	z-transform of $r(n)$
$R(k)$	Discrete Fourier Transform of $r(n)$
$R_{xd}(t)$	Cross-correlation between the reference and the disturbance signal
$R_{xx}(t)$	Autocorrelation of the reference signal
$R_{ss}(t)$	Autocorrelation of the primary excitation
$S_{xd}(k)$	Discrete Fourier Transform of $R_{xd}(t)$
$S_{xx}(k)$	Discrete Fourier Transform of $R_{xx}(t)$

Symbols

A_n	modal amplitude
c	speed of sound in air
D	coupling term
E_p	time averaged acoustic potential energy
f_s	sampling frequency
G	Green's function, secondary plant transfer funtion
g	secondary plant impulse response
i	index
I	number of control filter's coefficients
j	$\sqrt{-1}$
k	wavenumber, number of reference signals
K	number of reference signals and microphones
l, L	number of error signals and microphones
m, M	number of control signals and loudspeakers
N	FFT block length
p	sound pressure
r	distance
T_s	sampling period
w	control filter coefficients
z	z-transform indexing

Greek letters

ζ	damping ratio
μ	step-size
τ	time delay
ψ_n, ψ_m	mode shape (eigenfunction)
ω	angular frequency
ω_n	natural frequency

List of publications

Two peer reviewed conference papers and one journal publication were inspired from several parts of this PhD thesis and are presented in the following list:

• N. Zafeiropoulos, A.T. Moorhouse, A. Mackay, U. Senapati (2013). A comparison of two in-situ transfer path analysis methods, *International Conference on Recent Advances in Structural Dynamics.*

• N. Zafeiropoulos, M. Ballatore, A.T. Moorhouse, A. Mackay (2015). Active control of structure-borne road noise based on the separation of front and rear structural road noise related dynamics, *SAE International Journal of Passenger Cars-Mechanical Systems, 2015, 8. Jg., Nr. 2015-01-2222.*

• N. Zafeiropoulos, A.T. Moorhouse, M. Ballatore, A. Mackay (2015). Active control of road noise: the relation between the reference sensor locations and the effect on the contoller's performance, *Proceedings of the* 22^{nd}*,International Institute of Acoustics and Vibration (IIAV)*

Acknowledgements

I would like to take the opportunity to express my great gratitude to my supervisor Professor Andy Moorhouse for several reasons. First, for allowing me to take part in a such interesting PhD study and introducing me to vibro-acoustics and in particular in TPA methods. Secondly, for his academic guidance, support, proof reading the thesis and last but not least for encouraging me throughout difficult and stressful moments. I am also grateful and thankful to my technical manager from Bentley Motors Ltd, Dr. Marco Ballatore for his support, technical advices and also introducing me to vehicle structural dynamics. It is always great to work with people that are enthusiast, passionate and also want the maximum performance. I want also to express my warm thanks to Andy Mackay for bringing me in Bentley Motors, for his fruitful discussions and also sharing his experiences with ARNC technology for vehicles that have been an important feedback in many cases. An industrially funded project is not feasible without people with vision and technology interests that will provide the funding for a research project such as a doctorate study. Therefore I would like to acknowledge Uday Senapati, former Head of Whole Vehicle NVH of Bentley Motors, who created this project initially and hired me. Also, Marco Tarabra, my NVH manager for his great support and his help with budget issues. A special thanks to Jonathan Layfield, Head of Whole Vehicle Physics, who has been extremely supportive and also interested in the technical side of this Phd. I also appreciate the support of Bentley NVH team, especially Bob Kenyon, Francesco Naclerio, Dave Wilcox and Greg Wilshaw, who have been very helpful for setting and performing measurements with the vehicle. I would like to thank also some people that have significantly influence me to pursue a PhD, Dr. Stelios Koukoulas for introducing me in electrical/electronic engineering and stochastic processes, Dr. Stelios Potirakis for been a great mentor from my early years as an undergraduate student, Dr. Khaldoon Al-Naimi for been very supportive to purchase a PhD and Professor Finn Jacobsen for teaching physical acoustics with his unique simplistic way and also recommending me to Salford University. Lastly, I would like to thank Professor Colin Hansen and Professor Yiu Lam for their reviews. My sincere thanks to my sister, Dr. Aristea Zafeiropoulou for her support these three years and also for her great efforts in proof reading the thesis. I would like express appreciation to my mother, Georgia Dimitropoulou for been always supportive to achieve my goals.

"Perhaps I may clarify the historical background of the present situation if I say that the first industrial revolution, the revolution of the dark satanic mills, was the devaluation of the human arm by the competition of machinery... The modern industrial revolution [i.e., the computer revolution] is similarly bound to devalue the human brain... The answer, of course, is to have a society based on human values other than buying and selling. To arrive at this society, we need a good deal of planning and a good deal of struggle..."

Nobert Wiener ,"Cybernetics: Or the Control and Communication in the Animal and the Machine" (1948)

Chapter 1

Introduction

1.1 Noise vibration and harshness attributes

Modern vehicles are required to achieve specific targets in terms of acoustic performance, in order to become more attractive products, by improving sound quality and vehicle refinement. The sound character has become a crucial element of the development process of the vehicle. Several mechanical parts of the vehicle are designed and tuned in order to meet the targeted Noise Vibration & Harsheness (NVH) specifications. Apart from the sound character, vehicle refinement, which includes the noise and vibration levels, is also key to the overall NVH performance. The levels of interior noise depend on various mechanical sources that act on the vehicle structure and couple with the sound field in the compartment. Interior noise can also be generated due to the poor sound insulation of the cabin. All the previously mentioned sound and vibration issues belong to the interior NVH area and they are categorised in table (1.1) according to their frequency range and their sources.

NVH term	Frequency range [Hz]	Source
Powertrain noise	20 Hz - 3 kHz	engine, driveline, exhaust
Road noise (structure-borne)	20 Hz - 800 Hz	tyre cavity noise, structure
Road noise (airborne)	20 Hz - 2.5 kHz	tyre noise, air leaks,
Wind noise	50 Hz - 5kHz	exterior design, styling

Table 1.1: Interior NVH attributes.

The overall noise spectra in the vehicle's compartment can be decomposed to the three major sound attributes: powertrain, road and wind noise (figure

1.1). Powertrain noise covers the areas of the vehicle's engine, transmission and exhaust systems. The mechanical noises from the powertain sources vary in a broad frequency range as a function the engine speed and throttle loading conditions. In particular, engine noise is of harmonic nature since it is defined as the sum of the fundamental frequency plus its harmonics. Air conditioning systems and other ancillaries impact also to the total noise levels depending on the driving condition and their settings. In a luxury vehicle these disturbances are kept at a very low noise level as they can strongly influence the customer's perception in terms of the overall sound quality of the vehicle.

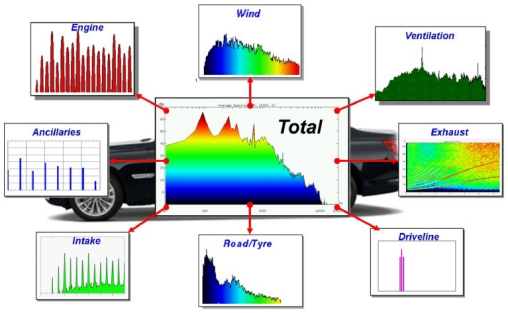

FIGURE 1.1: Interior NVH sound attributes. Taken from [Williams (2014)].

The primary noise sources such as the engine and the vehicle's structure are mostly concerntrated at low frequencies, typically below 500 Hz. In many modern vehicles dominant cavity booms (single frequency) can be created from the engine calibration settings or from the transmission systems, which can excite higher order acoustic modes of the cabin. In the case of road noise is caused by the tyre-road surface interaction that dominates mostly at low-mid frequencies. On the other hand, wind noise is broadband and it starts to be strongly perceivable at speeds above 100 km/h as it dominates the interior sound pressure levels.

1.2 Interior road noise

Tyre/road noise can be characterised as a band-limited random signal that is strongly influenced by the road surface. Road noise is generated by the interaction between the tyres and the road surface. The road roughness increases the applied forces on the tire contract patch and creates a large global displacements at low frequencies. The contact patch delivers strong vibration levels into the wheel hub. As a result, vibrations propagate through weak structural parts of the vehicle into the cabin, where the received floor panel vibrations couple with the sound field of the cabin.

At high speeds the cavities at the tread patent of the rolling tyres are excited by their interaction with the road surface and road noise is radiated that can be transmitted through airborne paths into the vehicle compartment. Figure 1.2 presents the two transmission mechanisms, airborne and structureborne of road noise inside the vehicle.

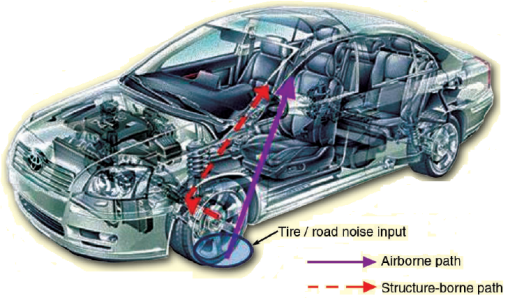

FIGURE 1.2: Structure-borne and airborne paths into the vehicle's cabin. Taken from [Cerrato (2009)].

Advanced NVH methods are used to analyse the road noise data and identify the various noise transmission paths that contribute to the interior road noise. Figure 1.3 illustrates an example of the airborne and structure-borne contributions from the front and rear part of the vehicle with data that were acquired with microphones close to the four wheels and accelerometers mounted at the front and rear axle.The structure-borne contributions of the front part are very close to the total noise level at driver's headrests 100-300 Hz, whereas at frequencies above 700 Hz airborne road noise starts to dominate.

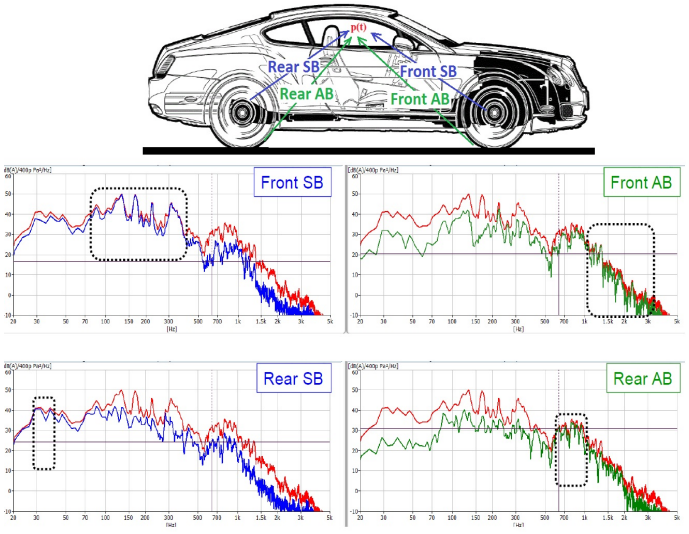

FIGURE 1.3: Structure-borne (SB) and airborne (AB) contributions to the interior noise spectrum at the driver's headrest at 90 km/h. –: Total noise level, –: Structure-borne road noise contribution, –: Airborne road noise contribution. Taken from [Williams (2014)].

The airborne paths in the vehicle body can be identified with advanced NVH measurement technique in order to apply sound insulation treatment. In the case of structure-borne road noise the transmission emerges from the tire through the suspension and body structure into the cabin. As a consequently, acoustic treatments are not so effective on this type of noise. Detailed analysis of the vehicle structural-acoustic interaction is required at a simulation and measurement level before applying any NVH solutions on the vehicle. Identification and ranking of the structural sources can be performed with the use of TPA (Transfer Path Analysis) [Plunt (1999)], [Elliott et al. (2013), Yoo and Chang (2005)]. The main assumption of TPA is that the vehicle is modelled as a *Multiple Input Multiple Output* (MIMO) vibro-acoustic system with several inputs are acting on the vehicle and cause interior road noise as output. TPA highlights also the most sensitive structural or airborne paths for various road input conditions, this type of analysis is referred as *contribution analysis*. Multiple coherence analysis can be alternatively used to find the total road noise contributions and also the incoherent road noise contributors as figure 1.4 demonstrates [Williams (2014)]. Additionally, the incoherent noise components that are not referenced

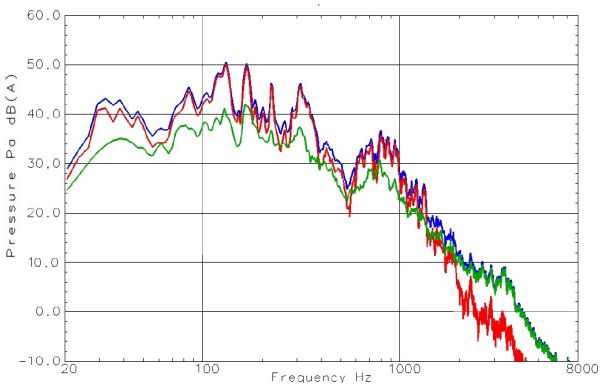

FIGURE 1.4: Interior road noise at 90 km/h. —: Measured interior road noise at the driver's headrest. —: Sum of airborne and structure-borne road noise contributions. —: Sum of other unreferenced noise contributions.

with accelerometers and microphones at the chassis and around the wheels can be separated with the use of multiple coherence method [Williams (2014)]. These components are generated from other noise sources such as wind noise that are incoherent with the road noise components. Wind noise some effects the interior noise spectrum at very low frequencies and also above 1 kHz [Cerrato (2009)]. Very low frequency interior noise can be a wind noise component that is referred as buffeting noise and it is caused by a small leakage path around the door or windows. If we compare the summation of the road noise contributions in figure 1.4 with the total sum of all the contributors (road and wind) of figure 1.5, then it can be noticed that the later accurately synthesises the measured spectrum at the driver's headrest. This indicates that there several noise sources acting at the same time, but still the main dominant noise component is related to

structural vibrations of front axles (1.3). Therefore at speeds from 50 km/h up to 100 km/h road noise reduction is important as it can improve significantly the refinement of the vehicle, since noise resonances can become annoying at these speeds and degrade the subjective NVH performance of a luxury vehicle.

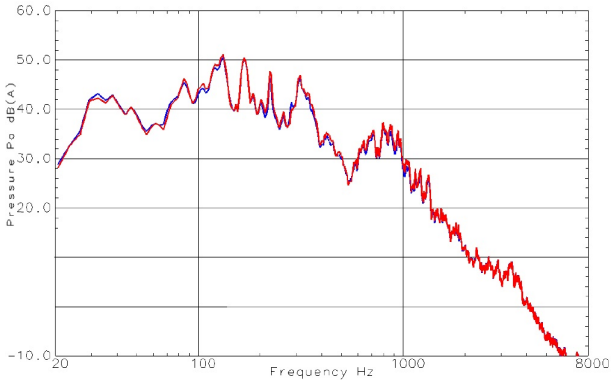

FIGURE 1.5: Interior road noise at 90 km/h. −: Measured interior road noise at the driver's headrest. −: Sum of airborne, structure-borne and other noise contributions.

1.3 Passive control of structure-borne road noise

The application of passive NVH control techniques on structure-borne road noise is not a trivial task, since design changes on the vehicle's structure are difficult to apply and most of the time not cost effective . Usually structure-borne road noise is treated by tuning the global and local dynamic stiffnesses of the vehicle structure during the design stage of the body structure [Kim et al. (2014)], [Duncan et al. (2011)]. Modern vehicle design techniques focus on the optimisation of the structural behaviour of the most sensitive structural parts in terms of road noise. The performance of the passive damping that is applied on the floor panel is estimated with numerical methods [Subramanian et al. (2003)], [Mohanty et al. (2000)]. Other local vibrations that are related to road noise cam be controlled by tuned mass dampers [Aubert and Howle (2007)] that block the road noise forces on sensitive vibro-acoustic paths. At the same time advanced NVH measurement techniques such as in-situ TPA [Elliott et al. (2013)] methods can identify these weaknesses within the structure and can allow to perform structural changes on the dynamic properties of chassis components in order to improve the levels of refinement in terms of road noise [Dohm et al. (2013)]. In practice though all the design changes and NVH control techniques treat structure-borne noise up to certain extent, typically 3- 5 dB(A) at frequencies below 300 Hz [Yoo and Chang (2005)]. As previously mentioned they can start compromising other vehicle performances. For example, if the suspension

mass and compliance need to be increased for reducing the road noise levels, then the steering performance can be potentially effected. Another example of the influence of road noise NVH solutions on the vehicle's performance metrics is the mass increase usually below 150 Hz for the control of global vibration levels of the whole vehicle structure. This type of solution can have serious effect on the fuel consumption and thus on CO2 emissions. As a result, active noise control technologies have the potential to offer useful NVH solutions in cases, in which the standardised NVH solutions begin to compromise other important characteristics of the vehicle.

1.4 Characteristics of structure-borne road noise

Structure-borne road noise is the outcome of different mechanisms that are excited from high levels of road-force inputs. Road noise is mostly perceivable while drving over rough asphalts, where the friction between the tire and the asphalt is high. Another issue is that road-forces are able to provide enough energy to the vehicle structure that can excite global and local vibrations that couple with the acoustic field of the cabin. The perceived sound can be analysed in terms of the various sources that contribute to the sound pressure response in the cabin. Previous studies have characterised road noise in terms of subjective perception [Gauterin (1994b)]. The outcome of [Gauterin (1994b)] has resulted in a metric that ranks the NVH performance of the vehicle and at the same time charecterises a vehicle in terms of the road noise perception [Gauterin (1994a)]. Similar assessments are currently used in the automotive industry for the subjective evaluation of road noise and vary between manufacturers according to the sound character of the vehicle. In table 1.2 the frequency bands of each road noise component with their corresponding structural source are presented.

Name	Frequency range [Hz]	Structural source
Boom/drum	10-70	Global vibrations
Rumble	70-170	Body, axle vibrations
Tyre Cavity	180-230	Tyre resonances
Midfrequency	230-500	Local body vibrations

TABLE 1.2: Structureborne road noise frequency bands and their structural source.

1.5 Variability of structureborne road noise

An important parameter of structure-borne road noise is that it has shown a variety of different levels and frequencies in the same vehicle model due to component tolerances and vehicle assembly. Kompella [Kompella and Bernhard (1993)] found that the manufacturing variability strongly affects the low frequency vibro-acoustic behaviour of the vehicle. As a consequence, vehicles are highly sensitive to changes or small variations in the assembly of the vehicle. The following figure presents the same vibro-acoustic system that is measured across 100 vehicles of the same model, typically sharp resonances in this frequency response function result to audible road noise components as we will discuss later in chapter 2.

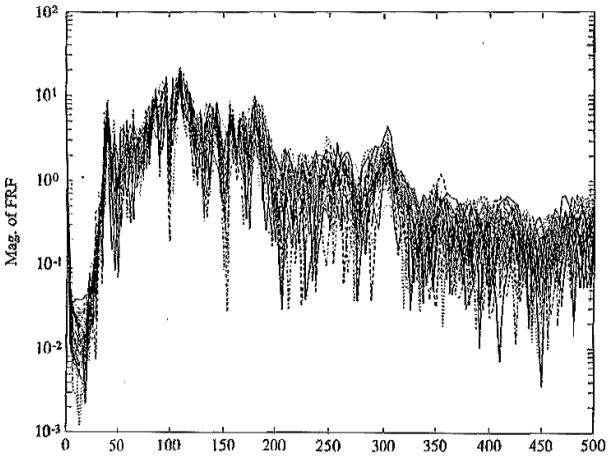

FIGURE 1.6: Variability in a vibro-acoustic path at measured at the driver's headrest for 100 vehicles. Taken from [Kompella and Bernhard (1993)].

Modern vehicle numerical modelling techniques [Durand et al. (2005)] take into account the statistical variations in the vibro-acoustic paths with the use of stochastic models as suggested by [Rustighi et al. (2008)] and [Durand et al. (2008)]. As a result these modern prediction tools can provide a guidance to the NVH design at the early stage of the vehicle. However, still accurate CAE methods that can correlate well with measured road noise data are not so far available at least in the literature.

It is also worth highlighting that passive NVH control techniques are not able to control changes in the road noise spectrum or any other uncertainties in the vibro-acoustic behavior of the vehicle over time. On the other hand active control techniques can potentially compensate for all these changes and uncertainties, since the adaptive algorithms are able to adapt to variations in the vehicle's structure-borne NVH performance. Previous work by Lotus [Mackay and Kenchington (2004)] and from other researchers in the field [Park et al. (2004)] applied the *active road noise control/cancellation* (ARNC) technology in a number of vehicles by using the use of the same hardware control platform. This

fact demonstrates the improvements that adaptive noise control solutions can offer to a wide range of vehicles in terms of noise reduction without constraining the mechanical design of the vehicle. The cost depends on the volumes and the accelerometer sensor pricing as modern DSP are already integrated in the audio systems. In terms of reliability of the controller this depends on the hardware platform, as currently adaptive ANC system are already implemented in several vehicle for powertrain noise reduction. The only thing that needs to be addressed is the fault detection of the accelerometer sensor that provides the input signals of the controller.

1.6 Active control of structure-borne road noise

During the last 30 years, several research groups as well automotive manufacturers have investigated whether *active noise control* (ANC) can offer an alternative to existing passive noise control techniques. This is mainly due to the fact that ANC does not require any changes in the structural design of the vehicle only access to the loudspeaker system and some sensors at specific locations of the vehicle. In addition to this active systems are very effective in the modal area of small cavity similar to the one of an automotive vehicle. In the early 90s, Nissan Motors managed to integrate noise cancellation systems for engine noise reduction into a production vehicle [Hasegawa et al. (1992)]. In Europe, Lotus Engineering has demonstrated ARNC and *engine order control/cancellation* (EOC) in a wide range of vehicles for different automotive manufacturers, but none of these vehicles have yet been released in the market with ANC. Up until now, ARNC technology has not been applied to any production vehicle, mainly due to cost requirements. However, recent advances in *digital signal processoring* DSP processors and sensor technologies offer ANC systems the possibility to be implemented in vehicles with a controllable cost. Besides the cost, there are also technical challenges that still need to be addressed. In particular, the high number of vibration sensors required for feedforward ARNC systems is another obstacle for the implementation and integration of the controller with the rest of the vehicle electronics.

1.7 The evolution of active road noise control

1.7.1 Principles of active noise control

The concept of active noise control is based on the destructive interference of two sound waves: the first is the primary noise field whereas the second is generated by the loudspeaker system in the cavity. Active noise control or active noise cancellation is a noise control technique that is mostly effective at low frequencies. A loudspeaker is used for emitting the canceling sound, also referred as *"antinoise"*, whereas a microphone sensor measures the sound pressure at the location where the noise is to be minimised. An electronic controller that contains the ANC filters generates the appropriate control signals that drive the loudspeaker units. This technique has a limited frequency range mainly due to the latency in the control loop and also the sound field becoming diffused at higher frequencies. Active noise control was first introduced as a concept by Paul Lueg in [Lueg (1936)], who presented a system that controlled sinusoidal sounds. Figure (1.7) present the configuration of Lueg's apparatus, where a microphone for measuring the noise source, an amplifier and a loudspeaker are usedto generate the secondary sound field.

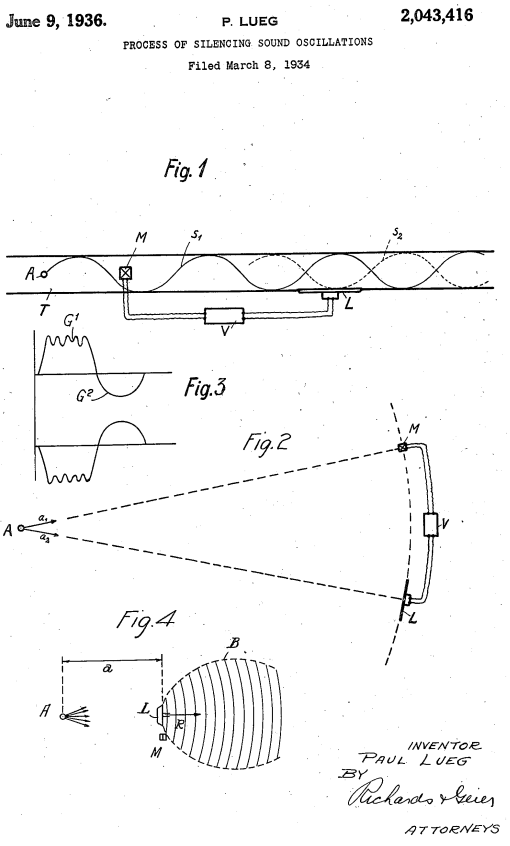

FIGURE 1.7: Drawings of Paul Lueg's apparatus.

An array of sensors and loudspeakers is used for reducing either to total acoustic potential energy in the sound field, *global control* meaning the average mean-square pressure across the space of an enclosure or only at specific locations in the field, *local control* [Nelson and Elliott (1991)]. The same principles of control can be also used for vibrational system in order to reduce the vibration levels across a structure, this type of technology is referred as *active vibration control*. The type of control depends on the number of microphone sensors that are measuring the sound pressure in the enclosed cavity and also the number of modes that contribute to the sound field at low frequencies. If the system is based on a large number of microphones, then a good approximation of the acoustic energy in the cavity at low frequencies can be achieved. As a consequence, global control of the sound is generally possible if there is low modal density in the cavity at low frequencies and the control sources couple directly with acoustic modes. For vehicles it has been demonstrated that the acoustic modes of the cabin can be partially controlled up to 150 Hz and above 200 Hz only *zones of quiet* are resulted by the presence of the *canceling* sound field.

One of the conditions for effectively reducing the noise is that the sound field at the loudspeaker position must be coherent with the primary noise source. This implies that the loudspeakers need to be placed at a location in the sound field where they can couple well with the primary noise disturbance. In addition to this the sensors that are measuring the variations of the noise source need to be placed at a point in the sound field or in the structure. In the case of vibro-acoustic noise transmission, where they can provide a signal that is coherent enough with the noise in the cavity.

The selection of the reference sensors for structure-borne road reduction is a difficult task, since various structural sources act on the vehicle. The coherence between the measured vibrational signals can be low due to the cross-coupling of the sources. As a result, the coherence between the accelerometers and the microphones in the cabin might be poor. To avoid that, a set of accelerometer sensors is used to tackle this problem, in order to capture all the structural road noise sources that contribute to the sound pressure in the compartment. The discussion regarding the coherence issue will be expanded in section (1.7.4) and in chapter 4.

1.7.2 Introduction to feedback active road noise controllers

Noise reduction in cars through active controllers has been an active research area since 1984 [Oswald (1984)], when the first control system to cancel engine

order harmonics was presented. In this thesis we mainly focus on active controllers of road noise, a challenging research topic in terms of vibro-acoustics, signal processing and control systems engineering. To that purpose, this section provides a detailed account of basic principal control strategies, which are used for the creation of the appropriate secondary sound field through the audio system of the vehicle. Figures 1.8 and 1.9 present a feedback control system.

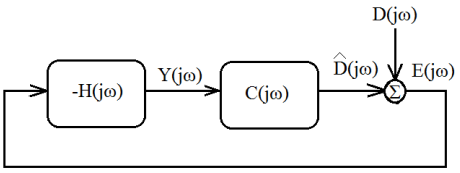

FIGURE 1.8: Block diagram of a single channel feedback ARNC system. $E(\omega)$: error input signal typically from a sensor at the cancelling point. $H(\omega)$: control filter. $Y(\omega)$: control signal that drive the transducer. $D(\omega)$: primary noise disturbance. $\hat{D}(\omega)$: estimated noise from the controller.

Multichannel feedback ARNC is recently developed and published by [Cheer and Elliott (2013)]. In this section we only introduce single channel feedback ARNC systems for the sake of simplicity. In figure 1.8, the signal $D(j\omega)$ is the main road noise disturbance and the signal $\hat{D}(j\omega)$ is the "*antinoise*" generated by the audio system. The superposition of $D(j\omega)$ with $\hat{D}(j\omega)$ results to $E(j\omega)$ that is the measured error signal by a microphone inside the vehicle's cabin. The output $Y(j\omega)$ of the controller $H(j\omega)$ can be expressed as

$$Y(j\omega) = -H(j\omega)E(j\omega), \tag{1.1}$$

whereas the noise canceling sound $\hat{D}(j\omega)$ that reaches the cancellation point through the electro-acoustic path between the audio system and the microphone $C(j\omega)$ is equal to

$$\hat{D}(j\omega) = C(j\omega)Y(j\omega). \tag{1.2}$$

The error signal that is measured by the microphone can be calculated as

$$E(j\omega) = D(j\omega) - C(j\omega)H(j\omega)E(j\omega). \tag{1.3}$$

The attenuation at the microphone's location depends on the control filter design $H(j\omega)$. The tuning of the control filter is very important for feedback control

since the poles of the filter must be negative real valued numbers to avoid instabilities [Nelson and Elliott (1991)]. A stronger stability condition is the Nyquist criterion as it takes into account the FRF of the acoustic plant $C(j\omega)$. According to Nyquist, the open loop FRF $C(j\omega)H(j\omega)$ must not contain the point (-1,0) in the complex plane [Elliott (2000a)]. The following function that is referred as *sensitivity function* defines the objective of the control filter design

$$\frac{E(j\omega)}{D(j\omega)} = \frac{1}{1 + C(j\omega)H(j\omega)} = S(j\omega). \tag{1.4}$$

Advanced feedback control design techniques such as H_∞ control and IMC (Internal Model Control) are used for optimising the sensitivity function $S(j\omega)$ [Adachi and Sano (1996), Adachi et al. (2001), Elliott (2000a)]. H_∞ control is a mathematical method for design stable optimal controllers and IMC is a feedback control strategy for generating a virtual reference signal instead of using an actual reference signal directly from the noise source. Sano [Sano et al. (2001)] applied feedback ARNC on a Honda vehicle based on H_∞ design. The system controlled the first acoustic mode of the cabin at 40 Hz at the driver's seat. The setup of the Honda feedback system is presented in figure 1.9, where the ARNC setup on a Honda Accord is presented.

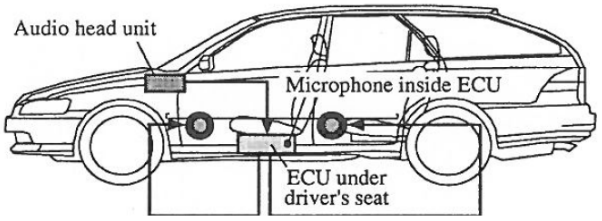

FIGURE 1.9: Feedback ARNC system of Honda Motors. Taken from [Sano et al. (2001)].

Sano's [Sano et al. (2000)] feedback controller caused enhancements at the rear seats as the system was only focusing on the driver's headrest without taking into account the sound pressure levels at the rear seats. As a result, he introduced an extra feedforward control system, in order to equalise the sound pressure levels at back seats. This side effect of the controller may be expected in sound field control, since suppressing the sound at one location in the cabin's sound field without observing the other locations could potentially cause enhancements at other areas in the cabin. The phenomenon of reducing the noise levels at the frequencies where the controller is phase leading the physical plant and increasing the noise levels outside of the frequencies, where it is phase is lagging the plant is referred as the "*waterbed*" effect [Sano et al. (2001)].

Apart from the stability and enhancement issues, the mixing between the audio and control signals of the loudspeakers needs to be carefully performed. Another significant feature of feedback systems is that the limitation of the distance between the loudspeaker and microphone must be kept as small as possible, since the acoustic propagation delay can significantly limit the performance of a feedback system [Elliott and Sutton (1996)]. For example, [Adachi et al. (2001)] proved experimentally (under free field conditions) that 0.1 m distance between the actuator and the sensor is necessary in order to achieve good control at 150 Hz.

In terms of the integration with the audio system, the microphone signal that is fed to the feedback controller needs to be separated from the audio signals that drive the loudspeakers before the control and audio signals. This way the road noise disturbance and the audio spectra are separated, since both are embedded in the measured microphone signal of the cabin. Otherwise if the microphone signals are directly fed to the controller, then the control might have an effect the performance of the audio system. Sano presented a solution for the integration of feedback controllers with the vehicle's audio system implemented in Honda vehicles [Sano et al. (2000)].

1.7.3 Review of feedback active road noise controllers

The first study of road noise cancellers is dated back in 1989, when a digital feedback controller was designed for reducing impact road noise [Costin and Elzinga (1989)]. The system was based on a headphone system mounted at the headrest of the driver. The feedback controller was designed with a *proportional integral* (PI) control theory that achieved 5-10 dB reduction between 20-60 Hz. Also a version of the controller with *genelarised minimum variance* theory was implemented that managed to cancel up to 20 dB in the same low frequency range. Another very interesting study in terms of control theory is found in [Brown (1995)], where a state space was used for developing a *linear quadratic gaussian* (LQG) optimal control for road noise cancellation with a single microphone mearusing the sound field in the cabin. Poor performance was reported in this study and the need for *multiple input multiple output* (MIMO) feedback design techniques was highlighted. As previously mentioned single channel feedback controller for ARNC with fixed filter coefficients has only been developed by Honda Motors in a production line vehicle [Sano et al. (2000), Sano et al. (2001)]. Yet, its effectiveness was limited to a single frequency of a road noise drum frequency at around 40 Hz. The main reason for the limited performance of feedback road noise controllers is the delay that is introduced by the physical

path between the loudspeaker and the microphone in the cabin that feeds back the sound signal to the controller.

A simulation study for road noise cancellation [Elliott and Sutton (1996)] showed that feedback systems are extremely sensitive to the acoustic plant delays, especially as the distance between the loudspeaker and the microphone increases. Adachi presented a more detailed design and analysis of feedback ANC [Adachi et al. (2001), Adachi (2003)]. The effect of the latency that is introduced by the acoustic plant is demonstrated under an ANC experiment with simulated road noise through loudspeakers in free field and varying distances between the control source and the cancellation position in the field.

In Elliott's study was suggested that the maximum distance should not be more than 0.3 m [Elliott and Sutton (1996)], whereas Adachi proved within an experiment that 0.1 m is required in order to attenuate 10 dB(A) at 150 Hz. The successful demonstration of Adachi was also based on the use of an extremely low order system for modeling the acoustic plant of the free field thus a simple control filter. In practice however, as the distance from the loudspeaker to microphone increases in the vehicle's cabin the complexity of the acoustic system between the transducer and the sensor increases. As a consequence, a high order control filter that compensates for the phase changes in the response of the physical system is usually required [Adachi (2003)]. As a solution to this problem, Cheer suggested a method that weights the control filtering according to the spatial distribution of the acoustic modes in the vehicle cabin [Cheer and Elliott (2012)]. However, the simulation findings were not particularly successful as the phase characteristics of the electro-acoustic path between the loudspeaker and microphone are always limiting factors for feedback strategies. As a further improvement of the suggested method, Cheer proposed an optimisation technique that calculates an *finite impulse response* (FIR) filter matrix for a multichannel feedback ANC with the use of operational data [Cheer and Elliott (2013)]. A comparison study based on simulations of road noise was published recently demostrated that the MIMO feedback controller was effective from 80 Hz to 180 Hz, but with the trade-off of small enhancements at frequencies above the range [Cheer and Elliott (2014)]. As a continuation of Cheer's work for multichannel feedback road noise control, the author performed a comparison between feedforward control with reference microphones inside the vehicle's cabin and feedback control [Cheer and Elliott (2015)], where good performance is obtained at the road rumble range, but above this band it has noticed that the coherence between the microphones is poor, due to other NVH attributes contributing to the sound field.

An interesting study in terms of hardware selection for feedback ANC systems for vehicles was presented by Howard [Howard and Leclercq (2006)]. The

control system was based on a single channel feedback ANC implemented in a *field programmable analog array* (FPAA) platform. The system was designed to cancel a very low frequency boom at 35 Hz, which created very high sound pressure levels in the cabin of a Holden Commodore station-wagon. Limited performance was reported as there were no attempts to optimise the loudspeaker and microphone placement.

Up until the point of writing this thesis, there have been no implementations of broadband feedback ANC for interior road noise in vehicles for the whole structureborne noise frequency range. Simulation results of new MIMO feedback ARNC design techniques have shown promising results up to 200 Hz [Cheer and Elliott (2013), Cheer and Elliott (2014)]. Recently, Honda demonstrated an interesting feedback technique of generating narrowband reference signals instead of using actual accelerometer sensors for removing some low frequencies road booms [Sakamoto and Inoue (2015)]. This method allowed Honda to use the active controller that is already integrated in their vehicles that is also capable of engine order cancellation.

1.7.4 Introduction to feedforward active road noise controllers

Modern control engineering control systems are augmented with a reference sensor that supplies a signal from the source. In the case of active road noise control the reference sensors are accelerometers that are positioned on the vehicle structure, suspension or subframe. The feedforward topology is presented in figure 1.10.

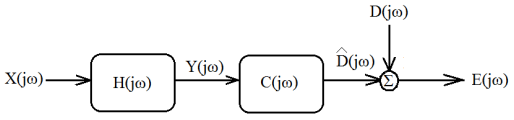

FIGURE 1.10: Block diagram of a single channel feedforward ARNC system. $X(\omega)$: reference input signals typically from a sensor at the noise source. $H(\omega)$: control filter. $Y(\omega)$: control signal that drive the transducer. $D(\omega)$: primary noise disturbance. $\hat{D}(\omega)$: estimated noise from the controller.

If the reference signal from an accelerometer demoted as $X(j\omega)$, then the output $Y(j\omega)$ of the control filter $H(j\omega)$ can be calculated as

$$Y(j\omega) = H(j\omega)X(j\omega) \tag{1.5}$$

and the error microphone signal can now be expressed as

$$E(j\omega) = \hat{D}(j\omega) + C(j\omega)Y(j\omega) \tag{1.6}$$

In order to find the controller's FRF the order of the $H(j\omega)$ and $C(j\omega)$ can be changed as in figure 2.1.

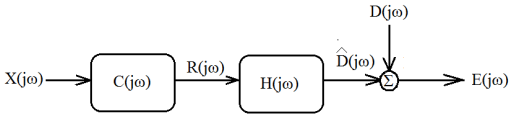

FIGURE 1.11: Alternative block diagram of a single channel feedforward ARNC system.

Feedforward controllers are usually developed based on adaptive algorithms, meaning that the control filter coefficients are adjustable. Figure 2.2(a) presents the general adaptive feedforward control strategy with the use of filtered reference LMS algorithm, also known as FxLMS.

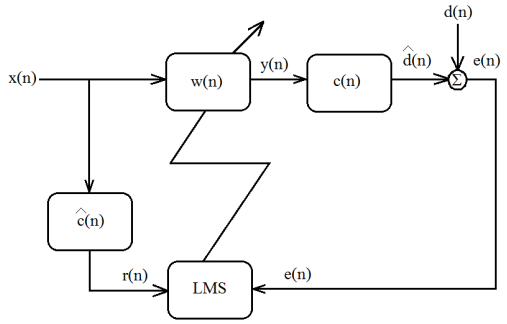

FIGURE 1.12: Block diagram of a single channel adaptive feedforward controller. $x(n)$: reference input signal typically from a sensor at the noise source. $w(n)$: control filter. $y(n)$: control signal that drive the transducer. $d(n)$: primary noise disturbance. $\hat{d}(n)$: estimated noise from the controller. $c(n)$, $\hat{c}(n)$: secondary path impulse and its estimate. $e(n)$: error signal.

In the case of adaptive feedforward ARNC the control filter coefficients are continuously adjusted in the time domain according to the variations of the sound pressure signal $e(n)$, which is measured by a microphone in the cabin, but also according to the variations of the filtered reference singal $r(n)$. The latter is the result of the convolution between the measured acceleration signal $x(n)$ and an estimate of the electro-acoustic plant $\hat{c}(n)$. The famous filtered reference LMS algorithm updates the control filter coefficients $w(n)$ according to the cross-correlation of $e(n)$ and $r(n)$ as follow

$$w(n+1) = w(n) + \mu e(n) r(n-i) \tag{1.7}$$

,where μ is the number between 0 and 1 that controls the speed of the converge of the algorithm and $r(n)$ is the so-called *filtered reference*, which is generated by the convolution between the refererence signal $x(n)$ and the impulse response of $\hat{c}(n)$. We will discuss further and analyse of the filtered reference LMS algorithm and its extension to a multichannel system in chapter 6.

As an introduction to multichannel feedforwad ARNC systems the typical configuration on a vehicle is shown in figure 2.2(b). This type of ARNC does not require any compensation for the audio signals since the controller cancels the part of the road noise that is coherent with structural vibrations measured by the accelerometers.

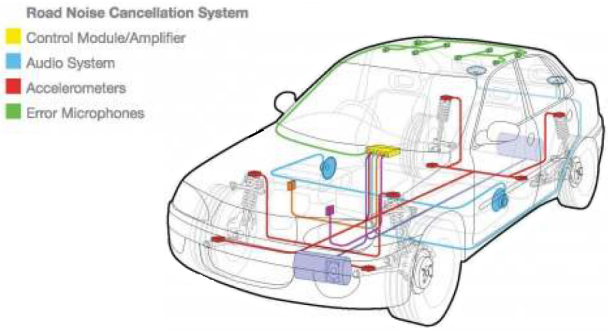

FIGURE 1.13: Feedforward ARNC system of Lotus-Harman. Taken from [Harman (2014b)].

In terms of hardware implementation, an ARNC controller consists of a DSP processor and an audio amplifier that drives the loudspeaker units. Figure 2.2(b) the accelerometer locations can be noticed around various suspension and body points, whereas the acoustic sensors are mounted on the roof lining. The location of the accelerometers significantly varies significantly according to the vehicle suspension setup and a structural design. Therefore an investigation is necessary for the defining number and the locations of the vibrational sensors. This depends on the number of structural road noise sources that act on the vehicle structure and are received in the cabin as road noise.

1.7.5 Review of feedforward active road noise controllers

Active control of road noise is a technology that was first successfully demonstrated on a small hatchback vehicle in the early '90s by Institute of Sound & Vibration (ISVR) and Lotus Engineering. In their study presented a multichannel adaptive controller based on an adaptive feedforward control strategy [Sutton et al. (1994)]. Apart from addressing the derivation of the adaptive algorithm, they pointed out the issue of the accelerometer placement. The authors performed time recordings on the road and then calculated the *cross-power spectral*

density (CPSD) matrix in order to identify the most important structural resonances that contribute to the road noise spectra. The also used *principal component analysis* (PCA) for calculating the virtual uncorrelated power spectra of the acceleration signals. The authors noticed two independent components in PCA. This fact implied two dominant structural sources acting in the structure of the vehicle. The Lotus-ISVR team used four acceleration signals for the implementation of the feedforward controller on a Citroen AX, since the combination of the accelerometers provided 7 dB(A) active reduction in their predictions. Two microphones were used at front headrests at the outer ear side in order to control the noise at the front headrests for reducing the noise in the front seats.

The latency in the controller feedforward path is also discussed, since the control filters need to be causal, meaning that the physical delay of the noise path from the structural source to microphone in the cabin needs to be greater than the sum of the electronic controller's latency with the acoustic plant delay from the loudspeaker to same microphone location in the sound field. The physical delay can be found from measured data and in particular from the cross-correlation between the acceleration signal and the receiving microphone in the vehicle's cavity. As a consequence, the distance between the vibrational and acoustic sensors controls the time required for the DSP hardware and analog electronics to generate the control signals that drive the loudspeakers in the interior of the car.

The ISVR-Lotus team installed and tested the multichannel controller in the Citroen AX on the road. Their system achieved 7dB(A) active noise reduction on average at the road noise bands, which is in good agreement with the authors predictions. Stother developed an improved version of the system in terms of computational load with the time domain multireference LMS requiring a high number of convolutions during each sample period, in order to calculate the filtered reference signals [Stothers et al. (1995)]. The proposed controller performs the adaptation stage in the frequency domain with the use of FFTs. The algorithm calculates the output of the controller in the time domain with the use of time domain convolution between the time series of the reference acceleration signals and the updated filter coefficients. In this way the computational requirements are significantly reduced, as blocks of sampled data update the algorithm. Instead in the standard multichannel filtered reference LMS algorithm [Elliott (1998)] that was applied by [Sutton et al. (1994)] the adaptation needs to be performed for each sample time. As a consequence, the sample based algorithm requires a high number of MMACS (Million Multiply Accumulate Cycles per Second). FFT based calculations allowed Lotus to develop an ANC that reduces the number of convolutions that are necessary for the generation of the filtered reference acceleration signals. Stothers used a constraint optimisation based on a

simulated annealing algorithm to optimise the selection of accelerometer sensors [Stothers et al. (1995)]. At the late '90s Lotus demonstrated again the technology to Mercedes. The system was integrated in a station wagon vehicle and the locations of the acceleration sensors were found with coherence analysis of the vehicle [Letens et al. (1999)].

A European research project that was mainly led by Katholieke Universiteit Leuven (KUL) conducted a comparative study between two active road noise control strategies [KUL et al. (1996), Sas and Dehandschutter (1999)]. The first was based on vibration actuators, which were mounted at sensitive structure-bone noise paths, whereas the second on the loudspeakers in the vehicle's cabin. The same algorithm was applied to both systems. The two control strategies were tested experimentally with the car mounted on four shakers that applied random uncorrelated forces. The researchers from KUL also explored the causality of the real-time controller, as they found that locations close to the vehicle's cabin did not allow enough time for the algorithm to converge [Sas and Dehandschutter (1999)]. The control system that was based on loudspeaker actuators performed better than the vibration control system as the required forces levels were close to the linearity limits of the inertia actuators.

As a continuation of the project this group of KUL developed a method for reducing the number of accelerometers in [Dehandschutter and Sas (1998)] based on Principal Component Analysis (PCA). The method was formulated in the time domain in order to derive a transformation filter matrix that can decompose the acceleration reference signals and increase the coherence between the vibrational and acoustic sensors. The time domain *singular value decomposition* (SVD) technique of the auto, cross-correlation matrix of the reference signals showed a dramatic reduction of the number of accelerometers without any degradation of the active noise reduction in the vehicles. The decomposition of the correlation matrix was extended to a recursive algorithm that is updated by multiplying with a Givens-like rotation matrix [Dehandschutter and Sas (1998)]. The author highlight that the adaptation of this covariance matrix of the reference acceleration signals under real-time conditions requires extremely high computations and only simulations were demonstrated. Therefore it is in question if such a complex algorithm is worth implementing as its real-time performance is unknown. Similar decomposition techniques techniques for multichannel feedforward active noise control have been also proposed by Elliott. A set of FIR filters are found from SVD methods and are used in the algorithm that help to decompose the references before they are fed into the adaptive controller, thus this type of algorithms are referred as *preconditioned LMS algorithms* [Elliott and Cook (2000), Elliott (2000b), Bai and Elliott (2004)].

A team of researchers from Centre of Noise and Vibration Control (NOVIC) in the Korean Advanced Institute of Science and Technology (KAIST) developed a multichannel ARNC system and applied their system on Hyundai Sonata [Kim et al. (1996)]. In their study a modified version of the filtered reference LMS was evaluated that converges faster than the standard algorithm. Four accelerometers were placed at the two front wheels and the active road noise reduction was limited. The authors presented a further improvement of the algorithm with the same sensor configuration on the Hyundai vehicle in [Oh et al. (2002)]. The proposed adaptive algorithm achieved better cancellation at a specific road noise band that was centered at 250 Hz. The key of the successful demonstration of this ARNC system was that it could focus the control effort at specific frequencies bands of road noise. In particular stable bandpass IIR filters may resolve specific road noise bands. The control focuses on certain frequency areas of road noise and also the convergence speed of the algorithm can be enhanced as the signal is band-limited. [Oh and Park (2000)] presented the full formulation of adaptive algorithm with IIR base filters.

Virginia Tech developed a broadband multichannel controller for active road noise cancellation up to 400 Hz [Couche (1999)]. The system was applied on a Ford Explorer and high levels of noise reduction were obtained for both ARNC and EOC at the dyno. Still, when the ARNC system was tested on the road, it achieved less reduction than on the dyno. This highlights the fact that the road conditions are strongly effecting the optimal performance of the ARNC system. Additionally, the Virginia Tech team developed a novel piezoelectric loudspeaker system for improving the phase response of the control sources and extending the frequency range of cancellation up to 400 Hz. These loudspeakers extended the ANC performance in the range of 200 Hz-500 Hz, which is the mid to high frequency range of structure-borne road noise.

The Virginia Tech group continued their research with Ford Motors and managed to apply ARNC into two different vehicles [Park et al. (2004), Park et al. (2002)]. The feedforward system was first developed for one vehicle and then it was installed in a second vehicle without any changes in the ARNC configuration. Additionally, the passive treatment at floor panels of the vehicles was removed, in order to investigate the NVH improvements from the active controller above 300 Hz, where the treatment started to be efficient. However, no information regarding the accelerometers placement and their number was published. For both vehicles, maximum 3.6 dB(A) active noise reduction was obtained at the driver's ear position, which was measurement location that was used to observe the performance of the controller far from the cancellation points where the maximum attenuation is achieved. It is also worth mentioning that the system was able to achieve global active control up to 350 Hz and and local

reduction at the cancellation points up to 475 Hz.

Lotus updated their ARNC system with more active sound technologies [Mackay and Kenchington (2004)]. The controller was integrated with engine order cancellation and engine sound synthesis. The updated Lotus controller was installed on a luxury diesel saloon with poor road noise performance. In particular the new system reduced by 10 dB(A) of road noise at headrest positions. Still, twelve accelerometers were necessary to capture all the road dynamics and achieve good active noise reduction in the demonstrator.

The decomposition of the acceleration signal matrix has not only been proposed for the optimisation of the sensor placement, but also for finding a set of filters that can decorrelate the vibrational signals that are recording on the chassis [Akiho (1995)]. In this way a reduced set of virtual reference signals can be used that increases the multiple coherence between the accelerometer output signals and microphone signals [Dehandschutter and Sas (1998)]. This method can potentially reduce the number of accelerometers as long as the virtual acceleration signals still contain all the spectral information of the actual road noise sources. The spatial position of the accelerometers is more important than making the signal uncorrelated and therefore in practice it has been suggested to use three locations per wheel for ensuring high multiple coherence in the structure-borne road noise range [Sutton et al. (1994)]. Mackay has highlighted the trade-off between the active road noise reduction and the number of reference accelerometers, where significant amount of reduction can be obtained with 6-12 accelerometers [Mackay and Kenchington (2004)]. However, there is no technique that locates the structural road noise sources on the vehicle as the majority of the proposed methods directly calculate the multiple coherence. It is therefore in question if a high number of sensing is signals is always necessary, as this depends on the complexity of each of the structure-borne road noise sources. This complexity is related with the number of locations that are coherent with the interior road noise and also the directions that the structure is vibrating at these locations.

A recent study presented another feedforward Active Vibration Control for road noise on a static shaker rig [Belgacem et al. (2012)]. The authors tried to optimise the actuators location around the suspension. An extensive and time consuming study on a separate test rig for the suspension is required in order to identify the most important vibration paths from the tire to the end of each suspension arm [Douville et al. (2006)]. Several shakers are also required at the suspension arms in order to control difference degrees of freedom that are important for road noise. Equivalent passive NVH refinement techniques [Aubert and Howle (2007)] that can control structural resonances are already

well-known in the automotive industry with tuned mass-dampers. Passive mass-damper isolators are easier to design and integrate on the suspension compared to miniature shakers with sensitivity output, as robust ways of mounting the actuators on the suspension will be necessary. This also explains the fact that all studies in active vibration control of road noise only static test rigs perform without the wheels. Yet, this technology can become feasible. If miniature vibration actuators can be mounted on critical road noise paths on the suspension system and they can also deliver high force levels under driving conditions, then *active vibration control* (AVC) could be potential applied in road noise reduction.

Currently the cost of the available minishakers with embedded controllers for automotive applications is extremely high and they still do not deliver enough force for reducing the vibration level under operational conditions across the whole frequency range of road noise. This kind of AVC are used as powertrain mounts for the reduction of vibration transmission into the cabin. As a result, this thesis explores feedforward active sound systems as previous findings in the area of active control of road noise have been rather successful in delivering high levels of reduction with the use of in-car loudspeaker setup.

As we discussed in this section several feedforward ARNC technologies have been demonstrated in vehicles for several automotive manufacturers, but none so far has been integrated into a production line vehicle. The main reasons are cost and complexity of the technology as for the time been the NVH development of the vehicle is not integrated with ARNC and the two sectors are treated as a separate piece of work. In reality, an ARNC development is necessary to come at early stages of the vehicle development in order to define sensor locations that can be latter used for a product. As once the vehicle is out from the production line the wiring that is necessary for the accelerometer sensors is not a simple task. In addition to that fault diagnostics of the sensors is necessary to be integrated with vehicle's electronics. All these limiting factors from the accelerometer side are can be highlighted once the vehicle is understood in terms of road noise performance, where candidate sensor locations are found. From the research point of view up until now there is no concrete method for the selection acceleration signals that relate to the main structural sources that cause road noise. Therefore we will investigate a more solid way of defining the necessary reference signals of the controller by analysing the vehicle with several NVH and signal analysis techniques that are widely used in the automotive industry for structure-borne road noise analysis.

1.8 Active control of engine noise and commercially available systems

Active sound controllers that can attenuate engine order harmonics (or amplify them) are already installed in vehicles that are available in the market. The technology that reduces engine order is referred as engine order cancellation (EOC) and recently it is modified in such a way that some order that are causing booming noise are attenuated and others are enhanced so that a specific engine order profile can be achieved. The concept of EOC started in 1984, where an analog controller was tuned to reduce the engine orders of a diesel motor truck [Oswald (1984)]. The controller achieved high noise reduction up to 200 Hz, but it was not capable to react fast to changes in the engine spectrum due to limitations of the analogue hardware. ISVR and Lotus developed a DSP based feedforward adaptive engine order controller in the '80s [Elliott and Stothers (1986), Elliott et al. (1988)]. Their system achieved maximum 10 dB noise reduction from 3000rpm-4000rpm. A filtered reference LMS algorithm with second order FIR filters was implemented as an adaptive controller [Elliott and Nelson (1988)]. The reference signal of the feedforward system was extracted from the rotational speed of the engine with the use of the output signal of the tachometer. In the early 90s Nissan Motors successfully developed and integrated an adaptive controller in a Nissan Bluebird [Kinoshita and Nakaji (1994)]. Their system did not significantly differ from the previous proposed systems in terms of algorithm development and system implementation. On the other hand, Honda Motors introduced a more efficient in terms of computational requirements adaptive controller that was implemented in a low cost microcontroller for production vehicles [Inoue et al. (2003)].

The latest EOC system is the *Active Sound Management* (ASM) system by Bose Corporation, which is integrated with audio system of Bose. The ASM of Bose can perform cancellation or enhancement of specific engine harmonics [Bose (2014), Ahrens and Feng (2014)]. The system has already been implemented in American vehicles: Buick, Cadillac, GMC and Acura and in Europe in Audi S-series vehicles. Recently, Ford Motors has already also introduced the EOC technology in Ford Fusion Hybrid and Ford C-Max Energi. The Bose system is actually an embedded software solution, which is integrated in audio DSP processor by NXP semiconductors [Bose and NXP (2014)]. Another software solution that can be downloaded to the DSP unit of the audio amplifier is provided QNX [QNX (2014)]. Although these type of systems are very attractive for production. However they are not complete NVH solutions as they do not take into account all the low frequency NVH attributes.

Lotus and Harman have presented so far the most complete ANC solution for commercial vehicles [Harman (2014a), Doyle (2014)]. Their system integrates all the active sound technologies in one unit [Halosonic (2014)]. Recently, Müeller Active Sound Technologies entered the market of ANC by introducing a software tool and a hardware control unit for ANC development in vehicles [Müeller (2014), Schirmacher (2010)]. The Müeller system is already integrated into an Audi s-series that has strong engine booming noise due to cylinder deactivation at some specific driving conditions [Schirmacher et al. (2012)].

To summarise most of the commercially available systems are limited to EOC and many of them cannot be used for road noise cancellation, since systems with high processing power and low hardware latency are required. In terms of integration to production line vehicles the main challenge is to define a generic low cost DSP architecture that could be used in different vehicles. However the vehicle physics related to NVH are always important and generic methods for design and integration of ANC are necessary.

1.9 Research objectives and contributions

This study aims to design and develop an ARNC system for a luxury vehicle by combining advanced NVH methods that reveal the main dynamics of road noise and adaptive DSP technologies. The main objective of the research is to provide a control strategy that is based on the structural dynamics of the vehicle that are related to the structure-borne road noise. As an outcome a low number of acceleration sensors and reference signals that are necessary for feedforward ARNC may potentially be used for feedforward ARNC systems.

Usually, the loudspeakers positions inside the vehicle's cabin is another element that effects the performance of the ANC system. However, in this case a technical requirement from Bentley Motors Ltd was set that the controller should make use of the existing loudspeaker arrangement of the vehicle. This way the controller could be applied to existing or future Bentley models without any modifications of the loudspeaker installation.

Alternative methods for the identification of the most important structural vibrations that are related to the interior noise are also another area of investigation. This also links to feedforward ARNC operation and performance as they depend on the observability of the structural resonances that are coherent with road noise resonances that are audible inside the cabin. As a consequence this is the main driving point of this thesis to enhance the link between ARNC

and structure-borne NVH analysis in order to create an integrated solution for future vehicle with enhanced structure-borne road noise performance.

The main objective of this PhD thesis are:

• The development of a method for reducing the number of acceleration sensors for feedforward ARNC systems.

• The development and the implementation a prototype ARNC system on a Bentley vehicle that can reduce the main road noise resonances.

1.10 Thesis structure

Chapter 1

In this first chapter a literature review of the application of Active Noise Control in commercial vehicle is presented. The evolution of feedback and feedforward Active Road Noise Control is also included in the literature review. At the last part of the review commercially available technologies of Engine Order Control are also discussed as this technology is currently available in several vehicles.

Chapter 2

In the second chapter the structure-borne noise field of the vehicle is described for three different cases: tyre-road interaction, hammer excitation and monopole source in the cabin. Before, measuring road and vibration data on the road it was necessary to find the acoustic and structural resonances of the vehicle, as they should highlight some of the sensitive structural inputs of the chassis that can cause structure-borne sound. As a starting point, experimental testing with the hammer and the monopole source are presented that allow to investigate structural and acoustical resonances separately. The operational data that were obtained from testing on the vehicle over a coarse chip road are shown as an introduction to the road noise field that is created under various speeds. Experimental data obtained by hammer testing the vehicle are used to calculate point and transfer mobilities of the suspension and subframe. The corresponding noise transfer functions are also shown for identifying significant paths of structure-borne noise. The investigation of monopole source measurements shows the dominant standing waves of the sound field below 500 Hz and their contribution to the sound pressure responses at the headrest locations.

Chapter 3

In the third chapter the development of a road noise simulator is discussed and the development of the experimental test bench is presented. The analysis of the vehicle's sound field is formed according to excitation that was applied at the front or rear tyres. Hence, the contributions and the control from front and rear axle were found and are presented in this chapter.

Chapter 4

In the fourth chapter, a methodology for identifying the location of the main structure-borne road noise sources based on coherence functions at each transfer path is developed. Multiple coherence analysis is usually applied to road noise data that are obtained on driving conditions in order to calculate the maximum reduction of feedforward ARNC system for a specific sensor arrangement. In this case coherence analysis is used for identifying the relative location of a road noise source on the vehicle structure and how much it contributes to the each of the structure-borne road noise bands. A low number of reference accelerometers was obtained and their combination resulted to high multiple coherence at the main road noise bands of the vehicle. The ARNC performance was calculated for the optimised set of the acceleration signals are presented and compared with a combination of high number of acceleration signals coming from important noise transfer paths.

Chapter 5

In the fifth chapter the multireference LMS algorithm is introduced for the identification of the impulse responses between the acceleration and sound pressure signals that were obtained from the road noise measurements. The sensor locations are evaluated with the use multireference adaptive filtering techniques. The scope of this study was to synthesise the interior road noise with the previously selected acceleration signals from chapter 4. The selected acceleration signals are highly correlated with the noise and they can allow to the algorithm to converge to a causal filter solution. The error signals of the adaptive algorithm simulation are compared with the predicted active noise reduction that was estimated previously from the multiple coherence function in order to evaluate the validity of the estimated impulse responses of the algorithm.

Chapter 6

In the sixth chapter, the multichannel filtered reference LMS algorithm is derived and used for predicting the performance of an adaptive noise controller for road noise data. The measured impulse response between the audio system and the headrest locations are first modelled with multirate signal processing and then truncated with an adaptive algorithm for system identification, in order to

include these estimated secondary paths of a small FIR length in the ARNC algorithm. A comparative study between various combinations and numbers of accelerometer signals is performed and the results of this study are discussed in this chapter.

Chapter 7

In the seventh chapter the development of the real-time ARNC experiment on the road noise simulator is presented. The selected accelerometer locations from chapter 4 that were evaluated in the models in chapters 5 and 6 are tested in this chapter on the vehicle road noise simulator. The preselected accelerometer locations are supported according to their performance for the various excitation cases on the tires, front, rear and whole vehicle.

Chapter 8

In this last chapter the outcomes of this thesis are summarised. The outcome of this study and the contributions to the area of structure-borne road noise and feedforward ARNC are discussed. Suggestions for future work are also included in this chapter since from this development many interesting case scenarios for ARNC can be investigated in the future.

Chapter 2

The sound field inside a vehicle

2.1 Introduction

In this chapter we introduce the physical quantities that are typically measured in a vehicle for sound and vibration analysis. We begin with the case of the excitation sources inside the cabin. Two sources may be used in this case, a volume velocity source and the low frequency transducers of the audio system. The first acoustic modes that dominate the sound field of the compartment are usually found with the assistance of a volume velocity source. For the purpose of this research we used a monopole source to measure the acoustic FRFs between the source and the microphones at the headrests. Additionally, the electro-acoustic transfer functions between inputs of the loudspeaker systems to the microphones at the headrests were measured. These systems are instrumental in the development of active systems as they define the so-called secondary path tranfer functions that used in the design of adaptive algorithms as we will discuss this later in chapter 6.

With regards to the structural sources that cause structure-borne noise it is worth clarifying the relations between the acoustical and structural quantities. These are useful for NVH analysis methods of structure-borne road noise and in particular in force identification methods such as TPA. In this thesis we are more concerned with the localisation of the structural sources that relate to road noise, thus we will mainly focus the analysis of the measured quantities that relate to road noise. We present a vibro-acoustic analysis of the front axle based on noise transfer functions (NTFs), which may reveal the relationship between the impact

forces applied to parts of the axle, which in turn are influential for the passive NVH design of the vehicle. Apart from experimental data obtained from vibro-acoustic testing of the vehicle, operational road noise data are also presented, in order to highlight the variability of road noise under driving conditions.

2.2 Chapter outline

In section 2.3 we begin by defining the acoustical quantities that are measured in the cabin. Green's function inside a rectangular cavity is defined in section 2.3.1, which describes the relationship between the acoustical excitation for a point source inside a cabin and the sound pressure response at a certain point in the sound field. In sections 2.3.3 and 2.4 we present the outcomes of the measurements of the electro-acoustic FRFs and their impulse responses of the audio system. In section 2.5 we introduce the vibro-acoustic theory that is applicable to MIMO system analysis for NVH in vehicles. As an extention to this, the TPA method is introduced in section 2.6.1 as well as the different vibro-acoustic FRF functions such as transmissibilities that are used in NVH analysis methods. In section 2.6.2 we introduce the problem of the incoherent sources, which is a common problem among all TPA methods as well as ARNC technologies. Finally, in section 2.7 we present operational road noise data as an introduction to the actual noise control problem.

2.3 Acoustic frequency response functions

2.3.1 Acoustic frequency response functions in a vehicle

The sound field inside a small cavity, such as a vehicle's cabin, can be modeled by the Green's function. More specifically, this function determines the frequency response function between two locations inside the sound field, one placed at the location of a point source, at $\mathbf{r}_0 = (x_0, y_0, z_0)$ and the other is located at the receiver, $\mathbf{r} = (x, y, z)$. Green's function for an enclosure is defined as the summation of the contributing acoustic modes $\psi_n(\mathbf{r})$ at the source and at the receiver $\psi_n(\mathbf{r}_0)$ [Jacobsen (2007),Hansen (2013)]

$$G(\mathbf{r}, \mathbf{r}_0) = \frac{1}{V} \sum_{n=1}^{\infty} \frac{\psi_n(\mathbf{r})\psi_n(\mathbf{r}_0)}{k^2 - k_n^2 - \frac{jk}{\tau_n c}}, \tag{2.1}$$

where the time constant is τ_n and the losses are included in the imaginary part of the function. The time constant of each n-mode reflects how much time is necessary for its corresponding standing wave to decay in the cavity due to the losses that are introduced by the wall surfaces [Jacobsen (2007)].

The Green's function of equation 2.1 is an FRF that can be also converted to a causal impulse response function, which is commonly used to investigate the decay of the sound energy over time in an enclosure. In complex shaped enclosures such as the ones in vehicles, the acoustic mode shapes are fairly complicated and numerical methods such as finite element method (FEM) are used to solve the eigenvalue problem of the mode shape functions [Beranek and Vér (1992)]. In practice, modern transfer function identification methods are used to determine the FRFs between two locations in the sound field. Omnidirectional volume velocity transducers can be used for these type of measurements. In particular, the acoustic FRFs inside a vehicle's cabin are defined by referencing the measured sound pressure to the volume velocity autospectra. The velocity spectra can be found based on the assumption that the velocity specta at the outlet of the source are the same as for a one dimensional tube [Gade et al. (2004)]. The following section presents FRFs that were measured with this type of technique with the purpose of exploring the low frequency acoustic resonances that are audible by the passengers at the headrest positions.

2.3.2 Cabin acoustic responses for a volume velocity excitation

A miniature omnidirectional acoustic source by LMS Siemens was placed at two locations on the front part of the vehicle in order to access the acoustic modes. Since the cabin has an irregular shape, two excitation positions were chosen. The first location $\mathbf{s}_1$ is at the corner of the dashboard and the second down $\mathbf{s}_2$ at the footwell at the driver's position as illustrated in figure 2.1. The measurement configuration with the volume velocity source is demonstrated with the microphones that were mounted at the headrests.

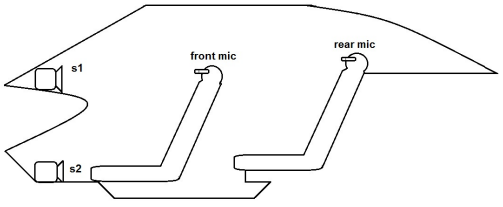

FIGURE 2.1: Microphone and volume velocity arrangement for acoustic FRF measurement inside the cabin. $\mathbf{s}_1$, $\mathbf{s}_2$: volume velocity source locations.

The FRFs between the two excitation source locations at the front part of the vehicle and the microphones were measured in a semi-anechoic chamber and the results are presented in figures 2.2(a)-2.2(d) and later in figures 2.3(a)-2.3(d) also the coherence functions between the volume velocity source and the microphones at the headrests are displayed. When the source is placed at the corner of the vehicle at the dashboard $\mathbf{s}_1$, then an acoustic mode that acts between 150-300 Hz appears in all of the FRFs at microphones at the right hand side.

As for the microphones at the left hand side only two resonances at the front headrest are noticeable at 190 Hz and 220 Hz, which they are in the tyre cavity range. In general, the frequency band of 150-300 Hz may play a significant role, since it is inside the structure-borne road noise range. It is likely that road vibrations may couple with this acoustic resonances in the cabin and thus generate audible levels of road noise. In section 2.5 we will explore this further with the introduction of the vibro-acoustic FRFs between important parts of the vehicle and the acoustic response inside the compartment.

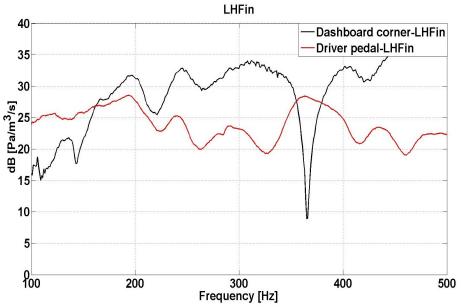

(a) FRFs from left hand front (LHF) woofer to microphones.

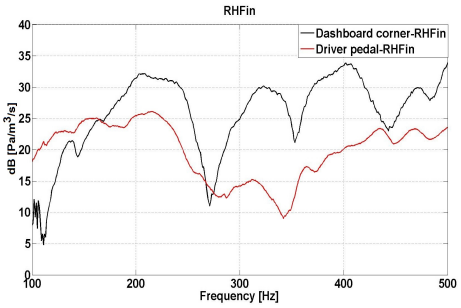

(b) FRFs from right hand front (RHF) woofer to microphones.

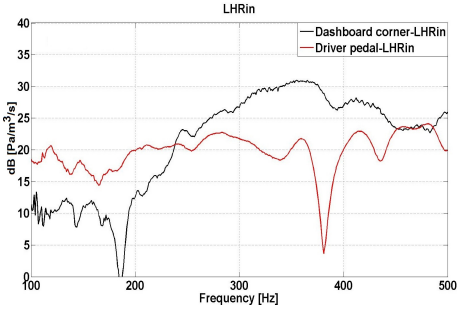

(c) FRFs from left hand rear (LHR) woofer to microphones.

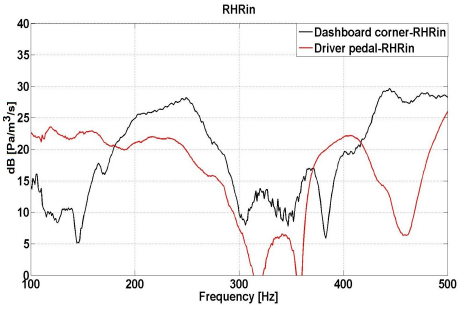

(d) FRFs from right hand rear (RHR) woofer to microphones.

FIGURE 2.2: FRFs between two volume velocity source locations and the microphones at the headrests. −: Dashboard corner. −: Driver's pedal.

Unfortunately, the volume velocity source did not succeed in exciting low-order modes of the sound field below 100 Hz, due to hardware limitations of the transducer. In figures 2.3(a)-2.3(d) the coherence is relatively poor below 100 Hz for the identification of the acoustic FRFs between the volume velocity source

and the microphones. This is probably caused by low frequency cut-off in the sensitivity of the transducer that limits the response of the transducer in the range of 200 Hz-10 kHz [LMS and Siemens (2014)].

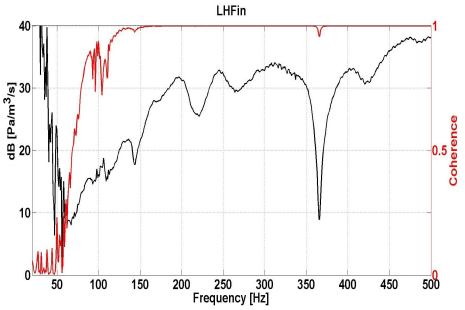

(a) Coherence and FRF from left hand front (LHF) woofer to microphones.

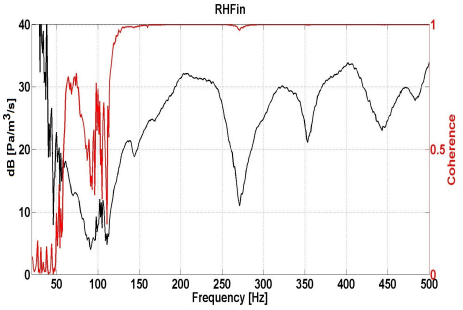

(b) Coherence and FRF from right hand front (RHF) woofer to microphones.

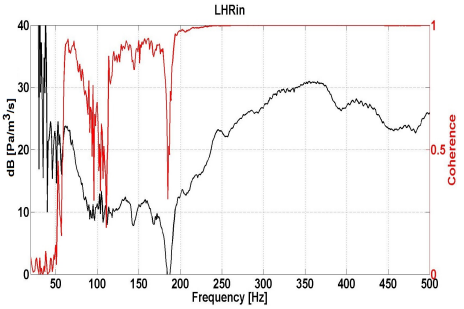

(c) Coherence and FRF from left hand rear (LHR) woofer to microphones.

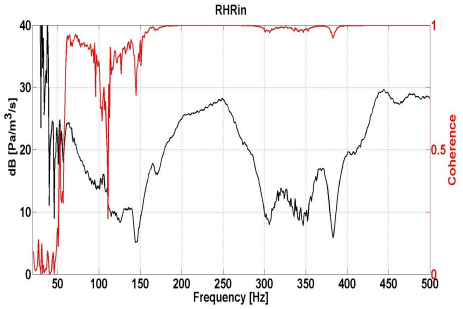

(d) Coherence and FRF from left hand rear (LHR) woofer to microphones.

FIGURE 2.3: Coherences and FRFs between two volume velocity source locations at the dashboard and the under the driver's pedal and the two microphones at the rear headrests. The microphones locations at the front headrests are noted as: LHR: Left hand rear. RHR: Rear hand rear. —: FRF. —: Coherence.

These two locations of the source may not be sufficient for measuring the sound field, since they do not directly couple with all the low order acoustic modes of the vehicle. More excitation and measurement locations are necessary to perform a complete acoustic modal analysis of the cabin, in order to map the sound field across the cabin. However, this is not a primary task in this study as the excitation does not come from inside the vehicle but it is due the vibro-acoustic coupling between structural and acoustical resonances of the vehicle. For feedforward active control it is necessary to further investigate the relation between several parts of the axle that could potentially used as reference locations for the vibration sensors that provide the inputs to the control filters. As a next step we will introduce the secondary paths transfer functions of the control systems that are the electro-acoustic systems between the loudspeakers and the microphones at the headrests.

2.3.3 Electro-acoustic frequency response functions

As previously mentioned, it is worth investigating the acoustic responses of the sound field at the microphone locations when the audio system of the vehicle is activated, as we will use it later on to generate secondary canceling field. In particular, for active sound control the loudspeaker arrangement is important to be able to excite the low frequency acoustic modes of the cabin [Nelson and Elliott (1991)] for the effective reduction of the low frequencies that coincide with the eigenfrequencies of the cabin. In this section we define the FRFs of the electro-acoustic systems and how we measured them in the vehicle. The sound pressure, $p_l(\omega)$ signal at the l^{th}-microphone in the cabin and the signal, $v_m(\omega)$ from the m^{th}-loudspeaker are used to identify the electro-acoustic FRFs that determine the secondary paths of the active control system. These electro-acoustic FRFs between the electrical inputs of the loudspeakers and the microphones outputs can be defined as

$$C_{lm}(\omega) = \frac{p_l(\omega)}{v_m(\omega)} \quad \left[\frac{Pa}{Volts}\right]. \tag{2.2}$$

The identification of these FRFs was performed through the use of white noise that was emitted by the loudspeaker system of the vehicle. Each loudspeaker was driven separately develop the matrix that contains all the FRFs between four loudspeakers and twelve microphones. The measurement configuration is shown in figure 2.4.

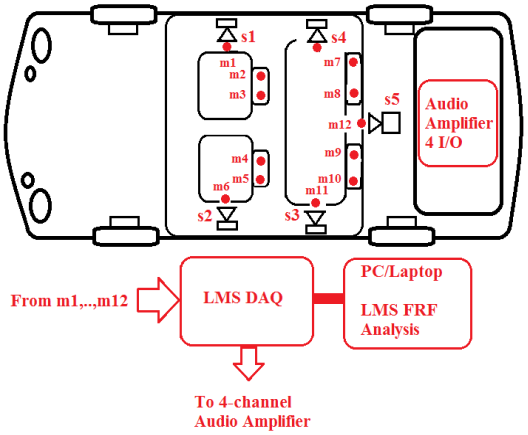

FIGURE 2.4: Loudspeaker and microphone placement inside the cabin. The LMS Siemens SCADAS DAQ systems was generating the white noise signals that was driving the audio amplifier and also measuring the microphone responses that were referenced back to the white noise signal, in order to obtain the electro-acoustic FRFs. The four loudspeakers are noted as $\mathbf{s_1}$, $\mathbf{s_2}$, $\mathbf{s_3}$, $\mathbf{s_4}$ and the twelve microphones as $\mathbf{m_1}$, $\mathbf{m_2}$, $\mathbf{m_3}$, ..., $\mathbf{m_{12}}$. •: Microphone positions.

An after-market car audio amplifier with four inputs and outputs was used to drive the loudspeakers of the vehicle with white noise between 0-1 kHz generated from the SCADAS Siemens LMS system. Each of the five loudspeakers was tested seperately in order to generate all possible combinations between the loudspeakers and the microphones.

From the perspective of an active control system, the low frequency transducers of the audio system are expected to generate the appropriate sound pressure levels at the road noise resonances, especially in the range of 0-300 Hz, where most of the structure-borne noise appears in the particular luxury vehicle. In addition to this the loudspeakers should not be placed at the pressure minima of the first standing waves of the cabin, so that the loudspeaker drivers are not driven with large voltage signals to compensate for the low acoustic impedance in front of them.

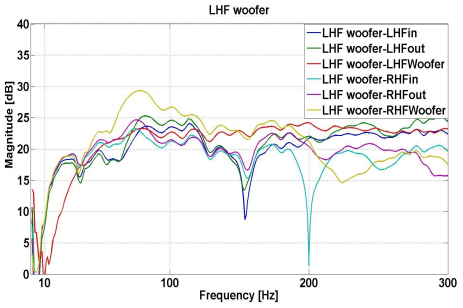

(a) FRFs from left hand front (LHF) woofer to microphones at the front headrests.

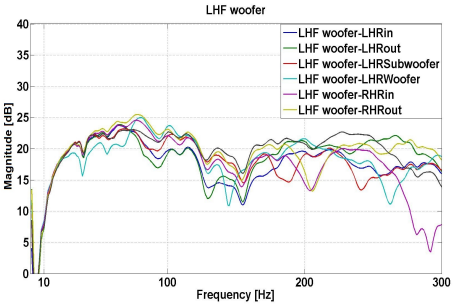

(b) FRFs from left hand front (LHF) woofer to microphones at the front headrests.

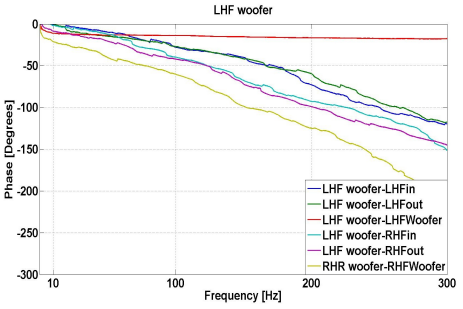

(c) Phase responses from left hand front (LHF) woofer to microphones at the right headrests.

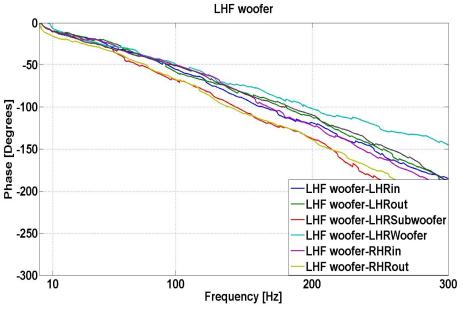

(d) Phase responses from left hand front (LHF) woofer to microphones at the right headrests.

FIGURE 2.5: Magnitude and phase responses of FRFs between the left hand front (LHF) woofer and the microphones in the cabin. The microphone positions are noted as LHFin/out: left hand front inner/outer, RHF: right hand front inner/outer, LHR: left hand rear inner/outer RHR: right hand rear inner/outer.

In terms of the phase responses, the microphone in front of the woofer does not roll-off as sharply as in other electro-acoustic paths, since it is very close to the near field of the loudspeaker and it is not effected by the cabin resonances. The same behaviour is noticed in figure 2.6(c), where the microphone is placed in front of the right hand front woofer. As for some of the magnitude responses in figure 2.6(b), sharp antiresonances above 200 Hz occur between the right hand front woofer and the microphones mounted on the right rear headrest.

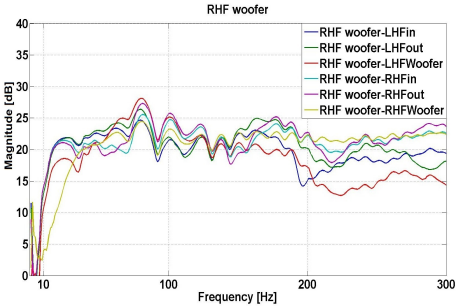

(a) FRFs from right hand front (RHF) woofer to microphones at the front headrests.

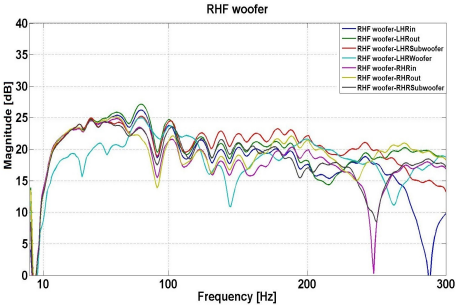

(b) FRFs from right hand front (RHF) woofer to microphones at the front headrests.

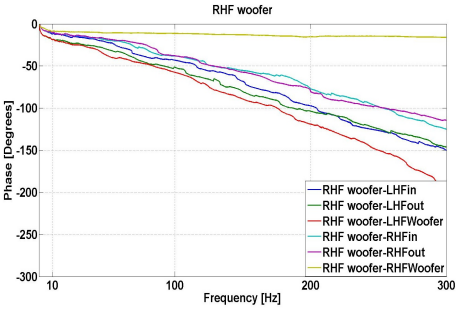

(c) Phase responses from right hand front (RHF) woofer to microphones at the rear headrests.

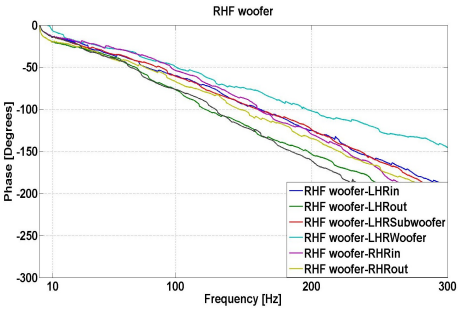

(d) Phase responses from right hand front (RHF) woofer to microphones at the rear headrests.

FIGURE 2.6: Magnitude responses of FRFs between the right hand front (RHF) woofer and the microphones in the cabin.

When the sound field is excited by the left rear woofer in figures 2.7(a)-2.7(c), the response levels for the front microphones are reduced in the frequency range of 100-200 Hz. This fact suggests that the front woofers are necessary as they can achieve 10-25 dB higher output levels compared to the rear woofers. In contrast to this the microphones at the rear headrests are not close with this loudspeaker and are almost insensitive to the acoustic resonances above 100 Hz, thus the magnitude levels vary in a smaller range within 5 dB.

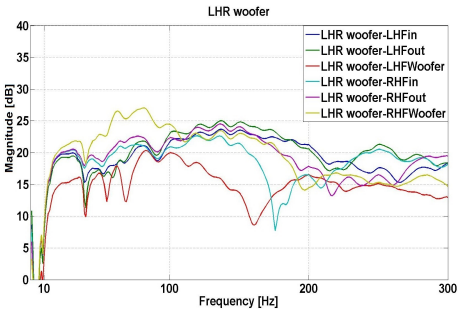

(a) FRFs from left hand rear (LHR) woofer to microphones at the front headrests.

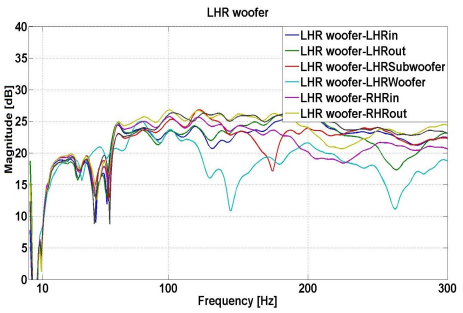

(b) FRFs from left hand rear (LHR) woofer to microphones at the front headrests.

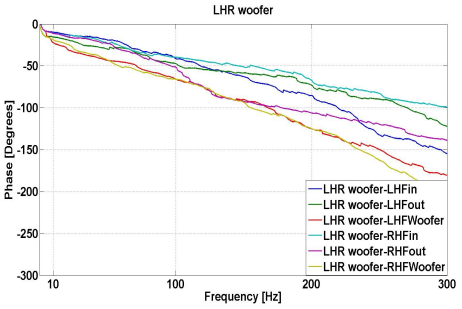

(c) Phase responses from left hand rear (LHR) woofer to microphones at the rear headrests.

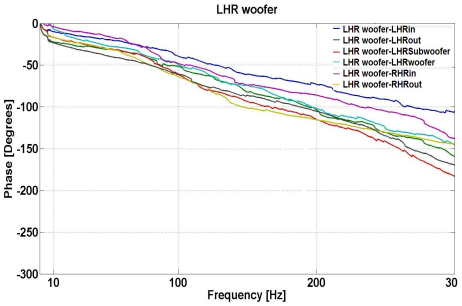

(d) Phase responses from left hand rear (LHR) woofer to microphones at the rear headrests.

FIGURE 2.7: Magnitude responses of FRFs between the left hand rear (LHR) woofer and the microphones in the cabin.

The fourth woofer at the right hand rear door was also measured. As figure 2.8(a) illustrates, several antiresonances are present in the FRFs between this woofer at the rear door and some of the microphones at the front of the cabin. This may influence the length of the FIR filters used for modelling these transfer functions for the development of the ANC system, as several taps might be required for accurately modeling such high order secondary paths. If several low frequency acoustics modes are includes in the secondary paths, then the decay of the impulse response is relative slow. As the sampling rate increase more taps are necessary to model the tail of the impulse response that corresponds to the low frequency contain of the secondary path. For example, for a sampling rate of 1 kHz and an acoustic impulse response of a duration of 0.1 seconds, an FIR filter with 100-taps is required.

The side-effects of poor estimation of the electro-acoustic systems is slow convergence of the adaptive algorithm and also instabilities [Hansen (2001)] and therefore precise estimation of the secondary paths is always necessary for the robustness of the system. The subwoofer located under the parcel shelf behind the rear headrests was also measured, since it is the only transducer that is only a short distance from the sensors at the rear headrests. The placement of this subwoofer is ideal for the active sound control as we will see later in the impulse

responses of the secondary paths, as the propagation delay is dependent on the distance between the transducer and the microphones in the cabin's sound field.

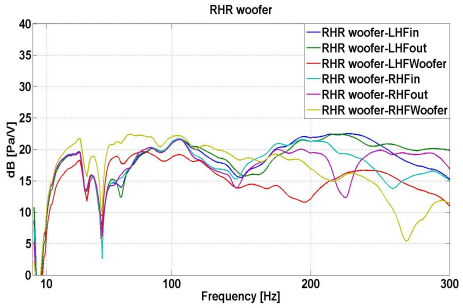

(a) FRFs from right hand rear (RHR) woofer to the microphones at the front headrests.

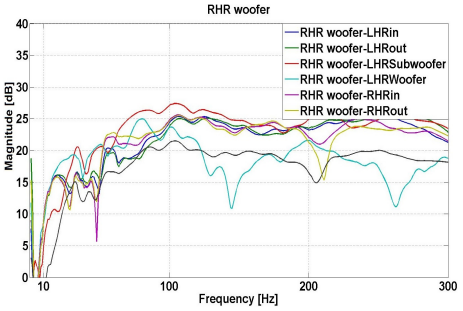

(b) FRFs from right hand rear (RHR) woofer to the microphones at the front headrests.

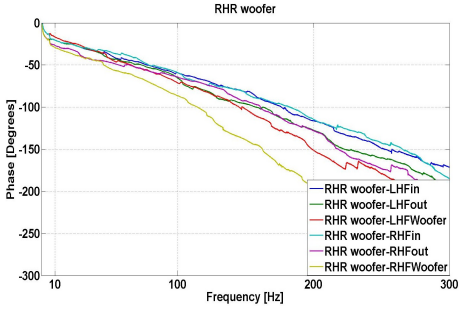

(c) Phase responses from left hand front (RHR) woofer to the microphones at the rear headrests.

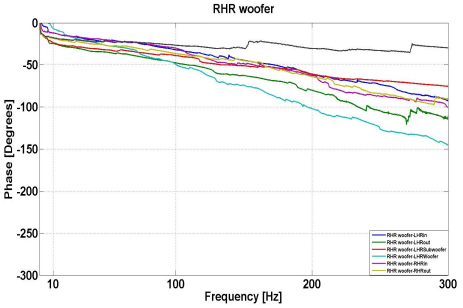

(d) Phase responses from right hand front (RHR) woofer to the microphones at the rear headrests.

FIGURE 2.8: Magnitude responses of FRFs between the right hand rear (RHR) woofer and the microphones in the cabin.

As a result, the phase responses of the rear microphones transfer functions, displayed in figure 2.9(d), decay at a low rate. As figure 2.10(a) illustrates, this subwoofer provides the highest sensitivities for the rear microphones, which may prove beneficial for high sound pressure levels at low frequencies.

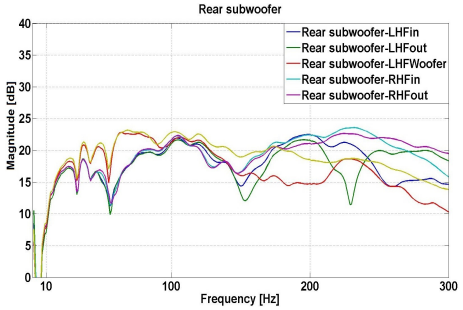

(a) FRFs from the rear subwoofer at the parcel shelf to microphones at the front headrests.

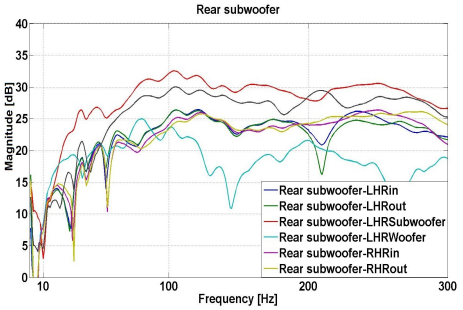

(b) FRFs from left hand rear (RHR) woofer to microphones at the front headrests.

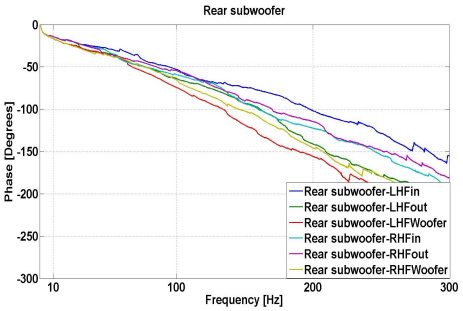

(c) Phase responses from the rear subwoofer at the parcel shelf to microphones at the rear headrests.

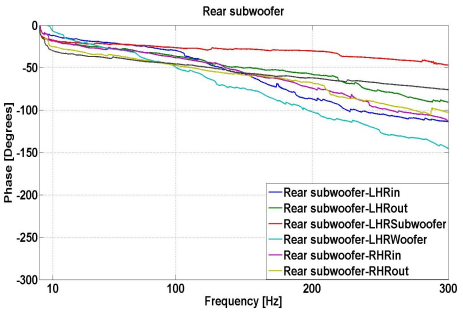

(d) Phase responses from the rear subwoofer at the parcel shelf to microphones at the rear headrests.

FIGURE 2.9: Magnitude responses of FRFs between the rear subwoofer and the microphones in the cabin.

In our experiments we observed that the sound field in the cabin is heavily damped. Some sharp notches are included in the FRFs between the front and rear part of the vehicle, which they may effect the amplification stage of the ANC controller in some cases. However, most of the loudspeakers provide a relatively high sensitivity response in the range of 100-200 Hz, where most of road noise energy is concentrated. The rear subwoofer has the ideal location for an active application, since it is close to the rear headrests. In the following section we discuss further the time delays that are inherited from the electro-acoustic paths.

2.4 Electro-acoustics impulse responses

In this section we continue further with our investigation on the impulse responses of the physical plants that determine the secondary paths of the control signals from the input of each transducer to the microphones inside the cabin. In this case the inverse FFT of the complex FRFs was used to transform the measured systems in the time domain.

In active systems of road noise the latency that is embedded in the controller can strongly downgrade the noise reduction of random disturbances as it was found by Sutton [Sutton et al. (1994), Elliott and Sutton (1996)]. For feedforward road noise control system reduction levels of 6 dB are possible with highly coherent sensor signals. Interestingly, in figures 2.10(a), 2.10(c) illustrate that around 5 milliseconds delay is required for the direct sound to travel from the left hand front woofer to the front microphones at the headrests. On the other hand, more time is necessary for rear microphones, more specifically 10 milliseconds, as displayed in figures 2.10(b) and 2.10(d). This latency is proportional to the distance between the source and the receiver and it can only

be compensated if the loudspeakers are located at the headrests [Sutton et al. (1994), Cheer and Elliott (2014)].

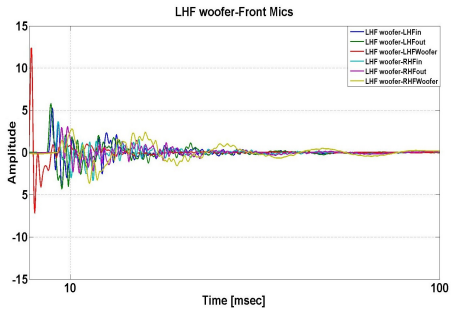

(a) IRFs from LHR woofer to microphones at the front headrests.

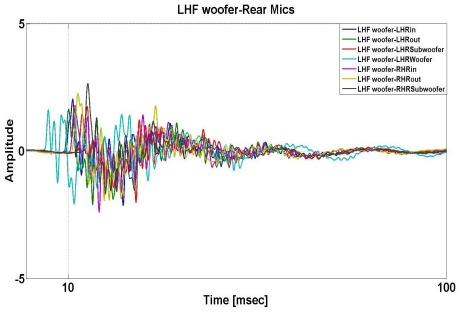

(b) IRFs from LHR woofer to microphones at the rear headrests.

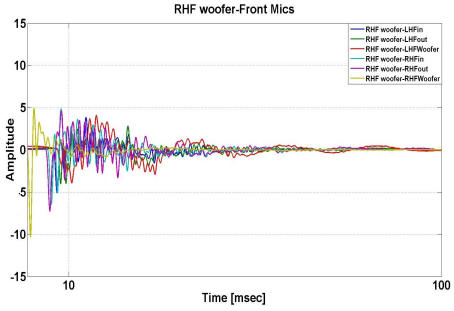

(c) IRFs from LHR woofer to microphones at the front headrests.

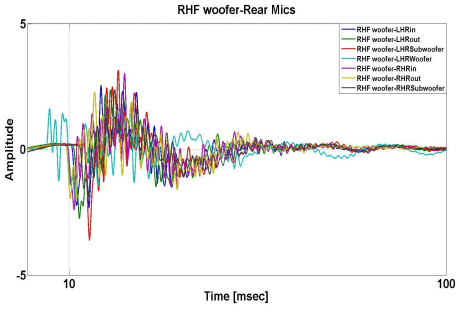

(d) IRFs from LHR woofer to microphones at the rear headrests.

FIGURE 2.10: Impulse response functions (IRFs) between the two front woofers and the microphones in the cabin.

Some modern commercial ARNC systems use loudspeakers and microphones that are integrated in the vehicle's headrests [Silentium (2014)]. This arrangment decreases signficantly the delay in the acoustic path between the control loudspeaker and the microphone, where the sound pressure minimum is created. For the purpose of our study we focus our design in the scenario that the standard loudspeaker system mounted at the doors is available and the microphones at the headrests. We measured for the impulse responses from the rear subwoofer to the rear headrests microphones, where the first peak that corresponds to the direct sound is 4 milliseconds, as illustrated in figures 2.12(a),2.12(b), due to the close proximity between the transducers and the sensors at the rear headrests.

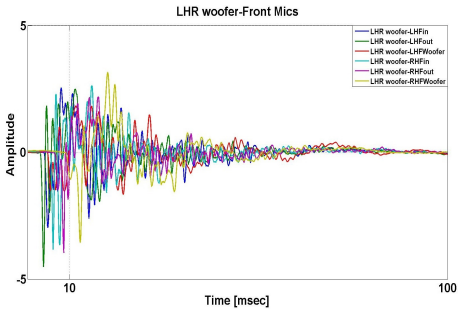

(a) IRFs from LHR woofer to microphones at the front headrests.

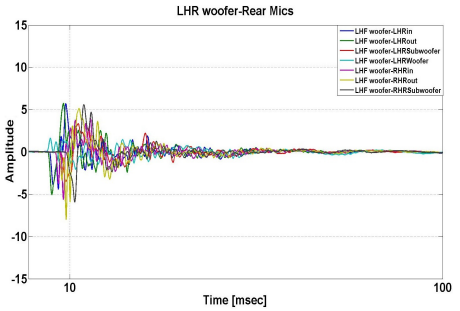

(b) IRFs from LHR woofer to microphones at the rear headrests.

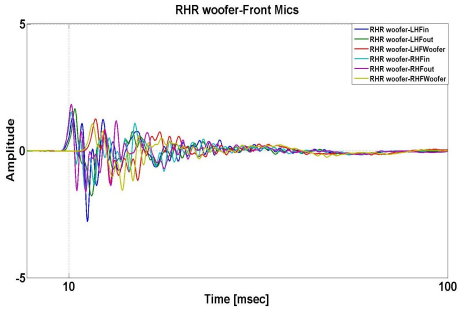

(c) IRFs from the LHR woofer to microphones at the front headrests.

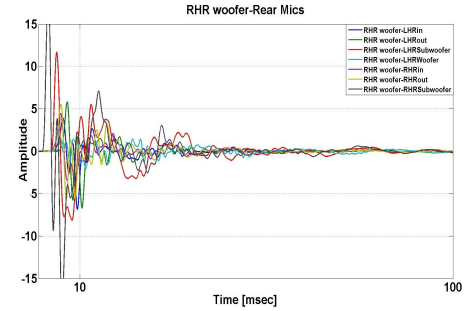

(d) IRFs from the LHR woofer to microphones at the rear headrests.

FIGURE 2.11: Impulse responses between the two rear woofers and the microphones in the cabin.

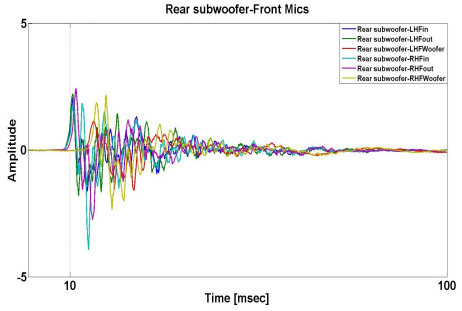

(a) IRFs from the subwoofer to microphones at the front headrests.

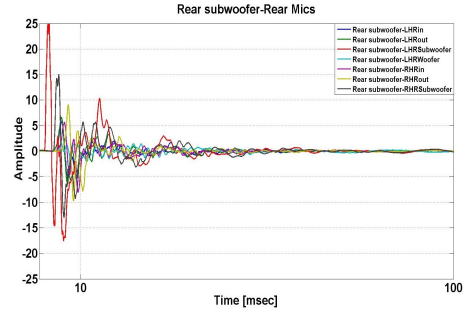

(b) IRFs from the subwoofer to microphones at the rear headrests.

FIGURE 2.12: Impulse response functions (IRFs) between subwoofer at the rear parcel self and the microphones in the cabin.

2.5 Vibro-acoustic frequency response functions

2.5.1 Structural mobility frequency response function

The analysis of mechanical structures in terms of structural dynamics is based on the assumption that harmonic forces are applied on *Linear Time Invariant* (LTI) systems. The vibrational responses of such mechanical systems are linearly

related with the excitation forces that applied across the structure. Coupled systems such as vehicles can be modeled with measurable vibrational quantities, in order to synthesise structural or acoustical responses across the mechanical system. In many cases complex mathematical functions such as mechanical impedance are used to estimate the operational forces at the interface between two structures. For example, the operational forces that are applied by a engine on an isolator that is used to reduce the transmission cannot be measured directly, thus methods for force identification are derived with the use of impedance functions. These methods are widely used in the automotive industry as NVH design and analysis. In particular, the so-called Transfer Path Analysis method uses mechanical impedance functions, as we will explore in a later section. As a first step we need to define some basic mechanical FRFs and their extensions to *Multiple-Input-Multiple-Output* (MIMO) systems. The mechanical impedance can be determined from the applied force on a structure divided by the response at a point on the structure as follows

$$Z(\omega) = \frac{f(\omega)}{v(\omega)} \quad \left[\frac{N}{m/s}\right]. \tag{2.3}$$

In practice, the inverse of the mechanical impedance is measured on the structures, the so-called *mobility function*. This is essentially the vibrational velocity at the response point on the structure referenced to the input force that is applied at the system as shown below

$$Y(\omega) = \frac{v(\omega)}{f(\omega)} \quad \left[\frac{m/s}{N}\right]. \tag{2.4}$$

2.5.2 Structural mobility matrix

For high order mechanical systems, the structures vibrate in different motions and their directions that contribute to the vibrational response of the systems. Each complex motion can be expressed by a number of independent movements that are referred as *DoF* (Degrees of Freedom). In vehicle structures, several vibrational resonances are effecting the structural response of the system and they are included in a matrix of a mobility functions of n-DoFs, which is usually measured with impact hammer testing on the decoupled system. This approach requires to disconnect the axles from the body, in order to identify the structural properties of the mechanical components of the vehicle. The most common measured property on a vehicle is the mobility matrix that contains all the mobility FRFs that are later used for various calculations in advanced NVH

analysis methods. The mobility matrix of such a high order system contains the transfer mobilities and the point (input) mobilities at the excitation points on the vehicle axles. The transfer mobility function of a structure can be defined under the condition that there is only one force applied on the structure at a j-point and the response is measured at another i-location [Fahy and Gardonio (2007)]

$$Y_{ij}(\omega) = \frac{v_i(\omega)}{f_j(\omega)}, f_j(\omega) \neq 0, \forall j = 0, \tag{2.5}$$

the special case of the response location measured at the excitation point, defines the point or direct mobility function

$$Y_{jj}(\omega) = \frac{v_j(\omega)}{f_j(\omega)}, f_j(\omega) \neq 0, \forall j = 0. \tag{2.6}$$

The inverted FRFs of the mobility functions provide the mechanical impedances of the system as follows

$$Z_{ij}(\omega) = \frac{f_i(\omega)}{v_j(\omega)}, v_j(\omega) \neq 0, \forall j = 0. \tag{2.7}$$

As we will explain later, this property of the impedance functions is useful for the TPA method where the input forces that act on a vehicle structure are estimated.

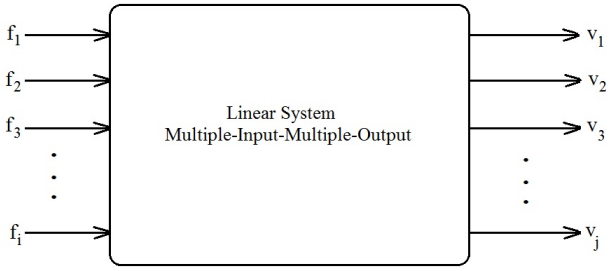

FIGURE 2.13: Multiple Input Multiple Output system (MIMO) that can be described by mobility frequency response function. The forces $f_1, f_2, f_3, ..., f_i$ are the inputs to the system and the velocity responses $v_1, v_2, v_3, ..., v_j$ are the outputs of the MIMO system.

In general, the mobility FRF matrix of the MIMO mechanical system is defined as

$$\mathbf{Y} = \begin{bmatrix} Y_{11}(\omega) & Y_{12}(\omega) & Y_{13}(\omega) & ... & Y_{1j}(\omega) \\ Y_{21}(\omega) & Y_{22}(\omega) & Y_{23}(\omega) & ... & Y_{2j}(\omega) \\ Y_{31}(\omega) & Y_{32}(\omega) & Y_{33}(\omega) & ... & Y_{3j}(\omega) \\ ... & ... & ... & ... & ... \\ Y_{j1}(\omega) & Y_{j2}(\omega) & Y_{j3}(\omega) & ... & Y_{ij}(\omega) \end{bmatrix}. \tag{2.8}$$

The diagonal terms of this matrix contain the direct or point mobility functions that relate to the mechanical impedances at the excitation points of the structure. The cross-diagonal terms contain the structural paths between the excitation at a certain DoF and the response at a location for the same or another DoF. If the inverted mobility matrix is multiplied with the velocities responses measured on a structure, the forces that act on a structure can be identified as follows

$$\mathbf{f} = \mathbf{Y}^{-1}\mathbf{v}. \tag{2.9}$$

Equation 2.9 is in fact the basis of inverse force synthesis, which is used in classic TPA [Plunt (1999)], but also lately in in-situ TPA for the coupled system [Elliott et al. (2013)]. As previously mentioned, the inversion results in the mechanical impedance matrix, which is sometimes hard to obtain with good accuracy due to numerical issues during matrix inversion operations. For the successful inversion of a mobility matrix the eigenvalues of the MIMO system must non-zero and positive defined [Moorhouse and Gibbs (1998)]. As a consequence, matrix reguralisation techniques are suggested to tackle with these issues [Thite and Thompson (2003a),Thite and Thompson (2003b)]. The mobility matrix can be also used to find ratios between the velocities or the forces depending on the interpretation of the matrices. These type of functions are related to the mechanical sensitivities of the system. They can be formulated into matrices that link the velocities or the forces at the two terminals of a MIMO mechanical system. In the case of the sensitivity functions between the vibrational responses at the two terminals of the coupled system, an alternative formulation of the mobilities function is used. If the transfer mobility matrix, $\mathbf{Y}_{bc}$ (c-connections b-receiving structure, body side) is multiplied with the inverted point mobility matrix, $\mathbf{Y}_{cc}^{-1}$ of the mobility at the c-connection inputs points such as mounts or bushing points as follows [Magrans (1981), Ribeiro et al. (2000) Maia et al. (2001)]

$$\mathbf{T}_{bc} = \mathbf{Y}_{bc}\mathbf{Y}_{cc}^{-1}, \tag{2.10}$$

$$\mathbf{T}_{bc} = \mathbf{Y}_{bc}\mathbf{Z}_{cc}. \tag{2.11}$$

The sensitivity function $\mathbf{T}$ is usually referred as *generalised transmissibility function* [Ribeiro et al. (2000)]. These FRFs are used in Advanced TPA method that is a method developed by Magrans in [Sapena et al. (2012) ,Malkoun et al. (2014)], which has been mostly applied mostly in NVH analysis for high speed trains. It is important to mention that the in-situ TPA and the ATPA are applied on the coupled system, whereas in classic TPA the source must be dismounted

from the receiver's structure. As a consequence, less measurement time is required and also information about the blocked forces and the weakest transfer paths can be obtained [Magrans (1981), Zafeiropoulos et al. (2013)]. A simpler version of the transmisibility function, which is commonly used in NVH and especially for the purposes of tuning isolator properties is the so-called *forced transmissibility* [Duncan et al. (2011)]. This function is defined as the ratio between the forces with or without the presence of an isolator

$$T_f = \frac{Y_{body} + Y_{suspension}}{Y_{isolator} + Y_{body} + Y_{suspension}}, \tag{2.12}$$

where Y_{body} is the mobility of the vehicle's body, $Y_{suspension}$ is the suspension's mobility and . The forces applied to the isolators are found with the use of the Hooke's law [Plunt (2005), Moorhouse et al. (2013)] and are calculated as follows

$$\mathbf{f}_{base} = \mathbf{K}(\mathbf{x}_{suspension} - \mathbf{x}_{body}), \tag{2.13}$$

where $\mathbf{K}$ is the dynamic stiffness matrix and the dynamic stiffness is defined as the input force normalised by the displacement response. Dynamic stiffnesses are widely used for structure-borne NVH design. If we now take into account that the stiffness is inversely proportional to the mobility function, then equation 2.12 changes as follows

$$T_f = \frac{K_{body}^{-1} + K_{suspension}^{-1}}{K_{isolator}^{-1} + K_{body}^{-1} + K_{suspension}^{-1}}. \tag{2.14}$$

Equation 2.14 is a useful method, as it is used to achieve a specific tuning between the structural properties of the chain source-isolator-receiver [Duncan et al. (2011)]. An example of dynamic stiffnesses at an important input to the body side of the luxury vehicle that we investigate in this thesis is presented in figure 2.14(a).

These local dynamic stiffnesses were measured on the coupled system and some interesting characteristics regarding the vehicle's structure can be obtained from these FRFs. First of all, the dynamic stiffness are fairly damped, as they are close to the suspension damper as it illustrated in figure 2.14(b). In addition low dynamic stiffness is necessary, in order to block the road related vibrations and avoid any modal coupling between the axles and the body. Ideally, the dynamic stiffness across the vehicle needs to be as high as possible and especially at mount and bushes locations, in order to decouple the mechanical systems and block vibrations that may cause structure-borne road noise [Neto and de Oliveira

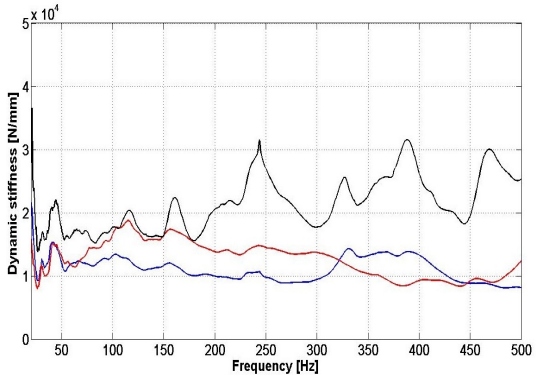

(a) Dynamic stiffnesses between the dome top and the control arms at the top suspension.

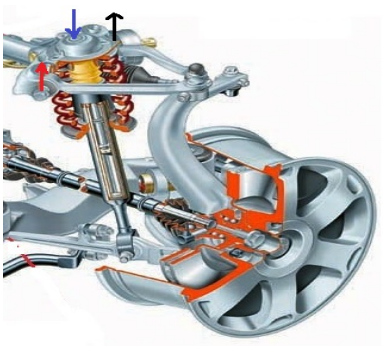

(b) ↑: Excitation and response at the damper top. ↓, ↓: Responses at the control arms

FIGURE 2.14: Local dynamic stiffness measured between the body side at the suspension damper top and the two suspension locations at the z-axis. −: Dynamic stiffness at the excitation point on the body side. −: Dynamic stiffness between the excitation point on the body side and first control arm. −: Dynamic stiffness between the excitation point on the body side and second control arm.

(2010)]. The methods that we have mentioned up until this point, such as TPA are crucial passive NVH techniques that highlight weaknesses in the vehicle structure and quantify the road forces. We will further investigate the vibro-acoustic FRFs that are used for NVH analysis methods in the following section, in order to gain a better understanding of structure-borne road noise transmission.

2.5.3 Vibro-acoustic frequency response functions

When road forces act on a vehicle structure, structure-borne sound is generated due to vibrations that are transmitted through multiple paths inside the cabin. There are points in the structure, which have such structural properties that can allow vibration transmission between the excitation source location and the sound field inside the cavity. The type of FRF that can describe the physical relationship between an excitation force that acts on the vehicle and the structure-borne sound is called noise transfer function (NTF) and it usually reveals the relationship between the sound pressure levels for an impact force applied on the vehicle structure and it is defined follows [Wang (2010), Lyon (1987)]

$$H(\omega) = \frac{p(\omega)}{f(\omega)} \quad \left[\frac{Pa}{N}\right]. \tag{2.15}$$

In reality multiple, excitation forces act on a structure and thus this relationship is also extended for a MIMO system as

$$H_{ij}(\omega) = \frac{p_i(\omega)}{f_j(\omega)}, f_j(\omega) \neq 0, \forall j = 0. \tag{2.16}$$

The FRF matrix of a vibro-acoustic system that includes all the FRFs between the input forces and the sound pressure responses is defined as

$$\mathbf{H} = \begin{bmatrix} H_{11}(\omega) & H_{12}(\omega) & H_{13}(\omega) & ... & H_{1j}(\omega) \\ H_{21}(\omega) & H_{22}(\omega) & H_{23}(\omega) & ... & H_{2j}(\omega) \\ H_{31}(\omega) & H_{32}(\omega) & H_{33}(\omega) & ... & H_{3j}(\omega) \\ ... & ... & ... & ... & ... \\ H_{j1}(\omega) & H_{j2}(\omega) & H_{j3}(\omega) & ... & H_{ij}(\omega) \end{bmatrix}, \tag{2.17}$$

and the total sound pressure at a m-location inside a cavity can now be expressed as the superposition of all the vibro-acoustic FRFs multiplied with the excitation forces

$$p_m(\omega) = \sum_{i=1}^{N} H_{ij}(\omega) f_j(\omega) \tag{2.18}$$

and in a more compact form can be written as the multiplication of the FRF matrix, $\mathbf{H}$ with the vector of the excitation forces, $\mathbf{f}$

$$\mathbf{p} = \mathbf{Hf}. \tag{2.19}$$

Equation 2.19 is also the quality check of TPA methods, where the estimated force spectra are used as inputs into the vibro-acoustic system of the vehicle and the predicted sound pressure spectra are compared to the actual road noise specta obtained usually on chassis dynamometers or on the road.

2.5.4 Vibro-acoustic FRFs for impact forces on the front axle

Many modern vehicle structures are assembled using advanced suspension systems to improve the ride and dynamic behaviour of the car. A typical multilink suspension system with four mounting points between the subframe and the body is shown in figure 2.15. In this case impact forces were applied in the

z-direction, since the other directions were not accessible with the hammer for obtaining reliable measurements.

Two resonances dominate in the NTFs between 100-200 Hz , the first one centered at 125 Hz and the second one at 200 Hz. At these frequencies road related vibrations could potentially be transmitted inside the cabin. It is evident that in figures 2.16(d), 2.16(e) and 2.16(f) that the sensitivity levels at the NTFs are around 60 dB [Pa/N] at 125 Hz, which indicates that these locations may allow road noise transmission. Some authors suggest this value to be also used as a generic target for a NTF [Wang (2010), Duncan et al. (2011)]. Still for a luxury vehicle with high levels of refinement the target is lower at 45-55 dB [Pa/N] across the road noise spectrum. Interestingly, the resonances at 125 Hz and 200 Hz for the subframe mounts and at the top of the suspension in figures 2.16(b), 2.16(c), 2.16(d) are well damped and below 55 dB [Pa/N], especially for the damper top in figure 2.16(d).

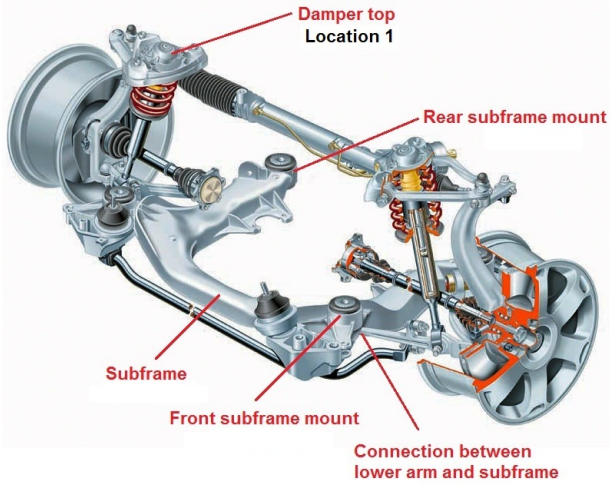

FIGURE 2.15: Front axle with multilink suspension system. The main parts of the structure are highlighted that were also included in the impact FRF testing.

If we take into account the geometry of the locations, there is only one case in which structural vibrations could result in road noise: when the subframe vibrations are well coupled with the vehicle's body. However, there is high isolation from the subframe mounts, since they are tuned to attenuate effectively the applied road forces at the subframe connection points.

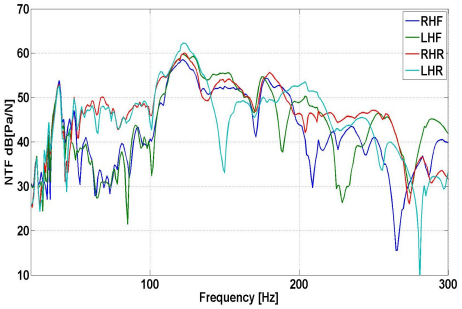

(a) Noise transfer function of an impact force applied at the connection between the lower front arm and the subframe.

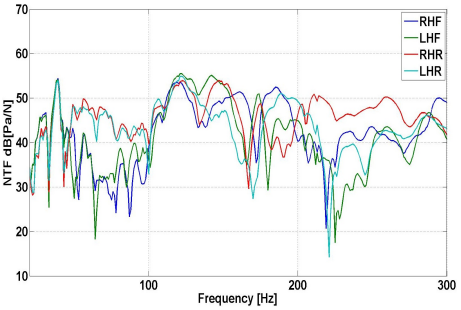

(b) Noise transfer function of an impact force applied at the rear subframe mount.

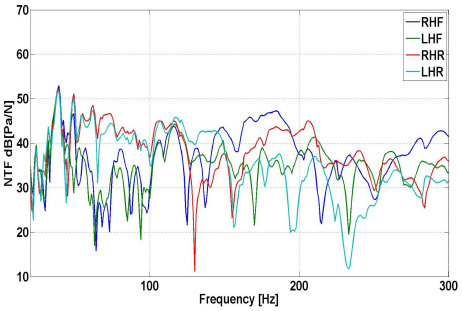

(c) Noise transfer function of an impact force applied at the front subframe mount.

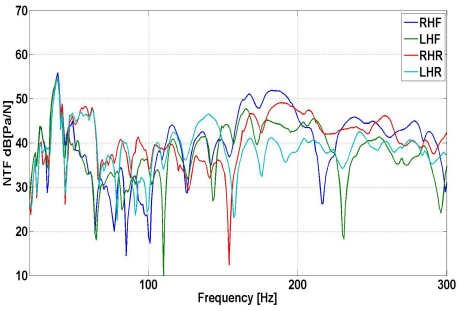

(d) Noise transfer function of an impact force applied at the damper top.

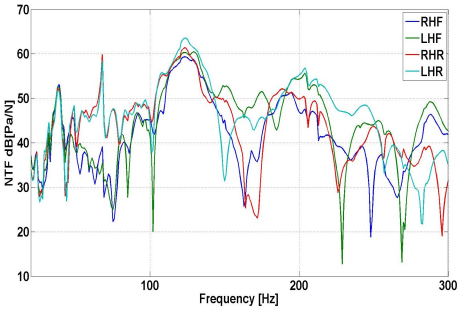

(e) Noise transfer function of an impact force applied at the left hand side of the subframe.

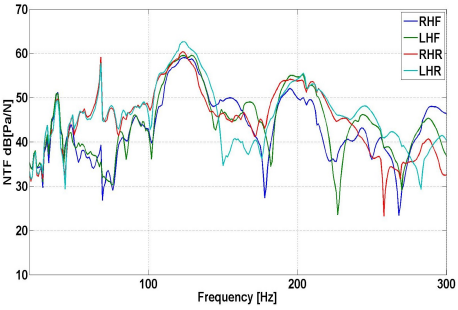

(f) Noise transfer function of an impact force applied at the right hand side of the subframe.

FIGURE 2.16: Vibro-acoustic FRFs between the excitation point on the front axle structure the four headrests microphones.

From the results of this measurement we may conclude that the front axle of the vehicle results in fairly damped structure-borne sound responses in the cabin. In addition to this, it is clearly evident that the main structural paths can reduce the vibrations of the front axle for forces that are directly applied on the axle's structure.

2.6 Methods for structure-borne road noise analysis

2.6.1 Transfer Path Analysis

In this section we present the formulation of the TPA method, in order to reveal the relevant points to ARNC technology. We will start first by introducing the parameters that are necessary for TPA and also highlight the similarities with feedforward ARNC. Modern vehicle structures are mechanical systems composed of various substructures. The structural dynamics of each substructure are tuned separately, in order to meet the NVH targets. In the case of road noise there is a limit to this fine tuning. In particular, at low frequency any mass increase of the vehicle structure for reduction road related vibrations can several implications on other vehicle attributes, as we mentioned in chapter 1. The mechanical subsystems of the vehicle couple with each other through some connection points. The applied forces excite dominant structural resonances that may couple well with the acoustic modes of the cabin. The general model of structure-borne road noise generation is based on the SPC (Source-Path-Receiver) theory. Modern NVH modelling techniques combine this method with the modal behaviour of the vehicle, in order to analyse road noise in terms of structural contributions [Wyckaert and Van der Auweraer (1995)].

Road noise depends strongly on the tyre-road interaction. The forces at the suspensions and subframes are important for the vehicle NVH design, as they vary according to the road surface type and speed. The forces that are applied directly to the vehicle body are also of a high significance, since they determine the tuning parameters of several parts of the suspension and subframe systems. Therefore, the road forces at the connection points between the suspension and the body structure are usually estimated with the use of TPA (Transfer Path Analysis). These are also the main inputs into the body structure that cause structure-borne sound inside the cabin. In figure 2.17 a block diagram of the transmission paths and also how TPA models the vibro-acoustic behavior of the vehicle is presented.

The NTF matrix of each axle from an a-source location at the wheel to a b-receiving point in the sound field of the cabin $\mathbf{H}_{ba}$ contribute to the sound pressure responses, $\mathbf{p}_a$. Alternatively, the vehicle system can be decomposed with a matrix $\mathbf{Y}_{ac}$ from the source to a b-connection point at the axles and to the vibro-acoustic paths $\mathbf{H}_{bc}$ from the connections to the cabin.

In the frequency domain the vector of the sound pressure is defined as the product of the forces at the tyre contact patch multiplied with the matrix of the

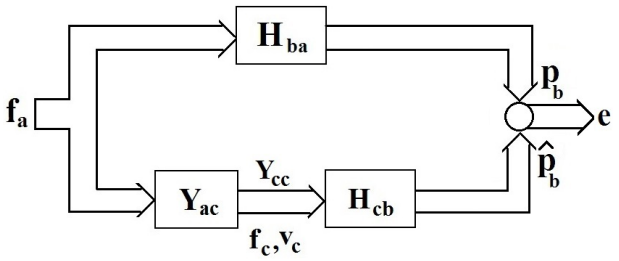

FIGURE 2.17: Source path receiver model (a): sources at the axle (b): receiver responses, (c): connections between the axle and the body structure. The forces at various points on the axle are denoted as $\mathbf{f}_a$ and the forces at various connection points are presented as $\mathbf{f}_c$. The vibration paths between the tyre and the connections are showed as transfer mobilities $\mathbf{Y}_{ac}$ and the point mobilities at the connections are noted as $\mathbf{Y}_{cc}$. The vibro-acoustics paths between the connections and the interior sound pressure $\mathbf{H}_{cb}$ and the primary paths of structure-borne noise are noted as $\mathbf{H}_{ba}$. The error between the estimated sound pressures, $\hat{\mathbf{p}_b}$ and the measured road noise responses $\mathbf{p}_b$ is denoted as $\mathbf{e}$.

primary transfer paths $\mathbf{H}_{ba}$

$$\mathbf{p}_b = \mathbf{H}_{ba}\mathbf{f}_a. \tag{2.20}$$

In practice, the forces at the connection points $\mathbf{f}_c$ are estimated and used as sources. These force spectra can be used for various body structure as long as the structural design of the suspension and the body have not changed dramatically. Usually, TPA methods are used to predict the forces and also to rank the most sensitive vibro-acoustic paths of road noise. The most common method of calculating the road forces is based on the matrix inversion of the mobility matrix $\mathbf{Y}_{cc}$ measured at the (c)-connection points. The point mobilities at the connection and are defined as the ratio between the velocity response at m-DoF and the driving force at the k-reference DoF as

$$Y_{c_m c_k} = \frac{v_{c_m}}{f_{c_k}}, \tag{2.21}$$

for the special case that $m = k$, the FRF is the point mobility at the connection. Now the point mobility FRF matrix at the interface can be defined as

$$\mathbf{Y}_{cc} = \begin{bmatrix} Y_{c_1c_1} & Y_{c_1c_2} & Y_{c_1c_3}\ldots & Y_{c_1c_k} \\ Y_{c_2c_1} & Y_{c_2c_2} & Y_{c_2c_3}\ldots. & Y_{c_2c_k} \\ \ldots & \ldots & \ldots & \ldots \\ Y_{c_kc_1} & Y_{c_kc_2} & Y_{c_kc_3}\ldots & Y_{c_mc_k} \end{bmatrix}. \tag{2.22}$$

The vibro-acoustic transfer function between the excitation point-k at (c) and the sound pressure response at a l-microphone location in the cabin is

$$H_{b_l c_k} = \frac{p_{b_l}}{f_{c_k}}. \tag{2.23}$$

Now the matrix $\mathbf{Y}_{cc}$ is measured either for the uncoupled system source-receiver in the case of classic TPA or for the coupled structure if in-situ TPA methods are used for the analysis. As previously mentioned in section 2.5.2 the forces at the connections, $\hat{\mathbf{f}}_c$ between the two structures are estimated with the use of matrix inversion methods, which in the case of TPA the point mobility matrix must be inverted $\mathbf{Y}_{cc}$. This is also the backward step of the TPA method the vibrational responses at the receiving structure are fed as inputs to the inverted FRF matrix in order to obtain a prediction of the road forces as shown below

$$\hat{\mathbf{f}}_c = \mathbf{Y}_{cc}^{-1}\mathbf{v}_c. \tag{2.24}$$

The second forward step of the TPA methods is to synthesise the sound pressure responses inside the vehicle's cabin and compare the estimated spectra with actual measurements for evaluating the quality of the predicted road forces.

$$\hat{\mathbf{p}}_b = \mathbf{H}_{bc}\hat{\mathbf{f}}_c, \tag{2.25}$$

where the estimated road noise is noted as $\hat{\mathbf{p}}_b$. The error of the TPA method is defined as the difference between the predicted noise spectra that indicates how reliable are the estimated road forces

$$\mathbf{e} = \mathbf{p}_b - \hat{\mathbf{p}}_b. \tag{2.26}$$

Now if we modify the diagram of figure 2.17 and include a feedforward controller we obtain the follow augmented system of figure 2.18. The reference inputs, $\mathbf{x}$ to the control filters, $\mathbf{W}$ are suggested to be placed very close to the wheel [Couche (1999)] or at axle locations with high vibrational responses [Bernhard (1995), Sutton et al. (1994)] or either to perform a simulating annealing algorithm for finding the optimum set of reference signals [Stothers et al. (1995)].

However, there are advantages of using the principals of TPA for ARNC design as it may be possible to obtain a better understanding regarding the

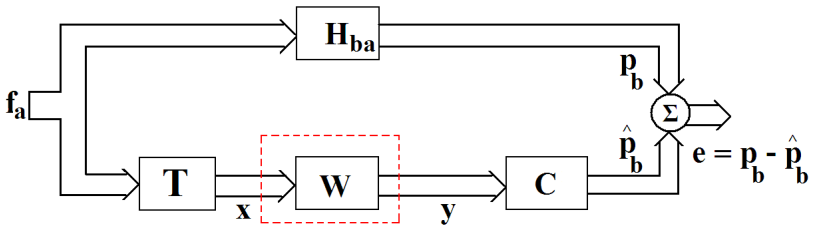

FIGURE 2.18: System diagram for Transfer Path Analysis and ARNC. $\mathbf{f}_a$: road forces, $\mathbf{H}_{ba}$: vibro-acoustic paths, $\mathbf{T}$: Structural transfer paths from the source to the reference sensor locations, $\mathbf{W}$: control filter matrix, $\mathbf{C}$: electro-acoustic paths from the loudspeakers to the microphones at the headrests, $\mathbf{x}$: vibrational responses as reference inputs to the controller, $\mathbf{y}$: control signals that drive the loudspeakers in the cabin, $\mathbf{p}_b$, $\hat{\mathbf{p}}_b$: are the measured and synthesised road noise spectra and $\mathbf{e}$: the residual error signals at the cancellation point in the cabin.

number of DoFs and the reference sensor locations that act on the vehicle and are related to structure-borne road noise before applying the technology. So far, most of the proposed techniques for reference sensor selection result in several locations and DoF, which indicates that they are not taking into account the structural design of the vehicle. Apart from the high number of reference vibrational signals the locations of the sensors should also correlate with the structure-borne noise sources at the axles. In the past it has been suggested that the number of dominant structure-borne noise sources should be equal to the references sensors used for the feedforward system [Sutton et al. (1994)]. On the other hand Park [Park et al. (2002)] proposed that a higher number of reference signals is required for ARNC for ensuring robust broadband performance as several DoF contribute at each road noise resonance. This is true for vehicles with very poor structure-borne NVH performance, but for luxury vehicles with several passive treatments a more systematic approach is required for using a number of reference signals that is related to the actual structure-borne noise contributions that are revealed from NVH analysis of road noise. Consequently, knowledge obtained from TPA method or from other NVH analysis methods regarding the locations may lead to a more solid approach for the selection of the reference inputs to the controller. In our case, we will make some assumptions that are used in TPA, such as the hypothesis that the connection points at the axles are the first candidates for road noise transmission and also important inputs to the vehicle and as an extension to the controller. We will further focus on the vehicle road noise analysis in chapter 4, where the statistical relation between the connection points at several axle locations and the interior noise for each of these paths is presented. Another problem that the controller has to face is the fact that the sources across the vehicle are partially correlated and that has an effect on the references. In figure 2.18 the reference signals $\mathbf{x}$ are mixed due to the spatial filtering through the matrix $\mathbf{T}$, which effects the performance of adaptive systems as demostrated by Elliott in [Elliott and Cook (2000)]. Before we present the structure-borne road

noise performance of the luxury vehicle that we investigate in section 2.7, we will first introduce the multiple coherence problem on vehicle structures in the following section.

2.6.2 Incoherent structural road sources

In most commercial structures several structural sources are interacting with each other, due to strong mechanical coupling that allows low frequency vibration transmission. Modern vehicles structures with advanced suspension systems are connected to complex subframe structures that cause a multi-source structural environment with multiple paths that allow the vibration transmission. The mechanical interaction between these structural parts randomises the phase of the vibration responses across the axles at low frequencies. Therefore, for operational modal analysis of structure-borne noise, decomposition methods based on PCA are applied to the acceleration matrix [Otte et al. (1988), Meillier and Mairesse (1996)], in order to analyse virtually independent phenomena instead of the actual operational vibrations that are partially correlated. The problem of the incoherent sources has been thoroughly analysed by Kompella in [Kompella et al. (1994)] and his method is very useful for understanding how many independent structural sources act on the structure and also for the force synthesis of TPA [Bernhard (2000)], where it is necessary to reference the vibrational responses at the connections to the the principal components before estimating the road forces [Elliott et al. (2013)].

Figure 2.6.2 demonstrates the mixing of the vibrational responses due to structural cross-coupling in the system. The road forces are causing various complex motions of the two axle with several DoF contributing at each resonant frequency of the system. In addition multiple structural paths that are strongly coupled allow the vibrations to be diffused across the structure, thus the recorded signals by the reference sensors are the summation of the contributions of each source. In chapter four we will apply PCA in operational data, in order to calculate the virtual multiple coherences according to [Price and Bernhard (1986), Otte et al. (1988)].

The matrix, $\mathbf{S}_{xx}$ contains the auto and cross-spectra between the k-reference signals measured by the sensors, thus the statistical relations between the sources are expressed as [Kompella et al. (1994)]

$$\mathbf{S}_{xx} = \mathbf{g}^H \mathbf{S}_{uu} \mathbf{g}, \tag{2.27}$$

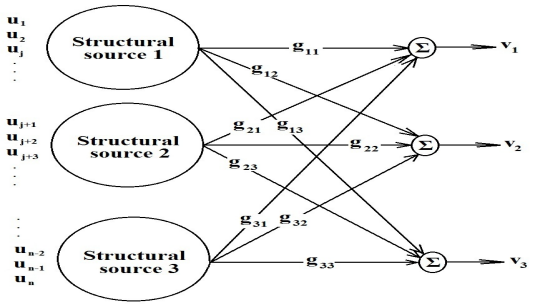

FIGURE 2.19: Interaction between various vibrational sources through structural transmission paths in a multisource environment. The vibrational responses at each source are noted u_i and the measured responses by the sensors as v_j. The stuctural paths between the i-inputs at the sources and the j-output responses at the reference locations are noted as g_{ij}.

where $\mathbf{S}_{xx}$ is a square non-diagonal matrix of size $k \times k$ and $\mathbf{g}$ is the FRF matrix between the structural responses at the n-structural sources to the k-reference points and $\mathbf{S}_{uu}$ is a diagonal matrix that contains the decorrelated autospectra of the reference. If the off-diagonal terms of $\mathbf{S}_{xx}$ are zero, then the forces at the input locations are uncorrelated and sources act independently. As previously mentioned in a vehicle structure the forces at the connections between suspension, subframe and body are interacting at various directions, but in a complex way such as several DoF are contributing to the vibrational response. As a result, the acceleration responses are partially correlated and their relations are included in the off-diagonal terms of $\mathbf{S}_{xx}$. As a result, the FRFs under operative conditions cannot be directly determined with conventional signal processing methods. Moreover, impact testing methods cannot be used in this case as the source location is not known and some locations are inaccessible for the hammer testing. An example of vehicle vibration measurement is presented in figure 2.20, where a tri-axial accelerometer was mounted on the wheel side for road noise measurements.

The data obtained from road noise measurements are usually analysed with PCA that we will introduce in chapter 4. If the primary vibro-acoustic paths were known and could be also measured reliably, then ANC design methods for feedforward control based on the primary paths [Nelson and Elliott (1991)] could potentially be used that are also applicable to feedforward control for ANC headphones technologies [AMS (2015)]. Unfortunately, the road noise responses vary significantly and thus adaptive methods are used, since they can compensate for changes in the acoustic environment of the cabin. In the following section we will introduce the variability of the road noise specta under various driving conditions.

FIGURE 2.20: Physical installation of the accelerometers on the front axle. ○: An accelerometer mounted on the wheel side.

2.7 Structureborne road noise responses

Structure-borne road noise is mostly dominant when cruising with medium to high speed (50 km/h-100 km/h) over coarse chip surface. In this section we present the road noise responses measured at the headret locations for four representative speeds, in order to find out the main structure-borne road noise resonances that are audible inside the compartment. In this particular luxury vehicle two main frequency bands of road noise can be identified between 90-120 Hz and 190-220 Hz for three incremental speeds, 50 km/h, 60, 80 km/h and 100 km/h. The tyre pressure was set to 2.2 bar that is recommended by the manufacturer. The main road noise resonances can be observed in the measured autospectra in figures 2.21(a)-2.21(d).

It can be observed that the noise levels increase as a function of the speed of the vehicle, due to the higher levels of vibrations at mechanical inputs of the axles as it illustrated in figure 2.21(e), in specific for one of the suspension control arms. This trend verifies the strong dependence on the tyre-road interaction and determines the magnitude and the frequency content of the forces that act the vehicle structure. The first low frequency band is the road rumble around 90-120 Hz that is 5 dB(A) louder at the rear headrests than in the front for all of the driving conditions. The rumble peaks at 60 dB(A) for 100 km/h at the rear headrests as shown in figures 2.21(c), 2.21(d). This could be explained by the fact that the rear headrests are close to the vibrating area of the vehicle that causes the road rumble. As for the second road noise band it is effective in the frequency range of 190-220 Hz and it is the typical tyre cavity resonances that travel from the tyre through the suspension links up to the rest of the vehicle structure. At medium speeds such as 50 km/h, two tyre cavity resonances are noticeable and at high speeds such as 100 km/h only one tyre resonance is created during the rotation of the wheel [Wang (2010)].

Figures 2.22(a)-2.22(d) present the spectrograms of the microphone signals

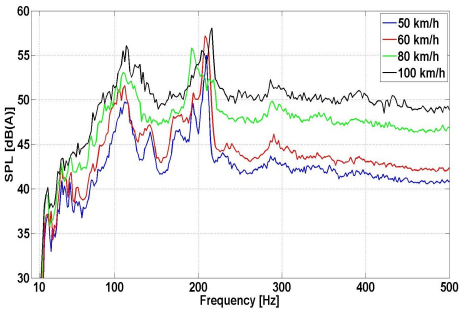

(a) Left hand front microphone responses.

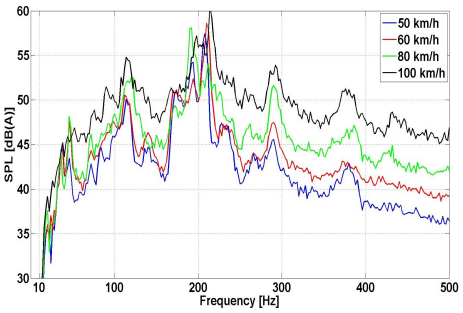

(b) Right hand front microphone responses.

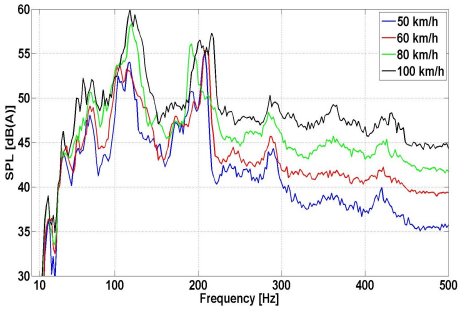

(c) Left hand rear microphone responses.

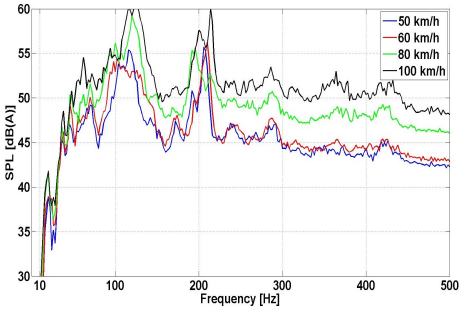

(d) Right hand rear microphone responses.

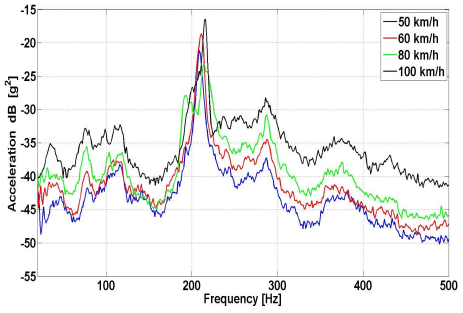

(e) Acceleration response measured at the lower arm at the left hand front suspension.

FIGURE 2.21: Structure-borne road noise response at the interior in a Bentley Flying Spur measured at the four headrests positions and an acceleration response at one of the suspension arms at the front axle. The measurement was conducted at a rough surface for providing high excitation inputs at the tyres. –: 50 km/h, –: 60 km/h –: 80 km/h, –: 100 km/h.

are presented, where the two main structure-borne road noise bands are noticeable. It should be noted that the amplitude of the noise in these two bands of road noise changes due to the randomness of the road surface. This is very important observation as even with a constant speed the noise levels are maintained at the same sound pressure levels as the road excitation are roughly consistent.

Structure-borne road noise resonances are usually predicted through modern CAE software packages with advanced FEA solvers. In addition to this, the resonant frequencies of tyre cavity noise can be predicted from an acoustic tube model with both sides open that couple with the rest of the vehicle structure. The

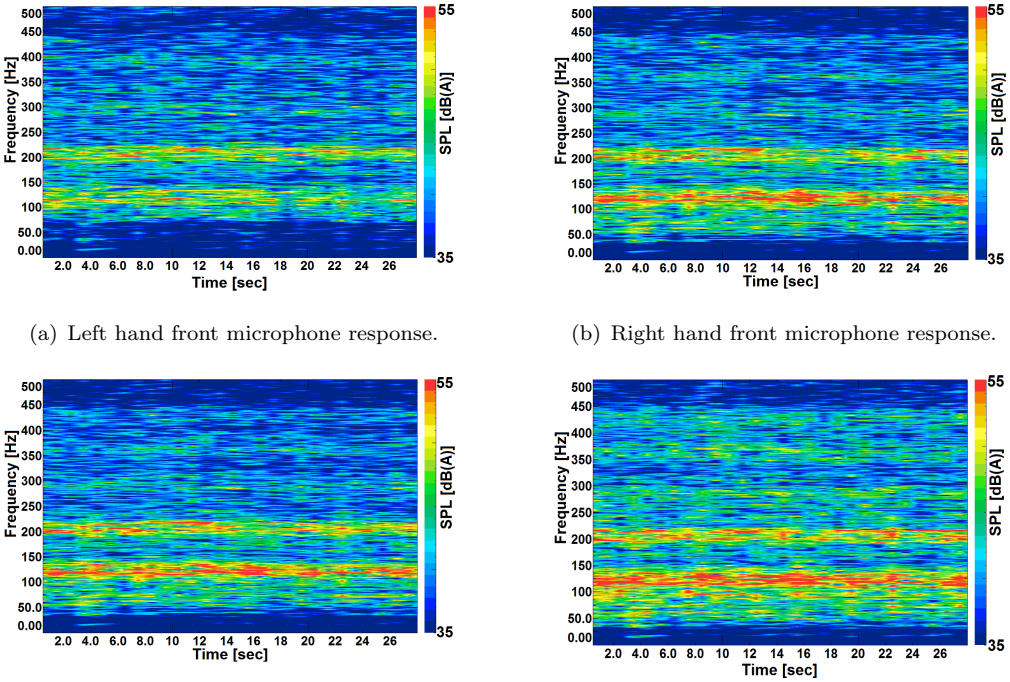

(a) Left hand front microphone response.

(b) Right hand front microphone response.

(c) Left hand rear microphone response.

(d) Right hand rear microphone response.

FIGURE 2.22: Spectrograms of the four microphone responses at 50 km/h for a 20 dB(A) amplitude spam.

acoustic tube model for tyre cavity noise was first introduced by Thompson in [Thompson (1995)]. The main assumption of this model is that at low frequencies plane waves propagate inside the tyre cavity, as the wavelength of the acoustic waves is larger than the dimensions of the cross-sectional area of the tyre. This is the case when rolling tyre is loaded by road forces and it is deformed. As a result, the cross-sectional area of the cavity is compressed, which may cause a volumetric air change inside the tyre cavity. The acoustic compliance changes and two standing wave are also created, one on the horizontal and one on the vertical direction of the tyre. These two acoustic waves couple with the rest of the suspension structure and propagate throughout the vehicle structure into the interior and cause a disturbing tonal component. The tyre mode is presented in 2.23(b), where also an acoustic model of the tyre is also illustrated.

Unfortunately, modifications on the structure cannot complete remove the noise levels of tyre cavity resonances, but only attenuate some part of the propagating wave as illustrated in 2.24(a)-2.24(b). As an example, a passive noise control technique is applied only at one of main paths at the front axle. The mass of the front axle was increased, in order to control the transmission of tyre cavity vibrations. In terms of noise reduction, 2 dB(A) at 188 Hz and 3 dB(A) at 211 were removed from the road noise spectra at the driver's headrest, whereas no reduction was obtained at the rear headrest. This happens because the fact

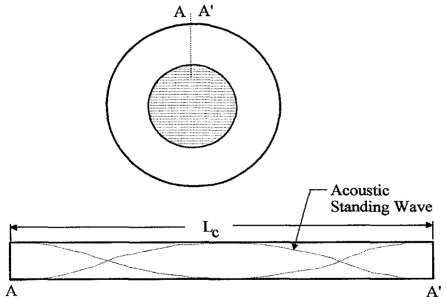

(a) Unloaded tyre cavity acoustic tube model.

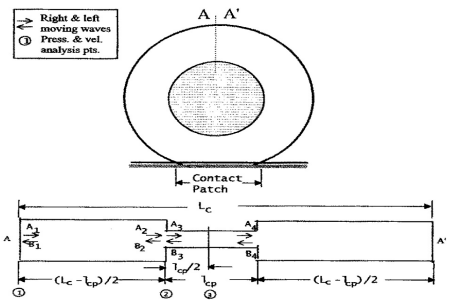

(b) Loaded tyre cavity acoustic tube model.

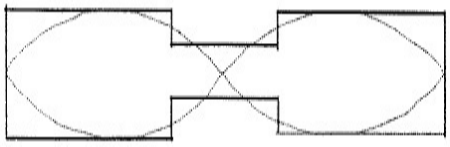

(c) Acoustic mode of the loaded tyre.

(d) Acoustic mode of the loaded tyre.

FIGURE 2.23: Tyre cavity acoustic tube models and the two first modes of the cavity. Taken by Thompson [Thompson (1995)].

that the rear axle was not modified or tuned to reduced vibrations at the tyre cavity range.

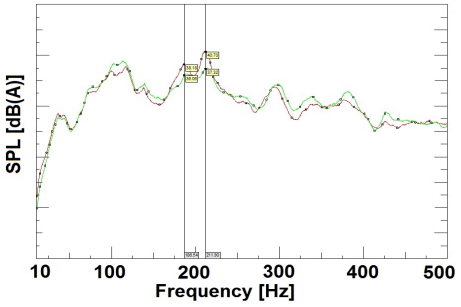

(a) Left hand front microphone response.

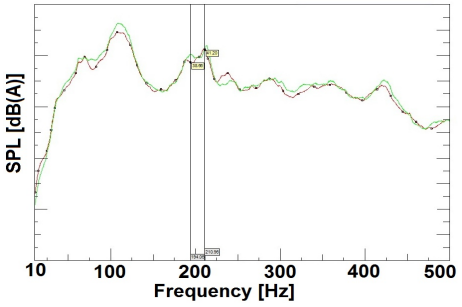

(b) Left hand rear microphone response.

FIGURE 2.24: Tyre cavity control, with a modified structural path at the front axle. —: Before passive treatment. —: After passive treatment.

Tyre noise cavity is the only road noise resonance, which is known and usually sensitive structural parts of the suspension system couple well with the tyre resonances and allow their transmission. Several modifications on the suspensions and the axles might be necessary for blocking all the paths that allow tyre cavity vibrations to propagate into the axles after finding the most significant transfer paths from TPA as demonstrated in [Neto and de Oliveira (2010)]. Another characteristic of tyre cavity noise are the two acoustic resonances of the tyre vary as a function of speed. Figure 2.25 demonstrates the variability of the two resonant frequencies of the tyre over a coast down from a high to a medium speed, because of the Doppler effect.

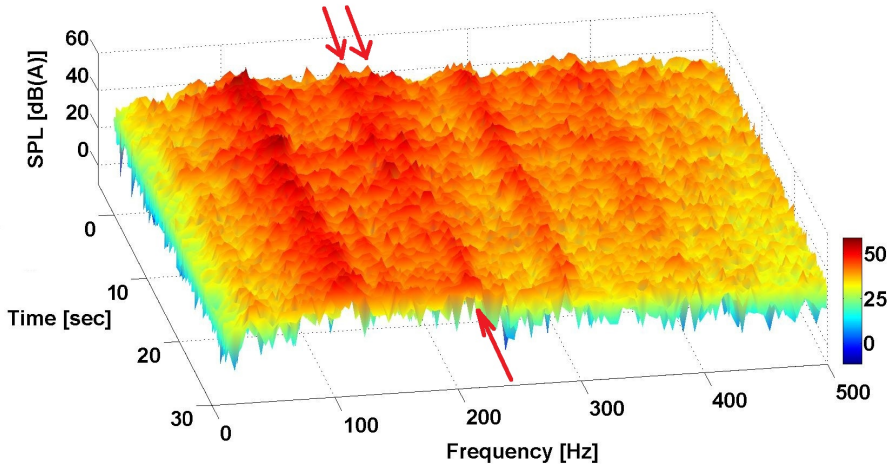

FIGURE 2.25: Tyre cavity resonant frequency drift over time and coast down speed sweep from 100 km/h to 50 km/h at the driver's headrest.

At high speeds the two tyre cavity resonances are evident from the beginning of the recording. A time increases and the vehicle reaches 50 km/h, only the high frequency tyre cavity resonance appears to dominate, whereas the distance of the two resonance has reduced significantly. A significant level drop is evident in the midfrequency road resonance at 290 Hz, whereas the rumble has not reduced by no more than 5 dB(A), which is also the case also for the constant speed measurements of same response (figure 2.21(d)). These are significant observations for an adaptive algorithm, since a multichannel controller with a high number of taps will not be able to adapt in such a short period of time ,as several minutes are required for the adaptation stage on the road [Stothers et al. (1995)]. Still under constant driving conditions this could be an issue and once the adaptive system is trained, the "frozen" coefficients of the filter will be able to generate the appropriate control signals to compensate for the rapid changes in the road responses.

2.8 Summary

In this chapter we performed several NVH measurements in a luxury vehicle, in order to analyse the physical FRFs, which are crucial in structure-borne road noise generation. We began with an analysis of vibro-acoustic FRFs in the road noise range and found that the NTFs of the subframe are around 60 dB [Pa/N] in the rumble range and 50 dB [Pa/N] in the tyre cavity. This indicates that the front axle subframe is the most sensitive part out of the five mechanical parts that were tested with the impact hammer technique. We also investigated the sound field of the cabin at low frequencies, in order to have an impression on

how the loudspeaker system of the vehicle affects the sound field inside the car. This is instrumental for the of of ANC system, as the physical distance between the loudspeakers and the location of the microphones may a strong influence on the adaptive algorithm, as we will explain later in chapter 6.

Chapter 3

Physical simulator of road noise

Structure-borne road noise is usually physically simulated with the use of controllable excitation sources such as chassis dynamometers or shaker transducers. The main benefit of using chassis dynamometers is that road noise can be tested at various speed ranges and sweeps. However, two drawbacks in this approach: the first one had to with background noise from the drum motors, whereas the second one deals with the pseudo-random excitation that is created by the periodicity of the rolling surfaces. Road noise is a signal of random nature, thus the use of shaker transducers, which are fed with random signals. In this way, the latency of the control system can be revealed as the performance of the ARNC system is sensitive to delays. Road noise simulators based on shaker transducers may also reveal the effects of delays in the control path [Dehandschutter et al. (1995), Sas and Dehandschutter (1999)], hence the experimental configuration of this chapter might be an alternative test bench for ARNC development, before testing on the road. In chapter, we focus on the development of a physical road noise simulator with shaker transducers as the primary source of the vehicle excitation. The outcome of this NVH technique development, will provide us with useful insight that will help us study the sound field inside the cabin when it is dominated purely by structure-borne sound without the presence of other NVH components and external noise sources during the measurements. Additionally, we will be able to analyse this NVH attribute without other contributions that are usually present under driving conditions and influence the repeatability of the

experiments. Previous studies have used road noise simulators to develop and demonstrate ARNC systems for various control strategies [Ferren and Bernhard (1991), Adachi and Sano (1998), Sas and Dehandschutter (1999)]. However, in most of these experimental studies a single shaker was attached to one of the tyres or directly mounted on a stiff location of the vehicle's structure with some parts of the vehicle dismounted. These changes in the vehicle were necessary, in order to access rigid locations on the vehicle's structure, which allow good coupling between the shaker source and the body structure. It is unknown to the us whether the experimental data were valid enough to allow the correlation between the simulated responses with actual measured noise under driving conditions. In addition to this limiting factor of the previous simulators, the low number of excitation inputs does not create a multi-source structural environment across the vehicle. In such a structural environment several sources interact with each other and the vibrational responses are partially correlated with the interior road noise resonances. In our study we hope to improve these conditions and develop a more realistic simulation of the structural behaviour of the vehicle for random inputs by including four excitation locations, one for each tyre. This addition in the hardware configuration of the simulator allows to replicate the road noise responses of the specific vehicle, so that feedforward ARNC systems experimentally at the main road noise resonances.

Recent advances in shaker transducers technologies enable the management of the force inputs to each tyre individually and replicate the acceleration responses on the axles that are acquired from road testing [Bräunig et al. (2013)]. However, this type of experimental setup requires extra sophisticated equipment and large shaker transducers that apply high output forces at very low frequencies. As an alternative in our experimental setup we focused to simulate the spectra of road noise responses that we acquired under driving conditions by exciting directly on the vehicle's tyres with random forces from 0-1 kHz, in order to create an uncorrelated vibrational field.

3.1 Chapter outline

This chapter is divided into a number of sections that aim to describe in detail our experimental setup and results. As a starting point we excite a front tyre with a band-limited force signal, while the microphone responses at the headrests are measured for a quarter vehicle analysis in section 3.2.1. An improved method of exciting the tyre and replicating the road noise responses is then developed and presented in section 3.2.2. In the final step of this development, the simulated responses are compared with road noise measurements (subsection 3.2.4), in

order to evaluate and compare the quality of the measured data of that were produced by the physical road noise simulator.

3.2 Technique development of physical simulation of structure-borne road noise

As previously mentioned, chassis dynamometers with special surfaces mounted on the roller are used for the simulation of road noise under rolling conditions. In this case, the surfaces of the rollers do not provide perfectly random inputs into the vehicle's structure, due to the periodicity of the rolling surfaces. Generally, two wheel rollers are available in the majority of automotive testing facilities and thus the structure-borne road noise contributions of the front and rear axle are measured separately. This may prove to be an issue for an all-wheel vehicle like the one we use in our study. In particular, mechanical parts of the powertain transmission must be removed such as the drive shaft to allow road noise testing. Still a simulator based on shakers can excite the whole vehicle under the condition that at least four shakers are used to provide the input forces at the four tyres. Four shaker transducers that are suitable for low frequency NVH testing are used in this development to ensure that high input forces can be applied to the tyres. In this way, audible structure-borne noise levels are obtained inside the compartment.

3.2.1 Quarter vehicle excitation

The first stage of this experiment involved a number of steps. First, the shakers were attached on the tyres almost diagonally, due to space limitations and placed the vehicle on top of some wooden blocks, as illustrated in figure 3.1(a). Force sensors for measuring the applied forces on the tyre were placed between the tyres and the shakers. The sensors were mounted between the beams that were bolted on the shakers and the metallic washers, which in turn were glued upon the tyre and was used as a contact area. This modification was found necessary, as tyre compliance compensates for forces coming from the transducer. Other parts of the wheels, such as the alloys, were difficult to excite and in turn produce consistent measurement results. Recently, sophisticated shaker technologies have been specially developed for simulating the acceleration responses at the suspension with the use of modern DSP controller that can compensate for the tyre compliance [Bräunig et al. (2013)]. The graphs in in figures 3.2(a)-3.2(d) illustrate

(a) Measurement setup outside the vehicle.

(b) Microphones at the headrests.

FIGURE 3.1: Static test bench for physical simulation of structure-borne road noise.

the noise responses of the quarter vehicle measurement (between 0-300 Hz), in relation to the band-limited input force signal. We observe several resonances, yet only the tyre cavity resonance centered at 200 Hz dominates the sound field of the cabin. Another interesting observation is that at the tyre cavity range, the microphones placed at the outbound facing side of the vehicle, measured slightly higher noise levels than the inbound ones. The road rumble appears at much lower sound pressure levels than the tyre cavity. This can be possibly due to the fact that the front axle vibrations are not the primary contributors of the road rumble and this highlights the fact that the rear axle needs to be included in the

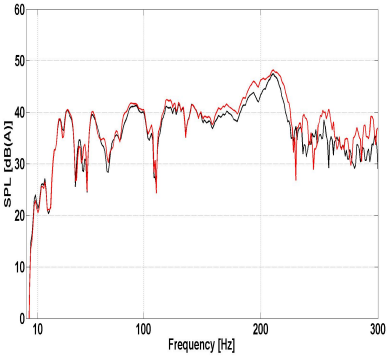

(a) Noise spectra at the left hand front headrest.

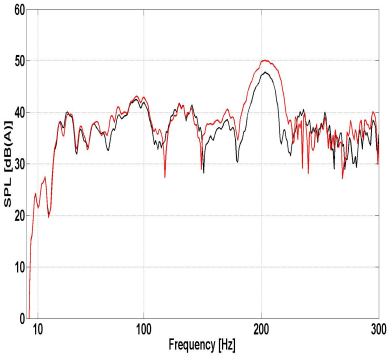

(b) Noise spectra at the right hand front headrest responses.

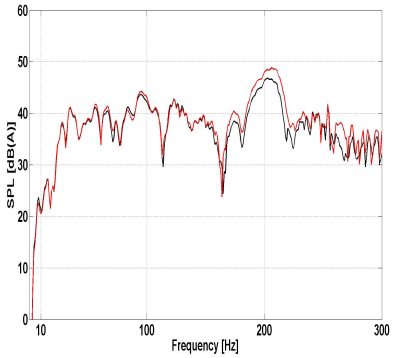

(c) Noise spectra at the left hand rear headrest responses.

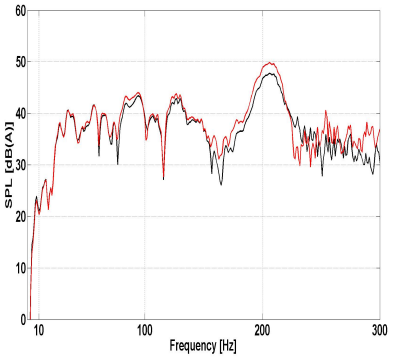

(d) Noise spectra at the right hand rear headrest responses.

FIGURE 3.2: Microphone responses at the four headrests for an input force from 0 to 250 Hz applied to the left hand front wheel. −: Microphone responses at the inbound facing side of the vehicle. −: Microphone responses at the outbound facing side of the vehicle.

3.2.2 Whole vehicle excitation

The simulated noise responses at the headrests with four input forces applied to each wheel are presented in 3.3(a)-3.3(b) and 3.4(a)-3.4(b). Two changes in the excitation technique were performed hoping to improve the simulated structure-borne noise responses . The first change deals with the input signal that drives the shaker transducers. The frequency range was set from 0-250 Hz to 0-1 kHz, in order to introduce broadband random forces into the structural system of the vehicle. A small metal cube was mounted between the metallic washer on the tyre side and the force gauge to improve the coupling between the shakers and the tyres. As a result, less losses between the shaker and the tyre were witnessed than in the previous setup. Interestingly, all the road noise resonances are now present in the simulated road noise spectra (figures 3.3(a)-3.4(b)).

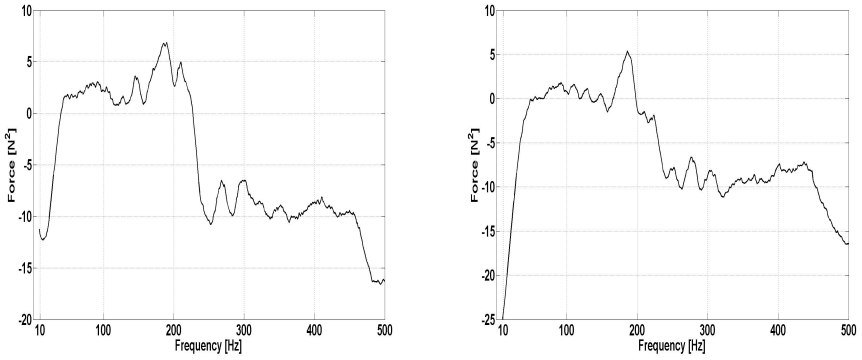

(a) Input force autospectra at the front tyres.

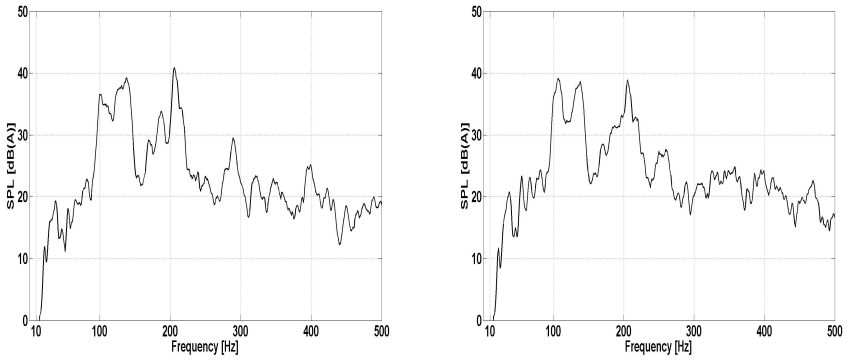

(b) Noise responses at the front headrests.

FIGURE 3.3: Forces applied at the diagonal of the front tyres and the corresponding sound pressure responses at the headrests of the front seats.

With regards to the input forces at the front tyres a resonance at around 180 Hz appears to dominate the force spectra (figures 3.3(a)-3.3(b)), whereas the tyre resonance of the noise spectra at the front headrests is centered slightly higher at 200 Hz. The force energy is concentrated between 20-200 Hz, while when it is above 200 Hz the forces decay sharply, due to the tyre dynamics that compensate for forces at higher frequencies. Two higher order resonances are also present in the force spectra at 290 Hz and 300 Hz, with the first one appearing also at the noise responses at the front headrests. Figures 3.4(a)-3.4(b) illustrate the input forces at the rear tyres and the noise responses at the rear headrests. In this case it is obvious that the force levels are slightly lower than in the front headrests.

In the cases, front and rear tyres above the tyre cavity resonance (220Hz) the input forces are significantly reduced. In general, the input forces seem to be high at the range of 20-200 Hz with some higher order tyre resonances present as we already discussed in the case of the front forces. Several reasons may cause this:

(a) the tyre stiffness that can effectively block input forces above 200 Hz

(b) the need for higher input force levels that are closer to the magnitude of road forces that are obtained on rough roads.

The main improvement of the developed experimental technique is that the simulated road noise spectra contain all the structure-borne road noise resonances, which appear under driving conditions at constant speed around 50 km/h. This is in contrast with the quarter vehicle excitation, in which only tyre cavity dominated the sound field in section 3.2.1.

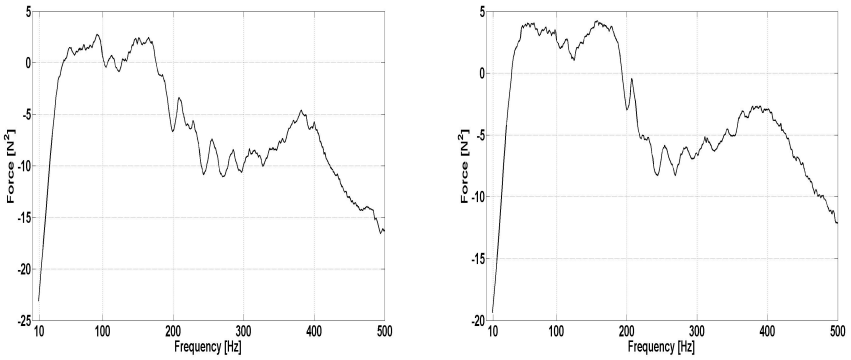

(a) Input force autospectra at the rear tyres.

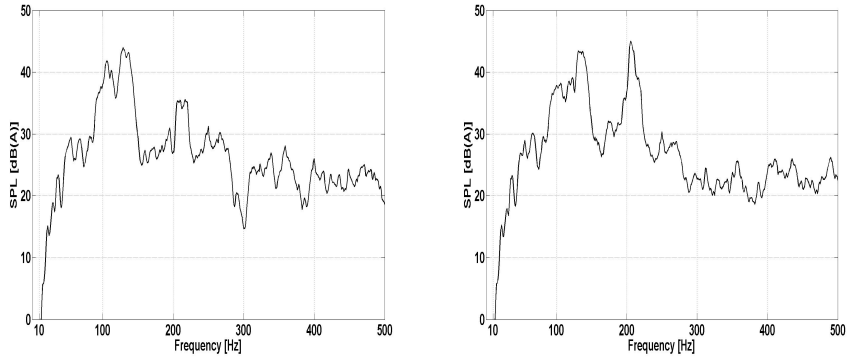

(b) Right hand rear microphone force.

FIGURE 3.4: Forces applied to the diagonal of the rear tyres and the corresponding sound pressure responses at the headrests of the rear seats.

3.2.3 Comparison between multiple coherence functions based on force and acceleration reference signals

As we discussed in chapter 2, various structural sources act upon the vehicle and multiple structural paths are responsible for the transmission of the vibrations related to structure-borne road noise. This happens because many parts of the vehicle are not mechanically decoupled or not optimise in terms of structural dynamics to block vibrations that can cause structure-borne sound. As a consequence, when we perform random road noise excitations the multiple coherence function at the microphones can be generally poor (since the acceleration signals are partially correlated). Figure 3.7 presents the location of the accelerometer sensors on the axles. In this section we investigate the alternative case, which uses force signals as references in the calculation of multiple coherence function between the input forces at the tyres and the responses at the microphone placed at the headrests. Figures 3.6(a)-3.6(d) illustrates the outcome of the comparison

FIGURE 3.5: Accelerometer locations at front and rear axles. The two front locations are symmetrical at the front suspension and one at the rear subframe mount at the rear axle. ■: One dimensional accelerometers

between multiple coherence functions based on force and acceleration autospectra as follow:

$$\gamma^2_{mk}(f) = \frac{|S_{x_m y_k}(f)|^2}{S_{x_k x_k}(f) S_{y_m y_m}(f)}, \tag{3.1}$$

where the k-input reference force autospectra are defined as $S_{x_k x_k}(f)$ and the m-acceleration autospectra are $S_{y_m y_m}(f)$. It is evident in these figures that the four force signals measured by the force sensors between and the tyre and the shaker transducers result to higher multiple coherence values in comparison with the three acceleration signals at the z-direction mounted at important mechanical parts of the vehicle, such as suspension links and subframe mounts. The multiple coherences used two acceleration signals that were measured at the front axle and one at the rear. Strikingly, the coherence is even lower at the rear microphones. This may happen because as only one accelerometer placed at the rear axle is used in this calculation. This verifies the fact that one sensor as reference is not enough to capture all the components of the rear axle vibrations, especially if we take into account the complicated geometry of modern subframe and multilink suspensions.

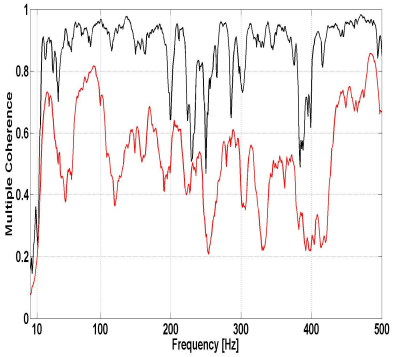

(a) Left hand front microphone.

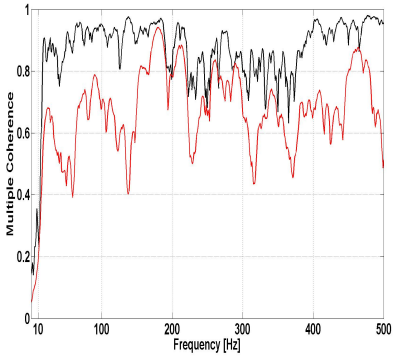

(b) Right hand front microphone.

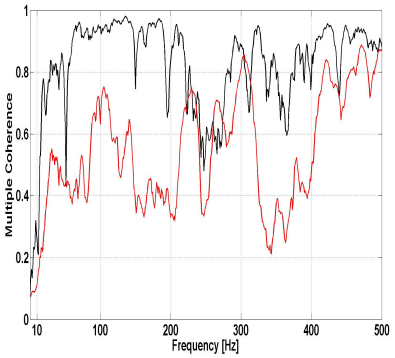

(c) Left hand rear microphone.

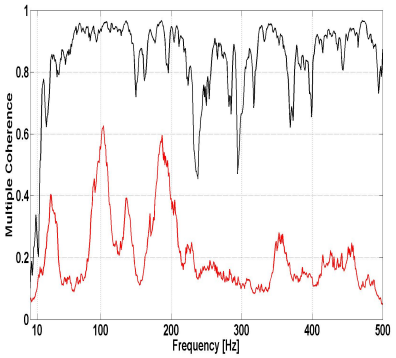

(d) Right hand rear microphone.

FIGURE 3.6: Multiple coherence between two types of the vibration signals (forces and accelerations) and the microphones at the headrests. −: Four forces as reference signals. −: Three acceleration as reference signals.

This acceleration signal set resulted to poor coherence at the rear headrests, especially for the right hand rear microphone response. Therefore, it is imperative to include further measurement locations, so that the correlation between the noise signals at the rear headrests and the vibrations from the rear axle increases. Two extra measurement locations at the rear axle were included at the rear as figure 3.7 illustrates. This increase in the reference sensor number

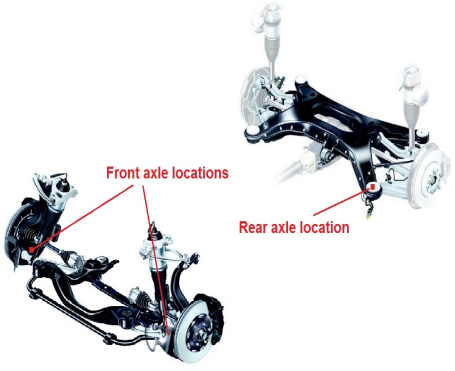

FIGURE 3.7: Accelerometer locations at front and rear axles. The two front locations are symmetrical at the front suspension and one at the rear subframe mount at the rear axle.

and location is followed by a significant improvement of the multiple coherence functions based on accelerometers as shown in figures 3.8(a)-3.8(d).

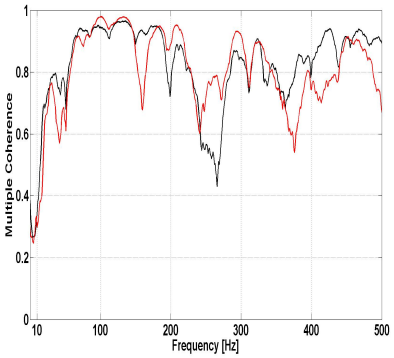

(a) Left hand front microphone.

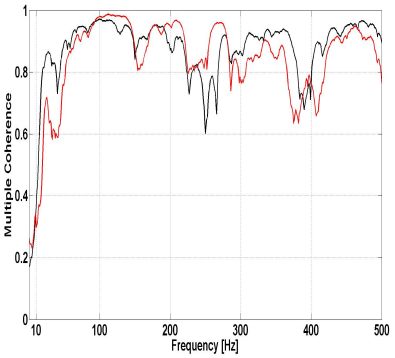

(b) Right hand front microphone.

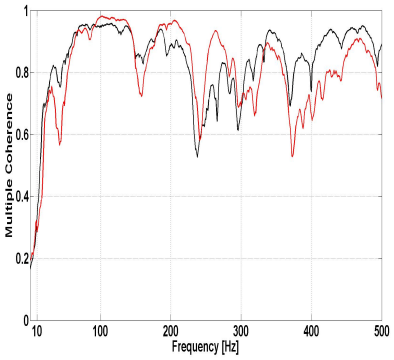

(c) Left hand rear microphone.

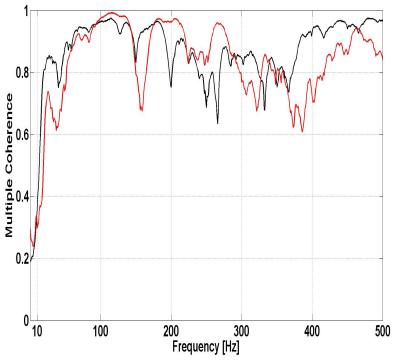

(d) Right hand rear microphone.

FIGURE 3.8: Multiple coherence between the vibration sensors (force gauges, accelerometers) and the microphones at the headrests. −: Four force signals as references. −: Five acceleration signals as references.

If we now compare the coherence functions based on the 4 force signals with the 5 acceleration signals, we observe that they agree with each other between 80-150 Hz. The acceleration based coherence is slightly higher, as the structure amplifies these vibrations, above this range and in particular in the tyre cavity range 180-220 Hz. In fact these are the most audible road noise components inside the car. Figures 3.9(a)-3.9(e) demonstrate the acceleration spectra at the five measurement locations on the axles. The acceleration autospectra of the control arms indicate that they are the main transmission paths of vibrations that relate to tyre cavity resonances.

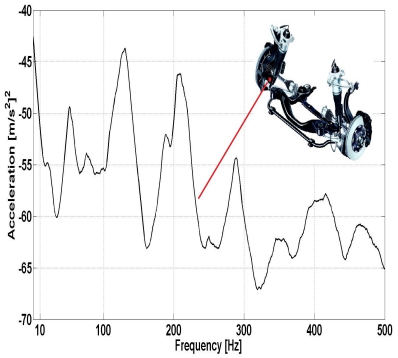

(a) Front axle: Left hand side front suspension, lower control arm.

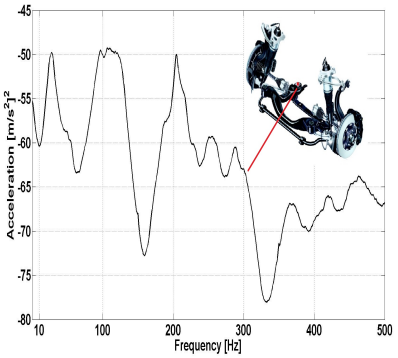

(b) Front axle: Right hand side front subframe mount.

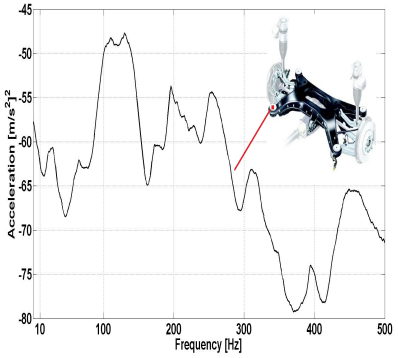

(c) Rear axle: Left hand side front mount.

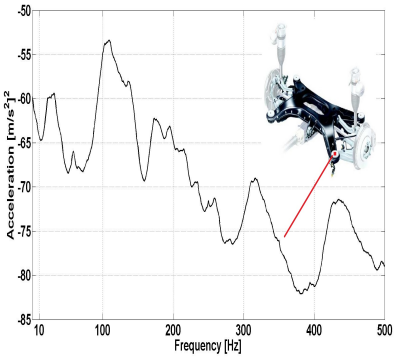

(d) Rear axle: Right hand side front mount.

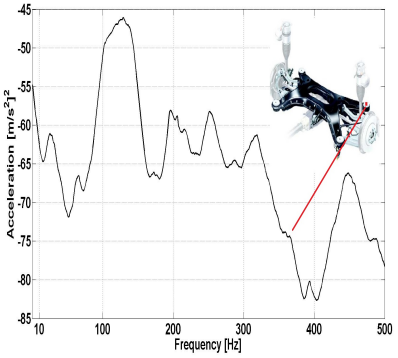

(e) Rear axle: Right hand side rear mount.

FIGURE 3.9: Five acceleration signals measured at the front and rear axle.

It then comes as no surprise that in figures 3.9(a)-3.9(e) several structural resonances appear at the road noise bands. Interestingly, high levels of vibration were recorded in the frequency of the tyre cavity noise at the accelerometer locations of the front axle (figures 3.9(a) and 3.9(b)). High acceleration levels at the rear axle were obtained mostly at the low frequency rumble band between 90-120 Hz for the figures 3.9(c)-3.9(e), whereas low levels of vibrations were measured at the tyre cavity range. This demonstrates that vibrations that relate to the road rumble dominate at the rear axle, whereas vibrations at the tyre

cavity range more noticeable at the front axle. Overall, road noise dynamics are present in all subframe mounts as the graphs in figures 3.9(b)-3.9(e) demonstrate.

3.2.4 Comparison of road noise and simulated road noise with shaker

This section presents a study that involves road noise measurements at the headrest at 100 km/h and the noise responses obtained by the shaker experiment. Figures 6.20(b)-6.22(a) illustrate the outcomes of the comparison between road noise responses and simulated road noise spectra with shakers.

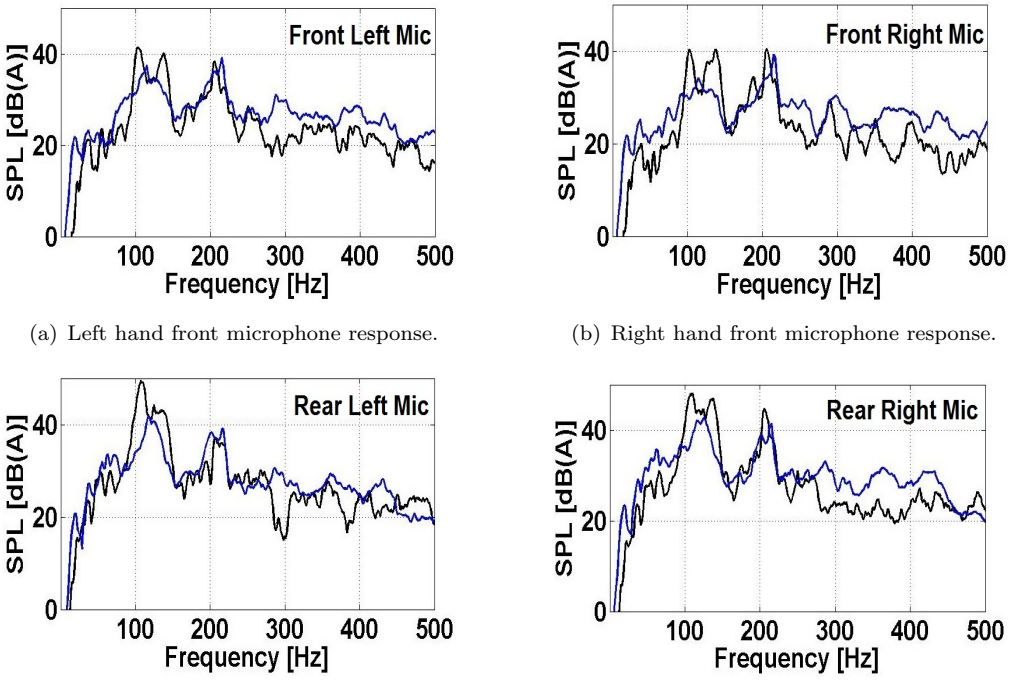

(a) Left hand front microphone response.

(b) Right hand front microphone response.

(c) Left hand rear microphone response.

(d) Right hand rear microphone response.

FIGURE 3.10: Comparison of interior noise at the four headrests. −: Simulated road noise with shaker transducers. −: Road noise measurement over a rough surface.

For the purposes of this comparison, the road auto-spectra were reduced by 20 dB(A). In this way the comparison is focused only at the spectral content, as the shakers cannot produce the same inputs that the actual tyre-road interaction generates. This reduction of road noise levels was performed deliberately as the shaker transducers were required to be driven with a certain voltage level limit to avoid any distortion products at the output of the transducers. Due to the limitations on the sensitivity of the transducers the simulated road spectra are lower than the actual spectra measured under operational condition.

In terms of the content of the simulated spectra, the road resonances they coincide with the ones of the road measurements. This is particularly evident in the road noise spectra at microphones placed at the two rear headrests.

The rumble band in the case of the simulated noise seems to have greater bandwidth compared to the measured responses on the road at the rear headrests in figure 6.20(d) and 3.10(d). This is probably caused by the fact that the shakers strongly excite two DoF as they are mounted on the diagonal of the tyres. This may trigger high vibrational levels on the z-direction at the rear axle, as we previously described in section 3.2.3. These structural resonances couple well with the sound field below 200 Hz as they appear at the microphone responses. Yet, the noise responses measured on the road strongly depend on the consistency of the surface and its roughness. Even if there are differences in the way that the tyres are excited during the road measurements compared to the simulation with the shakers, the shape of the road spectra is not that different, which is an important validation step of the physical road noise simulator.

3.3 Summary

In this chapter we developed a technique that simulates structure-borne road noise with controllable structural sources was developed. We began with a discussion on the noise measurements obtained by the quarter vehicle simulator, which several previous studies have used. We concluded that such an approach only reveals road noise contributions from the front axle. We also revealed that only one road noise component was detectable at the microphones that relates to a tyre cavity resonance is detectable at the microphones.

As a means to improve this NVH technique, we extended the system measurements using three extra shakers one for each tyre. Through this improvement we allowed four independent sources to act on the tyres. On this basis, we went on to study how the number of observation signals, which are used as reference inputs for the determination of multiple coherence function between the structural inputs and the corresponding noise response at each headrest. We verified that a small number of input sensor leads to low coherence values especially if the structural source is composed by several DoF. Instead of increasing the DoF at the initial measurement locations of the accelerometers we found an alternative method to improve the condition. We increased the observation points at the rear axle to capture all the vibrations at various input locations, which act as inputs into the rest of the vehicle structure. Then, we compared the multiple coherence functions against each other. We found that the four tyre forces, which were

the actual inputs into the vehicle system, provide higher coherency compared to three acceleration signals. For the improved sensor arrangement with the five acceleration signals was found enough to result to good agreement between the multiple coherence function based on the four forces and the one based on the acceleration signal set. This can be explained by the fact that the accelerometers at the rear axle were located at sensitive locations—i.e. the vibrations are highly correlated with the rumble noise. As a direct consequence, this configuration helped increase the multiple coherence functions with the acceleration as reference input.

In the final stage of the current study, we evaluated the performance of the physical simulator by comparing the simulated road noise spectra with road noise signals recorded on the road. It was found that the physical simulator can in fact replicate the noise responses, which were measured under driving conditions on a rough surface. The only disadvantage of this solution is that higher noise levels are measured on the road, but still the simulated road noise spectra are quite similar to the ones measured on the road. In particular, the simulated road noise resonances coincide with the actual ones from the road. These findings encourage the further use of this simulator in structure-borne NVH analysis as well as the development of active control systems in an experimental environment, where only this attribute is present.

Chapter 4

Signal analysis of road noise

The principal of coherent sound sources is the basis of active noise control, since the reproduced sounds by the loudspeaker system inside the vehicle's cabin must be coherent with the primary road noise disturbances in order to achieve satisfactory active noise reduction. As a consequence, feedforward controllers need to make use of a set of vibrational signals that are highly correlated with the road noise. This way they can generate a secondary sound field through the loudspeaker system that is highly coherent with the interior road noise. It is thus not suprising that the vibration sensors must be able to observe the main dynamics of road noise as the level of road noise control-attenuation depends on their location in the vehicle structure.

In this chapter an investigation of coherence function between the vibrations at the front and rear axle and the microphones at the headrest is presented. A coherence based method is developed for the selection of the number of accelerometers and their placement on the vehicle. As a first step the ordinary coherence functions are calculated between all the accelerometer and microphone signals. A colour map of the coherence at each of the transfer path is created in order to investigate in which channels there is some correlation between the measured vibrations and the interior road. As an outcome of this analysis the accelerometer signals that have relatively high coherence within the road noise frequency bands are then used to calculate the multiple coherence. We found that these set of accelereation signals are highly coherent with the road noise inside the cabin high and thus they were also used as reference-inputs for predicting the attenuation of a feedforward ARNC system.

In the past mathematical optimisation techniques [Stothers et al. (1995)]

have been used for obtaining an optimal set of accelerometer signals for implementing feedforward controllers in vehicles. Apart from this method techniques for the identification of the accelerometers location in the vehicle structure have been so far based on in-situ measurements on the car. Ussually, Principal Component Analysis (PCA) is performed on the Cross-Power Spectal Density (CPSD) matrix of the acceleration signals for ranking the structural sources and identifying their Principal Components (PC) [Wyckaert and Van der Auweraer (1995)]. The main drawback of the current available methods is that they always result to a large number of acceleration sensors in order to ensure that the controller is able observe the all the structural dynamics that are related to road noise. This is due to the fact that modern vehicles have many sensitive structural paths with different level of contributions to the interior road noise and by measuring all the degrees of freedom on the vehicle structure secures good performance of the contoller. This can be the general case for vehicles with very poor structure-borne road noise performance, but not vehicles that have only a couple of road noise components.

It is necessary to have a better insight of the coherent contributions to the interior noise before applying an ANC system, since as it will be shown in this chapter various locations on the vehicle structure can observe several road noise dynamics with good coherency. These locations may result to a low number of the reference sensors and used as an optimimum set of inputs to the controller.

4.1 Chapter outline

In this chapter the discussion is restricted to coherence analysis of road noise data that were obtained by road measurements. The coherence analysis is divided in three sections, quarter, half and whole vehicle analysis for identifying the location of the each road noise source around the vehicle and their coherent contributions. The methodology that is applied to the vibrational signals is presented in sections 4.2.3. The multiple coherence of the selected acceleration signals from the method and their predictions for a causally uncostrained ARNC are presented in sections 4.2.4 and 4.3 .

4.2 Coherence analysis

4.2.1 Introduction to road noise analysis

Road noise signals are often measured with accelerometers mounted at the suspension and subframe connection points. This way the main noise transfer paths are identified and ranked according to the vibrational energy that is observed at each path. Figure 4.1 describes the road noise transmission path problem.

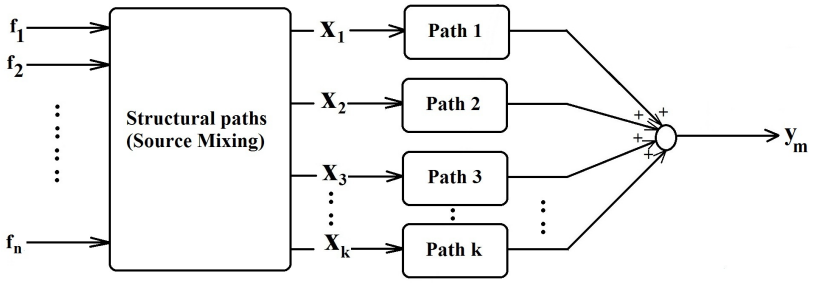

FIGURE 4.1: The road forces **f** result to vibrations that are measured by the accelerometer signals, $\mathbf{x_1}$,..., $\mathbf{x_k}$. The road noise response **d** inside the cabin is the superposition of all the output signals from the noise transfer paths.

The measurement setup of road noise on a quarter vehicle that was used to obtained the first road noise data is shown in 4.2. Four microphones were placed on the headrests in the vehicle's compartment and four tri-axial accelerometers at four different locations at the suspension of the left hand front wheel.

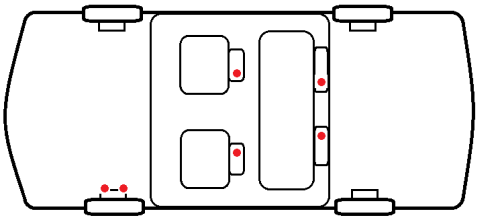

FIGURE 4.2: Sensor arrangement on the vehicle. The red dots indicate the measurement locations of the sensors. Accelerometers were mounted close the front wheel and four microphones were measuring the noise at the headrests.

At a first step the acceleration cross-spectra density matrix (CPSD) is calculated, in order to perform Principal Component Analysis (PCA). For vibrational signals with non-zero off-diagonal elements in the CPSD matrix, the virtual coherence function is calculated [Otte et al. (1988)]. This can performed by decomposing the CPSD matrix into a diagonal matrix that contains the virtual uncorrelated auto-powers of the measured acceleration signals.

For every noise transfer path the corresponding single-input, single-output coherence can be defined as

$$\gamma^2_{mk}(f) = \frac{|S_{x_m y_k}(f)|^2}{S_{x_k x_k}(f) S_{y_m y_m}(f)}, \tag{4.1}$$

and the acceleration CPSD matrix can be decomposed with the use of Singular Value Decomposition (SVD) as [Wyckaert and Van der Auweraer (1995)]

$$\mathbf{S}_{xx}(f) = \mathbf{U}(f)\mathbf{S}_{vv}(f)\mathbf{V}(f), \tag{4.2}$$

,where the virtual autospectra are in the diagonal matrix $\mathbf{S_{vv}(f)}$.The summed virtual coherence function based on the virtual auto-spectra can now be found, which is equivalent to the multiple coherence function as suggested in [Price and Bernhard (1986),Akiho (1995)] as follow

$$\gamma^2_{m:k}(f) = \sum_{k=1}^{K} \frac{|S_{v_k y_m}(f)|^2}{S_{v_k v_k}(f) S_{y_m y_m}(f)}, \tag{4.3}$$

,where $S_{v_k y_m}$ is the cross-spectrum between the m-th microphone signal and the k-th acceleration signal and $S_{v_k v_k}$ and $S_{y_m y_m}$ are the virtual auto-spectra of the acceleration and sound pressure signals respectively. The new matrix that contains the virtual auto-spectra can be used for identifying the number of independent vibrational sources that act on the vehicle structure [Otte et al. (1988)], [Sutton et al. (1994)].

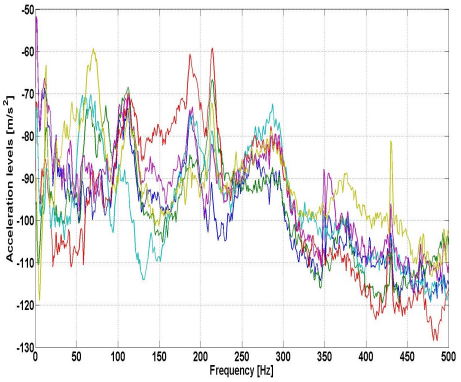

(a) Measured acceleration power spectral densities.

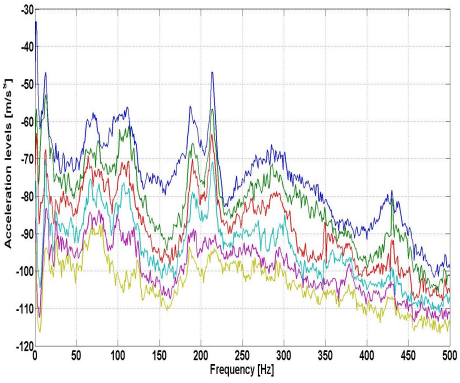

(b) Virtual uncorrelated acceleration power spectral densities.

FIGURE 4.3: Measured and virtual uncorrelated power spectral densities of the left hand front suspension.

The most dominant components for the front suspension are found at the tyre cavity region. In particular, in the frequency range of 180-220 Hz, four principal components are actually important in figure 4.3(b) and therefore four

independent contributors are acting at the left hand front suspension. Likewise, four independent contributors are also found in the rumble range 100-120 Hz. In contrast, in the road drum frequency range, six contributors are noticeable at around 20 Hz, 60 Hz, 110, 180 Hz, 220 Hz and 290 Hz. To conclude, maximum six independent structural sources are acting on the front suspension this observation correlates well also with previous findings [Park et al. (2002)]. However, it is questionable if all of them are necessary as inputs to a feedforward controller as in reality the structure-borne noise levels are dependent on the ranking of these sources that is usually found in TPA [Elliott et al. (2013)]. In chapter 6 we will investigate which axle locations and their DoF are actually important for the optimal performance of the controller.

4.2.2 Coherence analysis of quarter vehicle

The acceleration signals of the previous were used to calculate the coherence functions of each transfer path.Figures 4.4(c)-4.4(f) present the coherence functions for the front microphones and figures 4.5(c)-4.5(f) for the microphone at the rear headrests.

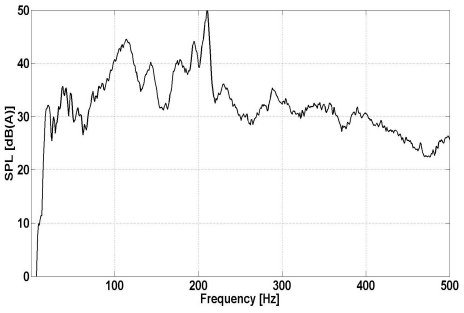

(a) Left hand front microphone response.

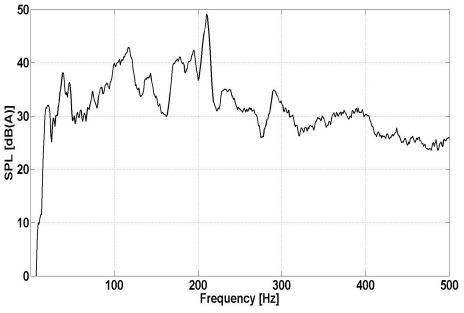

(b) Right hand front microphone response.

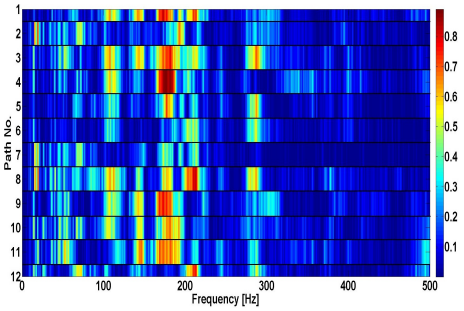

(c) Coherence map between the left hand front microphone and the accelerometers close to the front wheel.

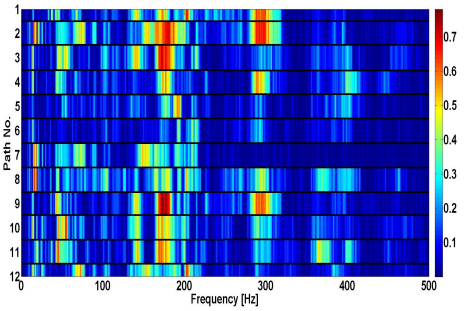

(d) Coherence map between the right hand front microphone and the accelerometers close the front wheel.

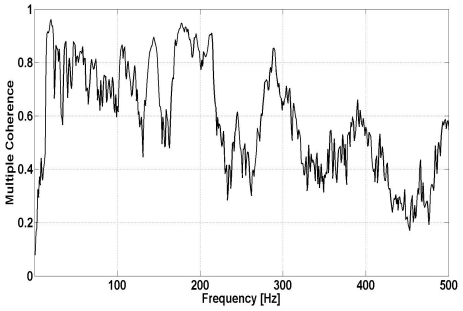

(e) Multiple coherence between the left hand front microphone and the accelerometers close to the front wheel.

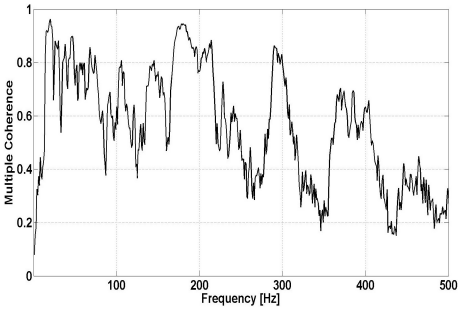

(f) Multiple coherence between the right hand front microphone and the accelerometers close to the front wheel.

FIGURE 4.4: Front microphones responses and coherence functions at 60 km/h.

In figures 4.4(c) and 4.4(d) relatively high coherence ($\geq$0.7) can be noticed around 180-220 Hz for most of the paths, where two tire cavity peaks at the sound pressure responses in figures 4.4(a) and 4.4(b) dominate. Some correlation can be also noticed around 290 Hz for some paths at a highly damped resonant peak around 290 Hz. High multiple coherence around 0.9 is obtained at the tire cavity range as it can be seen in figures 4.4(e) and 4.4(f) for the front microphones. Similar behaviour can be also observed for the case of the rear microphone: especially at the left hand rear microphone in figure 4.5(a) for most of its paths.

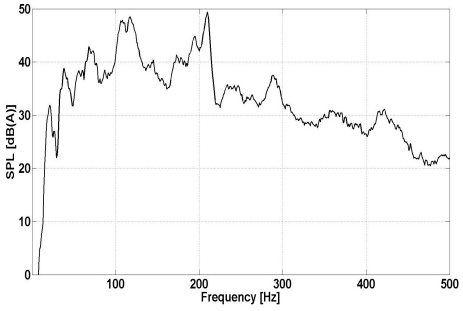

(a) Left hand front microphone response.

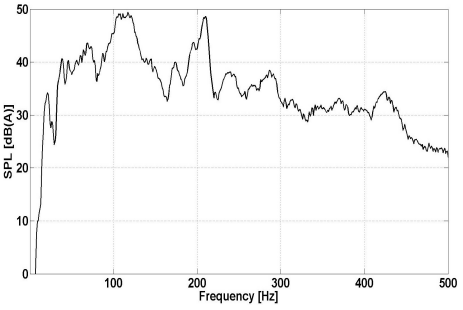

(b) Right hand front microphone response.

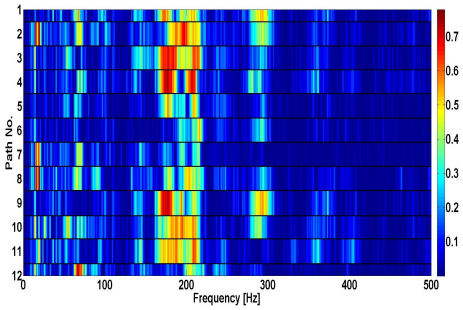

(c) Coherence map between the left hand front microphone and the accelerometer at the front wheel.

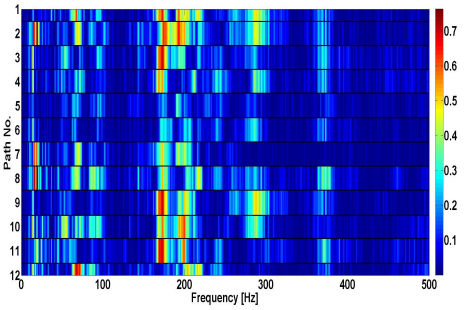

(d) Coherence map between the right hand front microphone and the accelerometer at the front wheel.

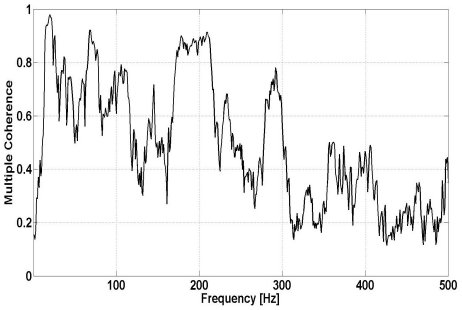

(e) Multiple coherence between the left hand front microphone and the accelerometer at the front wheel..

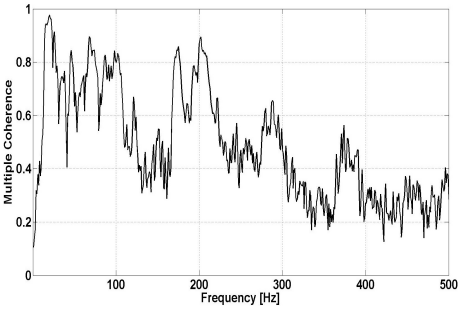

(f) Multiple coherence between the right hand front microphone and the accelerometer at the front wheel.

FIGURE 4.5: Rear microphones responses and coherence functions at 60 km/h.

At the frequency range of the rumble 100-120 Hz low coherence is noticed for all of the paths in figures 4.4(c), 4.4(d), 4.5(c) and 4.5(d). This fact indicates that there is low contribution of the front axle at rumble range. As a consequence, the multiple coherence is around 0.8 at 105 Hz for all of the microphones, but at the rest of the range is around 0.6 or less in the case of the rear microphones. As previously noticed in the PCA of the acceleration signals there were no significant independent components between 100-120 Hz. In addition the multiple coherence functions in figures 4.5(e) and 4.5(f) between the rear microphones and the accelerometer signals high coherence is only found in the tire cavity range 180-210 Hz. This indicates that it is very likely that the rumble is due to a source acting somewhere at the rear axle of the vehicle that is not included in this analysis.

In this quarter vehicle analysis it is revealed that not all the structure-borne road noise sources are identified. The accelerometers placed at the quarter of the car (around the right hand front wheel only) were not able to identify the source of rumble noise. Only accelerometer positions that have high coherence with the tire cavity noise were found. Therefore it is necessary to place more accelerometers around the vehicle for identifying the coherent paths from each wheel to the interior microphones.

4.2.3 Coherence analysis of half vehicle

In this section the results of the coherence analysis of half vehicle are discussed. More measurement locations were included in the front axle and 27 accelerometer signals were recorded. The data were obtained by driving the again on a rough surface and on coast down starting with a high speed from 100 km/h and going down to 60 km/h thus improving the excitation on the vehicle. The acceleration cross-spectra density matrix is calculated separately for the front and rear axle in

order to found out the contribution of each axle to the total road noise response in the cabin.

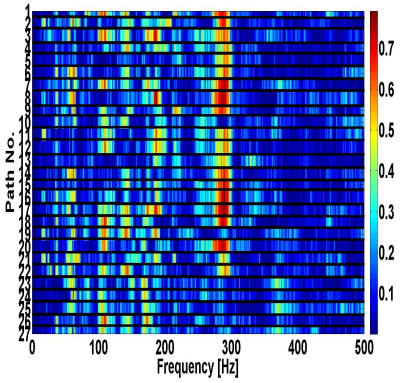

(a) Left hand front microphone coherence map.

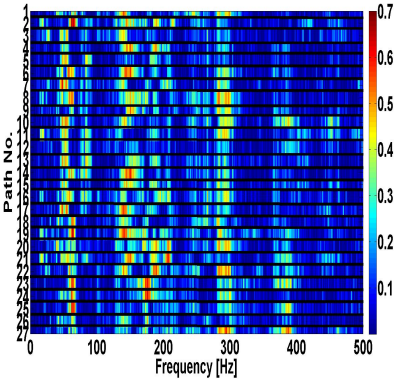

(b) Right hand front microphone coherence map.

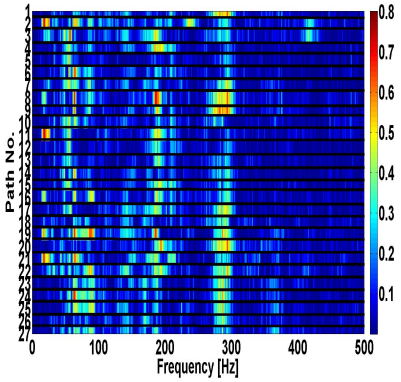

(c) Left hand rear microphone coherence map.

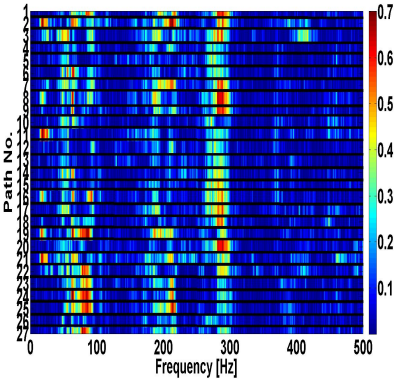

(d) Right hand rear microphone coherence map.

FIGURE 4.6: Coherence map between each accelerometer signals mounted at the front axle of the vehicle and the four microphones for a coast down from 100 km/h down to 60 km/h.

In the contour maps of figures 4.6(a) - 4.6(d) the results for the front axle are presented. Relatively good coherence (more than 0.7) can be found at 290 Hz for the left hand front microphone as before in the new accelerometer positions at the front axle. Tire cavity noise is still sensed at some of the sensors, since there is some coherence around 190 Hz for the left hand front microphone and around 214 Hz for right hand rear microphone. However rumble noise is still not coherent the front part of the vehicle. The following figures show the coherences between the paths coming from the rear part of the vehicle. Apart from the left hand front microphone in figure 4.7(c) the rest of the microphone coherence maps indicate that there is coherence between some paths and the rest of the microphones responses in the range of 100-110 Hz, where the rumble is located.

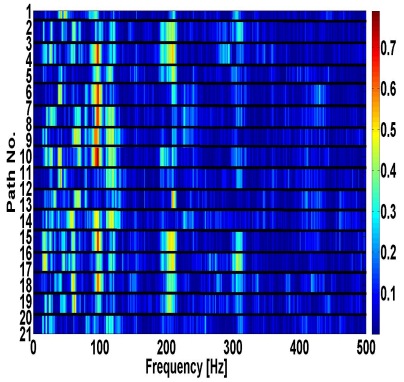

(a) Left hand front microphone coherence map.

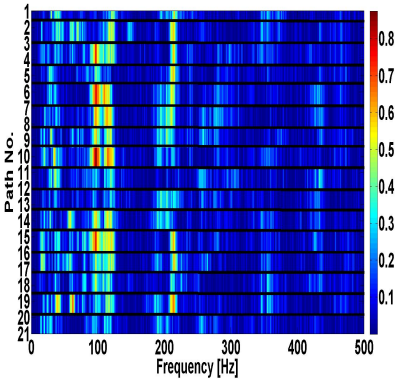

(b) Right hand front microphone coherence map.

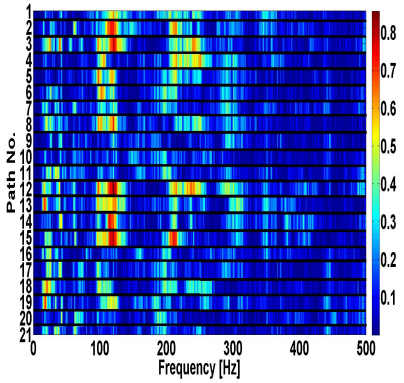

(c) Left hand rear microphone coherence map.

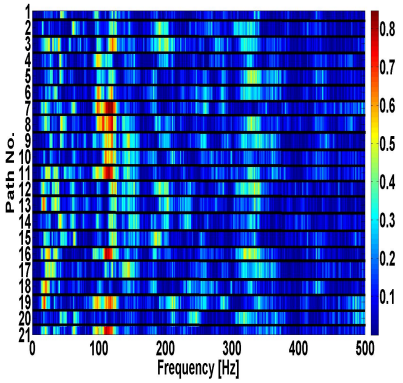

(d) Right hand rear microphone coherence map.

FIGURE 4.7: Coherence map between each accelerometer signals mounted at the rear axle of the vehicle and the four microphones for a coast down from 100 km/h down to 60 km/h.

4.2.4 Multiple coherence of whole vehicle

The multiple coherence analysis was extended to the whole vehicle by calculating the virtual cross-spectra density matrix that contains the front and rear axle acceleration signals for 60 km/h. It is obviously expected that a high number accelerometer will result to high multiple coherence in the range of structure-borne road noise, mostly in 0-300 Hz as it can be seen in figures 4.8(a))-4.8(d). It can be also noticed that there is high coherence between the front microphones and front axle vibrations compared to the rear axle in the 120 - 200 Hz. On the other hand, in the range 100 - 120 Hz there better coherence for the rear axle compared with the front axle, especially for the rear microphones. This validates that the most of the noise at the rumble range is due to contributions

from the rear axle that are highly correlated with the noise response at the four microphones.

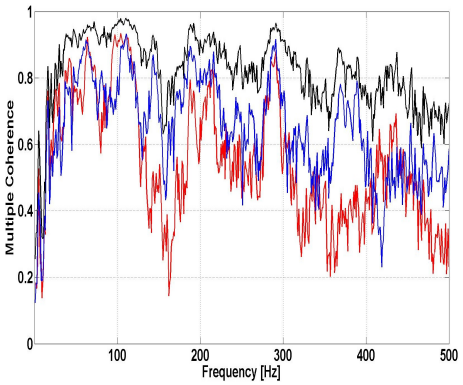

(a) Multiple coherences at the left hand front microphone.

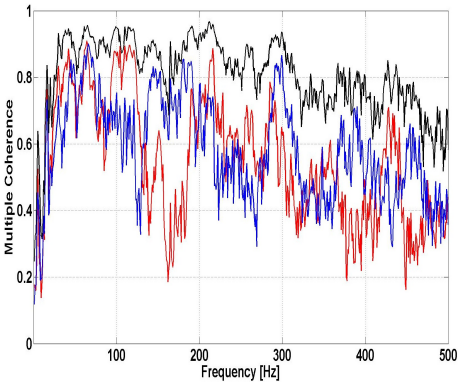

(b) Multiple coherences at the right hand front microphone.

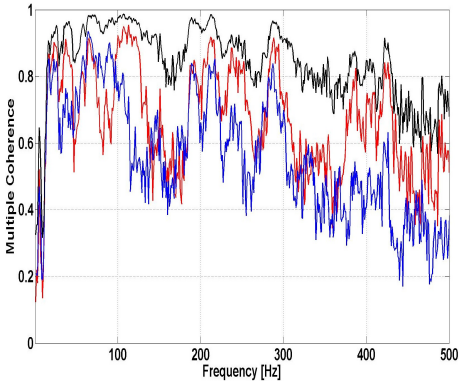

(c) Multiple coherences at the left hand rear microphone.

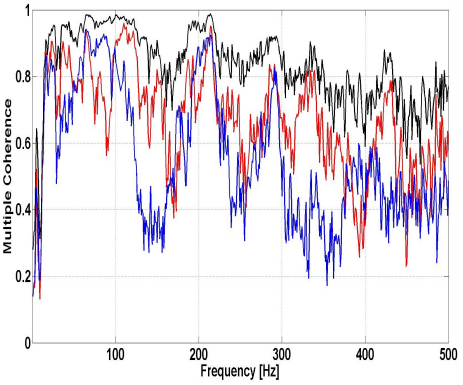

(d) Multiple coherences at the right hand rear microphone.

FIGURE 4.8: Multiple coherence functions between the four microphones and three cases of accelerometer signal inputs. Black line:Whole vehicle acceleration signals. Blue line: Front axle acceleration signals. Red line: Rear axle acceleration signals.

4.3 Evaluation of a reduced set of acceleration signals

4.3.1 Multiple coherence analysis

Only four accelerometer signals were used to calculate the multiple coherence. A good compromise has to use the two acceleration signals for tyre cavity from the front axle and two for rumble, which were coming from the rear axle. The acceleration locations of path 3 and 22 of the front axle (figure 4.6(a), 4.6(b)) were selected as they contribute highly to the range of 180 - 220 Hz. As for the

rear axle, the locations of path 11 and 12 are used for the rumble range (figure 4.7(c), 4.7(d)).

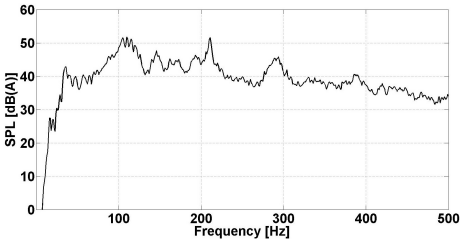

(a) Left hand front microphone response.

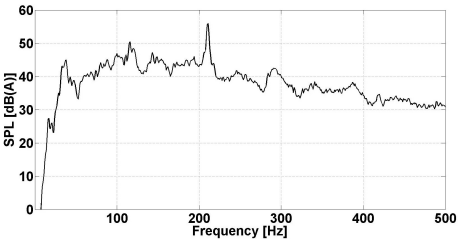

(b) Right hand front microphone response.

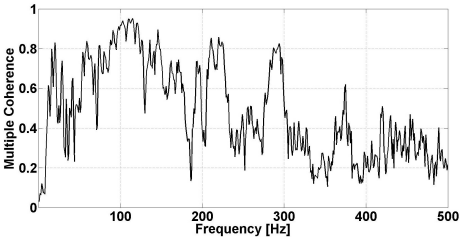

(c) Multiple coherence at the left hand front microphone.

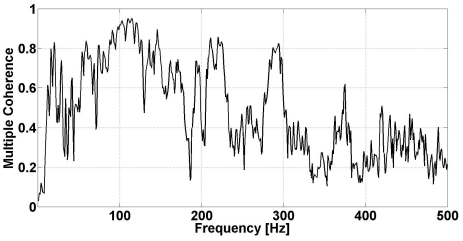

(d) Multiple coherence at the right hand front microphone.

FIGURE 4.9: Multiple coherence functions between the two front microphones and the four accelerometer signals at 60km/h.

Here the multiple coherence of their combination is demonstrated in order to shown that they can provide high coherence for an ANC system. In the rumble at 100-110 Hz and tire cavity range 190-220 Hz, the coherence was around 0.8. In addition good coherence is also noticeable at the midfrequency around 290 Hz.

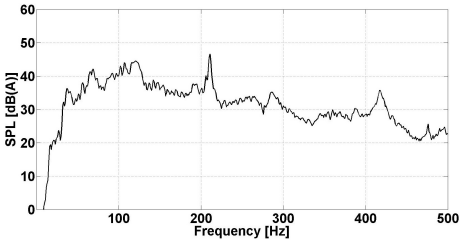

(a) Left hand rear microphone response.

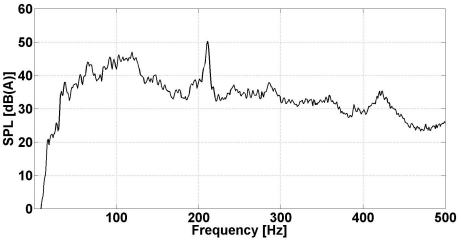

(b) Right hand front microphone response.

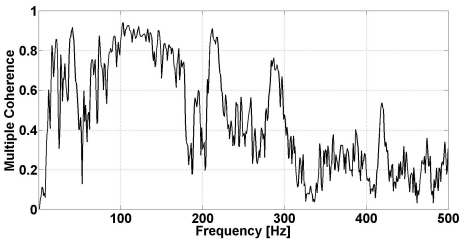

(c) Multiple coherence at the left hand rear microphone.

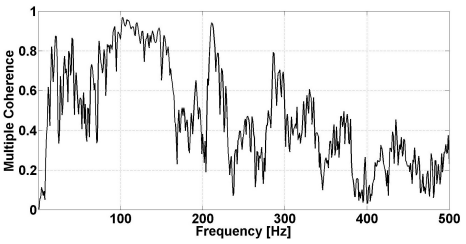

(d) Multiple coherence at the right hand rear microphone.

FIGURE 4.10: Multiple coherence functions two rear microphones and the four accelerometer signals at 60km/h.

Therefore these coherence values between the sensor may potentially be enough for achieving good ANC performance at the road noise bands. In figures 4.9(c), 4.9(d),4.11(b), 4.11(c) the multiple coherence for the selected four accelerometer locations are presented for stationary road noise data at 60 km/h. The same exercise is also repeated for signals obtained at 100 km/h in figures 4.11(a) - 4.11(d).

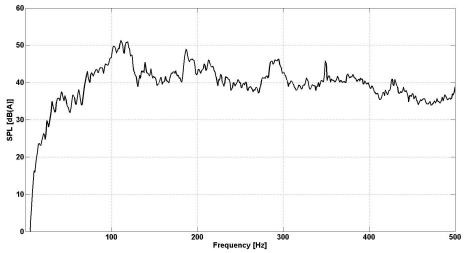

(a) Left hand front microphone response.

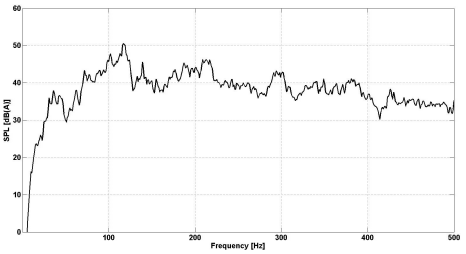

(b) Right hand front microphone response.

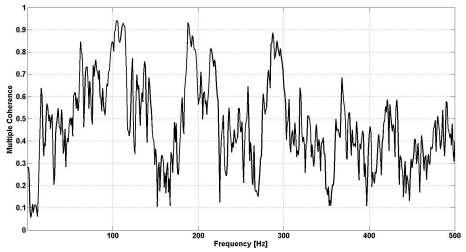

(c) Multiple coherence at the left hand front microphone.

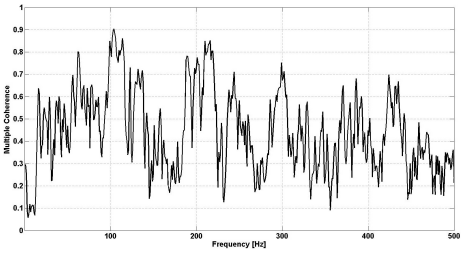

(d) Multiple coherence at the left hand front microphone.

FIGURE 4.11: Multiple coherence functions between the two front microphones and the four accelerometer signals. at 100 km/h

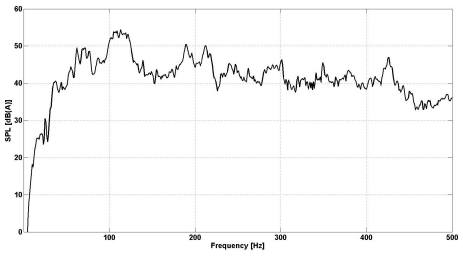

(a) Left hand rear microphone response.

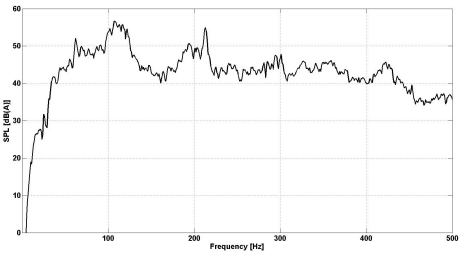

(b) Left hand front microphone response.

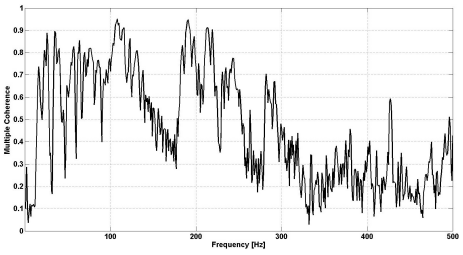

(c) Multiple coherence at the left hand rear microphone.

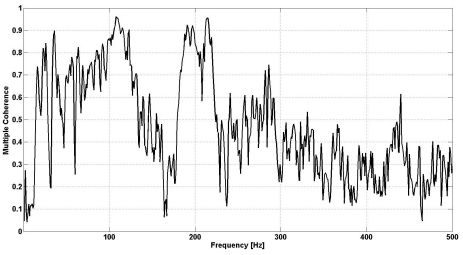

(d) Multiple coherence at the right hand rear microphone.

FIGURE 4.12: Multiple coherence functions between the two rear microphones and the four accelerometer signals at 100 km/h.

The coherence is still high at the main road noise bands, but outside these bands the coherence has dropped significantly due to other NVH attribute starting to taking effect on the sound field such as wind and traffic noise.

4.3.2 Non-causal prediction of feedforward ARNC performance

The multiple coherence of the four acceleration signals can be used to estimate the performance of a multichannel ARNC system without including the constraint of causality [Oh et al. (2002)]. This means that the physical delays of the secondary paths transfer functions and the electronic latency of the controller are not included in this type of prediction and only the coherency between the input-output signals is taked into account. The reduction as a funtion of frequency of an active road noise controller is usually estimated with the use of the multiple coherence between the accelerometer signals and a microphone signal in the cabin as follow

$$R(f) = -10log(1 - \gamma^2_{m:k}(f)) \tag{4.4}$$

Tables 4.1 and 4.2 present the predictions for the four optimised accelerometer positions and for twenty accelerometer signal obtained from the main paths of structure-borne road noise.

	Left hand front	Right hand front	Left hand rear	Right hand rear
Speed [km/h]	ARNC dB(A)	ARNC dB(A)	ARNC dB(A)	ARNC dB(A)
60	3.05	3.03	3.04	3.04
100	3.02	3.00	3.02	3.03

TABLE 4.1: Predicted ARNC performance for each of the four microphone at the headrests. The calculation is based on the four reference acceleration signals for the frequency range of 0-500 Hz.

	Left hand front	Right hand front	Left hand rear	Right hand rear
Speed [km/h]	ARNC dB(A)	ARNC dB(A)	ARNC dB(A)	ARNC dB(A)
60	3.27	3.26	3.29	3.29
100	3.26	3.26	3.28	3.28

TABLE 4.2: Predicted ARNC performance for each of the four microphone at the headrests. The calculation is based on twenty reference signals for the frequency range of 0-500 Hz.

By comparing the two tables it can be noticed that there is a very small improvement from four to twenty accelerometer signals as reference inputs. This is contradictory to what has been found in the past for other vehicles as an increase in the number of reference acceleration signal significantly improved the reduction [Mackay and Kenchington (2004)]. On the other hand, Bernhard has that four acceleration signals may result to 7 dB reduction for a Japanese sedan [Heatwole et al. (1993)]. This variation in the unconstrained prediction of the active reduction implies that there is a strong dependency between the estimated ARNC performance and the type of vehicle. In our case the luxury vehicle happens to have relatively high levels of refinement compared to typical high volume vehicles, which explains the fact that theoretically it can achieve more that 3.2 dB(A) reduction.

In our case the vehicle under investigation has relatively good structure-borne road noise performance especially for the front seats as we discovered in the analysis of the vibro-acoustic FRFs in section 2.5.3. As a result the ARNC system can provide a certain amount of improvement in this vehicle, since from the coherence analysis looks like that only two structural road noise sources are actually acting on the vehicle. Hence, sufficient control at the road noise resonances can be achieve also with a low number of accelerometer sensors.

4.4 Summary

Based on road noise measurement data, this chapter has investigated the most coherent transfer paths of noise. It was found that the contributions from the front axle are mostly related to tire cavity noise and also to a midfrequency resonance at 290 Hz. On the other hand, the rumble noise (100-120 Hz) is caused due to structural vibrations coming from several points at the rear axle. Two subframe mount locations from the front and two from the rear axle were selected to calculate the multiple coherence and evaluate the performance of a feedfoward ARNC controller. Reduction around 3 dB(A) at each headrest microphone are predicted, which is a good indication that the accelerometers are placed at sensitive structural points of the car that provide high levels of vibrations related to the interior road noise.

Chapter 5

Road noise synthesis

The coherence analysis of the vibro-acoustic paths in the previous chapter revealed that there are two main locations at the rear axle that are responsible for the road rumble between 90-120 Hz. As for the tire cavity band between 180-220 Hz the primary paths originate from the front axle of the vehicle. In this chapter we will demonstrate that these locations can be used to artificially synthesise the interior road noise with multireference adaptive filtering in the time domain. This technique is widely used in the identification of impulse responses of physical systems. In our case we determine the impulse responses of each NTF between the reference sensors and a microphone in the cabin in the time domain without the electro-acoustic paths between the loudspeakers and the microphones, which we will use later to model the ARNC system. The main target of this artificial synthesis of road noise is to highlight the contributions from the front and rear axle with the use of adaptive filtering instead of frequency domain methods, such as OTPA, which require matrix inversion of the CPSD matrix of the acceleration signals. In our case, we make use of adaptive filtering to identify the systems between the acceleration and sound pressure signals. This type of approach is a special case of adaptive noise cancellation that does not include the effects of the acoustic secondary paths. Therefore this can reveal the potential reduction with a given set of sound and vibration signals acquired from the vehicle without the effect of delays that are inherent in the secondary path impulse responses and also in the hardware of the controller. To summarise, this study aims to offer an impression of how close is the performance of adaptive filtering algorithms are to the attenuation, which is computed non-causally in the frequency domain with the use of multiple coherence function.

5.1 Chapter outline

In section we start with the introduction of the famous multiple reference LMS algorithm that is used in section 5.3 In section 5.4, 5.5, 5.7 and 5.7 the main structural inputs into the vehicle's body from the subframe are used for synthesising their vibro-acoustic contributions.

5.2 Multiple reference LMS algorithm

Before introducing the formulation of multichannel feedforward adaptive algorithms for active control, we first formulate the multireference LMS [Widrow and Stearns (1985)]. The necessity of multiple reference input signals was first presented by Widrow, where multiple electrical noise sources are generating noise at a the receiver of a transmission line [Widrow et al. (1975)]. Windrow also highlighted the constraint of causality for the cancellation of random signals. This was an important observation as the adaptive controller cannot converge to an optimal filter solution, if the delay in the controller is greater than that in the primary noise path. Therefore in the case of road noise large delays in the controller will limit the performance of the ARNC system [Sutton et al. (1994)].

If the reference signals, $x_k(n)$ at each discrete time instant n measured by k-reference sensors and also l-number is the primary disturbances that are observed at the cancellation points, then a set of control filters $w_{l,k}(n)$ is required to create the predicted l-disturbance signals as follows

$$\hat{d}_l(n) = \sum_{l=1}^{L} \sum_{j=1}^{J-1} w_{l,k}(n) x_k(n), \tag{5.1}$$

and the difference between the primary disturbance and the output of the adaptive filter can be found by the difference between the primary disturbance $d_l(n)$ and its estimate $\hat{d}_l(n)$

$$e_l(n) = d_l(n) - \hat{d}_l(n), \tag{5.2}$$

which defines the l-th error signal that is fed back to the adaptive algorithm. If we now jump some steps in the derivation of the multireference algorithm and

move directly to the update the equation of the MISO LMS algorithm [Widrow and Stearns (1985)]

$$w_{lk}(n+1) = w_{lk}(n) + 2\mu x_k(n) e_l(n), \tag{5.3}$$

where μ is the converge factor of the algorithm that controls the speed of the adaptation and also determines the stability of the algorithm. In our case x_k are the acceleration signals that were recorded on the axles and $d_l(n)$ the road noise signals. The signals $\hat{d}_l(n)$ are the estimated road noise signals from the outputs of the adaptive filters that will be compared to the actual structure-borne road noise spectra. In this artificial way of synthesing the structure-borne road noise spectra we will be able to have a first impression of how different sets of acceleration signals help the algorithm to generate the appropriate output signals that synthesise the road noise contribution of each signal set.

5.3 Road noise synthesis with multireference LMS algorithm

The raw data that were recorded in the vehicle are now used to build a model of an adaptive multireference algorithm that estimates the road noise contributions of various acceleration signals set that were measured on the front and rear axles. First, the multireference LMS was used to estimate the impulse responses between the reference sensors and the observation sensors in the cabin. Once these impulse response are found with a low estimation error, the reduction at the observing microphones is evaluated (before developing the actual active noise canceller). If the road noise is reduced effectively in this simulation, the reference sensors provide inputs highly correlated inputs with the microphone signals. As a consequence, this simulation allows to evaluate the accelerometers placed at axle locations; whether their structural responses are sensitive in terms of large road inputs that appear especially at coarse chip surfaces. The virtual synthesis of road noise also allows to identify a set of impulse responses that represent the vibro-acoustic paths between the vibrational and acoustical sensors with the acceleration responses as reference inputs. This is an interesting type of function for modern structural dynamics that it was defined in chapter 2.5.3 as transmissibility. In this case, we will estimate the impulse response functions with the use of adaptive filters for predicted the interior road noise for various combinations of acceleration data. The selection of this reference inputs is based

on the coherence analysis of chapter 4, where these structural inputs had high coherence at the main road noise resonances.

Widrow introduced the constraint of causality in the case of adaptive noise cancellation of random disturbances, such as road noise. It is necessary sometimes to delay the reference signals, in order to allow some time to perform the required convolutions that are necessary for generating the output signals. These signals synthesise the estimated noise signal by the multireference algorithm [Widrow et al. (1975)]. In reality though, this delay is only introduced if the main source is caused by an electrical system. In contrast, a physical system has an inherent delay that corresponds to the propagation time of the waves from the noise source to the receiving location.

Obviously, for road noise cancellation the main structural road noise sources cannot be delayed, unless the source is an electrical disturbance, i.e. a controllable source. Yet, in the case of tire force excitation, the control system is expected to perform the filtering stage in a very small time frame that depends on the propagation time of the noise from the reference sensors to the microphones in the compartment. Therefore, the accelerometer needs to be placed as far as possible from the microphone in the cabin, in order to increase the delay between the sensors. In this way, more time is gained for the controller's filtering, since the delay in the feedforward path cannot be compensated. Figure 5.1 illustrates the problem of the cross-coupling of the uncorrelated sources. The actual sources ψ_m are affected by the spatial filtering matrix $\mathbf{F}_{mk}$ of the structure, since the multiple structural paths are summed at the reference location, where the accelerometers are placed. The actual noise transmission paths $\mathbf{S}_m$ for the sources are also summed at the microphone position, where the primary road noise disturbance is located.

As shown in section 4.2.1 the measured acceleration signals are decomposed with the use of SVD in the frequency domain. The reference signals also become decorrelated by performing some filtering in the time domain. An interesting technique that is based on the decomposition of the correlation matrix of the acceleration signal was presented as a solution to the decorrelation of the reference signals in [Dehandschutter and Sas (1998)]. However, this technique cannot be implemented in a real-time system as it has very high computational requirements.

In the following simulation study, accelerometer locations on the subframe mounts are used as reference inputs to an adaptive algorithm for system identification. The purpose is to evaluate offline the perfomance of a causal feedforward controller. Additionally, the estimated impulse responses between the sensors are used to perform a time domain TPA analysis. It should be mentioned that

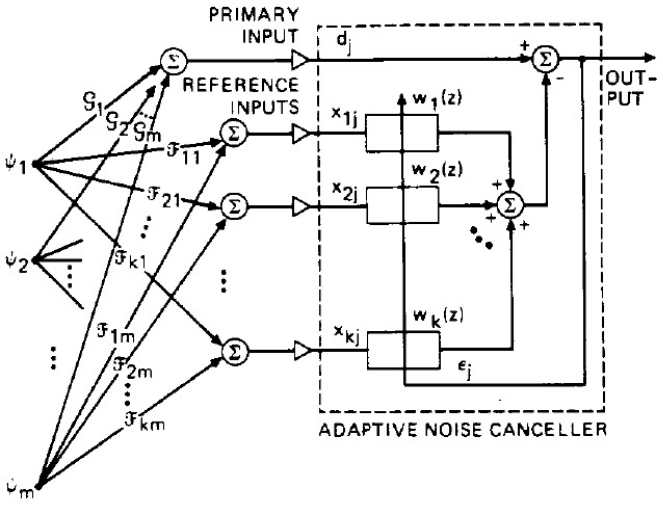

FIGURE 5.1: Multireference adaptive filtering problem with adaptive FIR filters. Taken from [Widrow et al. (1975)].

the acoustic plants (from the controller's ouput to the cancellation point) are not included, in order to present an idealised scenario, where these plants do not affect the magnitude and the phase of the cancellation signal.

5.4 Front subframe mounts as reference inputs to the system

The acceleration signals from the front mounts were used to train a set of adaptive filters with the multireference LMS algorithm that was described in the previous section. These filters are an estimate of the contributing paths of the front axle and thus a small estimation error would reflect how well correlated is this set of acceleration signals.

In particular, the spectra of the error signals are evidently lower for the front headrests (figures 5.2(a)-5.2(b)) compared to rear headrests (figures 5.2(c)-5.2(d)). The poor estimation is particularly noticeable at the rumble range for the microphones at the rear headrests. The only road noise component that is estimated with evidently low error is the tyre cavity, which verifies what we previously found in the coherence analysis.

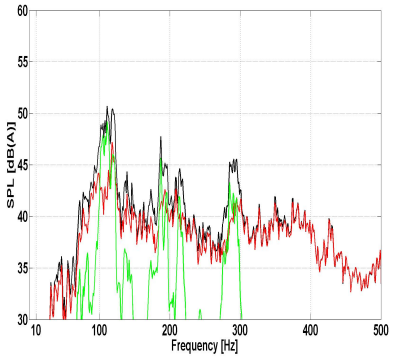

(a) Left hand front microphone responses.

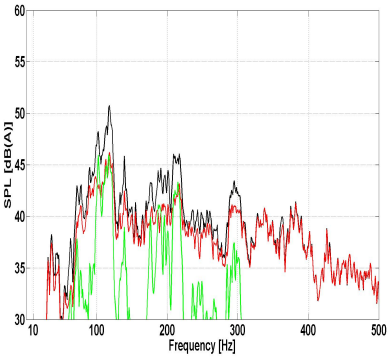

(b) Right hand front microphone responses.

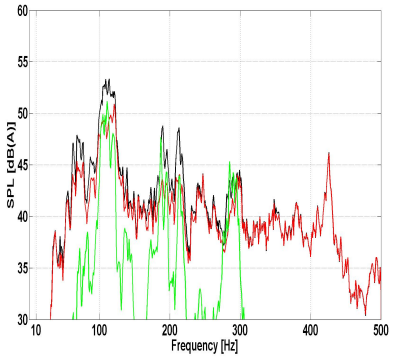

(c) Left hand rear microphone responses.

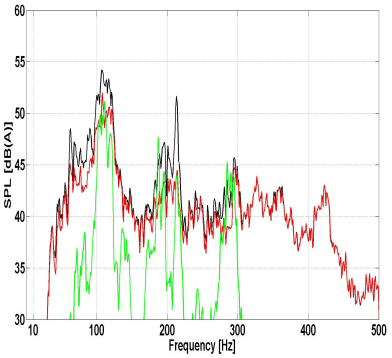

(d) Right hand right microphone responses.

FIGURE 5.2: Comparison between measured road noise spectra, synthesised/estimated with LMS and the difference between them (error signal). −: Road noise. −: Estimated front and rear subframe mount contribution. −: Estimation error.

5.5 Rear subframe mounts as reference inputs

The contributions from the rear axle are now evaluated using the measured acceleration signals measured at the mounts of rear subframe. We observe a rather poor synthesis of the road spectra for the microphones at the front part of the cabin (figures 5.3(a)-5.3(b)). In addition to this, it is almost the same as the measured road noise spectra for most of the error spectra. However, we notice a good estimation of the rumble range at the rear headrests, as figures 5.3(c)-5.3(d) illustrate. This indicates that high road rumble levels are caused by rear subframe vibrations.

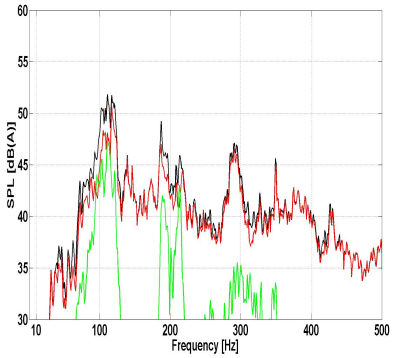

(a) Left hand front microphone responses.

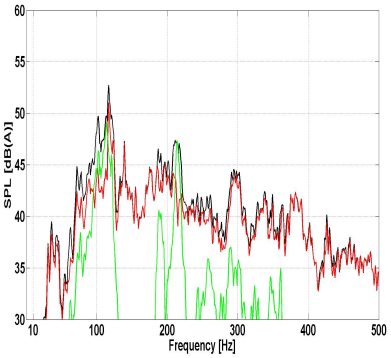

(b) Right hand front microphone responses.

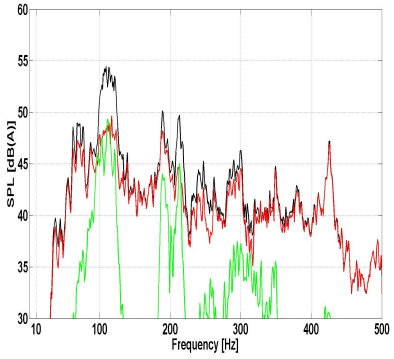

(c) Left hand rear microphone responses.

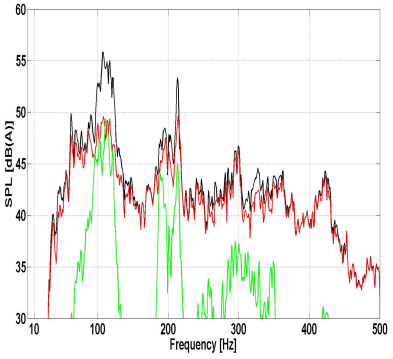

(d) Right hand right microphone responses.

FIGURE 5.3: Comparison between measured road noise spectra, synthesised/estimated with LMS and the difference between them (error signal). −: Road noise. −: Estimated front and rear subframe mount contribution. −: Estimation error.

5.6 Subframe mounts as references

In this section we use the three directions of the acceleration signals measured at the mounts at the front and rear subframe. The mounts are the last connections between the axles and the main vehicle's body, therefore they are regarded as the main structural inputs into the main vehicle structure. As it is illustrated in figures 5.4(a)-5.4(d) it is possible to capture all the dynamics that relate to low frequency road noise with the use of these reference points on the mounts. The estimation is very accurate at the road rumble, 90-120 Hz, as the subframe vibrations mainly contribute to this frequency range.

Previous studies compared the estimated performance of ARNC with adaptive filtering with the coherence-based calculation. We also perform this comparison, in order to evaluate the quality of the estimated impulse response by

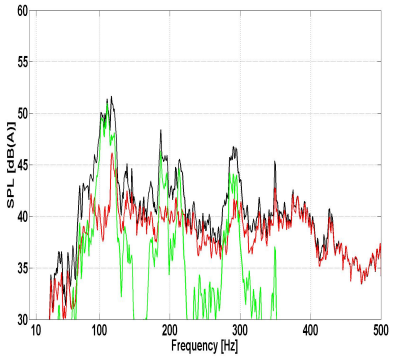

(a) Left hand front microphone responses.

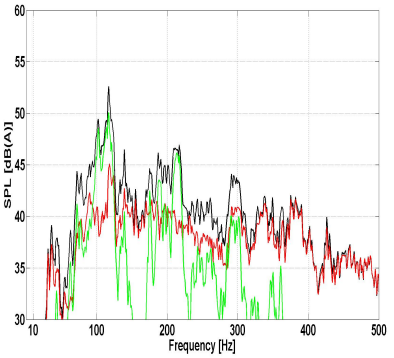

(b) Right hand front microphone responses.

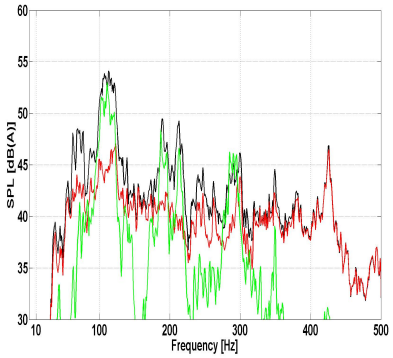

(c) Left hand rear microphone responses.

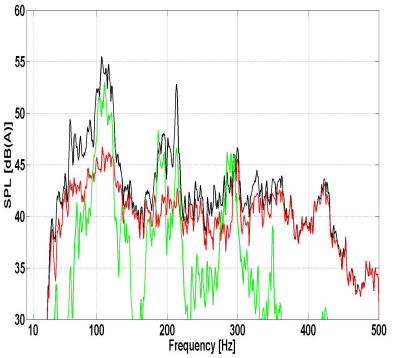

(d) Right hand right microphone responses.

FIGURE 5.4: Comparison between measured road noise spectra, synthesised/estimated with LMS and the difference between them (error signal). —: Road noise. —: Estimated front and rear subframe mount contribution. —: Estimation error.

the multireference LMS algorithm. Yet, we do not use it to predict the ARNC performance, since we aim to make more realistic prediction using MIMO ARNC systems, which we will introduce in the following chapter. It can be noticed that the adaptive algorithm is very close to the coherence predictions for this particular set of reference inputs. This is also verifies the fact that adaptive filters with very low latency can achieve reduction levels very close to the coherence predictions.

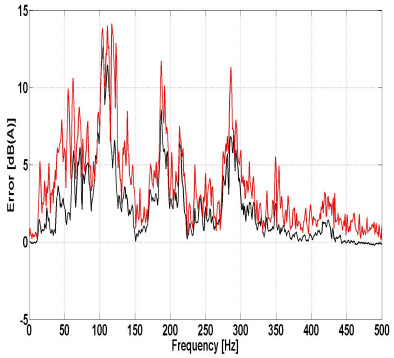

(a) Road noise cancellation for left hand front microphone.

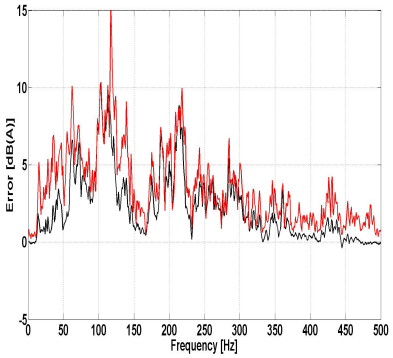

(b) Road noise cancellation for right hand front microphone.

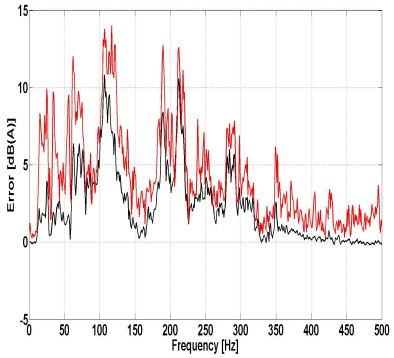

(c) Road noise cancellation for left hand front microphone.

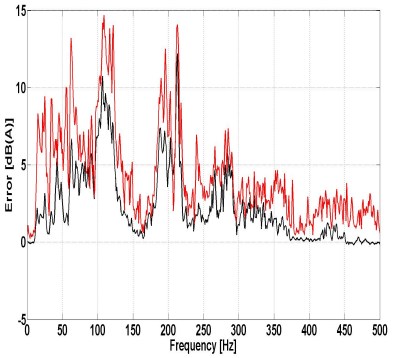

(d) Road noise cancellation for right hand front microphone.

FIGURE 5.5: Comparison between measured road noise spectra, synthesised/estimated with LMS and the difference between them (error signal). —: Road noise. —: Estimated front and rear subframe mount contribution. —: Estimation error.

5.7 Control arms and subframe mounts as references

In the final stage of this study we extend the adaptive system with the acceleration signals from the front suspension aiming to improve the estimation for the tyre cavity. From a first glimpse, it is evident that the synthesised road spectra are very similar to the measured ones, as low levels of error are obtained in figures 5.6(a)-5.6(d). Moreover, the error spectra are closer now to the ones from the coherence calculation as figures 5.7(a)-5.7(d) illustrate. This indicates that this is almost an optimal acceleration combination, as the simulation resulted into a low estimation error.

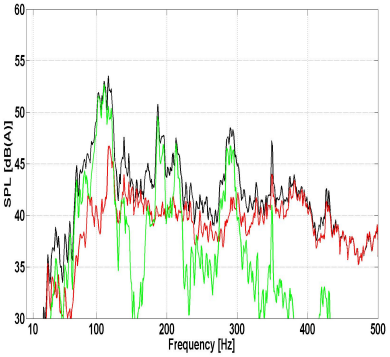

(a) Left hand front microphone responses.

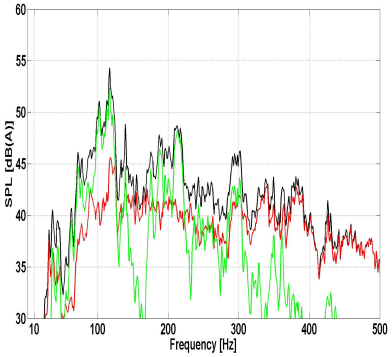

(b) Right hand front microphone responses.

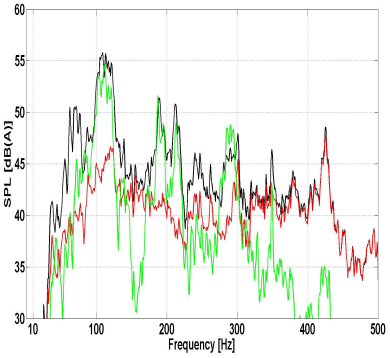

(c) Left hand rear microphone responses.

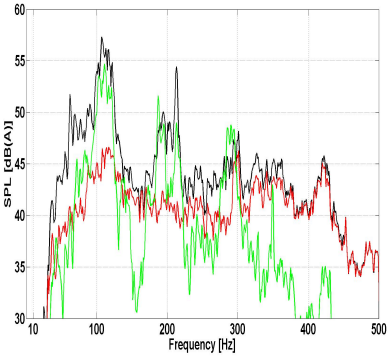

(d) Right hand right microphone responses.

FIGURE 5.6: Comparison between measured road noise spectra, synthesised/estimated with LMS and the difference between them (error signal). —: Road noise. —: Estimated front and rear subframe mount contribution. —: Estimation error.

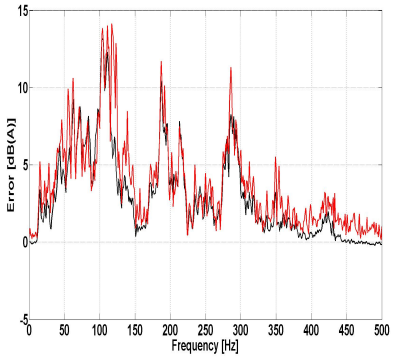

(a) Left hand front microphone responses.

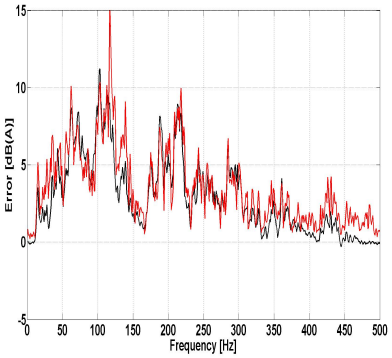

(b) Right hand front microphone responses.

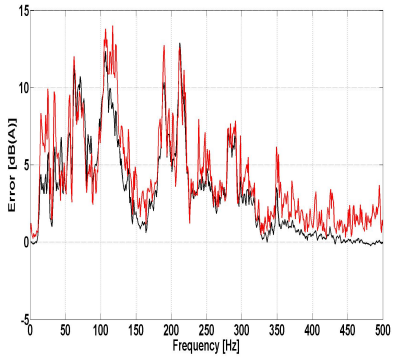

(c) Left hand rear microphone responses.

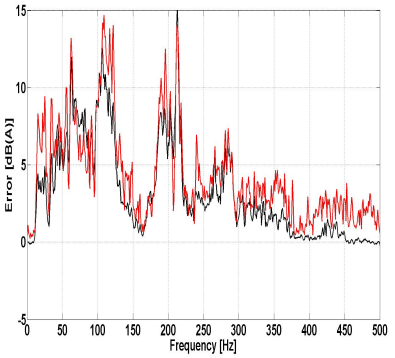

(d) Right hand right microphone responses.

FIGURE 5.7: Comparison between the estimated attenuation between the coherence limit and multireference adaptive filtering. −: Multiple coherence. −: Adaptive filtering error.

5.8 Summary

We performed a novel virtual synthesis of road noise by implementing an adaptive multireference LMS algorithm for system identification between the sensors at the vehicle's axles and the microphones mounted at the headrests. The main task of this simulation was to accurately synthesise road noise based on the most coherent structural locations of road noise. We managed to verify the origin of the road rumble, which is the rear axle and tyre cavity is mainly transmitted from the suspension arms at the front axle.

This method of synthesis of the structure-borne sound field highlights the sensitivity of the acceleration signals placed at the sources or at axle locations, when exposed at high levels of road excitation, which may offer sufficient estimation of the main road resonances. In terms of ARNC this method is useful is a useful starting tool that offers a first look at acceleration signals frequency content, since they can improve the performance of the adaptive algorithm for specific road noise bands depending on their location.

Chapter 6

Active Road Noise Control

A significant step prior to application of a real-time controller on the vehicle involves the and evaluation of the controller's performance at several accelerometer locations and directions. In this chapter we determine the fundamental adaptive algorithms for multichannel active noise control. We then, compare the reductions we achieved at different reference accelerometer locations and directions. This approach can allow to understand how locations that are essential in NVH road noise analysis, such as TPA-based methods are related to the performance of a multichannel controller, which uses the same input accelerometer locations as TPA. This could potential be advantageous, in case specific locations of the vehicle are known for their significant contribution to structure-borne road noise from TPA or other road noise NVH methods as the installation of the controller can be faster and more robust in terms of the reference sensor location. In this simulation study we examine the performance of a multichannel controller based on the geometry of the sensitive structural parts, in order to reveal the relation between the directions that are used in TPA methods. The common ground of ARNC and TPA is that both aim to synthesise accurately road noise, but with different input signals. In particular, TPA methods use force signals as inputs, whereas ARNC acceleration signals. However, both methods require measurement locations at several points on the suspension or other axle parts that are usually causing or allowing low frequency vibrations. On that basis, we will investigate most of the parts that are usually found in TPA analysis, in order to understand the physical relationship between the reference acceleration signals and the ARNC operation.

6.1 Chapter Outline

Twelve three dimensional accelerometers at twelve locations at front and rear axle were used to built up an ARNC model. In first section 6.2 the theory of multichannel adaptive feedforward controller is derived, in order to introduce the famous filtered reference LMS algorithm that is later used in the simulation study and also in the real-time system in chapter 7. Following that in section 6.4 the results of the causal time domain simulation with the use of vehicle data are analysed for estimating the potential performance of the ARNC for various combination of locations at the front and rear axles. In particular road data at high speed (100 km/h) obtained on coarse chip asphalt road are used deliberately as at this speed airbourne contributions from as wind and road noise may start to influence the microphone signals, thus the performance of the controller. However, the vibration levels are high on the accelerometer side thus most of the structure-borne sources that act on the vehicle are exciting during this drive. As a result it is a realistic scenario for simulating the controller with most of the disturbances been active and discussing the limitations of the adaptive cancelling algorithm in the last section 6.4.

6.2 Feedforward Active Road Noise Control

6.2.1 MIMO Filtered reference LMS algorithm

In the previous chapter we introduced the MISO LMS algorithm that is now extended to the MIMO filtered reference algorithm for active noise control. This algorithm and its modified versions adjusts the coefficients of the control filters in the time domain [Elliott et al. (1987), Douglas (1999)], since the adaptation can be also be performed in the frequency domain aiming to reduce the computational requirements of the algorithm for its DSP implementation [Stothers et al. (1995)].

The main difference between the multireference LMS and the filtered reference LMS is that the latter is expected to compensate for the secondary physical propagation paths between the actuators and the location where the noise or the vibration is about to be cancelled. It is worth mentioning that the same algorithm has been used for active vibration control of road noise [Dehandschutter et al. (1995), Belgacem et al. (2012)]. In our study, the secondary paths are defined from the output of the DSP controller to the microphones at the headrest

and they consist of the DAC, the reconstruction filters, the loudspeaker and the acoustic transfer fuctions to the microphones.

A multichannel feedforward system for ARNC is composed by k-reference accelerometer sensors, m-loudspeakers and l-microphones. So if the output signals of the MIMO controller are $y_m(n)$ and drive each m-transducer, the secondary estimated distrurbances at the microphone location are defined as

$$\hat{d}_l(n) = \sum_{m=1}^{M} \sum_{j=0}^{J-1} c_{lmj} y_m(n), \tag{6.1}$$

whereas the reduced sound pressure signal at the l-microphone is the difference between the estimate of the estimated disturbance $\hat{d}_l$ and the actual primary road noise d_l

$$e_l(n) = \hat{d}_l(n) - d_l(n). \tag{6.2}$$

The adaptive controller is required to compensate for the impulse response c_{lm} ,as demonstrated in adaptive inverse control in the special case of the FxLMS algorithm [Widrow and Walach (2008)]. The extension of the FxLMS algorithm for multi-reference signals is presented according to the derivation in [Elliott (1998), Elliott (2000b)]. The adaptation stage can become quite complicated compared to the multireference LMS algorithm for system identification. Moreover, the control filtering stage requires $M \times K$ convolutions for generating the canceling signals that are summed over the K-references for driving each M-loudspeaker

$$y_m(n) = \sum_{k=1}^{K} \sum_{i=0}^{I} w_{mki} x_k(n-i), \tag{6.3}$$

where the output signal at each l-microphone is the spatial summation of the refererence signals, x_k, which are inputs to the controller multiplied by the control filters coefficients w_{mki} and the sum of the controller's output multiplied with electro-acoustic paths c_{lm}

$$e_l(n) = d_l(n) + \sum_{m=1}^{M} \sum_{j=0}^{J-1} \sum_{k=1}^{K} \sum_{i=0}^{I-1} c_{lmj} w_{mki} x_k(n-i), \tag{6.4}$$

where the filtered reference signals derived from the convolution between the estimated impulse responses of the secondary plants between the M-loudspeakers

and the L-microphones

$$r_{lmk}(n) = \sum_{J=0}^{J-1} \hat{c}_{lmj} x_k(n-j), \tag{6.5}$$

and the vectors of the filtered reference signals are defined as

$$\mathbf{r}_l(n) = \begin{bmatrix} r_{l11}(n) & r_{l12}(n) & \dots & r_{l1K}(n) & r_{l21}(n) & \dots & r_{lMK}(n) \end{bmatrix}^T \tag{6.6}$$

and the control filters w_{mki} are adapted for each sample as follow

$$w_{mki}(n+1) = w_{mki}(n) - \alpha \sum_{l=1}^{L} e_l(n) r_{lmk}(n). \tag{6.7}$$

The *filtered reference LMS* is the topic of interest in a plethora of books and publications and it is commonly acknowledged as the main algorithm for active noise control applications [Hansen (2013), Elliott (2000a)]. A version of the MIMO filtered reference algorithm with IIR filters for the control filtering part of the algorithm has been presented by Melton and latter tested real-time in a reverberant room by Laugesen [Melton and Greiner (1992), Laugesen and Elliott (1993), Hansen (2013)]. However, careful design of the algorithm is necessary, as IIR filters are more sensitive to instability.

With regards to the computational complexity of the multichannel algorithms, Douglas has proposed modified versions of filtered reference LMS with a smaller number of calculations than the standard time-domain algorithm [Douglas (1999)]. However, the only algorithm that achieves high reduction in the required convolutions has been developed by Lotus [Stothers et al. (1995)]. In the special case of partially correlated reference signals the algorithm can be modified by prefiltering of the reference signals in order to decorrelate the signals as it shown in [Elliott and Cook (2000), Bai and Elliott (2004)]. In practice, this filtering adds more computation in inside the DSP processor. With that in mind, in our work we consider only the standard filtered-reference LMS.

Equation 6.7 can be also written in a more compact manner through matrix formulation [Elliott (2000a), Elliott (2000b)]

$$\mathbf{w}(n+1) = \mathbf{w}(n) - \alpha \hat{\mathbf{R}}^T(n) \mathbf{x}(n), \tag{6.8}$$

where $\hat{\mathbf{R}}^T(n)$ is a matrix that contains the filtered reference signals and is defined as

$$\mathbf{R}(n) = \begin{bmatrix} \mathbf{r}_1^T(n) & \mathbf{r}_1^T(n-1) & \mathbf{r}_1^T(n-2) & ... & \mathbf{r}_1^T(n-I+1) \\ \mathbf{r}_2^T(n) & \mathbf{r}_2^T(n-1) & \mathbf{r}_2^T(n-2) & ... & \mathbf{r}_2^T(n-I+1) \\ \mathbf{r}_3^T(n) & \mathbf{r}_3^T(n-1) & \mathbf{r}_3^T(n-2) & ... & \mathbf{r}_3^T(n-I+1) \\ ... & ... & ... & ... & ... \\ \mathbf{r}_L^T(n) & \mathbf{r}_L^T(n-1) & \mathbf{r}_L^T(n-2) & ... & \mathbf{r}_L^T(n-I+1) \end{bmatrix}, \tag{6.9}$$

and the vector of the FIR control filter taps is

$$\mathbf{w}(n) = \begin{bmatrix} w_0^T & w_1^T & ... & w_{I-1}^T \end{bmatrix}^T. \tag{6.10}$$

The minimum value that reduces the following cost function optimum

$$\mathbf{w}(n+1) = \mathbf{w}(n) - \alpha \hat{\mathbf{R}}^T(n)\mathbf{x}(n), \tag{6.11}$$

produces the optimum Wiener filter solution, which is calculated by multiplying the inverted correlation matrix of the filtered reference signals with the cross-correlation matrix between the filtered reference signals and the disturbances

$$\mathbf{w}_{opt}(n) = E\{[\mathbf{R}(n)\mathbf{R}(n)]\}^{-1} E\{[\mathbf{R}(n)\mathbf{d}(n)]\} \tag{6.12}$$

In practice ,methods for inverting the correlation matrix of size $MKI \times MKI$ are necessary, thus adaptive methods are preferable in practice ,since they can provide realisable filters that can be implemented into a DSP system.

The same algorithm can be modified by filtering the error signals $e_l(n)$ instead of the references x_k, in order to reduce the computational requirements [Wan (1996),Elliott (1998)]. This algorithm is usually referred as *adjoint LMS* or *filtered-error LMS* and the equation that updates the coefficients of the adaptive filters is now based on the cross-correlation between the filtered error signals f_m and the references x_k

$$w_{mki}(n+1) = w_{mki}(n) - \alpha x_k(n) f_m(n+i). \tag{6.13}$$

where the filtered error signals can be found from the filtering of the error signals $e_l(n)$ of the electro-acoustic paths c_{lm}

$$f_m(n) = \sum_{l=1}^{L} \sum_{j=0}^{J-1} c_{lmj} e_l(n-j) \tag{6.14}$$

Both the filtered reference LMS and the filtered error may take place the adaptation stage in the frequency domain and the new filter coefficients into the time domain with the use of inverse FFT transform. In this way, the controlling filtering part of the algorithm can still take place in the time domain without introducing the delays of the FFT blocks, which are essential in frequency domain calculations [Elliott (2000a)].

Lotus Engineering have developed and also patented the filtered error LMS in the frequency domain [Stothers et al. (1995), Stothers (1997)]. The main benefit of this algorithm is that compared to the time domain version it reduces the calculations of the algorithm significantly. This requires a great number of calculations of the cross-correlation between the reference signals x_k and the filtered error signals f_m. The equation that updates the filter coefficients of the FIR filters of the filtered reference LMS in the time domain, but performs the rest of the calculations in the transformed domain is the following

$$w_{mki}(n+N) = w_{mki}(n) - \alpha IFFT\{\sum_{l=1}^{L} R^*_{lmk}(k) E_l(k)\}., \tag{6.15}$$

and the filtered error LMS algorithm in the frequency domain can be expressed as

$$w_{mki}(n+N) = w_{mki}(n) - \alpha IFFT\{F_m(k) X^*_k(k)\}. \tag{6.16}$$

Rafaely has provided detailed information about the derivation of frequency domain adaptive algorithms in [Rafaely and Elliot (2000)]. Subband adaptive filters have become an research area over the past years, as they focus on algorithms on adaptive noise cancellation (especially for acoustic enviroments where the control needs to identify long impulse responses) [Qiu et al. (2006)]. However, studies have reported several issues with phase distortion in multiband filtering [Milani et al. (2009)]. Therefore, the fundamental filtered reference LMS was used in the modeling process of the ARNC system.

6.3 Active Road Noise Control strategy

In this simulation study we use the acceleration signals from sensitive structural locations in terms of road inputs. These signals are also used in TPA and other road noise analysis methods, such as operational modal analysis [Meillier and Mairesse (1996), Wyckaert and Van der Auweraer (1995)]. The data were recorded on a rough road, in order to ensure that main road resonances are captured. The diagram figure 2.18 illustrates the relationship between the TPA and ARNC is presented. It can be noticed that both methods reconstruct the road noise signals, still they use input signals. The measurement locations of TPA are typically mounting points, suspensions links and suspension dampers, which in this case also used to control of the recorded interior road noise signals. Heatwole showed that specific parts of the front and rear axle are effecting the performance controller depending on the vehicle [Heatwole et al. (1993), Heatwole and Bernhard (1994)]. This is somehow expected, given that the axle design changes depending on the targeted performance for vehicle dynamics. The same parts are also used in the NVH tuning of structure-borne road noise. Mechanical components, such as suspension dampers and subframe mounts are usually designed to block road forces and isolate the axles from the body, so that vibrations, which can cause road noise, are not transmitted into the cabin.

6.4 Comparison of reference sensor number and location

At this point we should out the importance of simulating and evaluating sensor locations in accordance with the architecture of the vehicle axles. To the best of our knowledge such a study has not taken place before, thus it is essential to improve the level of understanding between the structural dynamics at crucial mechanical parts of the axles and their effects upon the performance of an ARNC. The locations of these parts are usually used for TPA and also for tuning the local dynamic stiffness, which makes them the unique paths of structure-borne road noise transmission. In our study we performed various simulations that are based on these strategic locations. It should be noted that at an earlier stage of our research we already investaged these locations using coherence analysis (presented in chapter 4). Through our analysis we observed that some vibro-acoustic paths provide coherence value more than 0.5. The time recordings of these accelerometer locations are now used as reference signals to a multichannel feedforward system built in a Matlab/Simulink environment, with including

also the impulse responces of the paths from the loudspeakers to the headrest microphones.

6.5 Simulink model of ARNC

The Matlab environment offers Simulink, as a method for control system design and simulation. Simulink is a graphical programming languange for modelling dynamic. Signal processing algorithms can also be developed and compiled in C, which is especially useful for real-time systems and DSP processors. With that in mind, the first step involved the simulation of the algorithms as it is presented in this chapter, whereas as a second step we compiled it for an Analog Devices DSP processor that is embedded in the multichannel controller. In this way, we developed a system for road noise acquisition and control as we will see later in chapter 7.

Figure 6.1 illustrates the main parts of the algorithm. One of the main advantages of simulating a DSP system in Simulink is that its states are calculated in each time-step that is set before the simulation, but also for a specific time-span. In our case the time-step is the sampling rate of the recorded signals and the time-span is in fact, the time duration of the recording. Generally speaking, this type of modelling is preferable by modern control systems, as they expect a specific time response or processing time. Both these factors are critical, since model in a purely frequency domain modelling may result into non-causal filtering. Each Simulink block contains a specific signal processing process that is performed in each time step in this case as the model must simulate a real-time algorithm that is based on sample by sample calculations. The delays from the electro-acoustic are therefore significant in this type of simulation compared to causally uncostrained noise reduction predictions based purely on multiple coherence of section 4.3.2, which may overestimate the performance of the controller.

6.5.1 One directions reference signals

In this simulation study we initiate the controller with reference signals at the z-direction. The underlying reason behind choosing the z-axis is the fact that this direction is generally the main transfer direction of vibrations of the suspension [Wang (2010)]. Therefore we will initiate our study with vibrations coming the subrame and suspension points and only the z-axis.

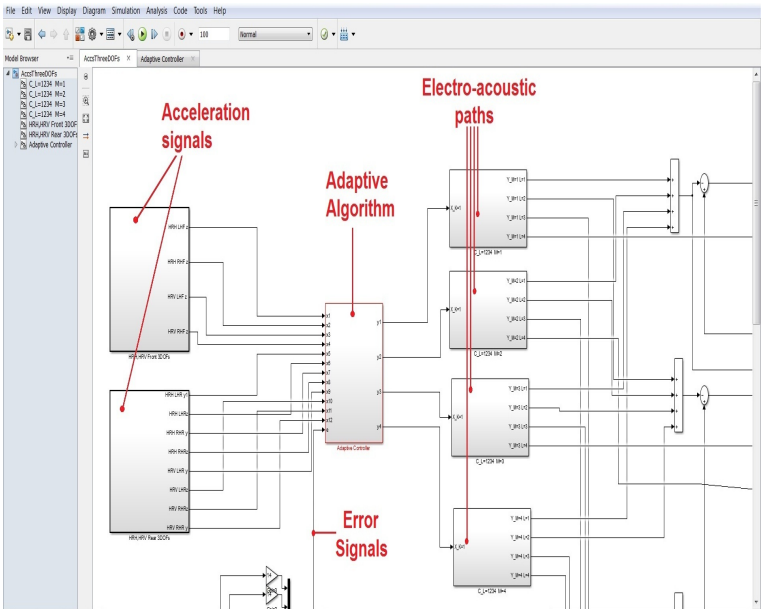

FIGURE 6.1: Simulink model for simulation and prediction of ARNC systems.

6.5.1.1 Case 1: Subframe mounts z-axis

The first case evaluates the four subframe mounting points of the front axle combined with also four mounting locations at the rear axle. As far as the directions are concerned, only the acceleration signals that come from the *z*-direction at the front and rear subframe mounts are used in this case, as illustrated in figure 6.2.

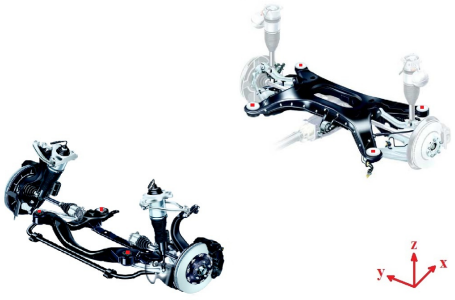

FIGURE 6.2: The locations of the accelerometers in the vehicle structure and the directions of the reference signals. ■: One direction.

Overall, eight reference signals are fed into the adaptive algorithm. The acceleration signals of the z-direction help the ARNC system to reduce by 5 dB(A) the noise levels at the tyre cavity range between 90-220 Hz, a fact that is evident in figures 6.3(a) - 6.3(d). It also help the controller to attenuate the road noise levels for a resonance at 290 Hz for the left hand front microphone. The rumbe is attenuated by at least 5 dB(A) at the driver's headrest and also of the headrest at the right hand rear seat,yet it is less than 4 dB(A) in the other microphones across the rumble range. This is apparent at the co-driver's

headrest, where only some part of the rumble resonance is removed. It is likely that more directions are necessary to use as references for noise reduction at the rumble band behind the co-driver's head.

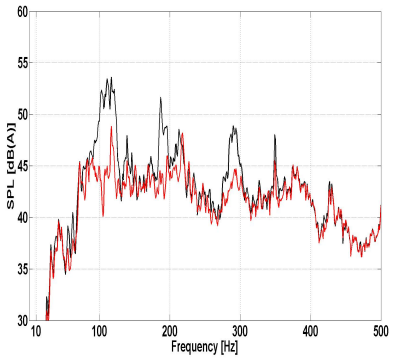

(a) Left hand front microphone response.

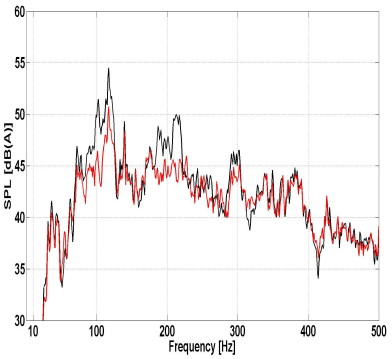

(b) Right hand front microphone response.

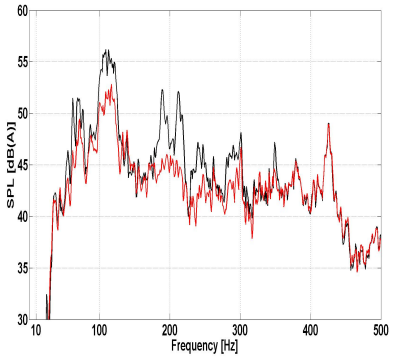

(c) Left hand rear microphone response.

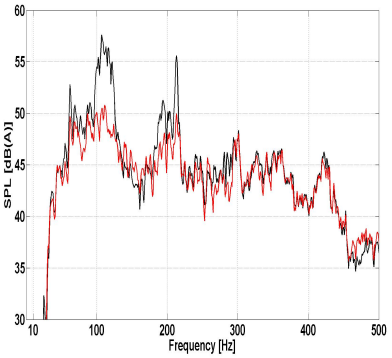

(d) Right hand rear microphone response.

FIGURE 6.3: Interior noise at the four headrests. −: ARNC off. −: ARNC on.

The average noise reduction of the controller in the range 0-500 Hz is slightly more than 2 dB(A) across the four microphones. The highest reduction is observed at the right hand front microphone with 2.8 dB(A) of active reduction in the road noise range.

LHF dB(A)	RHF dB(A)	LHR dB(A)	RHR dB(A)	Average dB(A)
2.4	1.5	2.3	2.4	2.2

TABLE 6.1: Total reduction for 0-500 Hz. LHF: Left hand front, RHF: Right hand front headrest, LHR: Left hand rear, RHR: Right hand rear.

6.5.1.2 Case 2: Subframe mounts and suspension z-axis

The set of the acceleration signals from the z-direction at the subframe mounts of the rear axle is maintained as shown in figure 6.4, but only two symmetrical locations at the front suspension, which observe the vibrations of z-axis, are now included in the ARNC model. Consequently, six acceleration signals are used as reference inputs to the feedforward controller. It must be pointed out that this is relatively low for an ARNC application, since several structure-borne sources are expected to be observed by the controller. The locations at the front axle are in fact rathen close to the wheel located at the lower control arm of the suspension. Therefore sufficient control of tyre cavity resonances should be easier to achieved easier.

FIGURE 6.4: The locations of the accelerometers in the vehicle structure. ■: One direction reference signals.

This change in the acceleration signal set may have implications on the controller's performance at other frequencies in the rumble range. For example, in figures 6.5(a) and 6.5(b) the reduction at the rumble of the front headrests is very limited. This may be due to the fact that there is some contribution from the front axle that is not fed into the controller as input, thus it remains uncontrolled. Interestingly, the reduction levels at the tyre cavity do not improved and the midfrequency resonance at 290 Hz is unattenuated for all the noise spectra.

The general poor performance affects on the total reduction for each headrest location, which becomes less than 2 dB(A). Still, the improvements are greater than to the trade-offs of other NVH control methods, especially the improvements in the right hand rear microphone of the rumble. Still, they are attractive enough fto turn the implementation of this echnology into a vehicle worthwhile.

The total reduction levels in all the microphones are poorer than the ones of the previous accelerometer configurations. As a matter of fact, only 1.6 dB(A) is the average attenuation across the four headrests.

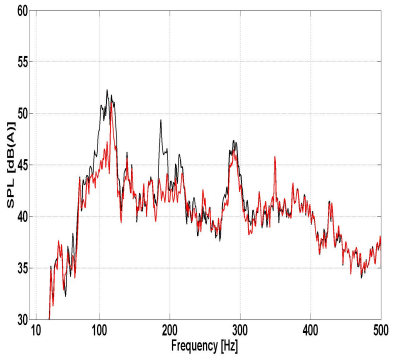

(a) Left hand front microphone response.

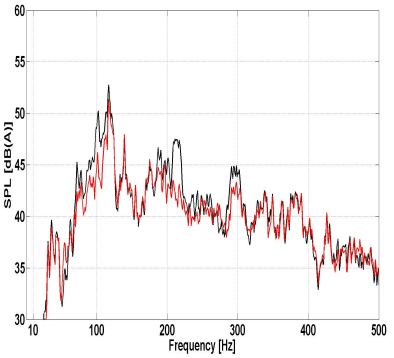

(b) Right hand front microphone response.

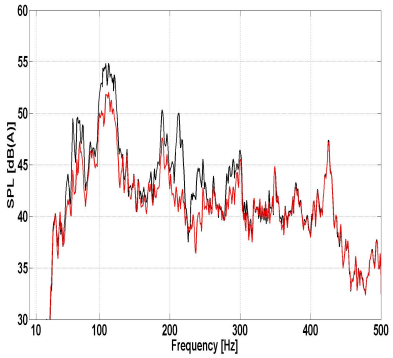

(c) Left hand rear microphone response.

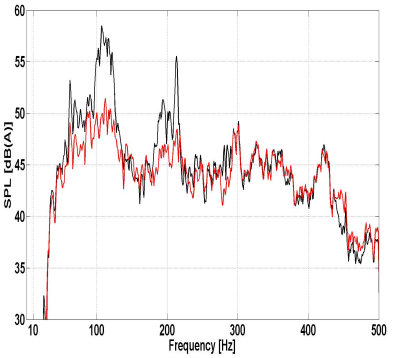

(d) Right hand rear microphone response.

FIGURE 6.5: Interior noise at the four headrests. −: ARNC off. −: ARNC on.

LHF dB(A)	RHF dB(A)	LHR dB(A)	RHR dB(A)	Average dB(A)
1.5	1.2	2.1	2.5	1.8

TABLE 6.2: Total reduction for 0-500 Hz. LHF: Left hand front, RHF: Right hand front headrest, LHR: Left hand rear, RHR: Right hand rear.

6.5.1.3 Case 3: Subframe mounts and suspension dampers z-axis

An important part of multilink suspension systems in road noise NVH is the top of suspension at the z-direction [Wang (2010)], where high road forces are usually applied. It is worth to investigate how this road noise input location can help the active systems control the rumble. In this case, only two symmetrical subframe mounts are used as displayed in figure 6.6. Apart from the top mount of the suspension strut also the bottom mounting point is also included for the front axle, thus in total ten reference signals were used for this case. The attenuation is slightly improved, especially for the front microphones in figures 6.7(a)-6.16. At the rear part of the cabin, the atternuation is improved at the tyre cavity range 180-220 Hz, but worse at the rumble of the microphone at

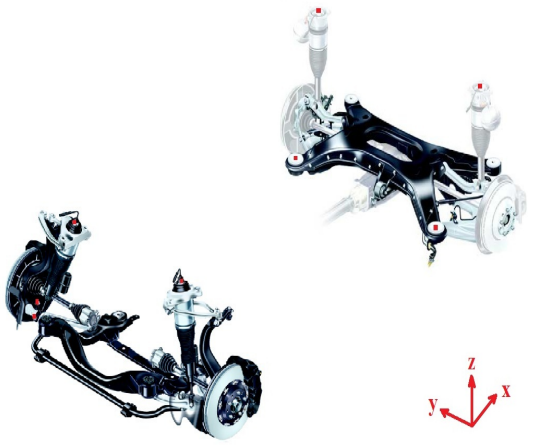

FIGURE 6.6: The locations of the accelerometers in the vehicle structure. ■: One dimensional accelerometers.

the left headrest. This change in the control focus deals with the fact that the acceleration singals at the front axle are close to the wheel, hence they should include spectral components that are related to tyre cavity noise. On the other hand, they do not contain any components that relate to the rumble range and also the midfrequency resonance at 290 Hz that appears at the front headrests. The limited performance of the controller is somehow expected, as they are far from the actual structural sources that cause these two road resonances at the interior noise spectra. In the following cases, we will not use the suspension damper locations anymore, since apparently they do not offer any significant improvements.

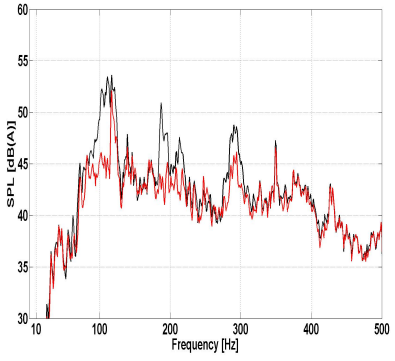

(a) Left hand front microphone response.

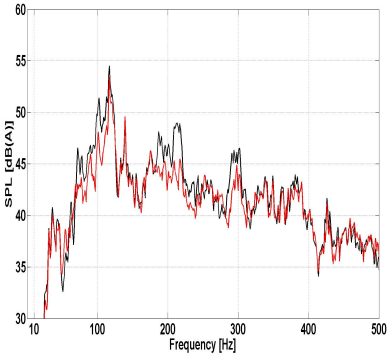

(b) Right hand front microphone response.

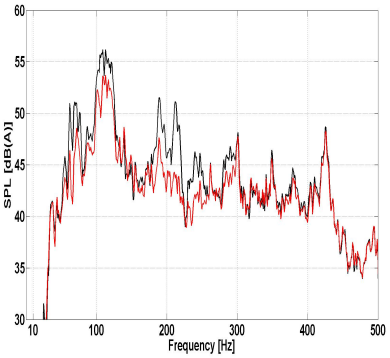

(c) Left hand rear microphone response.

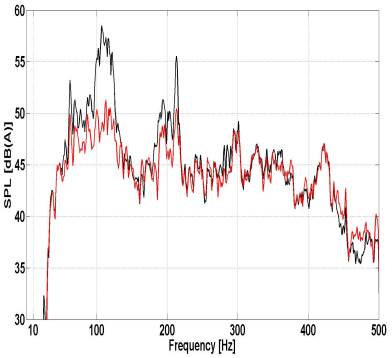

(d) Right hand rear microphone response.

FIGURE 6.7: Interior noise at the four headrests. −: ARNC off. −: ARNC on.

In comparison with the previous scenario, the total reduction levels are improved. More specifically, 2 dB(A) in the frequency range of 0-500 Hz are removed.

LHF dB(A)	RHF dB(A)	LHR dB(A)	RHR dB(A)	Average dB(A)
2.1	1.3	2.0	2.7	2.0

TABLE 6.3: Total reduction for 0-500 Hz. LHF: Left hand front, RHF: Right hand front headrest, LHR: Left hand rear, RHR: Right hand rear.

6.5.1.4 Case 4: Subframe rear mounts z-axis

In this case we further reduce the number of references with four acceleration signals coming from the z-direction the front subframe mounts of each axle. We already discovered that the front suspension part, e.g. the dampers and the control arms, do not improve in the performance.

This case is comperable with the first case 6.5.1.5, in which eight signals from the mounts were the reference inputs to the controller. Figure 6.8 presents the four locations at the front mounting points of the vehicle subframes, whereas figures 6.9(a)-6.9(d) present the corresponding spectra before and after ARNC.

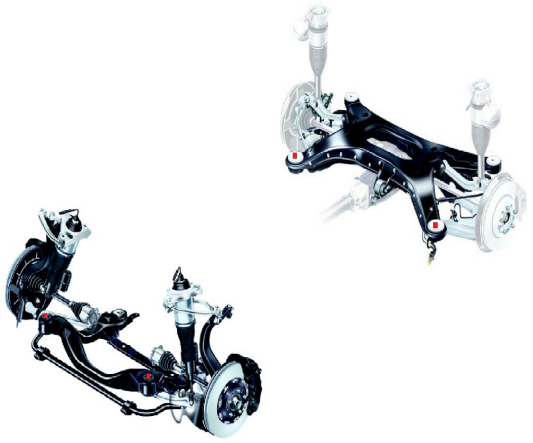

FIGURE 6.8: The locations of the accelerometers in the vehicle structure. ■: One dimensional accelerometers.

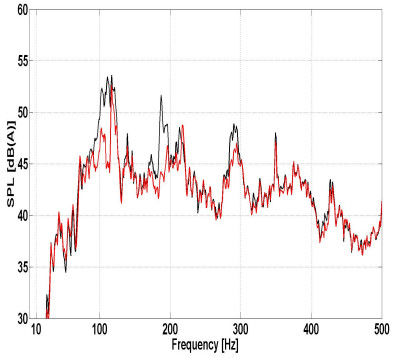

(a) Left hand front microphone response.

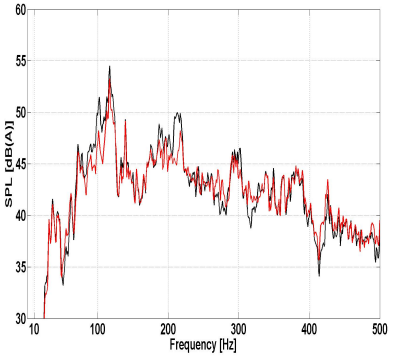

(b) Right hand front microphone response.

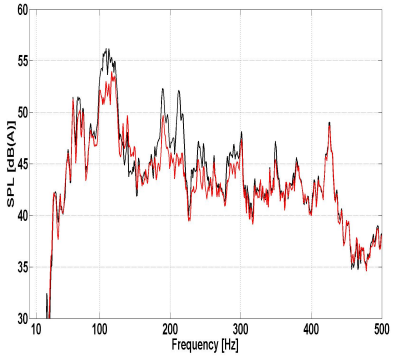

(c) Left hand rear microphone response.

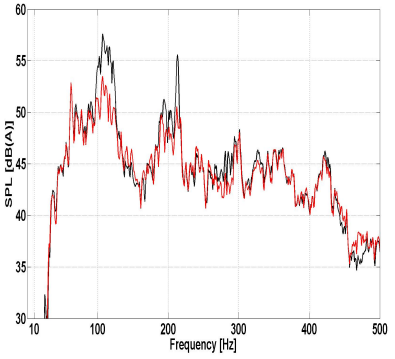

(d) Right hand rear microphone response.

FIGURE 6.9: Interior noise at the four headrests. −: ARNC off. −: ARNC on.

The performance is rather limited and effective only at the rumble range, 90-120 Hz. Some minor reductions can be seen in case in the left hand side microphones for the first tyre cavity resonance at 180 Hz. In addition to the limited success of this configuration, the total reduction level is only 1.4 dB(A) across

the microphones. It is becoming apparent that more directions are necessary to improve the active reduction levels of the system.

LHF dB(A)	RHF dB(A)	LHR dB(A)	RHR dB(A)	Average dB(A)
1.5	0.8	1.5	1.6	1.4

TABLE 6.4: Total reduction for 0-500 Hz. LHF: Left hand front, RHF: Right hand front headrest, LHR: Left hand rear, RHR: Right hand rear.

6.5.1.5 Case 5: Suspension and subframe only z-axis

In the final case of our investigation into one-dimensional signals, we emply sixteen measurement locations distributed across the axles at the z-dimension. As a consequence, this sensor arrangement is almost equivalent to map the axle vibrations of the whole vehicle in one axis. In return, all structure-borne sources should be now observable by the controller.

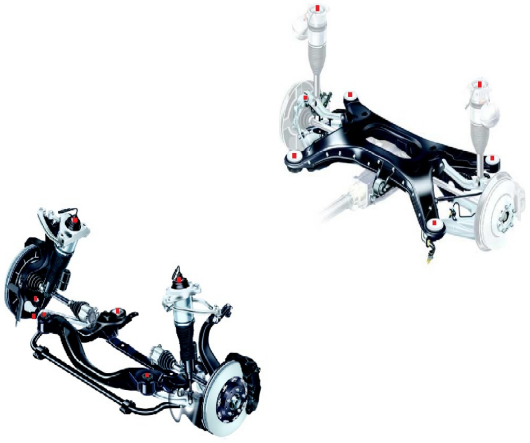

FIGURE 6.10: The locations of the accelerometers in the vehicle structure. ■: One dimensional accelerometers.

The increase in the acceleration signal number causes a drastic improvement in the ARNC performance. The controller can now reduce road noise up to 300 Hz. The noise levels at the second tyre cavity resonance are attenuated by 10 dB(A) at the rear headrests. Overall, the structure-borne road noise is attenuated by 3 dB(A) on average across the four headrests, from 0 to 500 Hz. If we now compare table 6.1 of the eight reference with the table 6.5, then it can be concluded that doubling the number of the reference signals at one direction can improve the reduction by 1 dB(A). An ARNC controller with a high number of references can significantly effect the specifications for its DSP implementation.

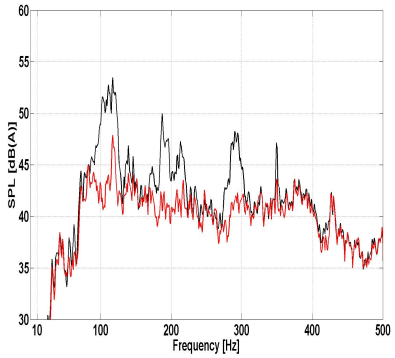

(a) Left hand front microphone response.

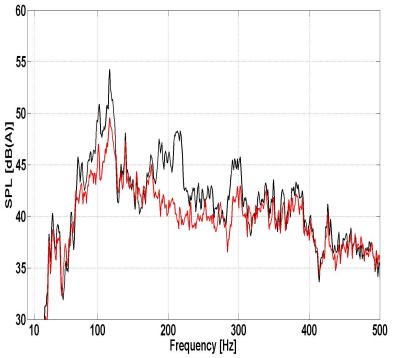

(b) Right hand front microphone response.

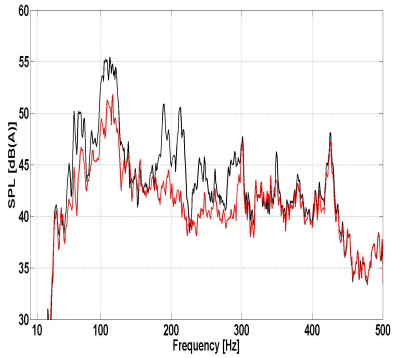

(c) Left hand rear microphone response.

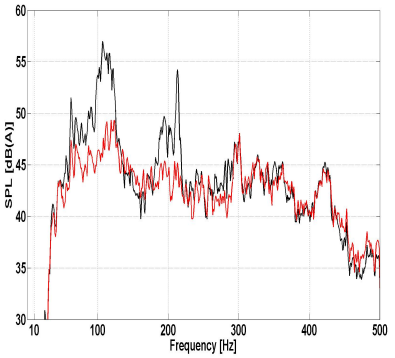

(d) Right hand rear microphone response.

FIGURE 6.11: Interior noise at the four headrests. −: ARNC off. −: ARNC on.

It is questionable if such a large system is necessary for achieving 1 dB(A) improvement compared to the case in section 6.5.1.3, where less sensor locations were used. With that in mind, we will continue our investigation into finding optimum set of signals can achieve between 2-3 dB(A) across each headrest with a maximum number references twelve input signals for the controller.

LHF dB(A)	RHF dB(A)	LHR dB(A)	RHR dB(A)	Average dB(A)
3.3	2.4	3.0	3.2	3.0

TABLE 6.5: Total reduction for 0-500 Hz. LHF: Left hand front, RHF: Right hand front headrest, LHR: Left hand rear, RHR: Right hand rear.

6.5.2 Two directions reference signals

Up until now, we have analysed the results of ARNC models based on single DoF reference signals. Only structure-borne noise contributions related to vibrations at the z-direction were mostly attenuated by the control system. in the following cases we will increase the complexity of the system with one more directions, the y-dimension. In this way, we are able to investigate, whether there are any significant benefits when more DoF are used as reference inputs.

6.5.2.1 Case 7: Front mounts z-axis and rear subframe rear mounts y,z-axis

Among the different case we have explored up until this point, the one with the best acceleration signal set with eight references measured at the z-directions at the eight subframe mounting locations was found for case in section 6.5.1.1. If we consider two directions y, z-direction for the mounts at the rear subframe, significant improvements can be obtained from 0-300 Hz for the rear headrests as illustrated in figures 6.13(c)-6.13(d). Twelve reference signals were used in total to make this ARNC prediction, which illustrates that an improvement at the rumble range for the rear headrests with the addition one extra DoF from the rear axle vibrations can be obtained.

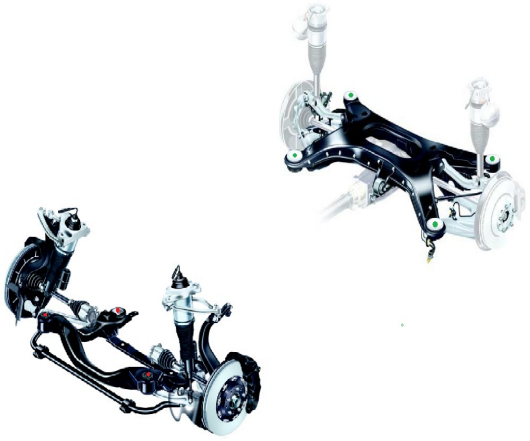

FIGURE 6.12: The locations of the accelerometers in the vehicle structure. ●: One direction reference signals. ■: Two directions reference signals.

The control is mostly effective up to 200 Hz for the rear headrests, but up to 300 Hz can for the front seats. The overall attenuation is slightly higher on the right side of the vehicle, while the right hand rear headrest has the highest reduction level at 3 dB(A) from 0 to 500 Hz.

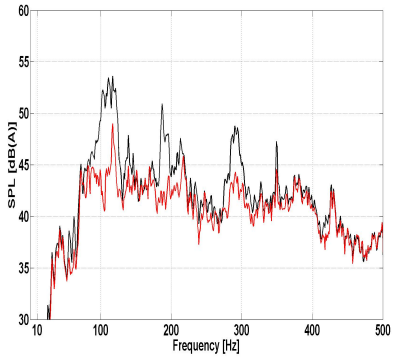

(a) Left hand front microphone response.

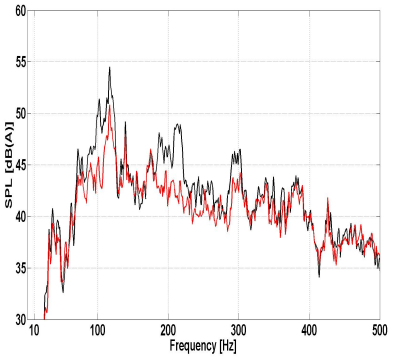

(b) Right hand front microphone response.

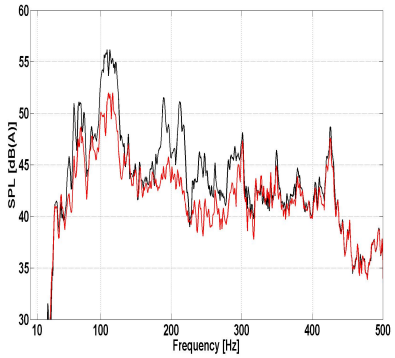

(c) Left hand rear microphone response.

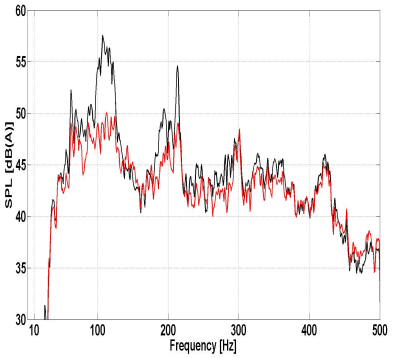

(d) Right hand rear microphone response.

FIGURE 6.13: Interior noise at the four headrests. −: ARNC off. −: ARNC on.

On average 2.8 dB(A) can be obtained from this reference signal combination. By comparing the total reductions of table 6.7 with the first one in table 6.1, which used one direction and the same locations, the y-direction provides very small improvements and only at the right hand side headrests.

LHF dB(A)	RHF dB(A)	LHR dB(A)	RHR dB(A)	Average dB(A)
2.9	2.1	2.9	3.0	2.8

TABLE 6.6: Total reduction for 0-500 Hz. LHF: Left hand front, RHF: Right hand front headrest, LHR: Left hand rear, RHR: Right hand rear.

6.5.2.2 Case 8: Front mounts y,z-axis and rear subframe rear mounts z-axis

In this case, the y-direction for the front axle mounts is also included (figure 6.14), aiming to emphasise once again the control at the front axle. We previously observed that the tyre cavity and the midfrequencies are harder to control,

as multiple paths are allowing their transmission through the front axle compared to the rumble. This also implies that it is harder to decompose the road noise dynamics at the front axle and advanced algorithms for decorrelating the reference signals have been suggested for improving several characteristics of the feedforward system such as decoupling the reference inputs and thus improving the coherence between the vibrational and acoustical sensors [Akiho (1995), Elliott and Cook (2000), Dehandschutter and Sas (1998), Bai and Elliott (2004)]. Despite the use of these algorithms, vibration signals that are close to the structural sources are still necessary, in order to achieve high SNR in the measured acceleration signals that contain several road resonances. Therefore the need for decomposing and uncorrelating the vibration singals may be only benificial in the case of faster convergence of the adaptive algorithm [Bai and Elliott (2004)].

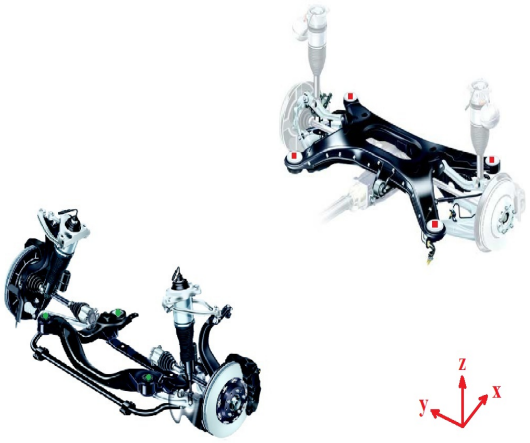

FIGURE 6.14: The locations of the accelerometers in the vehicle structure. ■: One direction reference signals. ●: Two directions reference signals.

Instead of increasing the complexity of the algorithm, we augment the controller with four extra signals at the y-direction from the mounts of the front subframe. Decorrelation filtering of the reference signal actually requires extra filtering before the signals are fed into the algorithm as suggested by reveral researchers [Bai and Elliott (2004), Tu and Fuller (2000)].

The attenuation is slightly impoved at the rumble range for the front headrests compared to the results from the previous section. Tyre cavity resonances are also better controlled as the filtered references and error signals are well correlated by the addition of acceleration signals. It is becoming more evident that contributors of the front axle are hard to be identified by the system if more directions are not included. However, the subjective levels of improvement will not be perceivable for this level of improvements for the front axle.

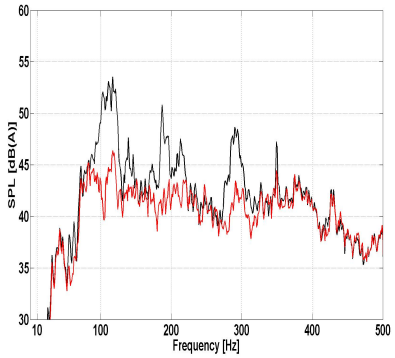

(a) Left hand front microphone response.

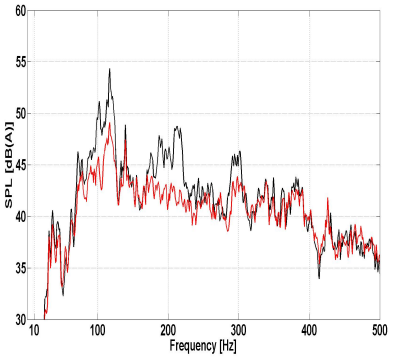

(b) Right hand front microphone response.

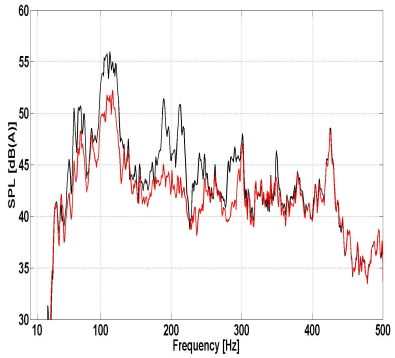

(c) Left hand rear microphone response.

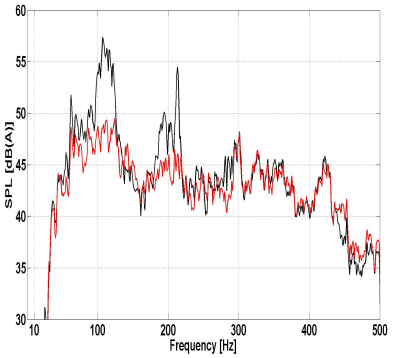

(d) Right hand rear microphone response.

FIGURE 6.15: Interior noise at the four headrests. −: ARNC off. −: ARNC on.

The active attenuation levels at the rear microphones are now slightly reduced and 2.7 dB(A) are removed from all the four headrests.

LHF dB(A)	RHF dB(A)	LHR dB(A)	RHR dB(A)	Average dB(A)
3.1	2.2	2.7	2.9	2.7

TABLE 6.7: Total reduction for 0-500 Hz. LHF: Left hand front, RHF: Right hand front headrest, LHR: Left hand rear, RHR: Right hand rear.

6.5.2.3 Case 9: Front suspension y, z-axis and rear subframe rear mounts z-axis

In section 6.5.1.2 we used acceleration signals at the z-direction that were recorded at front suspensions lower control arms. In this case we include also the y-axis of these suspension points, in order to investigate the level of improvement we

can obtain from these locations. The single direction signals of the front suspensions in section 6.5.1.2 were not able to help the system attenuate the road noise efficiently, especially at the front headrests.

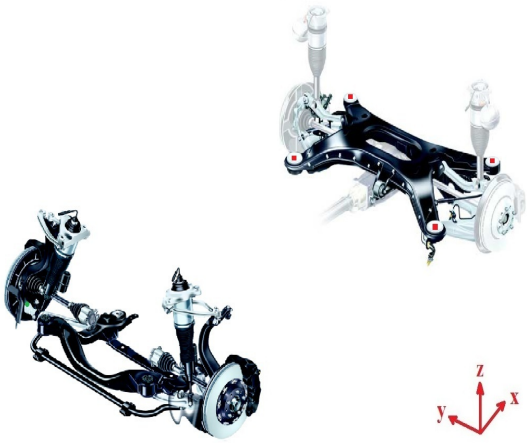

FIGURE 6.16: The locations of the accelerometers in the vehicle structure. ●: One direction reference signals. ■: Two DoF reference signals.

In figure 6.17(a) only a narrow part of the road rumble is attenuated. The first tyre cavity resonance is only canceled and the 290 Hz resonance is completely uncontrolled. In contrast to this the noise at right hand side headrest is attenuated by 5 dB(A) at the rumble and tyre cavity range, but the level of the midfrequency resonance at 290 Hz is still not reduced by the system. This is very likely to occur again if the right reference signal are not feed into the feedforward system.

The control at the left hand rear microphone is relatively limited between 2-4 dB(A) across 90-120 Hz. Interestingly, the effectiveness of the control is noticeable up to 300 Hz, whereas in the case of the left hand front headrest it was limited to 190 Hz. The combination of two directions at the front axle and one at the rear has a great effect on the ARNC performance at the front microphones as figures 6.17(a) and 6.17(b) illustrate. In particular, the reduction is around 5-7 dB(A) across 100-290 Hz for the front headrests. As for the rear headrests, high levels of reductions are obtained; between 90-200 Hz for the right hand microphone with almost 10 dB(A) been removed from the second tyre cavity resonance at 213 Hz. The controller with a reference signal set can potentially achieve reductions of 3 dB(A) across the road noise range. The only microphone that is difficult to control is the one located at the left hand rear, which is very likely to be affected by airborne contributions coming from the trunk. This happens because sound insulation material from the left hand rear wheel arches is necessary for blocking the low frequency airborne contribution. On that side of the vehicle the oil tank creates an opening that allows airborne transmission straight from the left hand rear tyre. More details on this will not

be revealed in this thesis due to a confidentially agreement with Bentley Motors. However, this problem highlights some limitations of the ARNC system that emerge when contributions from other NVH sources are not effectively attenuated in the frequency range of structure-borne road noise. The reduction levels are

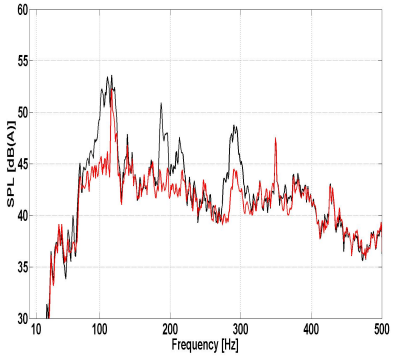

(a) Left hand front microphone response.

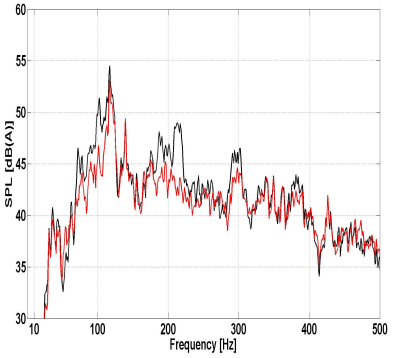

(b) Right hand front microphone response.

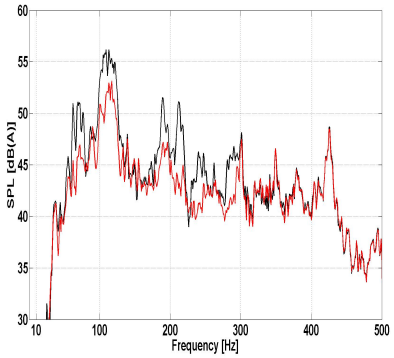

(c) Left hand rear microphone response.

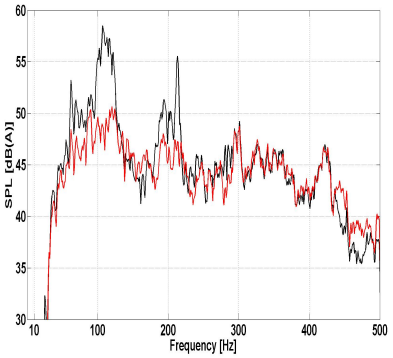

(d) Right hand rear microphone response.

FIGURE 6.17: Interior noise at the four headrests. −: ARNC off. −: ARNC on.

not significantly improved compared to the single direction systems that were presented in section 6.5.1 and especially to the first case in the subsection 6.5.1.1.

LHF dB(A)	RHF dB(A)	LHR dB(A)	RHR dB(A)	Average dB(A)
2.1	1.5	2.4	2.8	2.3

TABLE 6.8: Total reduction for 0-500 Hz. LHF: Left hand front, RHF: Right hand front headrest, LHR: Left hand rear, RHR: Right hand rear.

6.5.2.4 Case 10: Front suspension x, z-axis and rear subframe rear mounts z-axis

In the final case we use the front subframe mounts as reference locations for the input sensor. In particular, x and z-directions of the acceleration signals recorded at the front subrame mounts are combined, since we have not yet evaluated the x-axis has not been evaluated so far. Figures 6.18(a)-6.18(b) demonstrate the reduction at the front headrest, which confirms the necessity of front mount locations as inputs for reducing the front axle contributions. By comparing them with the previous results shown in figures 6.17(a)-6.17(d), we observe that the rumble was not complete reduced across its range, because of the wrong positioning of the accelerometers. Overall 3.1 dB(A) from the noise spectra can

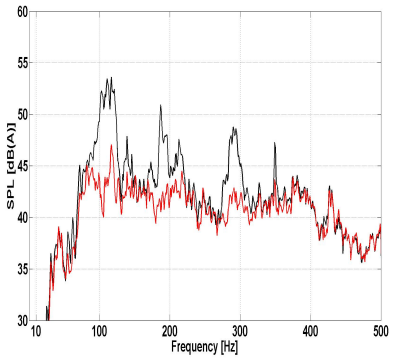

(a) Left hand front microphone response.

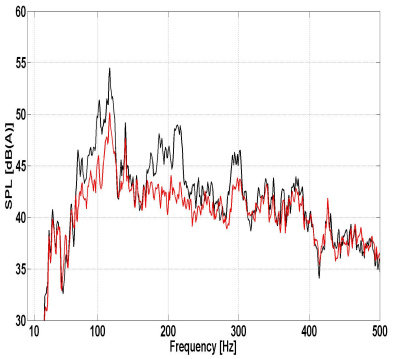

(b) Right hand front microphone response.

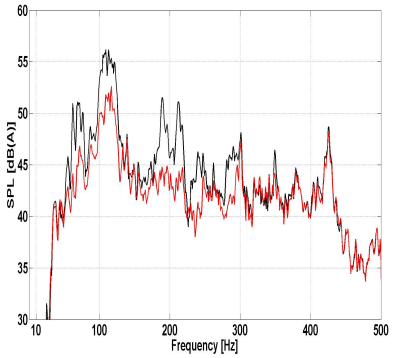

(c) Left hand rear microphone response.

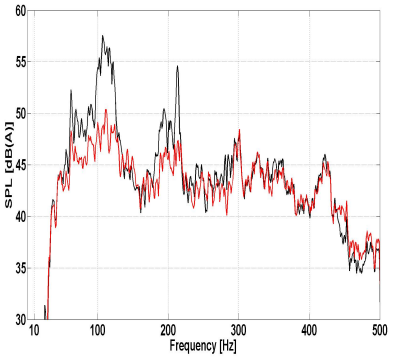

(d) Right hand rear microphone response.

FIGURE 6.18: Interior noise at the four headrests. −: ARNC off. −: ARNC on.

be attenuated at the driver's headrest and 2.4 dB(A) at the co-driver's, which we have constantly found always hard to attenuate in this simulation study possibly because other NVH contributions are also included in the recorded signals — the vehicle comes from the production line. As consequence, some airborne paths may affect the recorded signals in the cabin (at such a high speed) due

to the absense of underseats that would block the airborne paths of the body. However, this makes this simulation study even more realistic as deviations that may occur because of the modifications of the NVH packaging of the vehicle, are not expected to influence severely the operation of the ARNC system. It seems that even with these problems the estimated performance of the controller still provide good improvements for refinement levels especially at the rear headrests, where more close up to 3 dB(A) be removed from the road noise spectra.

LHF dB(A)	RHF dB(A)	LHR dB(A)	RHR dB(A)	Average dB(A)
3.1	2.4	2.8	2.9	2.8

TABLE 6.9: Total reduction for 0-500 Hz. LHF: Left hand front, RHF: Right hand front headrest, LHR: Left hand rear, RHR: Right hand rear.

6.5.3 Three directions reference signals

In this section we compare the reference signal by taking into account all directions for some of the locations. This will help us find out if there are any further improvements in the performance of the ARNC system or if there is a threshold in the maximum reduction that can be achieved with feedforward control for this luxury vehicle. Up until this point we have noticed that it is difficult to resolve the dynamics with only one direction from the accelerometer. These locations are located at parts that have multiple directions effecting the vibrational responses at low frequencies, for example subframe vibrations are approximately generated by a metallic plate and they are more complicated vibration responses than a suspension arm.

6.5.3.1 Case 11: Front suspension x, y, z-axis and rear subframe mounts z-axis

In the cases presented in the previous section we used the mounting points of the front and rear axle. In current case we change the locations of the front axle to the damper bottom, where the suspension strut is mounted and also the two front and rear control arms. Locations at the suspension strut and the control arms are often suggested by many authors as appropriate candidates for placing the reference accelerometers [Bernhard (1995), Park et al. (2002), Oh et al. (2002)]. As a result, the adaptive system may win time to perform the convolutions of the control filtering before the noise is received at the microphones inside the

vehicle's interior. This happens because the propagation time of the vibrations can be slightly longer for the locations around the suspension system.

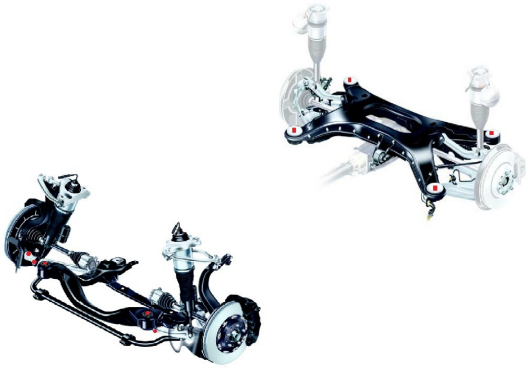

FIGURE 6.19: The locations of the accelerometers in the vehicle structure. ●: Tri-axial accelerometers position. ■: One dimensional accelerometers.

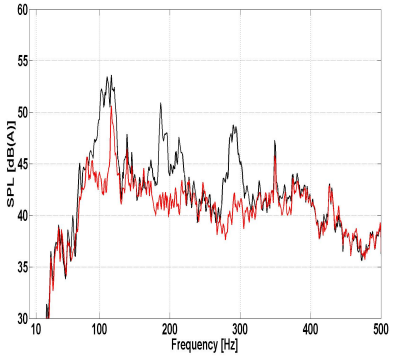

(a) Left hand front microphone response.

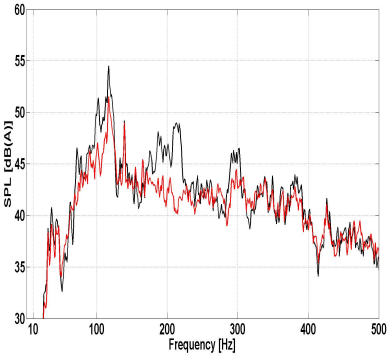

(b) Right hand front microphone response.

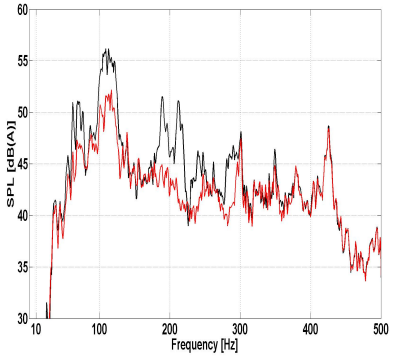

(c) Left hand rear microphone response.

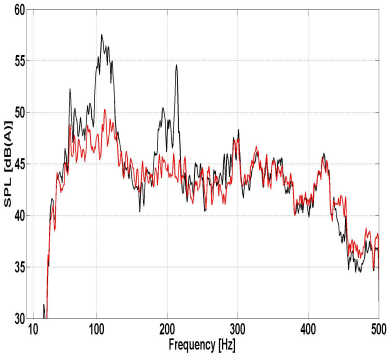

(d) Right hand rear microphone response.

FIGURE 6.20: Interior noise at the four headrests. −: ARNC off. −: ARNC on.

In the case of the luxury vehicle we study the structure-borne sources that act on the suspension parts are vibrations related to tyre cavity, since they are close to the actual excitation source. In fact, the suspension locations worsen the ARNC performance of the rumble range of the three headrests (illustrated in figures 6.20(a)-6.20(c)) because contributions from the front subframe locations are

not observed by the controller. However, the tyre cavity and the midfrequency performance are improved in the case of the front microphones.

The reduction levels at the front part of the vehicle are now 2.8 and 1.8 dB(A) at the two headrests. Overall, around 2.5 dB(A) can be obtained with this combination of acceleration signals. Even though, the average reduction is not much affected, at the front part of the vehicle cannot maintain the previous attenuation that was closer to 3 dB(A), due to the consistent performance at the rear microphones,

LHF dB(A)	RHF dB(A)	LHR dB(A)	RHR dB(A)	Average dB(A)
2.8	1.8	2.6	2.8	2.5

TABLE 6.10: Total reduction for 0-500 Hz. LHF: Left hand front, RHF: Right hand front headrest, LHR: Left hand rear, RHR: Right hand rear.

6.5.3.2 Case 12: Front subframe mounts x ,y, z-axis and front mounting point at the rear subframe only z-axis

Looking back at the previous simulations, we notice that the subframe mounts at the front axle can be employed to control the road noise in frequencies above 150 Hz. In this case we decrease the number of references from the rear axle and keep the four subframe locations of the front axle with three DoF per point.

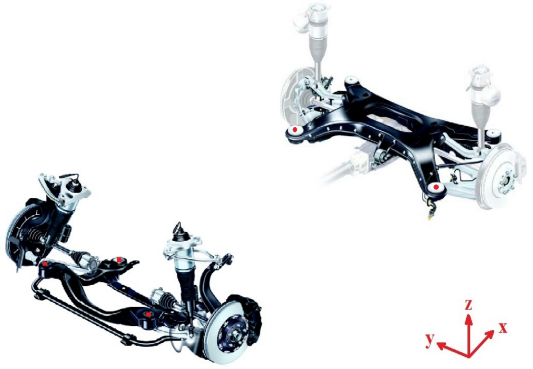

FIGURE 6.21: The locations of the accelerometers in the vehicle structure. •: Three DoF reference signals. ■: One direction reference signals.

Even if we keep a high number of references at the front axle, we achieve limited performance at road resonances transmitted from the front part of the vehicle. This fact can be observed for the levels at the two tyre cavity resonances and also at the resonance at 290 Hz, which are not totally removed from the road

noise spectra as in the previous case of section 6.5.3.1, where two directions were used at the fron axle. The reason behind this is the poor observability of the rear axle vibrations as only two summetrical locations are not enough to help the adaptive system to determine the dynamics of the rear axle contributions. As far as the rumble range is concerned, the reductions levels at the rumble range are lower, particularly at the left hand side headrests.

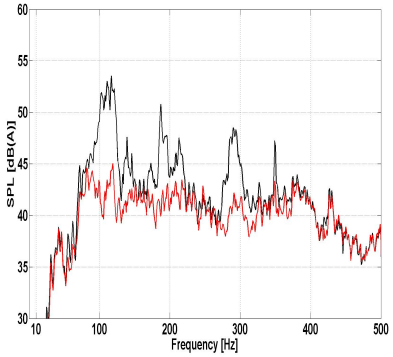

(a) Left hand front microphone response.

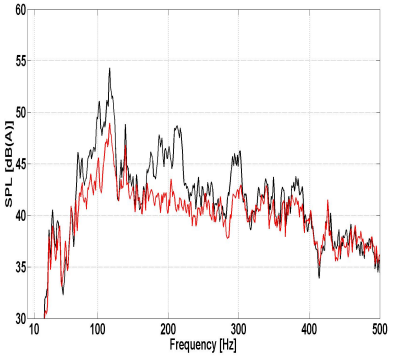

(b) Right hand front microphone response.

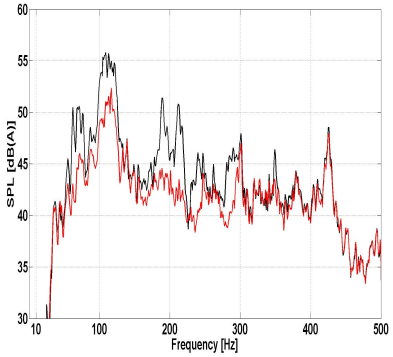

(c) Left hand rear microphone response.

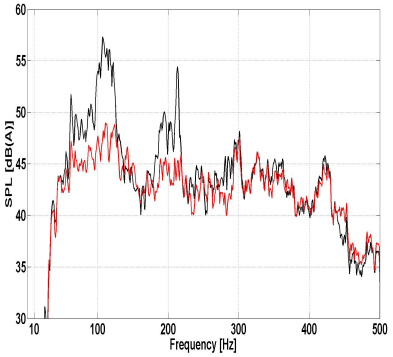

(d) Right hand rear microphone response.

FIGURE 6.22: Interior noise at the four headrests. −: ARNC off. −: ARNC on.

Increasing the directions at certain locations as a means to achieve better suspension vibrations is not a helpful solution for this vehicle design structure, since subframe vibrations seem to result to better control of the front axle contributions. Surprisingly, even when sixteen signals are used as references, the active reduction levels are not improved. This is a bit unexpected as one would expect a different outcome with such a high number of sensors. In the first case, presented in subsection 6.5.1.1, eight acceleration signals from the eight subframe mount locations were used and achieved better performance obtained across the four microphones. The average reduction levels are almost the same in both cases, in the current case the control performance is worsened at the left hand side of the vehicle. Consequently, there is a strong relationship between the

reference number and the locations that are structural sensitive in terms of vibrations that relate to road noise. The sensor number cannot be defined if there is no information about the location of the structural sources. Increasing the reference signals on the basis of improved coherence only or other optimisation methods can result to high number of sensors.

LHF dB(A)	RHF dB(A)	LHR dB(A)	RHR dB(A)	Average dB(A)
2.8	1.8	2.1	2.5	2.3

TABLE 6.11: Total reduction for 0-500 Hz. LHF: Left hand front, RHF: Right hand front headrest, LHR: Left hand rear, RHR: Right hand rear.

6.5.3.3 Case 13: Front subframe and damper top x, y, z-axis and rear subframe rear mounts z-axis

In the 13-*th* case we include location at the front axle hoping to improve the control at the tyre cavity and the midfrequency road resonance. In particular, the damper top signals and the front axle mounts at three directions are fed into the adaptive algorithm. As for the rear axle, only the z-direction is included with a single DoF that originates from the z-axis.

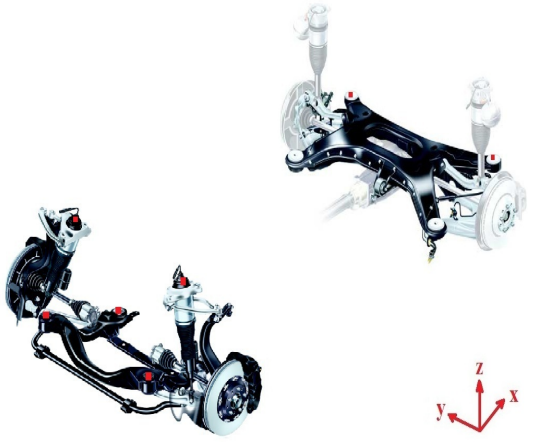

FIGURE 6.23: The locations of the accelerometers in the vehicle structure. •: Tri-axial accelerometers position. ■: One dimensional accelerometers.

Significant improvements are noticeable at the front headrests compared to the previous section, in which the damper at the top of the suspension strut was not included in the reference signal set. However, the attenuation levels at the front microphones are merely improved compared to the previous scenarios (figures 6.24(a)-6.24(b)). Yet, as figures 6.24(c)-6.24(d) show the performance at

the rear headrests has not changed a lot, a fact that implies indicates that more signals from the rear axle are necessary.

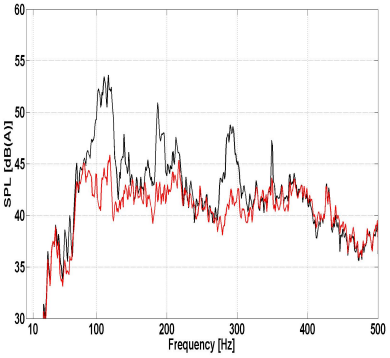

(a) Left hand front microphone response.

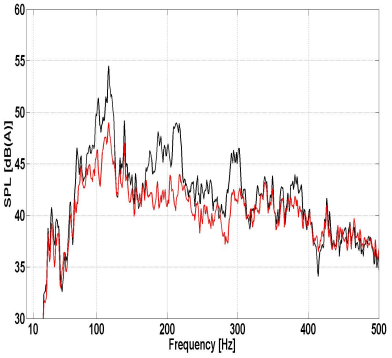

(b) Right hand front microphone response.

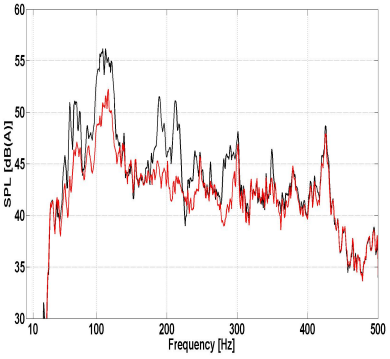

(c) Left hand rear microphone response.

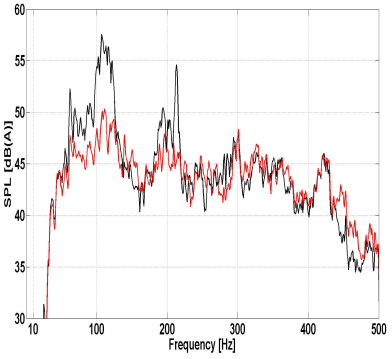

(d) Right hand rear microphone response.

FIGURE 6.24: Interior noise at the four headrests. −: ARNC off. −: ARNC on.

Up until this point, the increase of the directions and accelerometer locations has not achieved drastic improvements on the adaptive controller's performance. As we observe in table 6.12 the overall reduction levels are slightly more than 2 dB(A). It is starts to become apparent that improvement of more than 3 dB(A) might require a very high number of reference inputs for including locations that have some contribution to the road spectra. It is debatable if this extra reduction will improve the perceived reduction by the passengers and later we will try to verify this extreme case.

LHF dB(A)	RHF dB(A)	LHR dB(A)	RHR dB(A)	Average dB(A)
2.0	2.8	1.9	2.1	2.2

TABLE 6.12: Total reduction for 0-500 Hz. LHF: Left hand front, RHF: Right hand front headrest, LHR: Left hand rear, RHR: Right hand rear.

6.5.3.4 Case 14: Subframe mounts 3-directions front axle and z-axis for rear axle

In this scenario, we enhance the system with reference signals from the x, y, z-axis. These come from the front subframe mounts and at the top of suspension strut. As for the rear subframe, two signals from the z-direction of the rear mounts are set as references. Figure 6.25 illustrates the locations of the reference sensors and the corresponding DoF of the acceleration signals. It should be noted that all the mounting points between the front axle and the body are used to model this scenario.

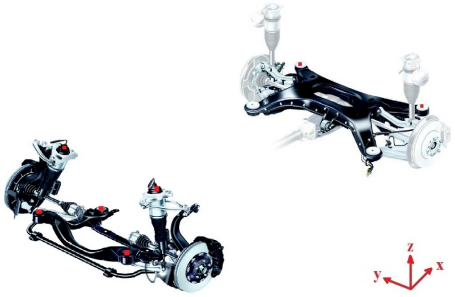

FIGURE 6.25: The locations of the accelerometers in the vehicle structure and the DoF of the reference signals. ●: Three DoF. ■: One DoF.

The road spectra are presented in figures 6.26(a)-6.26(d). It is evident that sufficient control for all road resonances at the front headrests can be achieved with this reference sensor arrangement. It is possible that the directions at these mounting locations at the front axle contain all the spectral components of structure-borne road noise. As a result, the controller is able to track changes in the vibrations that are related to road noise at the main structural input points of the suspension and subframe into the vehicle's body.

Notably, two acceleration signals at the rear headrests for the road rumble 90-120 Hz seem to be enough for reducing 5-7 dB(A). The low number of reference points at the rear axle is somethat expected, as only the structural source of the road rumble is contributing to sound field. As a consequence, the controller can resolve the rumble dynamics even with a pair of sensors.

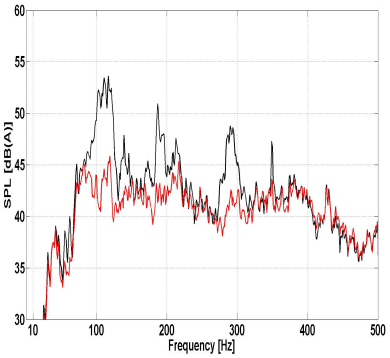

(a) Left hand front microphone response.

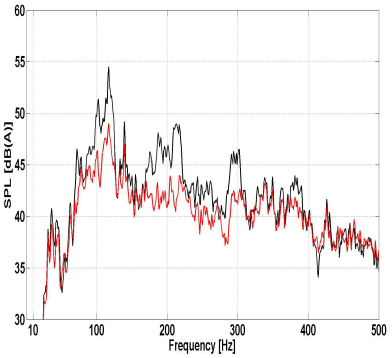

(b) Right hand front microphone response.

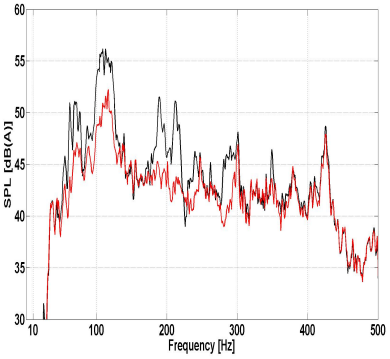

(c) Left hand rear microphone response.

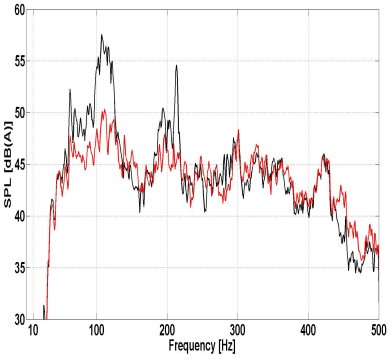

(d) Right hand rear microphone response.

FIGURE 6.26: Interior noise at the four headrests. −: ARNC off. −: ARNC on.

The reduction at the front microphones is now improved and the attenuation is noticeable up to 300 Hz. As a result, 3 dB(A) and 2.6 dB(A) are removed from the total road noise levels at the front headrests and 2.9 dB(A), 2.8 dB(A) for the two rear. From a NVH perspective this improvement is significant, but from a DSP perspective twenty signals need to be sampled from a hardware platform to increase the cost and the complexity of such an application. Therefore, in the following step we will reduce the acceleration signals number according to their structure-borne contributions and investigate the effects on the controller's performance.

LHF dB(A)	RHF dB(A)	LHR dB(A)	RHR dB(A)	Average dB(A)
3.2	2.6	2.9	2.5	2.8

TABLE 6.13: Total reduction for 0-500 Hz. LHF: Left hand front, RHF: Right hand front headrest, LHR: Left hand rear, RHR: Right hand rear.

6.5.3.5 Case 15: Subframe mounts 3-directions for front and rear axle

A feedforward system with twenty four acceleration signals was simulated in this case aiming to determine the trade-off between a high number of references and the performance of the controller. Figure 6.27 presents the eight subframe mount locations, where three directions were fed into the controller as references.

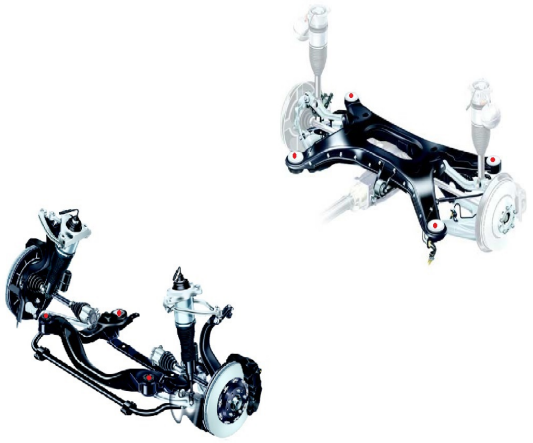

FIGURE 6.27: The locations of the accelerometers in the vehicle structure. •: Tri-axial accelerometers position.

Significant reductions in the road spectra are predicted for this reference set as shown in figures 6.28(a)-6.28(d). Small reductions in the front microphones are still noticeable up to 400 Hz in figures 6.28(a),6.28(b). As for the rear microphones a resonances around 410 Hz is slightly attenuated. However, the cancellation above 400 Hz is limited, due to low coherence (as we saw in chapter 4) and airborne paths possibly owing to these road resonances.

A control system with such a high number of input signals requires 96 ($K \times M = 24 \times 4$) convolutions, in order to generate the control signals that drive the loudspeaker system of the vehicle. Such a digital control system would probably require a DSP processor with high computational capabilities to perform the real-time convolutions. Another technical disadvantage is the fact that several sensors and complex wiring network across the vehicle structure would also be necessary. In the following case we will try to reduce further the number of reference inputs from the subframe mounts, in order to find out how much the performance of the controller would be affected by neglecting some reference locations and their DoF.

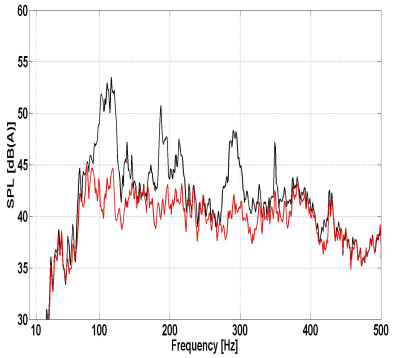

(a) Left hand front microphone response.

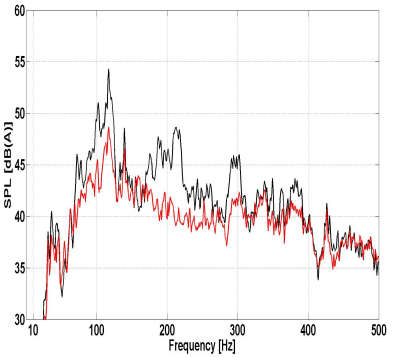

(b) Right hand front microphone response.

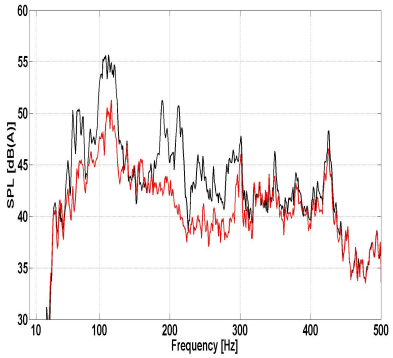

(c) Left hand rear microphone response.

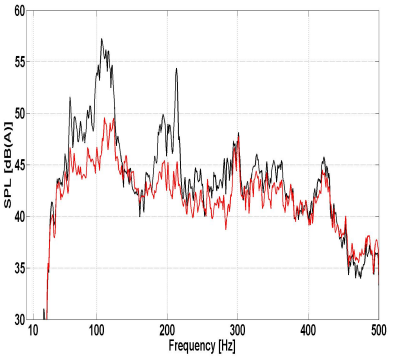

(d) Right hand rear microphone response.

FIGURE 6.28: Interior noise at the four headrests. −: ARNC off. −: ARNC on.

The reduction levels in the road noise range that derive from this scenario are important, as they define the threshold of the maximum achieve in attenuation of the particular vehicle. As table 6.16 demonstrates reductions more that 3 dB(A) were predicted for this scenario. This possibly indicates that the subframes are as the actual inputs to the vehicle system, therefore if the same inputs are fed into the controller very good performance can be achieved. As a result, the feedforward paths of the multichannel system can follow the behaviour of the vibro-acoustic systems of the vehicle, as the main structural inputs are observable by the controller.

LHF dB(A)	RHF dB(A)	LHR dB(A)	RHR dB(A)	Average dB(A)
3.7	2.9	3.5	3.6	3.2

TABLE 6.14: Total reduction for 0-500 Hz. LHF: Left hand front, RHF: Right hand front headrest, LHR: Left hand rear, RHR: Right hand rear.

6.5.3.6 Case 16: Reduced set of reference signals from subframe mounts

We continue further with effort to reduce the number of acceleration signals from the subframe mounts and in the current section we explore whether there is degradation in the performance by using only two directions from the front axle and one from the rear. In total, twelve acceleration signals are fed into the controller as reference inputs.

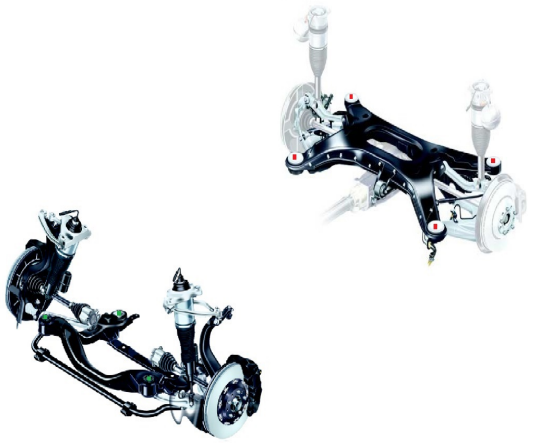

FIGURE 6.29: The locations of the accelerometers in the vehicle structure. ■: Two DoF reference signals. ■: One DoF acceleration signal.

If we now compare the road spectra in figures 6.28(a)-6.28(d) with the current case of figures 6.30(a)-6.30(d), we notice that the performance is not severely affected by the reduction from 24 reference to 10. This is a rather striking observation as it shows that minor improvements can be obtain even if we include all the structural inputs from the axles into the controller.

The controller improves the vehicle's NVH performance at frequencies, where the structural dynamics of the subframe cannot prevent the transmission of vibrations that are correlated with road noise. More specifically, the subframe mounts are the main inputs to the vehicle body and they are usually optimised in terms of local dynamic stiffness, in order to control structure-borne noise transmission [Plunt (2005), Noll et al. (2013)]. Therefore the improvements in the road noise spectra obtained from ARNC technology seem to depend on the amount of uncontrolled structural resonances, which come from the passive structural system that contributes to the sound field inside the cabin.

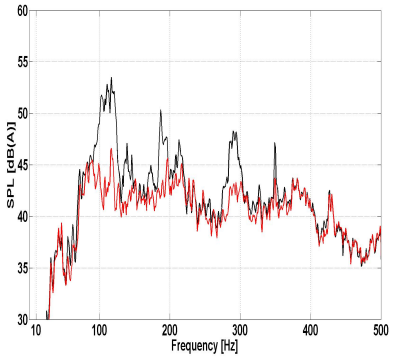

(a) Left hand front microphone response.

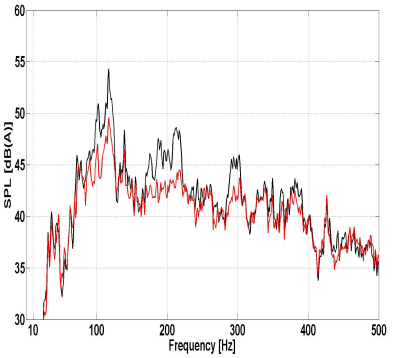

(b) Right hand front microphone response.

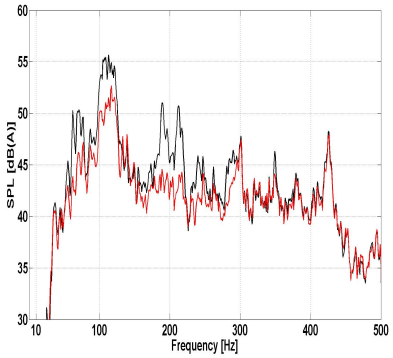

(c) Left hand rear microphone response.

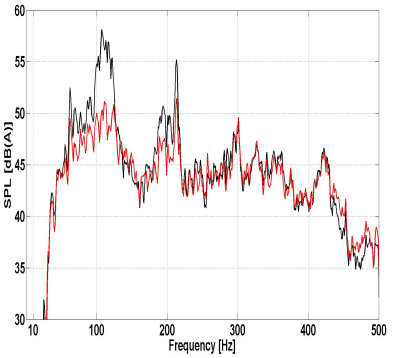

(d) Right hand rear microphone response.

FIGURE 6.30: Interior noise at the four headrests. −: ARNC off. −: ARNC on.

The overall attenuation is still maintained at 3 dB(A) across the four headrests. This means that minor improvements can be obtained for more than 10 acceleration signals in this vehicle.

LHF dB(A)	RHF dB(A)	LHR dB(A)	RHR dB(A)	Average dB(A)
3.0	2.3	3.2	3.3	3.0

TABLE 6.15: Total reduction for 0-500 Hz. LHF: Left hand front, RHF: Right hand front headrest, LHR: Left hand rear, RHR: Right hand rear.

6.5.3.7 Case 17: Reduced set of reference signals from subframe mounts with two reference locations at the rear axle

The same reference signals from the front axle as in the previous case of subsection 6.5.3.6 are now combined with two references locations from subframe mount of the rear axle. In total 10 acceleration signals are now the references of

the feedforward system. The single change deals with the references of the rear axle, as we only use signals from front subframe mounts at the z-directions.

FIGURE 6.31: The locations of the accelerometers in the vehicle structure. ■: Two DoF reference signals. ■: One direction acceleration signal.

The attenuation has been slightly degraded in the controlled spectra for the road rumble (figures 6.32(b) and 6.32(c)).

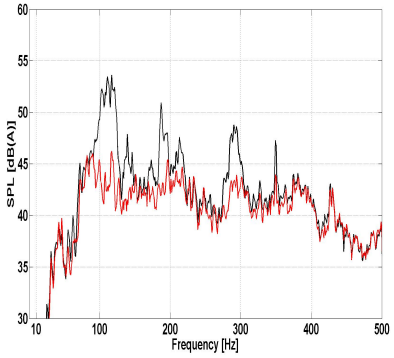

(a) Left hand front microphone response.

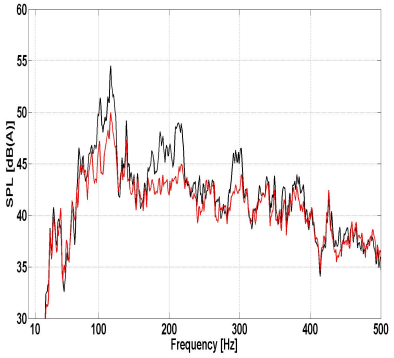

(b) Right hand front microphone response.

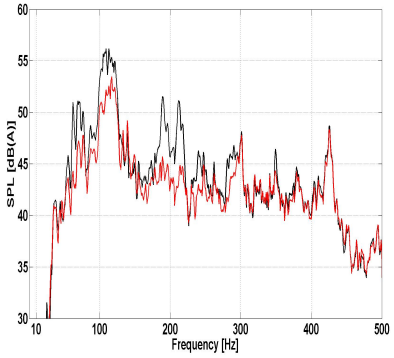

(c) Left hand rear microphone response.

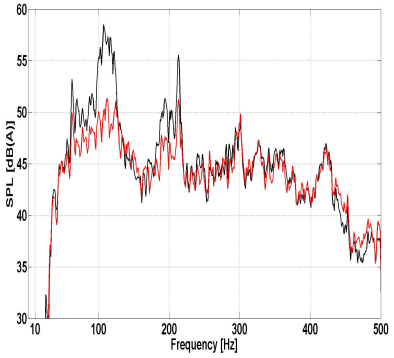

(d) Right hand rear microphone response.

FIGURE 6.32: Interior noise at the four headrests. −: ARNC off. −: ARNC on.

When it comes to the other two headrests, the reduction in the rumble range is still maintained at around 7 dB(A) across its range. The overall reduction in cabin is 2.5 dB(A) that is an acceptable improvement in the structure-borne NVH performance of the vehicle.

LHF dB(A)	RHF dB(A)	LHR dB(A)	RHR dB(A)	Average dB(A)
2.7	2.0	2.4	2.5	2.5

TABLE 6.16: Total reduction for 0-500 Hz. LHF: Left hand front, RHF: Right hand front headrest, LHR: Left hand rear, RHR: Right hand rear.

6.6 Summary

In this chapter we introduced the theory of multichannel adaptive filtering for active control and used it to develop a realistic model that estimates the performance of ARNC system. The prediction study focused on the identification of the most important direction and axle locations that can result to robust performance across the four headrests at a high speed. At the same time other NVH contribution start to influence the sound field in the cabin. We found that with one direction measured by eight sensors at sensitive location of the structure 2 dB(A) can be removed from the structure-borne noise spectra. It was found that reduction levels can go up to 3 dB(A) with 10 and 12 references. The main reason behind this improvement are that one more DoF was introduced into the system that helped to identify road noise contributions, which were previously partially controlled.

It was also found that this particular luxury vehicle cannot be further improved in terms of structure-borne NVH as we noticed in section 6.5.3.5, since all the DoF at the front and rear mounts that are the main inputs to the vehicle body were included in the model. At the driver's heardest 3.7 dB(A) can be achieved and across the four headrests 3.2 dB(A) on average, which is comparable to other cases with a smaller number of reference signals from the same locations.

We observed that there is no significant improvement when the reference signals are doubled from 8 to 16 signals. This is an entirely different finding to a previous study on ARNC predictions on an Alfa Romeo 156, which showed that 5 accelerometers can reduce 8 dB and ten sensor 11 dB [Mohammad et al. (2008)]. However, luxury vehicles with relative good refinement levels, such as a Bentley and a few passive NVH treatments for road noise can be improved up to a point

even with less than ten sensors. A rapid increase in the references might not offer extreme audible results. The following table summarises the best reference signals combinations that results to more than 2.5 dB(A) broadband reduction up to 500 Hz with the main use of subframe mount locations are reference inputs into the ARNC system.

Simulation case no.	Number of references	Reduction dB(A)
5	16	3.0
12	14	3.0
15	24	3.2
16	12	3.0
17	10	2.5

TABLE 6.17: Best reference signal combinations and the corresponding average reduction across the four headrests.

Chapter 7

Active noise control experiments on a road-noise simulator

Up until this point in this thesis we concentrated on the relationship between the various structural locations of the vehicle, which are sensitive to road noise inputs and are coherent with the interior road noise resonances. This study offered us a deeper insight into the relationship between the structural resonances coming from the two axles and the ones coming from interior road noise.

On that basis we evaluate a single reference input feedforward adaptive controller for three different excitation conditions, front tyres, rear tyres and whole vehicle. In this way, the structural sources that are located at the front and rear axle are physically decomposed and only the main contribution from each axle appears in the sound field inside the cabin. As a last stage all the tyres are excited by the shakers transducers (whole vehicle simulation) and each reference sensor location is once again tested in terms of performance. In addition to this, a multichannel system was developed. Road data were obtained using a multichannel control system and used to predict offline the performance of the system.

7.1 Chapter outline

We begin this chapter by introducing the experimental setup of the controller on the vehicle in section 7.2. We then move on to present an analysis of the measurement results. This is divided according to the different excitation locations (front tyres, rear tyres, four tyres-whole vehicle). In section 7.3 and 7.4 the cases of front and rear tyres excitation are presented and the measured performance after the training of the adaptive ARNC system is discussed. The next step involved testing the controller using four shaker sources that excited each tyre simultaneously. The results for this vehicle simulation are presented in section 7.5. Additionally, a multichannel road noise controller is presented in section 7.6 with computer predictions based on road noise data obtained through the multichannel system.

7.2 Experimental ARNC on a Bentley vehicle

7.2.1 Purpose of ARNC physical simulation

In the previous chapters we performed computer simulations that aimed to investigate how different locations of the axle, which are important for structure-borne NVH can either improve or degrade the performance of feedforward ARNC controllers. In the final stage of our study, we address the effects of the reduction obtained by a real-time feedforward controller with a single reference sensor.

The aim of this physical simulation of an ARNC system is to explore the application of a single channel feedforward controller that uses one sensor placed at a structure-borne noise source or at a part of the axle that allows the transmission or road noise related vibrations.

7.2.2 Real-time ARNC measurement setup on a Bentley vehicle

For the purpose of these tests an isolated environment was selected with also low levels of background noise, which was also employed in chapter 3 for the development of the experimental setup of the road noise simulator. This setup allows structure-borne noise to be measured at the microphone locations, so that the performance at each sensor location is evaluated without other NVH

attributes interfering with structure-borne noise and vibrations coming from the tyres.

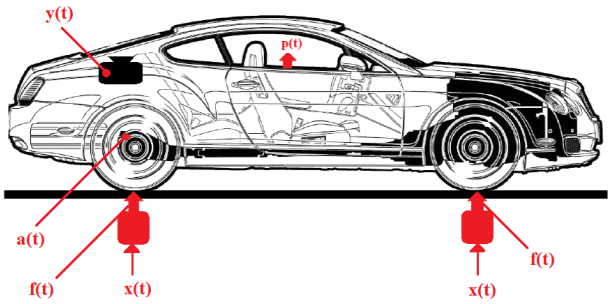

(a) ANC & LMS SCADAS setup on the vehicle.

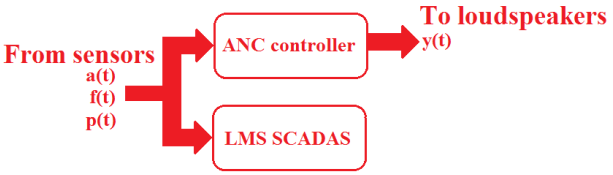

(b) Block diagram of the acquired signals by the two systems.

FIGURE 7.1: ANC configuration of the whole vehicle road noise simulator. The sensor signals $f(t)$, $a(t)$ and $p(t)$ are common inputs to the LMS SCADAS and the feedforward controller. The signal $y(t)$ is generated from the output of the adaptive controller and drives the audio amplifier unit.

The four signal generators of the LMS SCADAS system drove four shaker transducers with white noise from 10 Hz to 1 kHz. It is worth mentioning that the shakers were placed at the diagonal of each tyre, so that they do not excite a specific directions, but a mixture of x-, z-directions. As a result, the road noise resonances that act on the vehicle during rolling conditions are included in the simulated road noise spectra as it was presented in chapter 3.

The signals of the controller and data acquisition chain are displayed in figure 7.1(b). A data acquisition system by LMS was used to measure the applied forces, $f(t)$ at the tyres and the vibro-acoustic responses $a(t)$ and $p(t)$ on the vehicle. A commercial adaptive controller by Causal systems Ltd was integrated with a Monacor four channel car audio amplifier. The crossover filters of the audio amplifier were set to low-pass filtering with a cut-off frequency at 500 Hz. Figure 7.2(a) illustrates the actual ANC setup in the vehicle, including the wiring between the controller, the audio amplifier and louspeaker of the vehicle can be seen. Figure 7.2(b) shows the headrest microphones that provide the error signals of the adaptive algorithm.

The structure in figure 7.3 presents the sensor and loudspeaker arrangement inside the vehicle. Four microphones were placed at the headrests in similar manner to the measurement studies. The three woofers that were mounted at

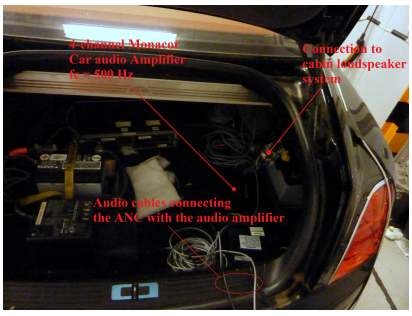

(a) Setup of the car audio amplifier in the vehicle.

(b) Interior microphones at the headrests.

FIGURE 7.2: ANC hardware setup in the vehicle.

the front doors and at the left hand rear door integrated the feedforward control path. Additionally, the subwoofer at the parcel shelf behind the rear headrests was also chosen to generate of the secondary canceling field, since its secondary path delay is short (as we found in section 2.4). In terms of reference inputs, an example of a reference sensor location with an accelerometer mounted close to the left hand front wheel is shown in figure 7.3.

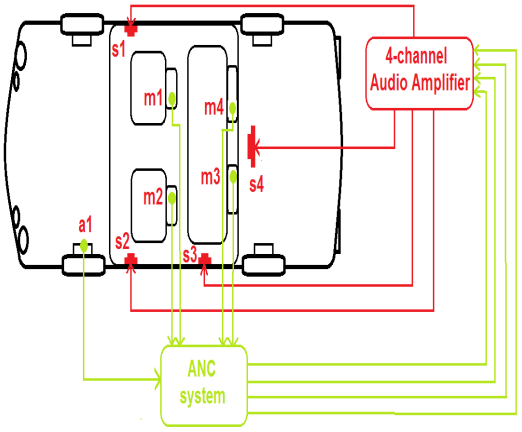

FIGURE 7.3: ANC configuration for feedforward control in a vehicle. The sensor signals are noted as **a1**: for the accelerometer, **m1**,**m2**, **m3**, **m4**: for the microphones and for the loudspeakers are displayed as **s1**, **s2**, **s3** and **s4**.

The adaptive ANC controller that was used in these experiments has a single reference input and four error microphone sensors. Four output signals were also allowed in this setup, which were connected to the four channel input car audio amplifier. It is worth pointing out that the Monacor audio amplifier has only a low pass and a high pass filtering setting, since modern digital car audio amplifiers are equipped with high-order filtering for room equalisation. It is very likely that this type of audio filtering may include extra delays from the DSP hardware, which constitutes the reason why we chose this analog amplifier in this study.

7.2.3 Structure of the real-time experimental study

The following section presents the experiments we undertook. We distinguish among a set of different experiments based on two factors: *a*) the excitation on the tyres *b*) the parameters that affect the operation of the adaptive algorithm, such as the number of FIR taps and the sampling rate. Therefore, the structure of the following sections is organised as follows

1. Front tyres excitation and reference accelerometer at the lower control arm at the front axle
   (a) **Case1**: FIR control filter I=256-taps, number of error microphones L=3 and control loudspeakers M=4 at f_s=4 kHz
   (b) **Case2**: FIR control filter I=512-taps, number of error microphones L=4 and control loudspeakers M=4 at f_s=4 kHz
   (c) **Case3**: FIR control filter I=256-taps, number of error microphones L=4 and control loudspeakers M=4 at f_s=4 kHz
2. Rear tyres excitation and reference accelerometer at the rear subframe mount of the rear axle
   (a) **Case4**: FIR control filter I=512-taps, number of error microphones L=3 and control loudspeakers M=4 at f_s=4 kHz
   (b) **Case5**: FIR control filter I=1024-taps, number of error microphones L=3 and control loudspeakers M=4 at f_s=4 kHz
3. Rear tyres excitation and force signal as refererence measured at one of the rear tyres
   (a) **Case6**: Force signal as refererence, FIR control filter I=512-taps, number of error microphones L=4 and control loudspeakers M=4 at f_s=4 kHz
4. Rear tyres excitation and reference accelerometer at the front subframe mount of the rear axle
   (a) **Case7**: FIR control filter I=750-taps, number of error microphones L=4 and control loudspeakers M=4 at f_s=8 kHz without anti-aliasing
   (b) **Case8**: FIR control filter I=128-taps, number of error microphones L=3 and control loudspeakers M=4 at f_s=2 kHz
5. Whole vehicle excitation and reference accelerometer at the rear subframe mount of the rear axle

   (a) **Case9**: FIR control filter I=128-taps, number of error microphones L=3 and control loudspeakers M=4 at f_s=4 kHz

6. Whole vehicle excitation and reference accelerometer at the rear subframe mount of the rear axle

   (a) **Case10**: FIR control filter I=256-taps, number of error microphones L=4 and control loudspeakers M=4 at f_s=4 kHz

7. Whole vehicle excitation and reference accelerometer at the front subframe mount of the rear axle

   (a) **Case11**: FIR control filter I=256-taps, number of error microphones L=4 and control loudspeakers M=4 at f_s=4 kHz

8. Whole vehicle excitation and reference accelerometer at the lower control arm at the front axle

   (a) **Case12**: FIR control filter I=512-taps, number of error microphones L=4 and control loudspeakers M=4 at f_s=8 kHz

   (b) **Case13**: FIR control filter I=128-taps, number of error microphones L=4 and control loudspeakers M=4 at f_s=2 kHz

7.3 ARNC simulation: Excitation at the front tyres

As a starting point, broadband forces from two shaker transducers excited the two front tyres, in order to reduce noise levels from the contributions that are mainly generated from front axle vibrations. In particular, tyre cavity resonances were transmitted through several parts of the front axle into the rest of the vehicle as we discovered in chapter 4. The effect of having only the structural sources from the front part of the vehicle was simulated, in order to cause structure-borne noise in the cabin that corresponds only to the vibro-acoustic contributions of the front axle. The shakers at the rear tyres are inactive thus there are no forces applied at the rear axle, which simulates the case of having the rear tyres with very low air pressure. The reference accelerometer was placed close to the tyres at one of the suspension arms to capture high levels of coherent vibrations with the tyre cavity resonance inside the cabin.

7.3.1 Experimental procedure for front tyres excitation

Two shaker sources excited the front wheel as presented in figure 7.4. The diagram in this figure demonstrates the noise transmission because of the excitation applied to the two front wheels and its control through the SIMO feedforward system.

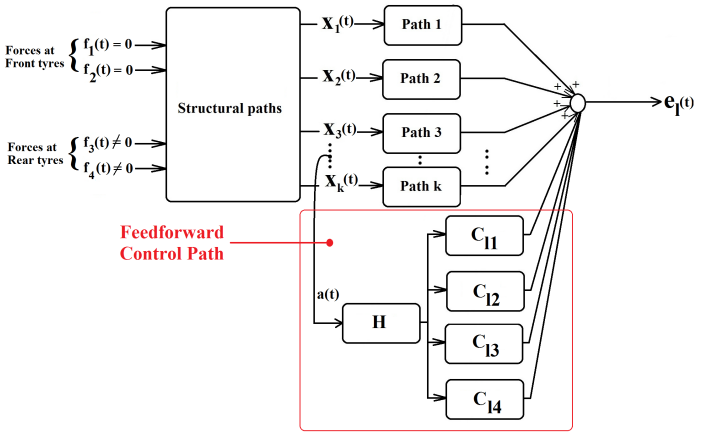

FIGURE 7.4: Block diagram of a single channel adaptive feedforward controller, where $f_1(t)$, $f_2(t)$ are two uncorrelated forces applied on the front tyres, $a(t)$ is acceleration signal that is fed to the control filter matrix $\mathbf{H}$ and c_{l1}, c_{l2}, c_{l3},c_{l4} are the cancellation paths from the loudspeakers to the headrest location of the attenuated signal $e_l(t)$.

As it is evident in figure 7.4, the adaptation stage is excluded, since the controller's performance was tested after the system was adapted to a solution for the FIR filter set. The performance of the controller was averaged for a minute of random excitation applied to the tyres with the filters coefficient been fixed to their converged values. It should be noted that between 10 to 15 minutes were required in the experiment to converge to a solution. In practice, modified versions of the FxLMS algorithm can be used that converge much faster than the conventional time domain FxLMS that was used in our case [Qiu and Hansen (2007), Sun et al. (2015)].

In this case the shaker transducers at the rear part of the vehicle did not apply any forces to the rear tyres, therefore structure-borne contributions coming from the rear axle were not included in the sound field in the cabin. As a result, vibro-acoustic coupling occurred only in the case of the front axle vibrations and the acoustic resonances in the compartment. Therefore, the suggested principle of reducing the noise that is caused independently by the structural sources on the front and rear axle was used to verify the selected accelerometer locations from chapter 4. The road noise analysis indicated that there are two structural sources acting globally in the front and rear axle with relatively low structural interaction. However, their modal contributions aggregate and generate the road

noise field in the cabin, which, in this study, is controlled by a single reference channel feedforward control with an accelerometer placed at the main structural sources of each axle.

7.3.2 Secondary path estimates

Before starting the adaptation process of the FxLMS algorithm, the secondary paths impulse responses are necessary for the algorithm as it is shown in the controller's setup in figure 7.4. Figure 7.5 demonstrates a comparison between a high resolution and high sampling rate impulse response that was modeled as an FIR filter with 1024-taps at 8 kHz and another one with 256-taps at 1 kHz. In both case the estimation error was 20 dB lower that the original noise signal that was used to train the filter set of the secondary paths. As it can be observed the 256-taps FIR is very similar to the 1024-taps filter above 0.04 seconds, where the accuracy of the filter is important at the tail of the impulse response contains the low frequencies that are important in the ARNC case. The high rippling that represents the high frequencies of the secondary path between 0-0.02 seconds is not same for the two FIR filters as the 1 kHz sampling rate limits the modeled system up to 500 Hz.

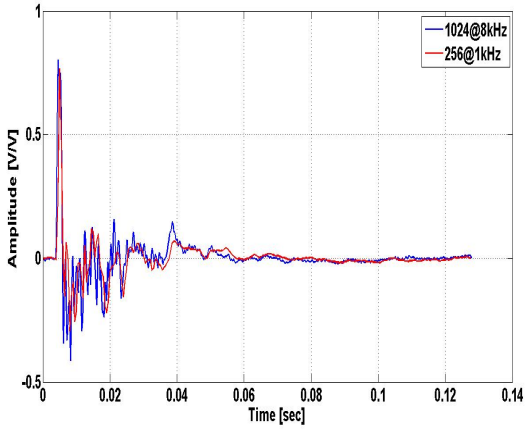

FIGURE 7.5: Comparison between secondary path estimates. ■: Measured with the dual channel FFT analysis.

7.3.3 Sensor arrangement on the front axle

In chapter 4 we demonstrated that the tyre cavity noise is related to structural vibrations located at the front axle. Specific locations, such as the control arms of the suspension, were found to be highly correlated with the interior road noise

in the coherence analysis. One of the suspension control arms is used at this stage to reduce the noise levels at the tyre cavity band as it is shown in figure 7.6.

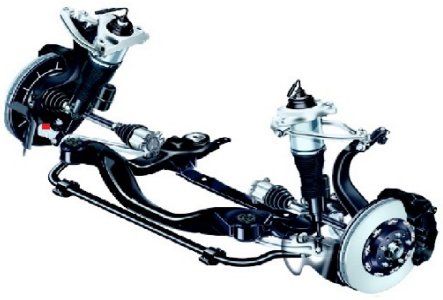

FIGURE 7.6: Reference sensor at the control arm of the suspension. ■: Acceleration signal from the z-axis.

7.3.4 Case 1: Reference at the lower control arm and control filter length I=256

The first step of the experiment dealt with the control over the simulated structure-borne road noise at the three headrest locations: co-driver and rear passengers seats. The microphone at the driver's headrest was used as an observing tool to examine, whether there are side-effects on the rest of the sound field. Changes on the road surface are useful acoustic cues for the driver, thus it might be the only area in the sound field that the controller does not attenuate the sound pressure levels.

FIGURE 7.7: Cancellation zones at the three passengers headrest marked with. • and uncontrolled zone at the driver's headrest with.

In the past this type of ARNC configuration, in which the cancellation at the front part of the vehicle, resulted to sound pressure increase at rear seats [Sano et al. (2000)]. However, in our study the cancellation is focused mostly to the rear headrests, where road noise resonances are perceptually very noticeable. The experimental setup in figure 7.4 shows that the controller was set to reduce the road noise when the forces from the shakers were applied only at the front

tyres. The digital controller sampled the all the input signals at 4 kHz and the length of the control was set to 256 taps. Figures 7.8 and 7.9 present the preliminary results of the structure-borne noise reduction within the cabin. As the figures illustrate, a significant reduction was noticed between 120-220 Hz for the right hand front microphone, with 11 dB(A) at the tire cavity band and 10 dB(A) around 120 Hz. A reduction of 10 dB(A) was also noticed at the 290 Hz resonance for the left hand rear microphone and 11 dB(A) at around 120 Hz for the right hand rear microphone.

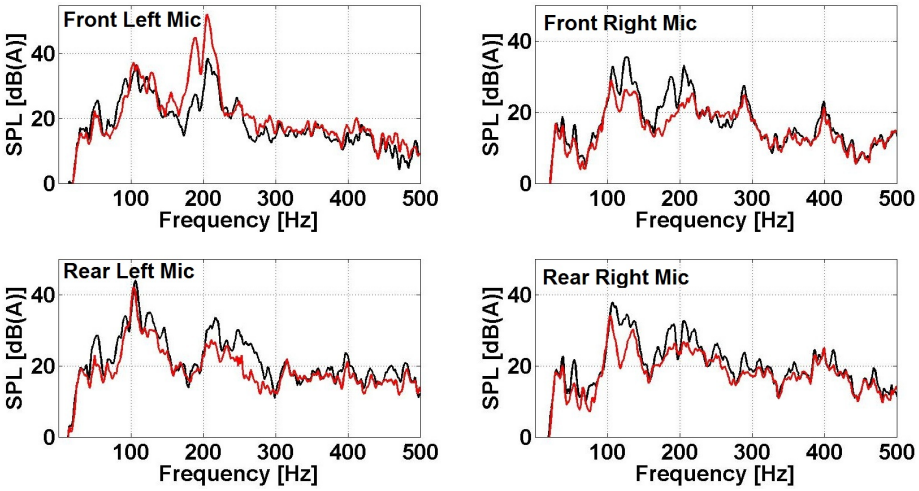

FIGURE 7.8: ARNC at the four headrests for front tyres excitation, when only the front tyres are excited by the shakers.−: ARNC off. −: ARNC on.

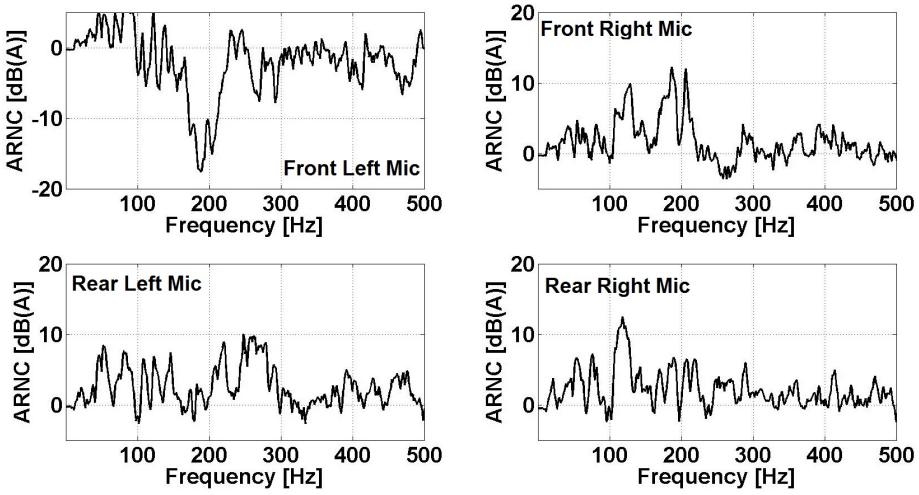

FIGURE 7.9: ARNC performance at the four headrests.

However, a rapid increase in sound pressure at the left hand front microphone (driver's headrest) was noticed at the tyre cavity band. As a consequence, the spatial averaged reduction of the four microphones is not significant (see figures 7.10(a), 7.10(b)), especially at the targeted noise band (200-220 Hz).

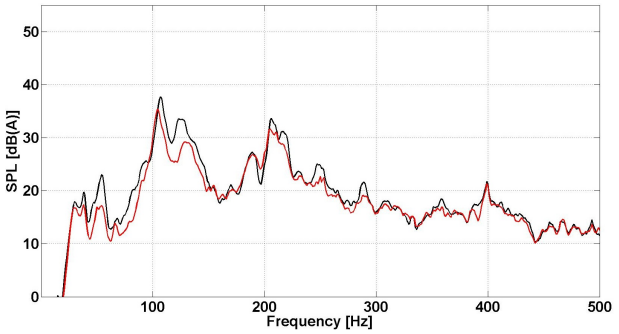

(a) Averaged interior noise. −: ARNC off. −: ARNC on.

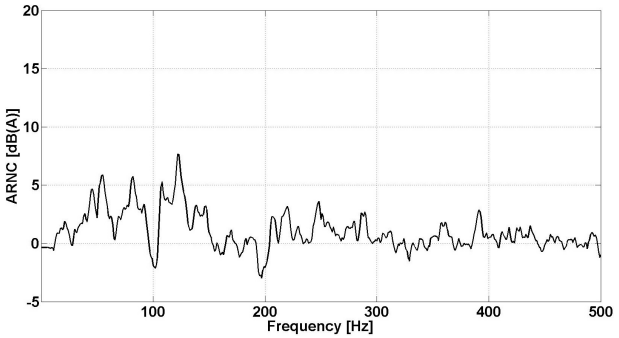

(b) Averaged Attenuation.

FIGURE 7.10: Averaged ARNC performance at the four headrests.

Another observation is that 5-7 dB(A) attenuation was obtained between 105-120 Hz. However, the total reduction remains relatively low at 1.9 dB(A) as table 7.1 demonstrates. Even if the reduction was 2-4 dB(A) at the three headrest microphones, the amplification at the observation microphone was high.

LHF dB(A)	RHF dB(A)	LHR dB(A)	RHR dB(A)	Average dB(A)
-9.3	4.5	2.6	4.0	1.9

TABLE 7.1: Total reduction for 0-500 Hz. LHF: Left hand front, RHF: Right hand front headrest, LHR: Left hand rear, RHR: Right hand rear.

7.3.5 Case 2: Reference at the lower control arm and control filter length I=512

In this section we present our second effort to improve the performance of this ARNC configuration. The length of the control filters was doubled to 512 taps and better reduction was measured at the three cancellation areas, as figure 7.11 shows.

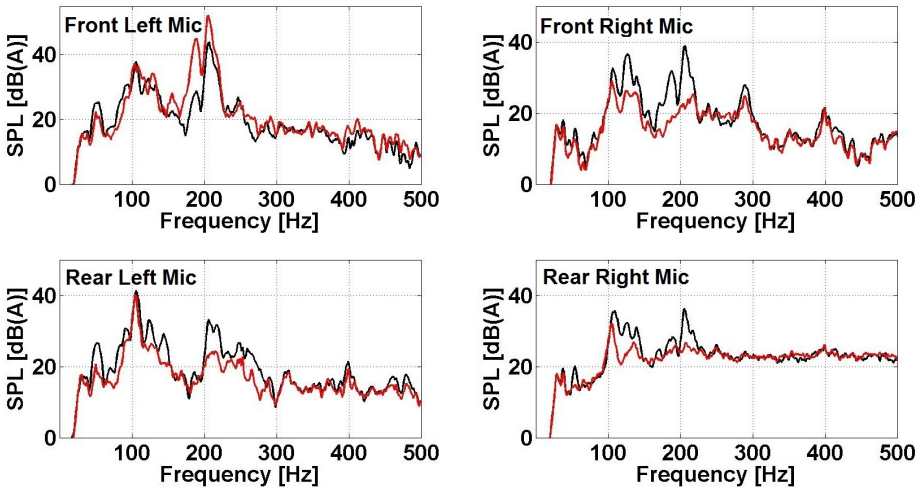

FIGURE 7.11: Interior noise at the four headrests, when only the front tyres are excited by the shakers. −: ARNC off. −: ARNC on

A significant improvement at the right hand front microphone (co-driver's headrest) can be noticed in figure 7.12. Tyre cavity resonances dominate the noise spectrum at 180 and 220 Hz, where the controller manages to reduce the noise to 12 dB(A) and 17dB(A) respectively.

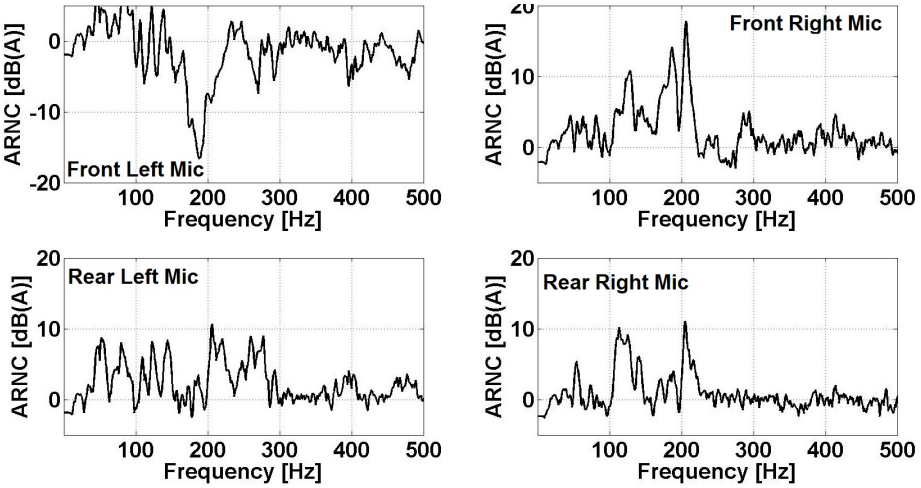

FIGURE 7.12: ARNC performance at the four headrests.

This high active noise reduction may be close to the optimal performance of the coherence limit. The peak reduction of 17 dB(A) should correspond to 0.87 according to equation 4.4, which is a high value for the coherence function at the tyre frequency range. This also confirms that the accelerometer sensor was placed at an optimum location, where the vibration levels that relate to tyre cavity noise were high. Significant cancellation maximum of 10 dB(A) in the range of 200-220 Hz was achieved at the rear headrest microphone. Another important achievement is that good reduction is also noticed between 100-120 Hz for the front axle contribution to the rumble band at the three headrests. In

the case of the observation microphone the amplification peaks at the tyre cavity resonance at 180 Hz. This indicates that including a fourth microphone in the control loop is necessary in order to eliminate the high sound pressure increase at the driver's headrest.

However, for determining the minimum number of sensors was rather advantageous, since a production line application on a vehicle requires a low number of sensors. To the best of our knowledge, such reductions have not been achieved in the past with such a low number of sensors at an experimental level with simulated structure-borne noise [Ferren and Bernhard (1991), Bernhard (1995), Dehandschutter et al. (1995), Sas and Dehandschutter (1999)]. In fact, as a rule of thumb it is proposed that the number of accelerometer sensors should be equal to the number of independent structural sources that act on the vehicle [Sutton et al. (1994)]. In contrast to this, Park and Fuller suggested that the number of sensors should be more than the vibrational sources of structure-borne noise [Park et al. (2002)]. In this way, it is ensured that the controller observes all the structural resonances that are correlated to road noise. Still, in both cases the location of sensors is not found by the TPA analysis, but only the decomposition of the acceleration spectra with PCA. Therefore, the path analysis based on the coherence (presented in chapter 4) has improved the placement of the accelerometers.

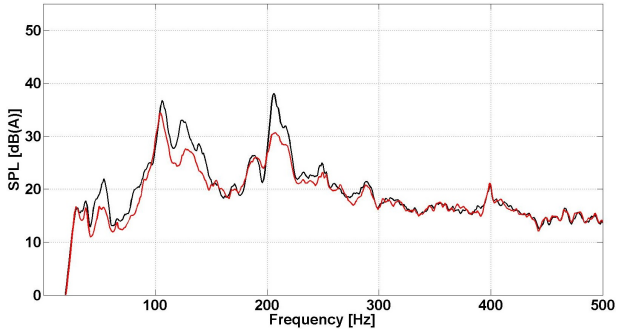

(a) Averaged interior noise. −: ARNC off. −: ARNC on

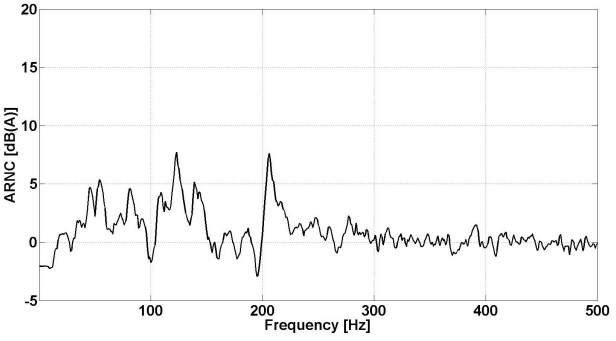

(b) Averaged Attenuation.

FIGURE 7.13: Averaged ARNC performance at the four headrests.

As mentioned previously, existing methods for reference sensor selection may result in a high number of sensors, as they do not take into account the partial contributions of each vibro-acoustic path to the interior noise response. In this case, the suggested approach was based on the most sensitive locations in terms of structure-borne road noise dynamics, where the ordinary coherence at each path can be high at the road noise bands. This makes us select locations with high contributions at the microphone response at the headrests. This approach was validated with the use of a single accelerometer — proposed as reference sensor location in chapter 4. A second accelerometer at the symmetrical location of the front axle should be used, but the hardware constraints of the controller allowed only one reference input. With regards to the number of microphones in the cabin, the performance was once again lower than expected due to the amplification at the left hand front microphone (driver's headrest). On the other hand, the average reduction is improved compared to the first trial and 5-6 dB(A) is achieved at the main road noise bands. This is also reflected on the average reduction in table 7.2, which is around 2.8 dB(A). An impressive reduction of 6.4 dB(A) on the co-driver headrest is also noticed.

LHF dB(A)	RHF dB(A)	LHR dB(A)	RHR dB(A)	Average dB(A)
-6.7	6.4	2.8	2.4	2.7

TABLE 7.2: Total reduction for 0-500 Hz. LHF: Left hand front, RHF: Right hand front headrest, LHR: Left hand rear, RHR: Right hand rear.

7.3.6 Case 3: Reference at the lower control arm and control filter length I=256 and four error microphones

In this trial the left hand front microphone becomes the fourth error microphone, aiming to compensate for the sound pressure increase at the left hand front microphone. Figure 7.14 illustrates that tyre cavity noise is attenuated effectively for the microphone at the left side of the cabin, which is also the side of the accelerometer. Approximately 19 dB(A) reduction is obtained for the left side in figure 7.15. In addition to this high reduction is also observed for the rumble range for the left hand side microphones with around 5-10 dB(A) in the range of 110-120 Hz.

At the other side of the cabin the reduction is much lower at the tyre cavity band for the co-driver's microphone around 5 dB(A) at 180 Hz. This is probably due to the fact that at the co-driver's headrest the noise is incoherent with vibrations coming from the left side of the axle, as a main contribution is not effectively reduced. An extra accelerometer is necessary at a symmetrical location

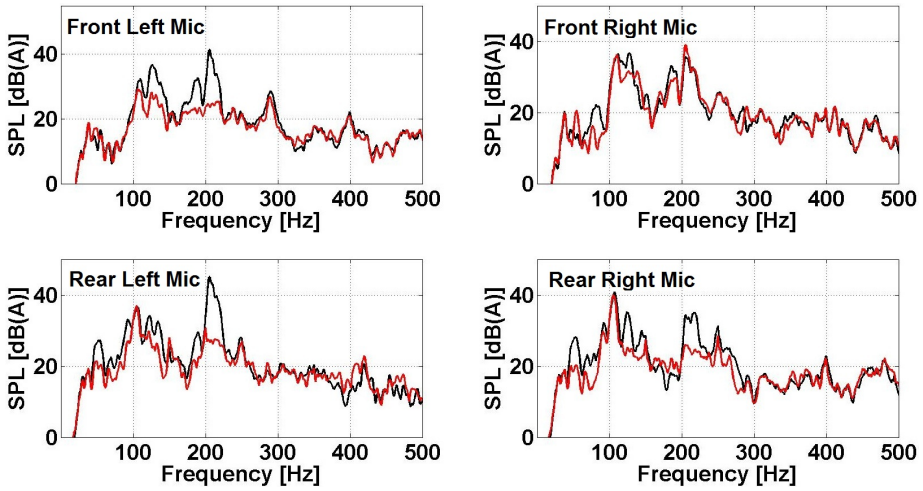

FIGURE 7.14: Interior noise at the four headrests, when only the front tyres are excited by the shakers. −: ARNC off. −: ARNC on.

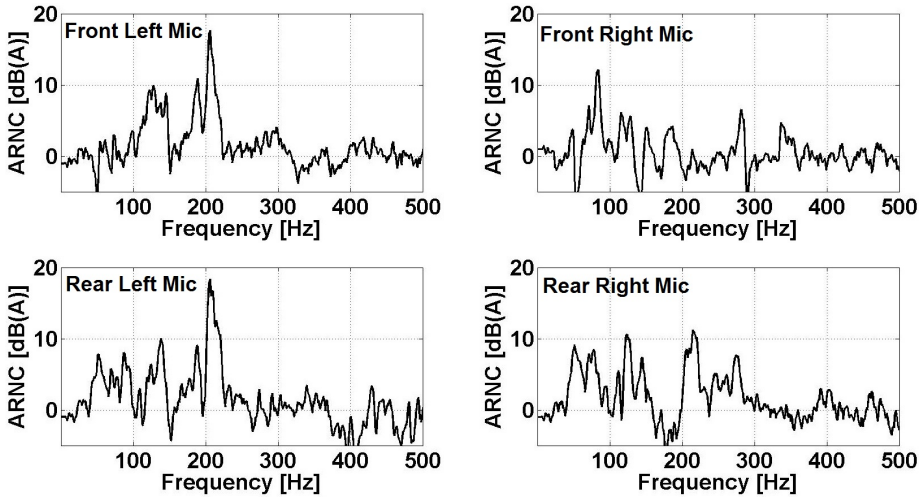

FIGURE 7.15: ARNC performance at the four headrests.

on the side of the co-driver for measuring the in-phase vibrational components of road noise. On the hand, the road boom around 80 Hz is attenuated by 11 dB(A) at the right hand front microphone. For the right hand rear microphone, better performance was measured compared to the front microphone and 8-10 dB(A) reduction was obtained between 200-220 Hz.

The averaged reduction at the four headrests is 4 dB(A). This implies that the sensor position on the suspension system is one of the weakest links in terms of road noise dynamics, the controller takes advantage of the high contribution of this point to the noise at the headrests. As a result, the controller is able to cancel effectively most of the road noise resonances that are generated by front axle vibrations. Very good overall performance between 0-500 Hz was measured according to table 7.3, where the noise levels are reduced by 4 dB(A) across the four microphones. The highest reduction is obtained at the side of the reference

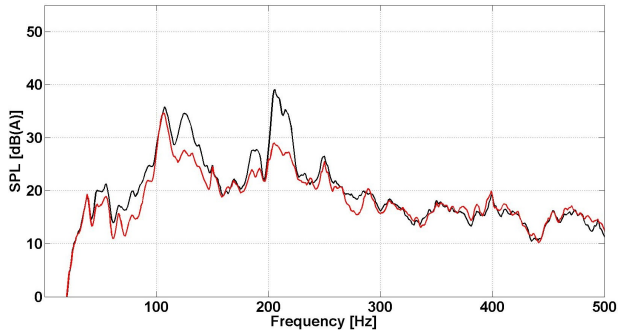

(a) Averaged interior noise. −: ARNC off. −: ARNC on.

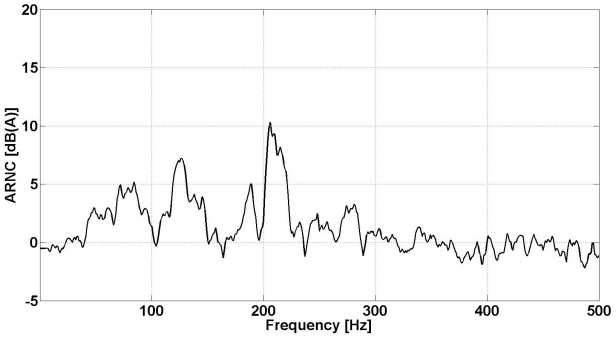

(b) Averaged Attenuation.

FIGURE 7.16: Averaged ARNC performance at the four headrests.

sensor, where around 6 dB(A) are removed from the structure-borne noise levels.

LHF dB(A)	RHF dB(A)	LHR dB(A)	RHR dB(A)	Average dB(A)
6.6	0.5	6.3	2.7	4.0

TABLE 7.3: Total reduction for 0-500 Hz. LHF: Left hand front, RHF: Right hand front headrest, LHR: Left hand rear, RHR: Right hand rear.

7.4 ARNC simulation: Excitation at the rear tyres

In this section the two locations at the right side of the rear axle of the vehicle were evaluated as references to the feedforward controller. In chapter 4 we found that these two locations on the rear axle are responsible for the road rumble and in this study were used to provide coherent reference signals to the controller. The two locations at the rear subframe that are investigated in the following sections are presented in figure 7.17, where only the z-axis was found to be the most important direction for road noise and its active control in chapters 6 and 4.

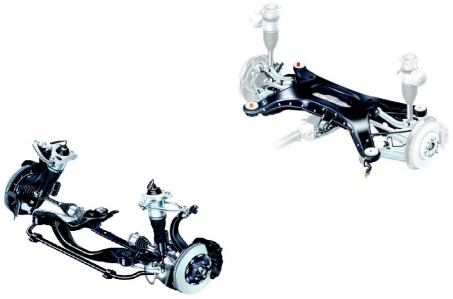

FIGURE 7.17: Reference sensors at the subframe mounts of the rear axle. ■, ■: Acceleration signals from the z-axis.

7.4.1 Case 4: Reference at the rear subframe mount and control filter length I=512

The first reference sensor location was at the right hand mount on the rear axle. For the purpose of this experiment, the sampling rate was set at 4 kHz and filter length was 512 taps, which is twice the length of the FIR filter used for the front axle, since the rumble band is broader than tyre cavity.

As in the previous section three microphones were used as error microphones as a point and the microphone at the driver's hearest was used as an observation microphone. In figure 7.18 the simulated road noise responses are presented. In can be noticed that cancellation is very effective also at the front part of the vehicle at the co-driver's headrest (right hand front microphone) in the rumble range. The measured reduction at that position was around 9-10 dB(A) from 100-120 Hz as presented in figure 7.19. Similar levels of reductions are also recorded for the rear headrest at the right hand side of the vehicle.

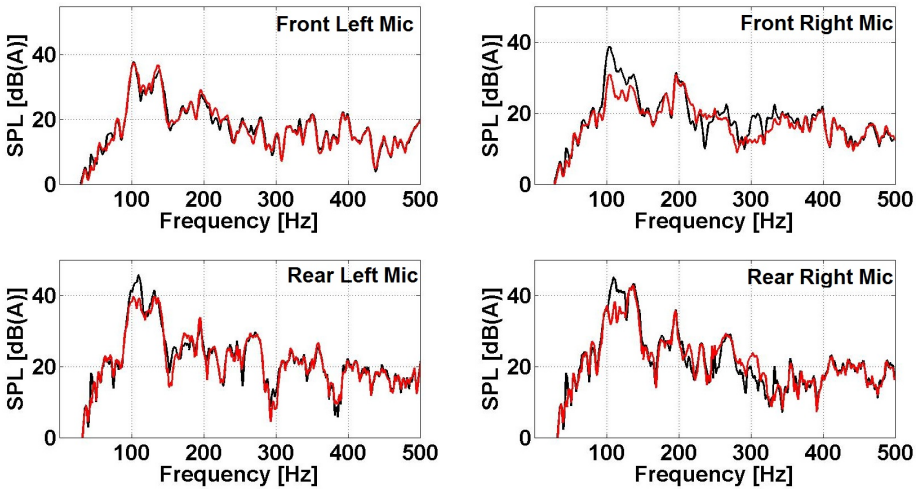

FIGURE 7.18: Interior noise at the four headrestswhen only the rear tyres are excited by the shakers. −: ARNC off. −: ARNC on

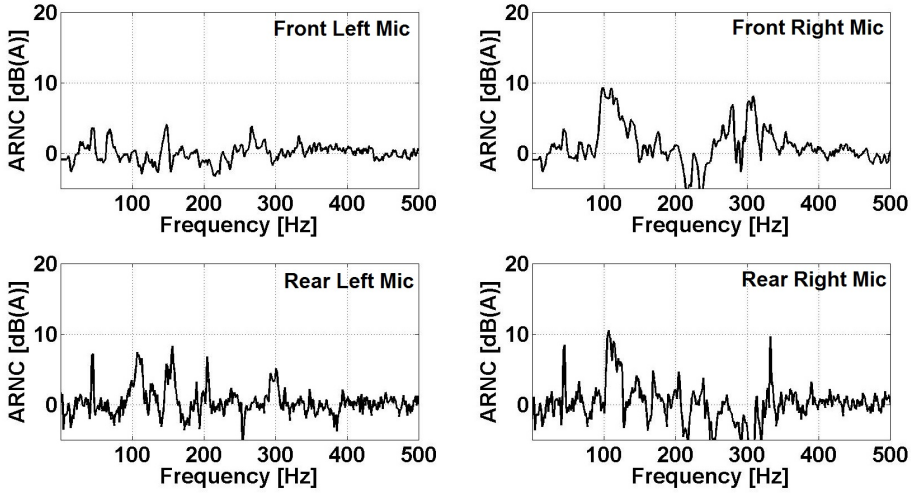

FIGURE 7.19: ARNC performance at the four headrests.

For the third microphone at the left hand rear headrest the reduction is close to 8 dB(A) but over a narrower frequency range, 100-110 Hz. In terms of the observation point at the driver's headrest, no significant reduction or amplification was obtained, due to the fact that source is coming from the back of the vehicle.

In the previous section for the tyre cavity noise, high amplification was noticed, since the structural sources of the front axle directly couple with the sound field at the front headrests. Therefore if selective zone of quiets are designed such as the driver can hear the road surface changes, then the location of the road noise sources must be considered as side-effects can occur if they have strong contribution to the driver's headrest.

In figure 7.20(a) the operation of the controller is mainly effective from 100 to 120 Hz for the three microphones and the attenuation is ranging from 7-10 dB(A). This is expected as the road rumble requires more acceleration signals, in order to observe the rear subframe vibration. In chapter 6 we found that the four rear subframe locations are necessary for completely canceling the road rumble. However, significant improvements were obtained even with the single sensor, as the total averaged attenuation in the road noise range according to table 7.4 is 2.2 dB(A).

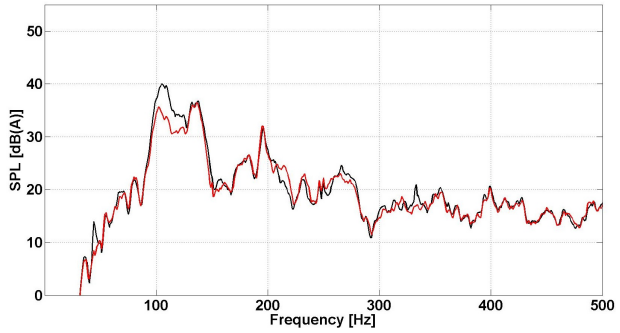

(a) Averaged interior noise. −: ARNC off. −: ARNC on.

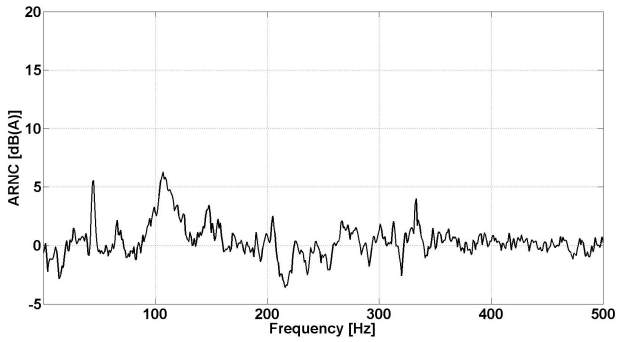

(b) Averaged Attenuation.

FIGURE 7.20: Averaged ARNC performance at the four headrests.

LHF dB(A)	RHF dB(A)	LHR dB(A)	RHR dB(A)	Average dB(A)
-0.6	4.0	2.5	2.7	2.2

TABLE 7.4: Total reduction for 0-500 Hz. LHF: Left hand front, RHF: Right hand front headrest, LHR: Left hand rear, RHR: Right hand rear.

7.4.2 Case 5: Reference at the rear subframe mount and control filter length I=1024

In the second experiment for the front axle in section 7.3.5 it was demonstrated that doubling the control filter length can increase the level of reduction. Similarly, the length of the FIR control filters was doubled from 512 to 1024 taps.

This change in the configuration of the adaptive controller improved the performance of the system as illustrated in figures 7.21 and 7.22 with the longer filters.

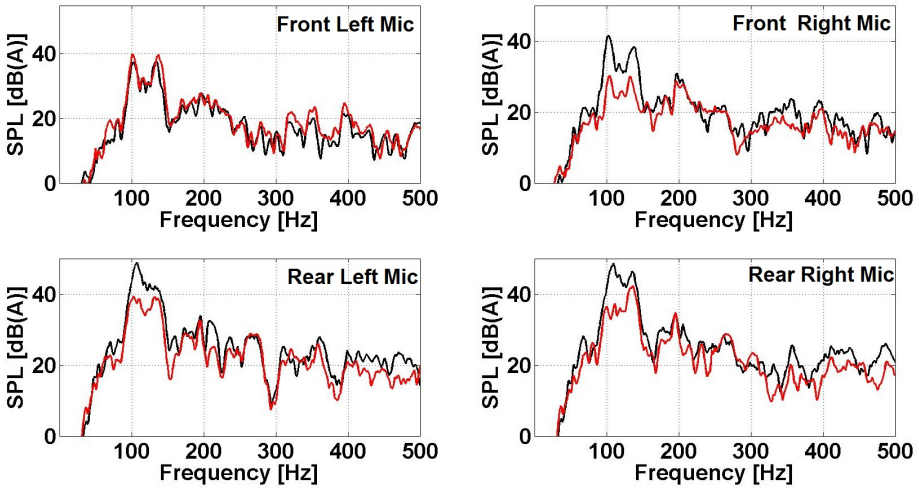

FIGURE 7.21: Interior noise at the four headrests, when only the rear tyres are excited by the shakers. −: ARNC off. −: ARNC on.

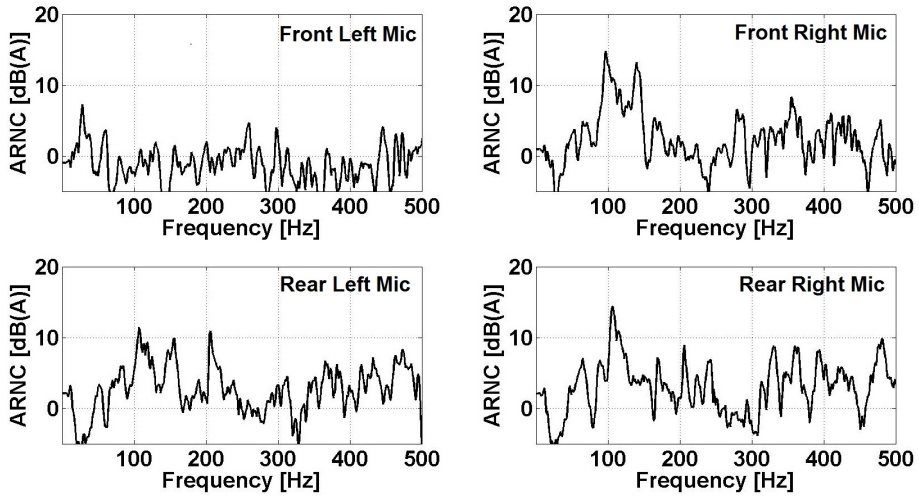

FIGURE 7.22: ARNC performance at the four headrests.

The rumble is effectively reduced up to 12 dB(A) for the right hand front microphone and 5-12 dB(A) for the rear headrests. Good control of the rumble can be noticed across the three headrests, which results to 4.6 dB(A) overall reduction. In table 7.5 an impressive 7 dB(A) reduction was measured for the right hand front microphone and around 6 dB(A) for the rear headrests. Some small enhancements are noticed at sound pressure level at the driver's headrest (front left microphone), which for once more it was not included as an input to the controller.

In a past research study for ARNC it has been shown theoretically that an increase of 100 taps in the control filter length, can improve the reduction by 1 dB [Bernhard (1995)]. If table 7.4 and table 7.5 are compared, then it can be observed that the attenuation is increased from 2.2 dB(A) to 4.6 dB(A) for the same reference signal.

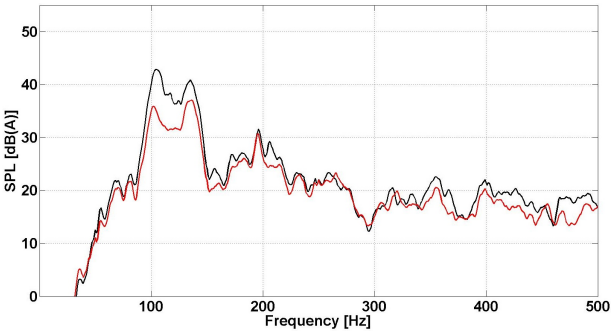

(a) Averaged interior noise. —: ARNC off. —: ARNC on.

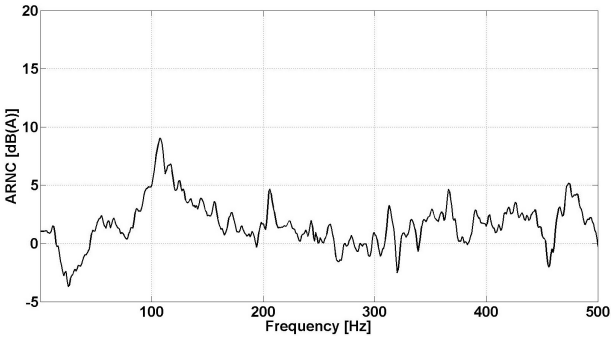

(b) Averaged Attenuation.

FIGURE 7.23: Averaged ARNC performance at the four headrests.

LHF dB(A)	RHF dB(A)	LHR dB(A)	RHR dB(A)	Average dB(A)
-1.7	7.0	6.0	6.2	4.6

TABLE 7.5: Total reduction for 0-500 Hz. LHF: Left hand front, RHF: Right hand front headrest, LHR: Left hand rear, RHR: Right hand rear.

7.4.3 Case 6: Force signal as reference and control filter length I=512 and four error microphones

Force signals have been used as references for the theoretical modeling of the performance of a feedforward ARNC system [Mohammad and Elliott (2006),Mohammad et al. (2008)]. The random force signals were used as the reference inputs to a multichannel feedforward controller and it was shown that they do not provide significant attenuation. In the same studies it was also demonstrated that sixteen force signals are necessary to cause 4 dB of the acoustic potential energy in a rectangular cavity.

In this experiment a force gauge that was placed inbetween the shaker and the left hand rear tyre and the output signal of the sensor was used as reference. Therefore this case investigates how the controller performs, when it is using one of the uncorrelated inputs as a reference input to the controller. As it can be

noticed in figure 7.24 the control is effective only at the rear headrests. Around 10 dB(A) of attenuation was obtained at the rear headrest microphones between 100-120 Hz. The limited effectiveness at the front headrests might be expected, since the spatial filtering of the structure and the contribution of the second shaker limit the performance with only one single sensor.

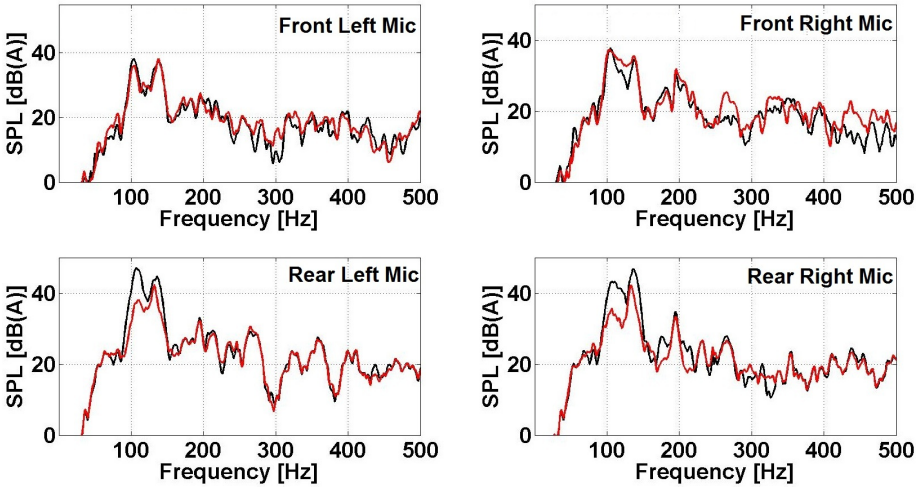

FIGURE 7.24: Interior noise at the four headrests, when only the rear tyres are excited by the shakers. −: ARNC off. −: ARNC on

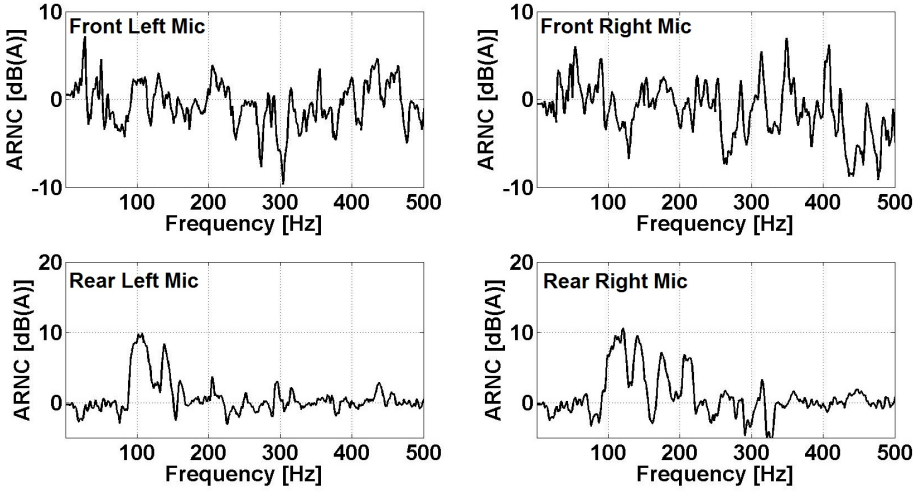

FIGURE 7.25: ARNC performance at the four headrests.

Unfortunately, some amplification at the front sear can be noticed, especially above 200 Hz, which justifies the necessity for a second reference signal coming from the rear right shaker transducer. However, it can be expected that if force sensors can be somehow placed in the vehicle structure, then better control of structure-borne noise can be achieved. Therefore, it might be possible to use also the forces from various sensitive structural points in the axles instead of the forces that are directly applied on the tyres. However, in this study we did not concerntrate on the design of sensors that may also to measure directly the forces at the points on the structure, but it is strongly recommended for future

research studies. Especially, if the car is analysed with the use of TPA, where the force spectra at several points of the vehicle are already know and might be used for ARNC prediction studies, before applying the technology.

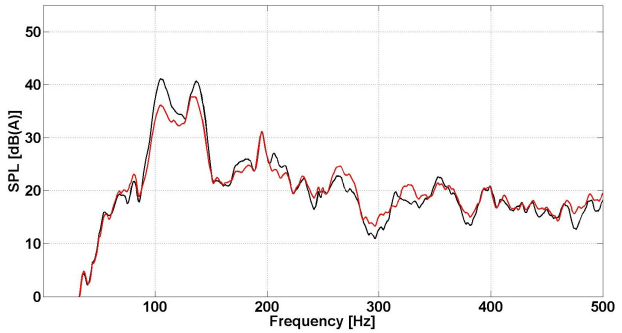

(a) Averaged interior noise. —: ARNC off. —: ARNC on.

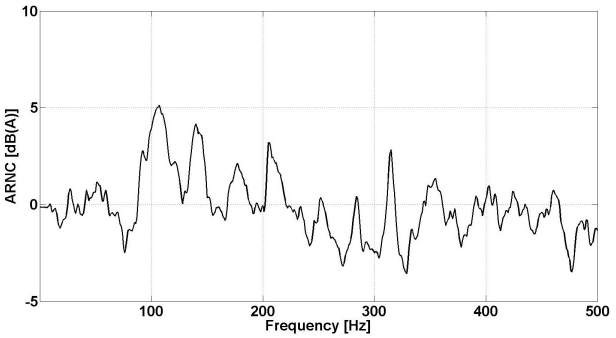

(b) Averaged Attenuation.

FIGURE 7.26: Averaged ARNC performance at the four headrests.

The total reduction at the two rear headrests was slightly more than 5 dB(A) as can be seen in table 7.6 and the average reduction across the four microphone 2.5 dB(A). This is a strong proof that force sensors at the tyres may potentially provide good reduction and also in general force signal could be also used for this type application instead of acceleration signals.

LHF dB(A)	RHF dB(A)	LHR dB(A)	RHR dB(A)	Average dB(A)
0.6	-1.4	5.1	5.6	2.5

TABLE 7.6: Total reduction for 0-500 Hz. LHF: Left hand front, RHF: Right hand front headrest, LHR: Left hand rear, RHR: Right hand rear.

7.4.4 Case 7: Reference at the front subframe mount and control filter length I=750 and f_s=8 kHz

For the purpose of this experiment the system was augmented with the microphone at the driver's headrest as the fourth error sensor of the control system. Maximum reduction of 10-15 dB(A) was noticed for the rear microphone between 95-120 Hz. As for the front headrests, the attenuation was less, around 5 dB(A) in the rumble range.

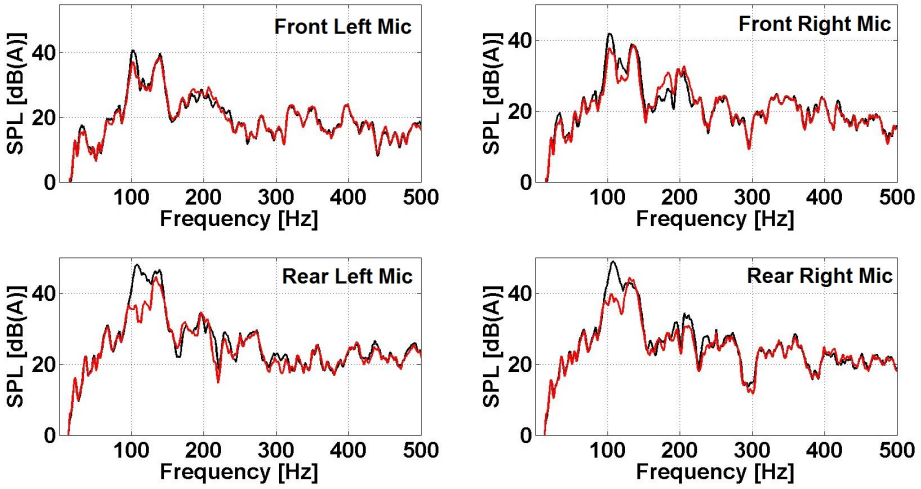

FIGURE 7.27: Interior noise at the four headrests, when rear the front tyres are excited by the shakers. −: ARNC off. −: ARNC on

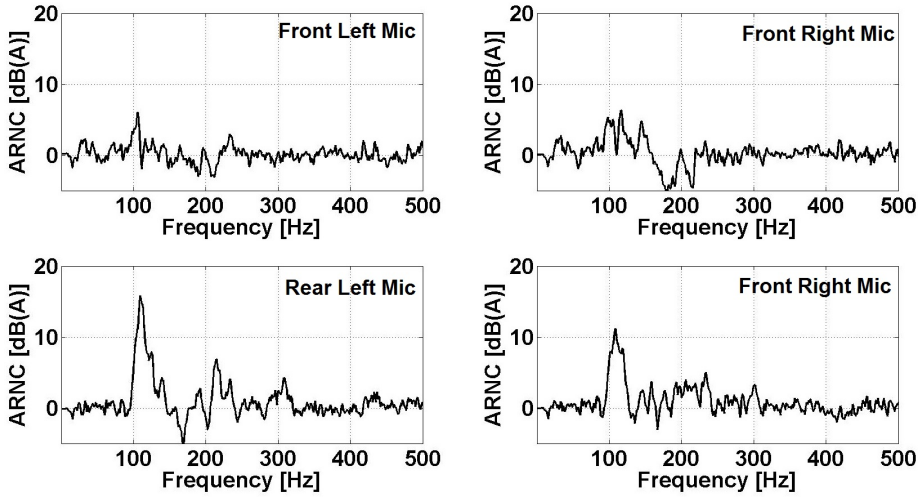

FIGURE 7.28: ARNC performance at the four headrests, when only the rear tyres are excited by the shakers.

The effectiveness of the controller at the front microphones was very limited. This again relates to the fact that the controller can manage only a single reference signal, since more locations at the rear are actually contributing to the rumble range. The averaged reduction was around 5 dB(A) in the rumble

range and 2 dB(A) at 220 Hz for the tyre cavity band. Consequently, the overall reduction is lower than the previous experiments and 1.8 dB(A) across the four headrests were obtained according to table 7.7.

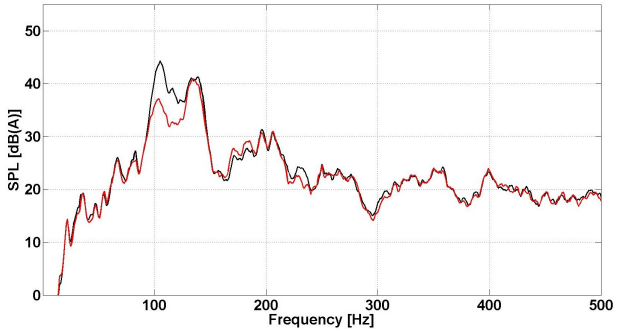

FIGURE 7.29: Averaged interior noise. −: ARNC off. −: ARNC on.

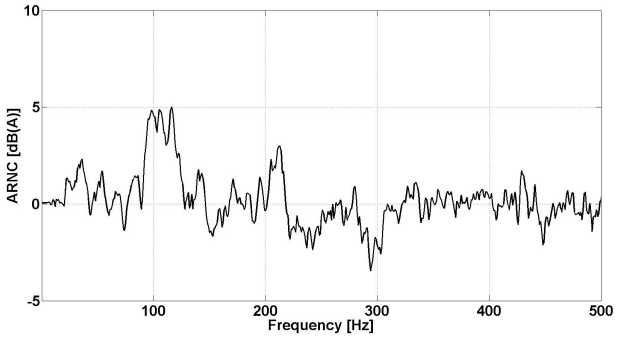

FIGURE 7.30: Averaged ARNC performance at the four headrests.

LHF dB(A)	RHF dB(A)	LHR dB(A)	RHR dB(A)	Average dB(A)
1.6	0.7	3.5	2.0	1.8

TABLE 7.7: Total reduction for 0-500 Hz. LHF: Left hand front, RHF: Right hand front headrest, LHR: Left hand rear, RHR: Right hand rear.

7.4.5 Case 8: Reference at the front subframe mount and control filter length I=256 and f_s=2 kHz

The second location that also highly contributes to the rumble noise was used as reference, but with a different configuration. The FIR filters were longer with 750 taps and 8 kHz sampling rate and the anti-aliasing filters been deactivated, in order to investigate if there is any effect of the controller's delay at the system. This location is actually slightly closer to the body side of the vehicle thus it was thought that a high sampling rate might reduce the latency of the control filtering stage in the case it has any severe effects on the adaptation stage.

In figure 7.31 it can be noticed that the reduction is somehow limited to the first resonance for the rear microphones of the road rumble. In addition the system was not able to provide broadband attenuation for the rear axle contributions to the front microphones and 5 dB(A) were measured at narrow frequency range as it can be seen in the graphs of figure 7.32.

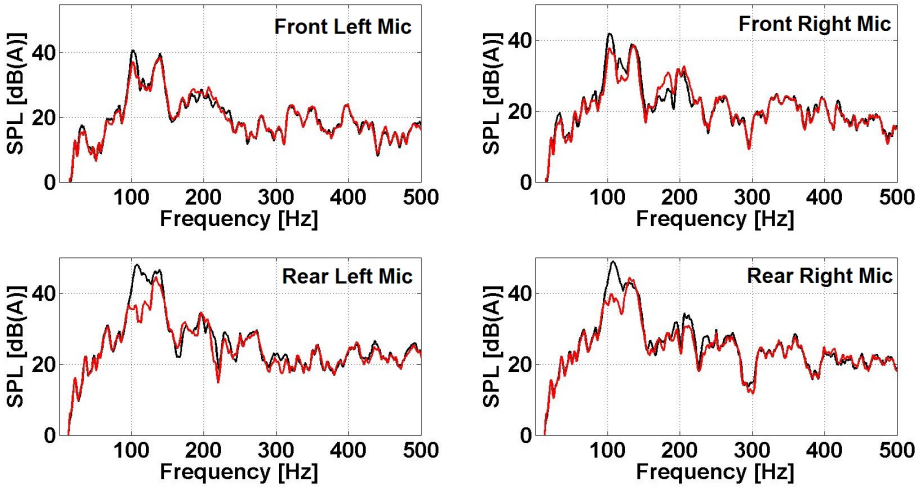

FIGURE 7.31: Interior noise at the four headrests, when the rear tyres are excited by the shakers.. —: ARNC off. —: ARNC on

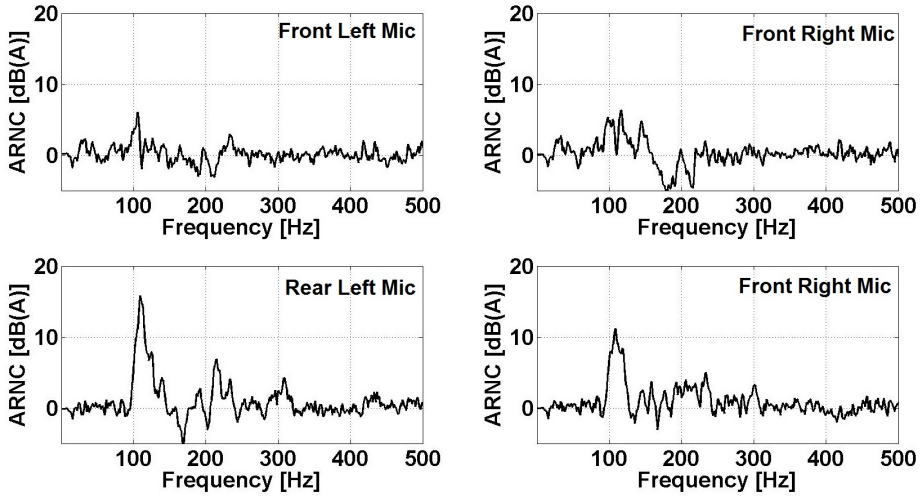

FIGURE 7.32: ARNC performance at the four headrests.

This limited performance of the system is probably due to the fact that actually 2-4 accelerometers are necessary at the rear axle. This way all the structural vibrations can be observed simultaneously and possibly controlling all the rear axle contributions. However, as mentioned before the controller allowed only one reference and thus the performance also for front microphones was limited to a narrow frequency range as not all the structural sources were fed into the controller that are contributing to the rumble. Even if the attenuation is limited to 1.3 dB(A) and 1.6 dB(A) for the left and right hand front headrest

microphones, the performance at the rear is more than 2 dB(A) for a single reference signal. In figure 7.32 that the attenuation was around 5 dB(A) from 90-120 Hz.

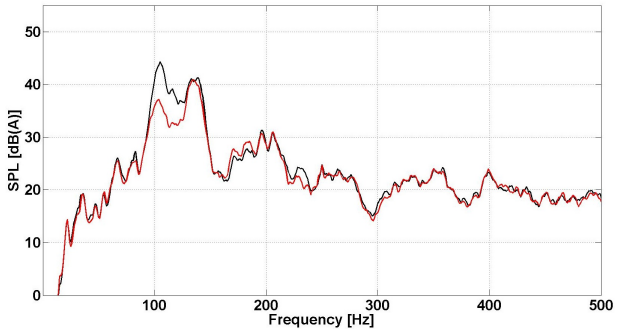

FIGURE 7.33: ARNC performance at the four headrests.

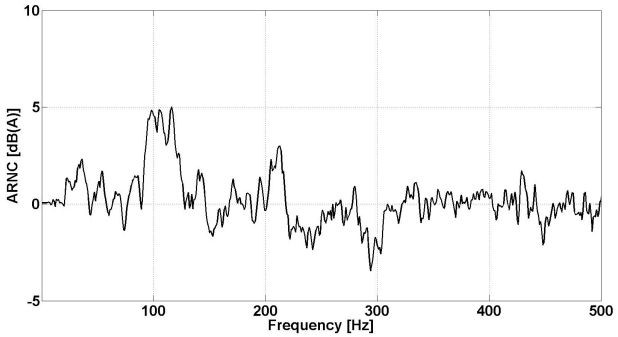

FIGURE 7.34: ARNC performance at the four headrests.

In total 2.7 dB(A) were obtained from this ARNC configuration with the reduction been focused at the rear headrests according to table 7.9. As for the rear headrest the noise levels were reduced by 4.7 dB(A) and 3.2 dB(A) for the left and right side respectively.

LHF dB(A)	RHF dB(A)	LHR dB(A)	RHR dB(A)	Average dB(A)
1.3	1.6	4.7	3.2	2.7

TABLE 7.8: Total reduction for 0-500 Hz. LHF: Left hand front, RHF: Right hand front headrest, LHR: Left hand rear, RHR: Right hand rear.

7.4.6 Case study 9: Reference at the rear subframe mount and control filter length I=128 and f_s=2 kHz

So far a sampling rate far from the Nyquist frequency was used for reducing the latency that may be introduced by anti-aliasing filtering at the inputs of the

feedforward controller. In this case the sampling frequency was set to 2 kHz and thus the antialiasing filtering was necessary. The length of the control filter was selected to be 128-taps, in order to find also the minimum required number of coefficient required for this vehicle structure.

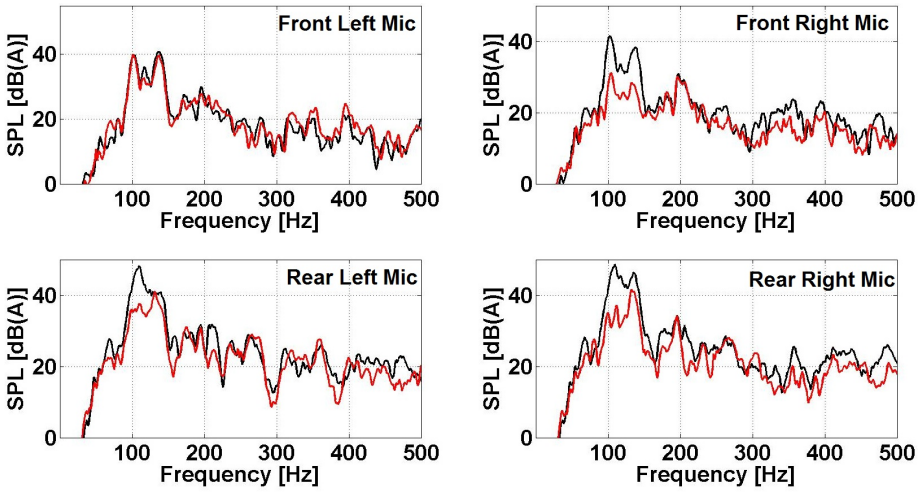

FIGURE 7.35: Interior noise at the four headrests, when only the rear tyres are excited by the shakers. −: ARNC off. −: ARNC on.

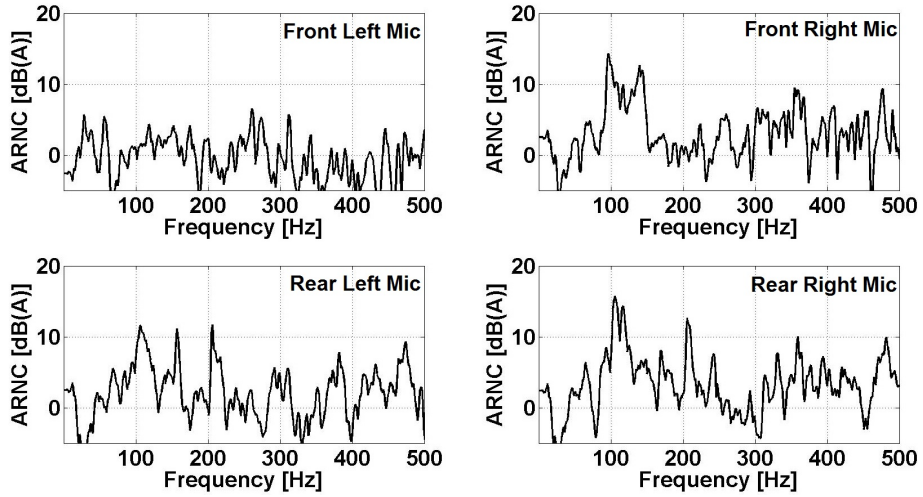

FIGURE 7.36: ARNC performance at the four headrests.

Actually the reduction of the filter length was proven to be beneficial for the adaptive system, as the adaptive algorithm was able to achieve faster convergence to a filter set in less than 10 minutes. Moreover reductions up to 500 Hz are noticeable, since also the location of the rear subwoofer is relatively close to the headrests, around 20 cm distance, thus it directly couples acoustically with the radiated rumble noise from the vehicle's panel.

Therefore the reduction of the sampling rate and the introduction of the anti-aliasing filters did not actually affect the controller's causality as it was

been noticed in a past study with feedforward control [Sas and Dehandschutter (1999)].

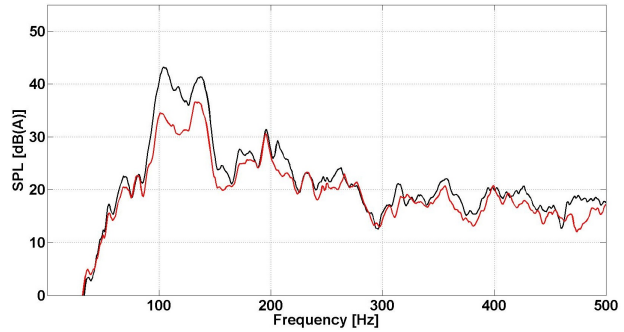

(a) Averaged interior noise. −: ARNC off. −: ARNC on.

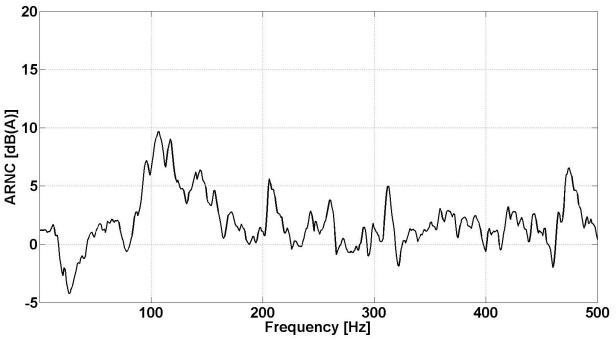

(b) Averaged Attenuation.

FIGURE 7.37: Averaged ARNC performance at the four headrests.

The attenuation was significantly improved and the noise was reduced by 10-15 dB(A) at the three error microphones as it can be seen in figure 7.35. In addition to that the averaged attenuation at the four microphones in figure 7.36 deviates from 5-10 dB(A) between 90-160 Hz, which shows the effectiveness of the controller across the headrests.

The total reduction from 0 Hz to 500 Hz at the co-driver's headrest was 7 dB(A), which previously the controller with the force sensor signal as reference was not able to attenuate at all. The setup with 1024 taps at 4 kHz had also provided exactly the same reduction for that microphone in table 7.5.

Moreover the averaged attenuation across the headrests was 5.6 dB(A) according to table 7.9, which is 1 dB(A) higher than the one obtained in the experiment of section 7.4.1 for the rear subframe mount. It seems that this second location at the rear axle provides good road rumble performance, which validates the fact that the structural location at the axles with the most coherent signal provides also better control of the noise as this location and DoF was also used for the coherence predictions in section 4.3.2. This setup also could be also potentially used in real application in a production line luxury vehicle for

reducing the road rumble at the rear headrests with a pair of accelerometers at the rear subframe of the rear axle.

LHF dB(A)	RHF dB(A)	LHR dB(A)	RHR dB(A)	Average dB(A)
1.1	7.0	5.7	7.4	5.6

TABLE 7.9: Total reduction for 0-500 Hz. LHF: Left hand front, RHF: Right hand front headrest, LHR: Left hand rear, RHR: Right hand rear.

7.5 ARNC physical simulation: Excitation at the four tyres

7.5.1 Case study 10: Reference location at the rear subframe mount of the rear axle

The location at the rear axle of section 7.4.1 was for once more used as a reference input to the controller. In this experiment the performance of the controller was evaluated for the case of the front and rear axle vibro-acoustic paths contributing to the sound field simultaneously as it is on actual driving conditions on the road. As it was shown in section 3.2.4, this shaker setup can simulate fairly well the structure-borne road noise profile for a low speeds as the transducer sensitivity limited the output levels that could provide a higher excitation input into tyres.

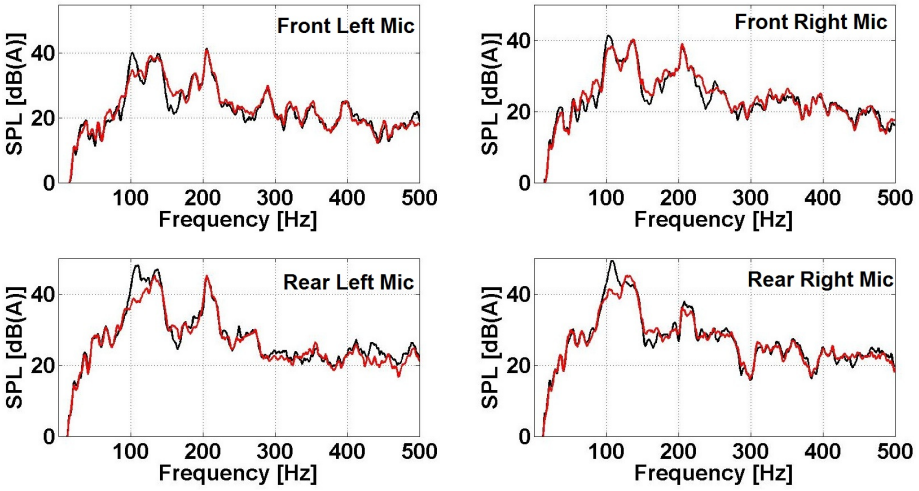

FIGURE 7.38: Interior noise at the four headrests, when all the tyres are excited by the shakers. −: ARNC off. −: ARNC on

The reduction in this case is not impressive for the front headrest microphones. At the driver's headrest maximum 2 dB(A) were obtained and 7 dB(A) at the co-driver's headrest in the road rumble range. At the rear headrests the noise was reduced up to 10 dB(A) between 90-110 Hz. The total noise levels in the frequency range of 0-500 Hz were reduced at the rear headrests by 2 dB(A) according to table 7.10 and an average of 1.3 dB(A) was obtained for the four headrests.

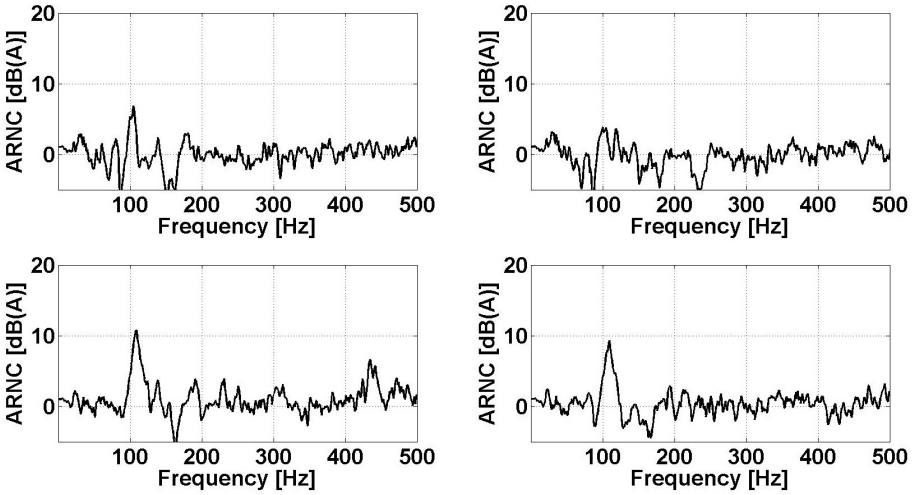

FIGURE 7.39: ARNC performance at the four headrests.

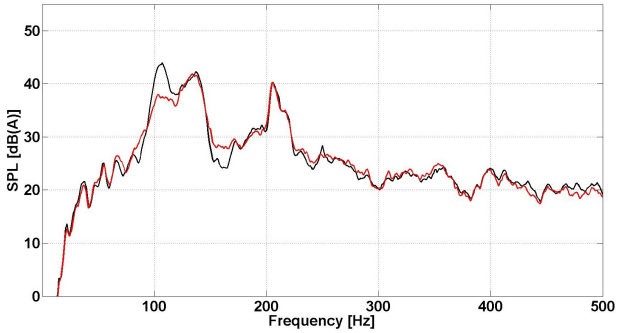

(a) Averaged interior noise. −: ARNC off. −: ARNC on

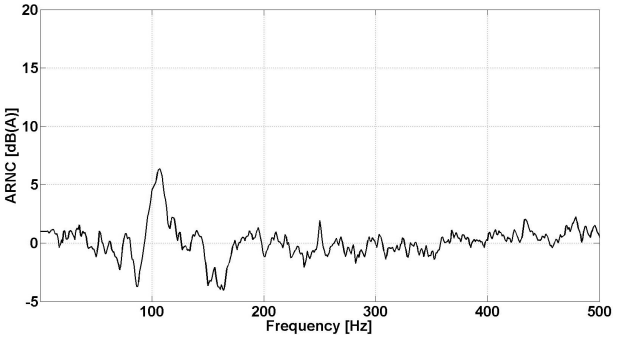

(b) Averaged Attenuation.

FIGURE 7.40: Averaged ARNC performance at the four headrests.

This limited performance for the rear axle is due to the fact that a single reference is not enough for observing all the structural sources that contribute to the structure-borne noise at the headrests. However, this location provides good control at the targeted frequency region (road rumble) that was initially selected for. We now observe a loss of performance as the vibration field now is closer to the actual one that is caused by the interaction of the tyres and the road surface. Even though still 2 dB(A) were attenuated from the noise levels at the rear headrest microphones as it can be seen in table 7.10.

LHF dB(A)	RHF dB(A)	LHR dB(A)	RHR dB(A)	Average dB(A)
0.3	0.3	2.6	2.0	1.3

TABLE 7.10: Total reduction for 0-500 Hz. LHF: Left hand front, RHF: Right hand front headrest, LHR: Left hand rear, RHR: Right hand rear.

7.5.2 Case study 11: Reference accelerometer at the front subframe mount of the rear axle

The second location of the rear axle that was used in section 7.4.6, which is the z-direction at the front mount of the rear subframe and it is the one that has provided the best reduction at the rear seats so far. It was observed in previous measurements for this accelerometer location at the rear axle that the cancellation was limited for the front microphones. In contrast, the reduction levels at the rear microphone are more noticeable in figure 7.41, where the noise levels between 100-120 were reduced by a maximum of 10 dB(A) as can be seen in figure 7.42. If table 7.10 and 7.11 are compared, then it can be noticed that the attenuation of the structure-borne noise at the rear headrest microphone is increased by almost 1 dB(A) in the frequency range 0-500 Hz. This improvement should be expected as in sections 7.4.5 and 7.4.6 it was shown that this accelerometer location provided better noise reduction at the rear headrests microphones. This again relates to the high structural sensitivity of this part of the rear axle that allows the vibrations to be transmitted into the vehicle's panel. Unfortunately, the noise levels at the tyre cavity range were not attenuated at all in sensor arrangement, since the main transfer paths of this noise are located at the front axle in this vehicle. Therefore, measurements with the accelerometer located at the front axle had to be repeated and are discussed in the following section.

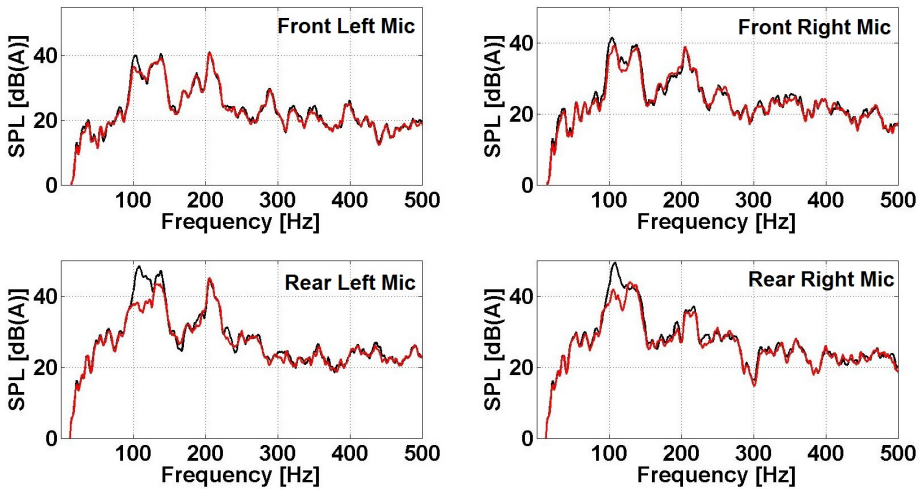

FIGURE 7.41: Interior noise at the four headrests, when all the tyres are excited by the shakers. −: ARNC off. −: ARNC on.

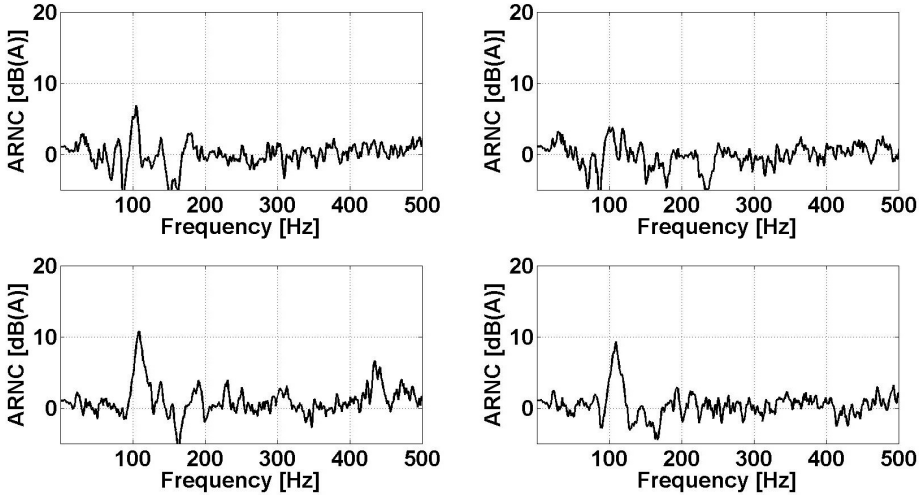

FIGURE 7.42: ARNC performance at the four headrests.

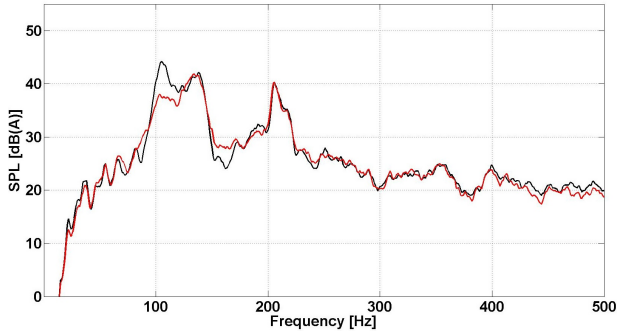

(a) Averaged interior noise. −: ARNC off. −: ARNC on.

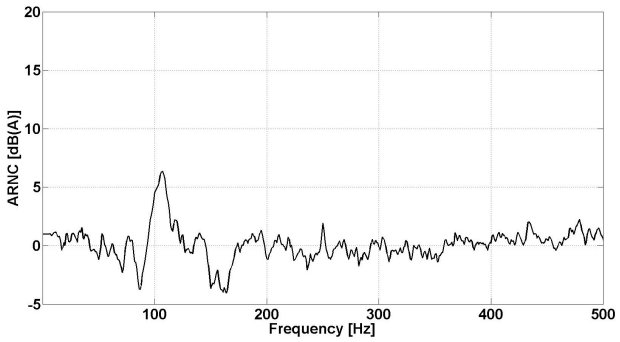

(b) Averaged Attenuation.

FIGURE 7.43: Averaged ARNC performance at the four headrests.

LHF dB(A)	RHF dB(A)	LHR dB(A)	RHR dB(A)	Average dB(A)
0.5	0.9	3.2	3.1	1.8

TABLE 7.11: Total reduction for 0-500 Hz. LHF: Left hand front, RHF: Right hand front headrest, LHR: Left hand rear, RHR: Right hand rear.

7.5.3 Case study 12: Reference accelerometer at the lower control arm at the front axle

The accelerometer location that was in section 7.3.4 at front lower control arm of the left hand front suspension is again providing the reference input for controlling the sound pressure levels of tyre cavity at the four headrests.

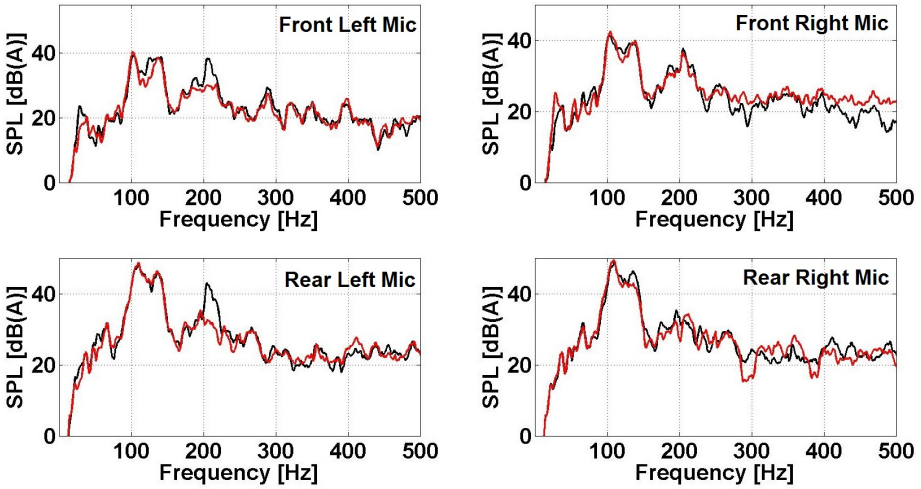

FIGURE 7.44: Interior noise at the four headrests, when all the tyres are excited by the shakers. −: ARNC off. −: ARNC on.

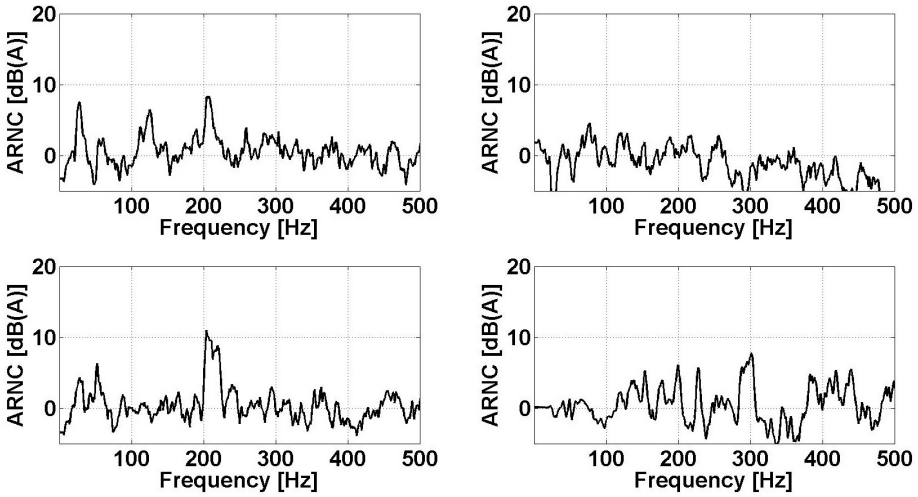

FIGURE 7.45: ARNC performance at the four headrests.

The reduction is only noticeable at the left side of the vehicle according to measured microphone responses in figure 7.44. As a starting point a high sampling and long FIR filter were used for this experiment. A sampling frequency of 8 kHz was used in order to avoid using any anti-aliasing filtering for the sensor signals. However, this change required longer FIR filters and thus 512-taps were trained for each controller. The effectiveness of the controller is again noticeable in the tyre cavity range for the left hand front and rear headrest microphone signals was resulted after training the system with adaptive algorithm. In particular 8 dB(A) and 10 dB(A) reduction can be seen in these two headrest locations in the tyre cavity range between 200-210 Hz. The averaged reduction is 5 dB(A) around 205 Hz, but the overall reduction is negligible according to table 7.12. However, there might be a subjective benefit of having this smoothing of the road spectrum with the ARNC even at the narrow frequency range of the tyre cavity resonance. This poor overall performance is likely to be caused by the settings of the adaptive controller, since in experiments for the front tyres the cancellation of the tyre cavity noise was effective in all of the microphone signals.

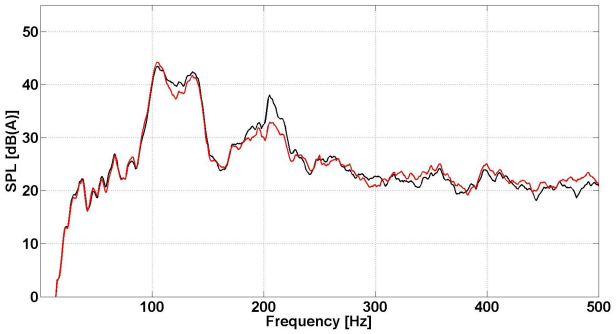

(a) Averaged interior noise. −: ARNC off. −: ARNC on.

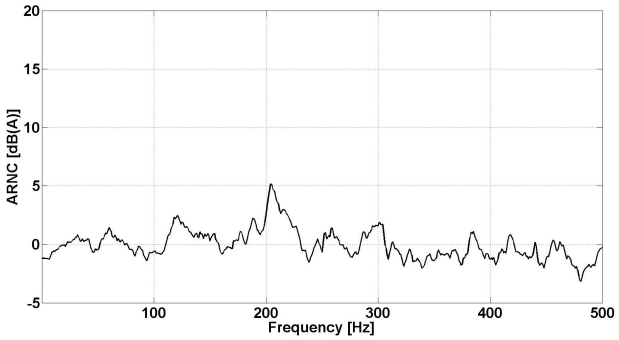

(b) Averaged Attenuation.

FIGURE 7.46: Averaged ARNC performance at the four headrests.

LHF dB(A)	RHF dB(A)	LHR dB(A)	RHR dB(A)	Average dB(A)
1.5	0.0	0.2	0.3	0.5

TABLE 7.12: Total reduction for 0-500 Hz. LHF: Left hand front, RHF: Right hand front headrest, LHR: Left hand rear, RHR: Right hand rear.

7.5.4 Case study 13: Reference accelerometer at the lower control arm at the front axle and f_s=2 kHz I = 128-taps

The previous ARNC sensor setup was used again, in order to investigate the effects of the long FIR filters and high sampling frequencies. In this case the length of the FIR control filters was shortened to 128 taps and the sampling rate was set to 2 kHz with also antialiasing filter also introduced into the control path.

According to figure 7.47 the reduction in the sampling rate and filter length of the adaptive system looks like they did actually improve the levels of cancellation at all of the microphone locations. It can be noticed that good reduction of tyre cavity noise was obtained 200-220, the maximum cancellation was 10 dB(A) at 205 Hz. Interestingly, the controller was also able to reduce by 10 dB(A) the 290 Hz resonance at the left hand front headrest.

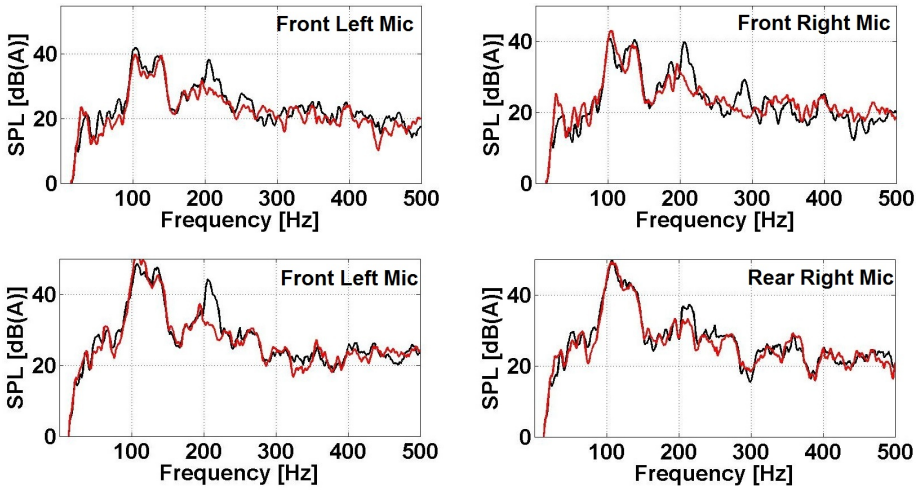

FIGURE 7.47: Interior noise at the four headrests, when all the tyres are excited by the shakers. −: ARNC off. −: ARNC on.

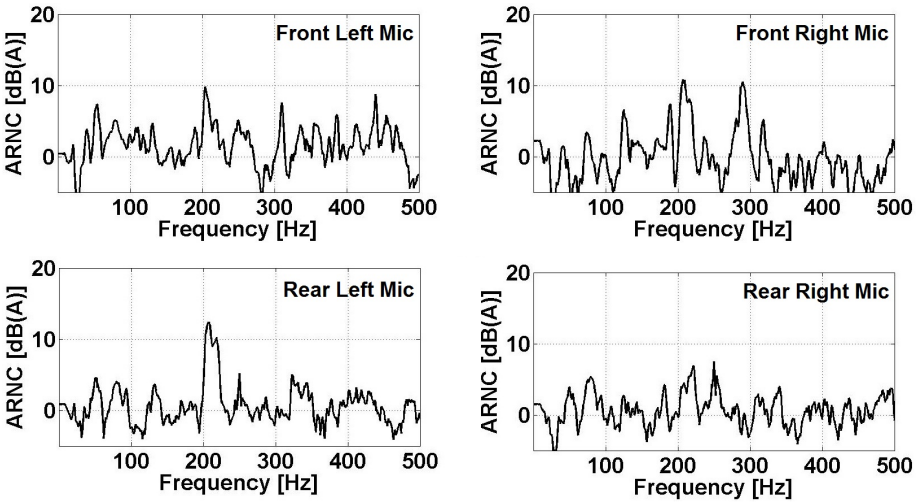

FIGURE 7.48: Averaged ARNC performance at the four headrests.

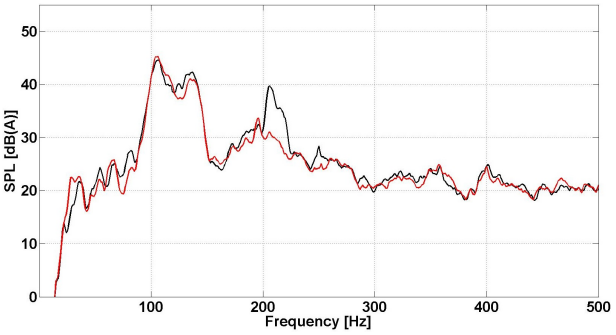

(a) Averaged interior noise. −: ARNC off. −: ARNC on.

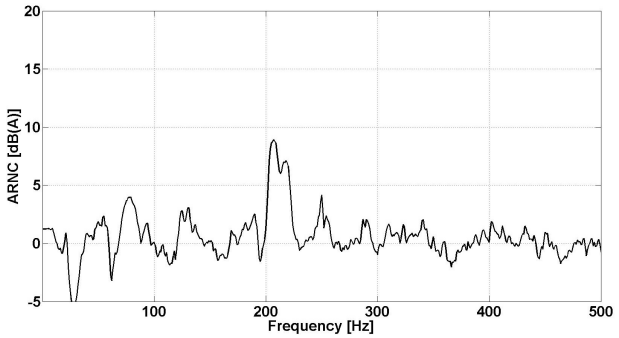

(b) Averaged Attenuation.

FIGURE 7.49: Averaged ARNC performance at the four headrests.

The averaged attenuation in the tyre cavity range at the four microphones deviates from 7-9 dB(A) as it can be noticed in figure 7.49(b).

LHF dB(A)	RHF dB(A)	LHR dB(A)	RHR dB(A)	Average dB(A)
2.1	0.5	-0.6	0.0	0.5

TABLE 7.13: Total reduction for 0-500 Hz. LHF: Left hand front, RHF: Right hand front headrest, LHR: Left hand rear, RHR: Right hand rear.

7.6 Multichannel active road noise

A portable system based on the ADwin Gold II was developed for the evaluation of a multichannel system. Four accelerometers were mounted on the locations that were used in the previous experiments. The ADWin system is a multichannel programmable controller through Matlab/Simulink environment for hardware in the loop simulations and also for real-time control and data acquisition. The following figure presents the arrangement of the hardware equipment for the portable controller inside the vehicle.

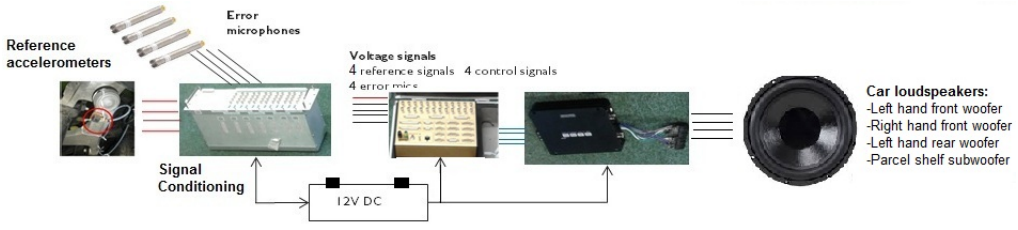

FIGURE 7.50: Hardware equipment for ARNC inside the vehicle. The arrangment of the units can be seen with the corresponding signals that flow in and out from the controller.

As a first step the ADwin system was used to acquire road noise and vibration data, in order to predict the performance of the system with the use of causal time domain simulation in Simulink with the use of the algorithm that was developed in chapter 6. Four acceleration signals were measured at two symmetrical locations at the front axle and two at the rear. The multiple coherence functions for the four microphones at the headrests were calculated and are illustrated in figures 7.52(a)-7.52(d).

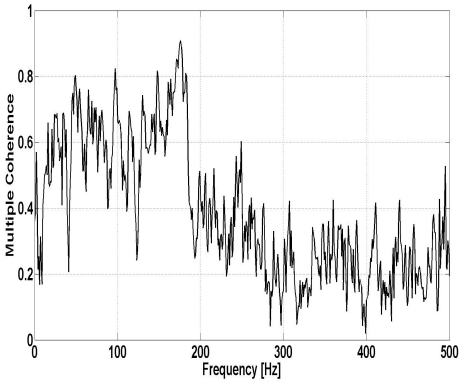

(a) Multiple coherence for the left hand front (LHF) microphone.

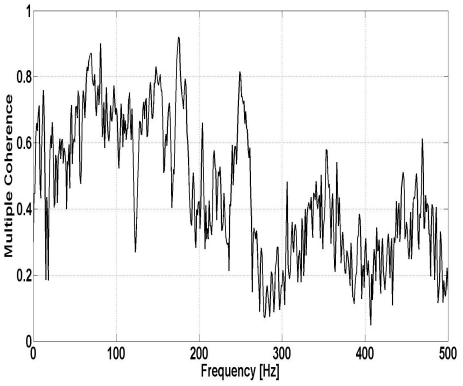

(b) Multiple coherence for the right hand front (RHF) microphone.

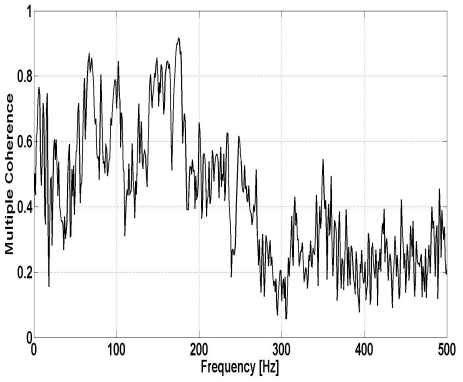

(c) Multiple coherence for the left hand rear (LHR) microphone.

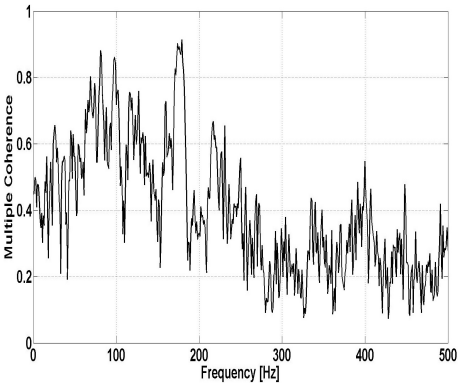

(d) Multiple coherence for the right hand rear (RHR) microphone.

FIGURE 7.51: Multiple coherence functions for the four microphones at the headrests.

Fairly good coherence is obtained in rumble band of 90-120 Hz, but even better for the tyre cavity noise in range of 160-180Hz. The road data were combined with the measured impulse responses of the audio system and the cabin for predicting the performance of the prototype system. Unfortunately, the development of this controller had to be terminated, due to severe electrical issue of the vehicle. Electrical transients were transmitted from the vehicle battery and burned the fuses that were protecting the prototype and also the power supply of the ADWin controller. Therefore only simulation results of the ADwin data are shown in figures for estimating the performance of the multichannel controller.

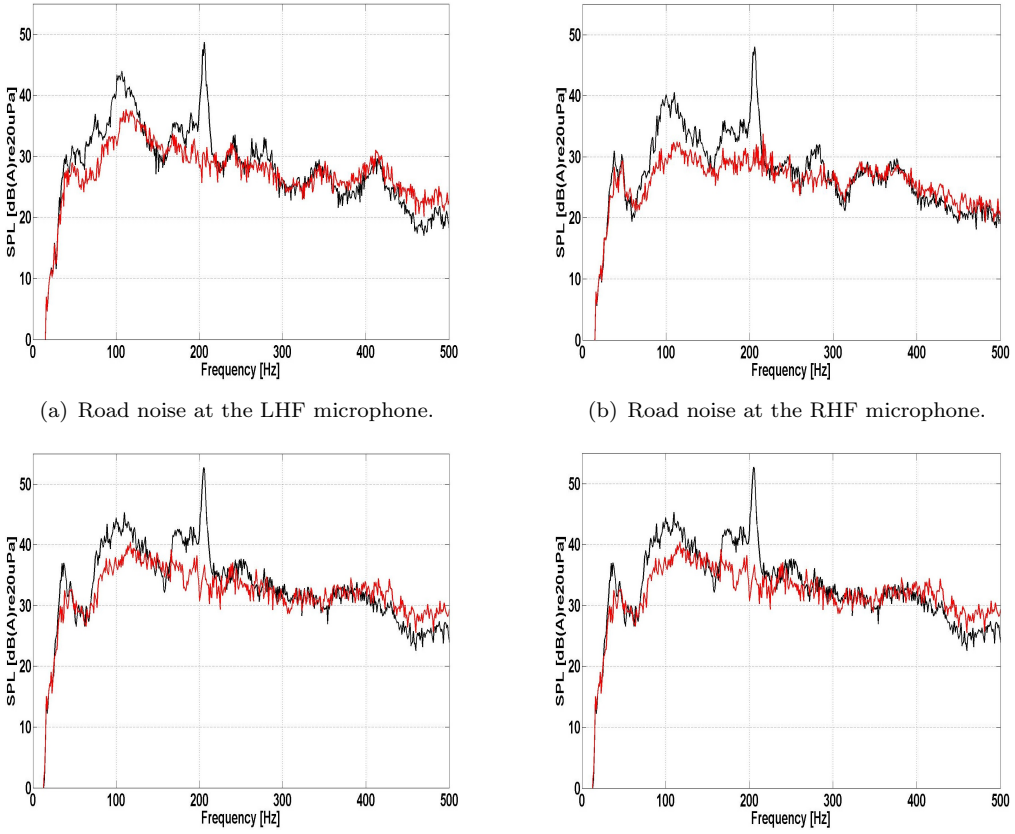

(a) Road noise at the LHF microphone.

(b) Road noise at the RHF microphone.

(c) Road noise at the LHR microphone.

(d) Road noise at the RHR microphone.

FIGURE 7.52: Interior noise at the four headrests at 50 km/h. −: ARNC off. −: ARNC on.

Good control can be obtained at this medium speed with four accelerometer locations measuring one direction only. This is mainly due to the fact that the accelerometers at this speed the main contributor is coming from the z-direction and thus more DoF are not necessary. However, at high speeds above 90 km/h more directions from the axles are contributing, thus more directions are necessary as we saw in chapter 6. If the controller is to operate in a specific speed range, where structure-borne dominates the sound field of the cabin, then this sensor configuration is apparently enough to achieve the necessary improvements in the NVH performance of road noise. It is also apparent that if the main vibrational inputs of the vehicle structure are not used as reference to the controller, then it can be difficult to demonstrate the technology and also the risk of using a large number of sensors is increased.

LHF dB(A)	RHF dB(A)	LHR dB(A)	RHR dB(A)	Average dB(A)
4.2	5.2	4.0	4.2	4.4

TABLE 7.14: Total reduction for 0-500 Hz. LHF: Left hand front, RHF: Right hand front headrest, LHR: Left hand rear, RHR: Right hand rear.

7.7 Summary

An ARNC system was implemented on Bentley Motor vehicle, in order to investigate under real-time conditions the accelerometer sensor placement on the vehicle chassis. The system was validated on the physical road noise simulator that was developed in chapter 3, in order to control the structure-borne noise contribution of the front and rear axle separately and also the whole vehicle that replicates the road noise under a medium driving speed around 60 km/h.

Excitation at the front tyres

As a first step only the front tyres were excited and three microphones were providing the feedback loops of the system and the four microphone the driver's headrest was used as an observation point. The reference input to the feedforward input was the z-direction of the lower control arm of the left hand front microphone. It was found that 2-6 dB(A) reduction levels are possible for the structure-borne noise contributions of the front axle and the system was very effective especially at the tyre cavity range. This validated the reference sensor location as in the coherence analysis it was found that this location is necessary for having high coherence value at the tyre cavity band. Unfortunately, this microphone configuration had caused enhancements at the tyre cavity range at the driver's headrest. Therefore for the last case of this excitation scenario the microphone at the driver's headrest was included as the fourth error microphone and the level at the centre frequency of tyre cavity was reduced by 19 dB(A), which is possible for a coherence value of 0.89 between the sensors. In the past the performance of the feedforward ARNC controller was found to be exceed slightly the coherence estimates [Park et al. (2004)]. This high reduction at the tyre cavity resonance relates to the fact that the reference sensor location at the control arm of the front suspension is actually one of the main vibration transmission of tyre cavity noise into the rest of the vehicle structure, which allows the algorithm to identify the relavant dynamics. As a result, the adaptive system converges to a filter set that is focused on that frequency area without any extra filtering in the algorithm side that is usually necessary for ARNC controllers [Stothers et al. (1998)].

For this case it was also found that 6 dB(A) can be removed from the noise spectra at the headrest at the left hand side of the vehicle, where the reference sensor was also placed. Unfortunately, the reduction was lower at the other side of the vehicle and thus 4 dB(A) reduction was obtained across the four microphones at the headrests.

Excitation at the rear tyres

When the rear tyres were excited by the shaker transducers, then the road rumble was simulated and controlled with one reference signal from the z-direction of the front or the rear mount of the rear subframe. It was found that the front subframe mount provides better reduction than the rear. Moreover, various filter lengths were investigated for 128-taps up to 1024-taps. High sampling rates had to be used for 512, 1024-taps for also avoiding the antialiasing filtering that adds an extra time delay in the system. We noticed that doubling the filter length and maintaining the same sampling rate improved the reduction by extra 2 dB(A) at the rear headrest, where the road rumble dominates.

In general, it was found that longer filter slightly improved the cancellation, but at the end it was verified that 128-taps at 2 kHz are enough. As 7 dB(A) reduction was achieved in the structure-borne road noise range at the microphones at the right hand side of the cabin, which is also the side of the reference sensor at the rear axle. At the co-driver headrest, where also the road rumble is audible in total 5.7 dB(A) attenuation was achieved by the system and the no noise enhancements at the driver's headrests were found as the microphone at that location was used only as an observation sensor for the rest of the sound field.

Excitation at the four tyres

The sensor locations were again evaluated for the case that all the tyres are excited with broadband random noise for replicating the randomness of the vibrational and acoustic fields that are generated under driving conditions over a coarse road. It was found that the front subframe mount provides 3 dB(A) reduction at the rear headrests with the controller focusing at the rumble range, which is 1 dB(A) more than the resulted attenuation when the rear mount was used with the same DSP configuration. The last experiment targeted the reduction at the tyre cavity range and the controller successfully managed to reduce the tyre cavity resonance at the left hand side as the sensor was placed at the lower control arm of the left hand front suspension. The overall reduction was very low as the tyre resonance is very narrow compared to the rumble that dominates the road noise range.

However the locations that were used in the initial two first experiments with the separate excitation of the front and rear axle seem to still provide good control of the noise levels at the main road noise bands. The sensor locations reveal the fact that a sensor close to the tyre at one of the structurally weak suspension arms allows consistent performance for the controller at the tyre cavity range. As for the road rumble the rear axle

subframe mounts are the main locations that the controller can observe most of the vibrations that generate the rumble. In our case only the z-direction was used for all the locations, but one more DoF for controlling the rumble is necessary are the vibrational response of the rear part of the vehicle at that frequency range is relatively complex and thus one DoF is not enough for measuring all the components that contribute to the noise responses at the rear headrests.

The following table summarises the best noise reduction cases that were obtained from the road noise simulator for the control of the two main road noise bands that the Bentley vehicle suffers from:

Shaker location	Filter taps and samping rate	Reduction dB(A)
Front tyres	256 @ 2 kHz	4.0
Rear tyres	1024 @ 4 kHz	4.6
Rear tyres	128 @ 1 kHz	5.6

TABLE 7.15: Best road noise simulation cases for tyre cavity and road rumble ARNC.

Chapter 8

Conclusion and future work

8.1 Summary

In this thesis we have presented the full cycle of a study of structure-borne road noise on a luxury vehicle along with the application of ARNC as a treatment for improving the NVH performance. Luxury vehicles such as Bentleys, contain several passive treatments for controlling the road forces at various points on the vehicle's structure, which play an important role for reducing the structure-borne road noise levels inside the cabin. Therefore, performing NVH analysis of the vehicle was essential, in order to highlight the most important structural locations of the vehicle that are related with the random noise inside the cabin. With that in mind coherence analysis proved to be essential in the successful application of a feedforward controller. As the accelerometers that were used as references input to the controller were placed at the locations, which were found to provide coherent signals with the interior structure-borne noise at specific road noise resonances.

The first step in our study was to analyse the vehicle with acoustically and structurally advanced NVH methods, which are currently used in the automotive industry in chapter 2. The second step was to develop a physical simulator for road noise, which was presented in chapter 3 and it was used later on employed in chapter 7 for the real-time implementation of a feedforward controller. In chapter 4 we presented the outcomes of a study for the sensor arrangement and the coherent vibrational sources that act on the structure, which aimed to find a minimum set of acceleration singals that can be used for ARNC. In

chapter 6 a time domain ARNC model for the Bentley vehicle was focused on the investigation of the various combinations of accelerometer locations and the DoF at each location. In chapter 7 a feedforward controller was presented for real-time experiments on the physical road noise simulator for evaluating the control strategy that made use of the locations that were found to important for road noise in the previous chapter. A multichannel system with low hardware latency was used for the development of a multireference adaptive system, the same system was used for data acquisition and ARNC predictions. An electrical issue with the vehicle's electrical system did not allow further development of the controller on that particular vehicle, as a consequence only the predictions based on the acquired data are presented in the thesis. Nevertheless, an ARNC model based on data that were initially acquired with the multichannel controller was developed, in order to estimate its performance. The model was based on data from four reference accelerometers, the error microphones at the headrests and the impulse responses between the five loudspeakers of the vehicle. The accelerometer reference sensors were placed at the same locations that were used for the experiments with the shakers. The control arms at the suspensions of the front axle and the two front subframe mounts at the rear axle were used as inputs for the ARNC model. The predictions based on this multichannel system with the low latency hardware were found to achieve active noise reduction up to 4 dB(A) across the four headrests.

8.2 Structure-borne road noise

In chapter 4, the coherence analysis method for structure-borne NVH was modified in such a way that the coherent contributions of each axle part can be identified from coherence functions between the DoF that act on important axle points, such as subframe mounts and the interior noise. In this way we can identify which parts and DoF are highly correlated with the structure-borne noise responses in the cabin under operative conditions and create a map of the coherence between the reference inputs and the microphone responses. Coherence values more that 0.7 at the road noise bands were found for several locations on the axle. In particular, the accelerations signals at suspension control arms of the front axle were found to be very coherent for tyre cavity noise, but generally the signals from the subframe mounts were very coherent for both road rumble and tyre cavity resonances.

During the development of an experimental ARNC configuration for simulating road noise in control conditions a physical road noise simulator was resulted

and it is presented in chapter 3. Another outcome of this experimental development was the good replication of the interior noise responses for four uncorrelated broadband random forces applied directly to the tyres. It was also found that with more acceleration signals than the four applied forces on the tyres, the multiple coherence between the structural inputs and the interior noise improves significantly. This was particularly evident when the accelerometers were placed at some mechanical parts of the axle that are close or at the structural sources that relate to the road noise bands. This implies that the interaction of the structural sources can be slightly compensated with sensors mounted at the main road noise contributors. As for the benefits of the physical road noise simulator, it may prove to be a useful and cost effective method for NVH testing of structure-borne noise, as it avoids many drives on proving grounds or other areas where the vehicle is evaluated for road noise. The main benefit of using shaker transducers is that the excitation forces that are applied on the tyres can be focused on either quarter, half or the whole vehicle, in order to identify from which axle the structure-borne sources originate from and validate it with road data as it was performed in our case. This way of testing prove to be potentially useful for benchmarking vehicles for road noise and evaluating design modifications of front and rear axle that are usually performed to later versions of the same vehicle.

The main was to improve excisting signal processing methods of road noise analysis, in order to apply these to an ARNC design method. An investigation on the generation of the structure-borne noise was performed through the physical simulator and managed to achieve a good synthesis of the actual noise field.

8.3 ARNC technology

The main target of this study was to improve the methods for the reference sensor selection, which are necessary for the application of multichannel feedforward ARNC. We approached this using coherence analysis combined with adaptive noise control predictions. Coherence analysis was proved to be useful in indicating the frequency content of the acceleration signals. The main conclusion is that there is a relation between the coherence and the structural sensitivity of the parts, in the sense that the higher the coherence, the higher the contribution to the interior noise response. Therefore it is of utmost importance to create a map of the coherence between the acceleration signals and the sound pressure response inside the vehicle's cabin before applying PCA and multiple coherence. As the two later methods will not show any information about each measurement

location on the structure, but only for the number of the independent sources and their correlation with the noise instead.

Another part of this research focused on the relationship between the most important axle parts and the performance of an ARNC controller. These parts are optimised for dynamics and structure-borne NVH, but they still allow the vibration transmission into the rest of the vehicle body. We focused on finding which DoF at these parts are the most significant by combining also the knowledge that we obtained from the coherence analysis of the vehicle. We found that two DoF are necessary from the front for the reducing effectively the noise levels at the front headrests. On the other hand, on the rear axle one DoF placed at the structural sources was enough to provide good control at the rumble range. The reason for having more DoF at the front axle is that the adaptive controller cannot resolve the frequency components of the acceleration signals. This is necessary as the accelaration signals are close to the noise floor of the measurement and by including more DoF the coherence is improved. Consequently, the cross-correlation between the filtered reference signals and the error signals of the microphones is higher in the adaptation stage and thus the algorithm can converge to filter solution that can control effectively the resonances that come from the front axle. The inspiration behind this control strategy came in fact from TPA, in which the sensor locations and the DoF are important for the appropriate synthesis of road noise. For tyre cavity control we chose a suspension part that provides high coherence at the tyre resonances. This type of approach for optimising the sensor placement is therefore related to the structural dynamics of the vehicle that relate to structure-borne road noise.

The real-time implementation of the adaptive feedforward systems was based on the independent excitation of front and rear axle. In terms of performance, reduction levels up to 10 dB(A) were achieved at some of the road resonances. This mainly happens because we allowed adaptive algorithm to converge to an optimum set of filters. Apart for that other NVH sources were inactive during the physical simulation of road noise. Three locations were tested for referencing the feedforward controller: one for the front axle and two for the rear. Each location was evaluated separately and only the z-direction was tested as the controller was limited to one reference only. As a consequence, broadband control was not feasible, due to this limitation of the controller. Additionally, we investigated the effect of reducing the noise at three passengers headrests, co-driver and rear seats. The noise at the driver headrest was deliberately excluded from the control system, in order to investigate any control spillover effects. It was fairly evident that tyre cavity noise was amplified as most of it comes from the front axle and it was interfered with the cancelling field that was generated by the loudspeaker system at the front doors. When four microphone sensors were used

as error singals in the adaptive algorithm, then good performance was measured across the headrests. It is therefore necessary to use at least four microphones, at least one per headrest as several resonances contribute to the sound field and a high number of sensor ensures that the acoustic field is overdetermined by the controller.

To conclude, good performance was achieved on the real-time experiments at road resonances even if one reference sensor was used. When the front tyre were excited, the spatially averaged reduction was 4 dB(A) across the four headrests. As for the rear tyre excitation, the noise levels from rear axle structure-borne contributions were attenuated by 5.6 dB(A) on average. For the last case of the whole vehicle excitation, the around 2 dB(A) were removed from the noise spectra across the four headrests.

8.4 List of contributions in structure-borne road noise NVH

In this thesis we primarily focused on analysis methods and simulation of structure-borne road noise, in order to create the baseline for the ARNC development that treats this NVH problem. In this section we discuss some outcomes that spin-off from this study and are highlighted as follow:

- A whole vehicle road noise simulator for analysing the structure-borne road noise behavior of a vehicle with a set of random tyre forces. The setup can be used for TPA analysis and modal analysis of the whole vehicle. In this case it was used for measuring the main transfer paths of road noise also for the developement of the ARNC controller.

- The method for the placement of the accelerometer sensors of feedforward controller was based on the coherence function as a continuation of the work performed by Bernhard in the early 90s [Ferren and Bernhard (1991), Kompella et al. (1994), Heatwole et al. (1993)]. In our study though all the transfer paths of the vehicle are included and a coherence function map for source identification is created. The road noise is analysed according to the contributions coming from the front and rear axle separately. This way the structural sources that act on each axle can be identified. It was found that several accelerometer signals have high coherence values with more than one road noise resonance in the cabin. A set of these acceleration signals can be selected in order to synthesise the road noise with the use of multireference adaptive filtering. It was found that

these acceleration signals are enough to describe and control the sound pressure response in cabin. This methodology is an improvement of what was suggested in the past as a rule of thumb for the number of reference sensors of feedforward ARNC. As in our case the selection relies on the location of the most sensitive structural parts for road noise. The control strategy with an optimised spatial arrangement of the sensors and with a low number of acceleration signals is demonstrated at simulation level and compared with various combinations of reference signals.

In terms of the accelerometer selection method up until now there was no strict guidance for the placement. In this thesis we defined a selection process with the following steps:

1. A coherence path analysis of front and rear axle that reveal the location of the main sources and transfer paths of each audible road noise resonance in the cabin.
2. Calculation of the multiple coherence with the use of the main transfer paths and sources that are highlighed in step 1.
3. Road noise synthesis of each microphone response at the headrest with the selected sets.
4. As a last step for validating the performance before installing the controller into the vehicle, ARNC predictions with FxLMS (or other ANC algorithms).

8.5 List of contributions in ARNC technology

The outcomes of the NVH analysis of structure-borne road noise constituted the basis for the ARNC development and provided a better understanding of how the ARNC performance is linked with the behaviour of the vehicle in terms of road noise in conditions under which other NVH attributes are also present in the cabin. The following points summarise the most significant outcomes of the ARNC development study of this research study:

• A real-time adaptive feedforward controller with a single reference input was successfully employed on the whole vehicle road noise simulator aiming to prove the validity of the accelerometer positions. The developed control approach was based on the principal that one reference signal at the road noise source can effectively reduce the noise levels at the corresponding road resonance in the

cabin. Therefore the reference sensor location does not relate with a random selection at some suspension locations that optimises the cancellation levels or with the fact that more sensors than the sources are necessary for observing all the road noise dynamics, but on the fact that the sensor is axle locations that are sources or transmission paths of structure-borne road noise. This was revealed from coherence analysis in chapter 4, where a map of the coherence functions across the vehicle was constructed and revealed several weak paths of road noise.

• In terms of ARNC performance the reduction levels with a single reference sensor are promising, as they could lead to a low cost controller design for reducing the levels at specific road noise resonances. In particular, tyre cavity noise can be removed completely from the road spectra and it was found that maximum reduction 10 dB(A) at the tyre resonance with a single reference at one of the control arms at the front suspension are possible. This is an important result, as in the past four sensors were observing tyre cavity vibrations at the wheel for the effective reduction of noise levels that relate to tyre cavity resonances [Sutton et al. (1994), Kim et al. (1996)]. An overall reduction of 3 dB(A) was achieved in the frequency range of 0-500Hz for the road rumble spectra at the rear headrests with the sensor placed at the most sensitive part of the rear axle in terms of road noise inputs. The microphone at the driver's headrest was sometimes used as an observer, in order to explore the scenario of the driver having the auditory cue from the road. It was obvious, when it comes to the road noise components generated from the front axle vibrations, there is room for enhancements as the microphone signal at the driver's head is not included in the cost function of the controller. With regards to the road noise components that originate from the rear axle there were no side-effects. Some modifications in the algorithm to allow for the audio feedback the road could be performed, as it is questionable if the ARNC affects the driver's awareness during long drives with the ARNC system activated. To the best of our knowledge, it is the first time that this configuration has been explored, therefore further research is necessary, in order to optimise the efficiency of adaptive algorithms and allow controllable levels of reductions at each headrest.

• A study into the relationship of the performance of an ARNC, DoF at vehicle components that are optimised, for passive road noise control, was presented in chapter 6. We discovered that once the location of the sensor with a single DoF is optimised in terms of ARNC performance, then the introduction of extra DoF provide improvements up to 1 dB(A) to this luxury vehicle. This increase of references happens mainly at high speeds, where high road inputs are applied on the vehicle and also airborne road noise is also present at the microphones. With regards to eight references at one DoF, around 2 dB(A) can be achieved across the headrests and with ten or twelve around 3 dB(A). Taking this into

account, we may conclude that the doubling of the number of references and the increase in the DoFs that observe the vibrations across the vehicle structure is not a general rule. This can be the case for specific types of vehicles, with poor levels of road noise refinement, where several structural sources are contributing to the sound field.

• The coherence analysis of each structure-borne road path provided significant input to the development, since it highlighted the locations of some highly correlated vibration signals with the interior noise. These also offered sufficient control over targeted road noise bands that are mainly audible in the cabin. The locations that came from the coherence are also critical for passive road noise NVH, they are the main sources and transmission paths of road noise. The advantage of this technique is that it can achieve a reasonable number of reference sensors without compromising the ARNC performance. Another advantage is that it can possible integrated in the NVH development process. During the structure optimisation with passive control techniques someone could use the knowledge obtained by the NVH analysis to introduce an active solution to improve further the performance.

• A novel feedforward ARNC control strategy has been developed that makes use of the location of either the structural sources or the main transmission paths. The latter identified through advanced NVH methods that employ signal processing methods, such as coherence. More specifically, the ordinary coherence helped us to locate the paths and the sources across the two axles. If the coherence is more that 0.7 between the accelerometer sensors, this is either an indication of the main path or that the sensor is close to the structural source. As a next later four locations were selected based on this condition, each two symmetrical for each axle. The criterion used for the selection was the highest coherence value and later on we calculated the multiple coherence.

We found that the combination of the sensor signals of these locations results to multiple coherence that is high at the road resonances. This validates the fact that the selected sensor locations are sufficient to observe the structural dynamics that are highly correlated with the road noise resonances. Following the coherence study, we examined the DoF that are important for ARNC and discovered that the z, y-directions mainly affect the controller's performance. The x-axis on the selected locations does not notably improve the performance. However, it was observed that for the front axle two directions are necessary. This has to do with the complexity of the front axle design that causes more complex structural behavior than the rear axle. Therefore we can conclude that the number of reference signals depends purely on the complexity of vibrations at each axle and their modal response.

The previous studies established a relationship between the control arms at the front axle and tyre cavity, but also a relationship between the subframe mounts of the rear axle and the road rumble. This spatial arrangement of the structural sources and transmission paths was the basis of the sensor placement in the vehicle. On that basis, the real-time system was tested and we noticed that 3 dB(A) can be reduced at the rear headrests, where the structure-borne road noise is mostly audible. The suspension arm was used to reference the controller and reduce the noise levels of tyre cavity resonance. Maximum 10 dB(A) can be attenuated at its centre frequency. As for the subframe mounts that were used as inputs for road rumble control, we discovered that 5-12 dB(A) across the rumble band can obtained when only the rear axle vibrations are contributing to the sound field. The direct link between the main mechanical inputs of road vibrations in the axles that are correlated with structure-borne noise and the reference inputs of feedforward control is also important in terms of the controller performance and robustness. In that way, the control system may be able to cope with all road changes as the all the mechanical inputs are able to observe the uncertainties at the mechanical inputs in the chassis.

8.6 Future work

In this thesis we investigated fundamental concepts of feedforward control with the use of well-established NVH methodologies. It was proven that are very helpful for the develop of such a system. Therefore this thesis sets the foundation for several future developments, which are the ones listed here:

• Knowledge obtained from structure-borne and air-borne TPA measurements can be used to develop an ARNC system with a mixed type of sensors for extending the operating range of active systems at speeds above 100 km/h, where airborne road noise contribution becomes audible at low frequencies. The advantage of this approach is that it reduces significantly passive treatments and their weight that are used for blocking air leaks around the vehicle.

• To the best of our knowledge, there is no evidence in the literature of the effects of very low frequency wind noise, usually referred to as buffeting noise, which is caused by opening the windows, this creates low frequency resonances. It would be of a great interest to explore whether controller with mixed type of sensors is able to cope also with that issue.

• Another potential line of research would be to control specific cancellation zones as well as the levels of reduction, so that it allows the driver to hear changes

in the road surface under driving conditions. This control approach would be extremely beneficial and innovating as modern vehicles are becoming more in terms of technology and that sometimes restricts the driver's driving capabilities and road awareness. This can potentially introduce novelty in the current adaptive control algorithms, as some of their parameters will need to adjust to achieve this type of control. Knowledge from modern sound reproduction systems could be helpful for achieving this type of control with the necessary adjustments on the algorithms side.

• In terms of adaptive signal processing, it was found that the time domain filtered reference LMS is converging slowly to a filter set. This is common problem with the filtered error LMS algorithm and needs to be addressed in the future for a road noise cancellation application, in order to allow real-time control.

• Another are of research in terms of signal processing and control is the robust stability of the control under severe changes in the acoustic environment that determine changes in the secondary paths of the controller that are strongly influencing the controller. Road impacts are partially cancelled by current algorithms, but further improvements can result to significant improvements in the RNC performance for impact road noise.

• The subjective performance of RNC systems is a dark area as most of the time the vehicles are evaluated in terms of how many decibels the ARNC controller can reduce from the overall levels. It would be of a great value for modern NVH technologies that currently use psycho-acoustic models to integrate such models with the algorithms so that specific frequencies that are strongly effect the perception of the passengers are more biased than others. This approach could potentially improve the overall subjective performance of the vehicle and creating a more acoustically balanced compartment.

• With regards future ARNC vehicle demonstrators and production line vehicles, the cabin NVH treatments above 500 Hz should be not underestimated by future studies, as low reverberation inside the cabin helps to maintain control filters of low orders. Panel damping for low frequency vibration control could be removed as it will allow more vibrational energy to couple with the sound field at low frequency and thus the structure-borne noise levels at the microphones will be higher. Taking this into account, it might be fruitful to further improve the correlation between the sensor signals and thus the convergence and the attenuation of the controller, as damped road resonances can be harder to identify.

8.7 Concluding remarks

In this thesis we developed a design method for feedforward active control aiming to reduce the levels of structure-borne noise in the compartment of a luxury vehicle. The method takes two factors into account: *a*) the multiple structural road sources that optimise the accelerometer sensor locations *b*) the cancellation at specific road resonances that are audible in the cabin. This novel approach enabled us to develop a system with a small number of reference signals. We then demonstrated that the structural locations across the vehicle, which are critical to TPA, are also the reference inputs to the feedforward controller. This is a valuable outcome, as it enables automotive manufacturers the use of their NVH tools, in order to apply the technology quicker, but also treat specific frequency regions with high structure-borne road noise contributions.

Reducing interior noise in vehicles is a great challenge for the automotive industry. Therefore, a significant number of research is currently active in this field. The advances in this field aim towards a future, in which cars with a grid of sensors will allow the integration of feedforward controllers. This will turn the concept of silent cars into a reality. Significantly, vehicle design will shift towards the implementation of advanced sensor networks and electronics that support integrated active sound technologies. Further improvements in the vehicle's electronic systems are required to enable the use of a grid of sensors — on the chassis or at other parts of the vehicle — for the application of feedforward active controllers. This scenario is not far from reality, as the so-called networked vehicles support the use of several sensor networks, thus one such network could be used to develop ARNC systems. On that basis, feedforward ARNC is closer to a production line solution with consistent performance across various vehicle platforms.

Appendix A

Appendix A

A.1 Instrumentation for NVH measurements

For most the NVH measurements an LMS Scadas was used for conducting the measurements. Integrated Circuit Piezoelectric (ICP) sensors from PCB were used for measuring acceleration and sound pressure in the car. In the case of ARNC a signal conditioner was necessary before sending the sensor output signals to the controllers. The equipment for the road noise simulator outside the vehicle is shown in figure A.1.

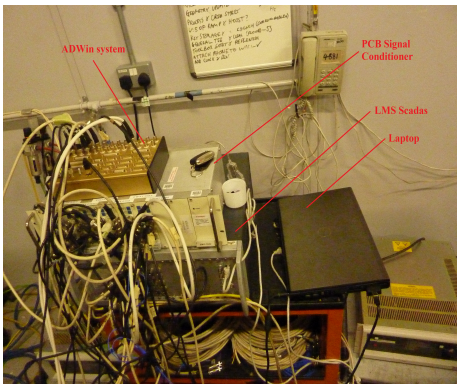

FIGURE A.1: Instrumentation for the road noise simulator. The LMS Scadas for data acquisition is shown that was used for data acquisition and also as a signal generator for driving the shaker transducers. The set-up of the multi-channel controller is also shown with a signal conditioner that was interfered between the controller and the ICP sensor in the car.

A.2 Hardware arrangement for ARNC

A portable multichannel controller was developed, in order to use the vehicle's battery for powering the system. The controller consisted fro a Brüel and Kjær Nexus preamplifiers for signal conditioning and also transforming the sensor ICP outputs to AC signals for the controller. At the output stage an analog audio amplifier was used for driving the vehicle's woofers and subwoofer. In terms of controllers, two systems were integrated, the Antysound ANC Lite II (figure A.2), which is a single reference feedforward controller. Additionally, a programmable multichannel system from Jäger GmbH was programmed through Simulink with a multireference filtered reference algortihm. Unfortunately, some electrical issues of the vehicle did not allow to develop any further the multichannel system. In particular electrical transients at the idle damaged the fuses that were protecting the controller and also the analog board of the power supply of the controller.

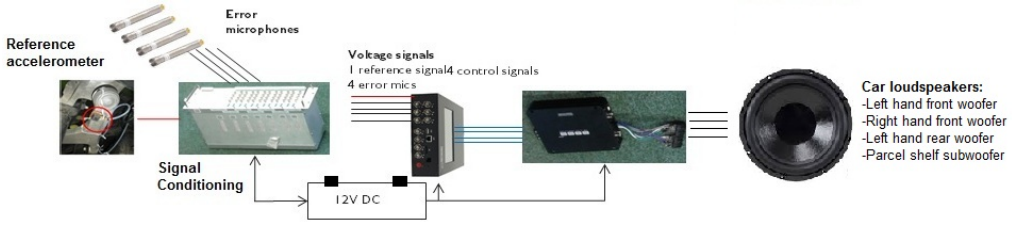

FIGURE A.2: Hardware for ARNC.

A.2.1 Audio amplifier

An audio power amplifier was necessary for this project, since the current audio system of Bentley does not have extra inputs for integrating an ANC controller. Therefore an analog audio amplfier based on Darligton transistors was selected, since an analog system would provide less latency than an digitally based amplifier. Modern digital car audio amplifier have digital equalisers that will introduce and extra delay in the feedforward control path, which cannot be compensated through the control system. However, the four channel audio amplifier that was used for this study had an analog low pass filtering stage for reducing any artifacts that could be generated from the control unit.

FIGURE A.3: The Monacor 404 four channel audio amplifier.

Pameter	**Value**	**Pameter**	**Value**
Max. power	300 Watt	SNR	96 dB(A)
RMS power 2 Ω	4x60 Watt	THD	¡ 0.07
RMS power 4 Ω	4x40 Watt	Low-pass filer	50-500 Hz, 12 dB/Octave
Frequency range	20 Hz - 30 kHz Watt	High-pass filer	50-500 Hz, 12 dB/Octave
Load impedance	2Ω	Supply voltage	11-16 V 30A
Input levels	0.15-5V Watt	Connector	2 x RCA Left & Right speakers
Cross-talk	55 dB	Weight	1.5 kg

TABLE A.1: Technical specifications of the Monacor audio amplifier.

A.2.2 Real-time controller: ADWin Gold II

A real-time multichannel system manufactured by Jäger GmbH was used for the implementation of an ARNC in the vehicle. The system can allow for 16-mulitplexed input channel and also 8-analog outputs. It is programmable with embedded C or assembly through Analog Devices compilers or from Jäger software tools. In our case it was programmed through a high level graphical languange, in particular Matlab/Simulink.

(a) ADwin controller.

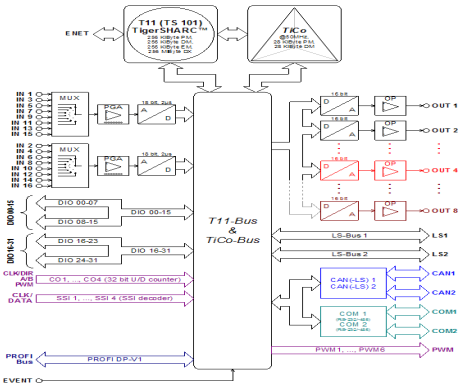

(b) DSP hardware architecture.

FIGURE A.4: ADwin Gold II system for real-time control and acquisition.

Pameter	**Value**	**Pameter**	**Value**
DSP Processor	ADSP TS101S	Resolution	16 bits
ADC/Resolution	2 ADC @ 16bit	Input range	± 10 V
ADC conversion time	5 μs	CAN	high & low speed
Multiplexer	2	PWM	6 outputs @ 50MHz
MUX settling time	5 μs	External memory	FIFO
Output channels	2/8	Ethernet	100 Mbit/s
No. of DAC	2/8	Supply voltage	9 to 28 V

TABLE A.2: Technical specifications of the Monacor audio amplifier.

A.2.3 Real-time controller: Causal systems TigerANC Lite II

Currently, there not many commersially available active noise controllers that can be used for the development of an ARNC system. There are only two companies that supply ANC systems with the algorithm already programmed in the DSP hardware. The first is an Isreally company, Silentium that provides a SISO system, which unfortunately was not suitable for our application. The second option, which was a very interesting ANC system with high hardware specification and also a user friendly environment for the performing real-time experiments was for Antysound. The TigerANC Lite II was chosen from Causal Ltd, since it is a portable device with a touch screen that allows access to the parameters of the adaptive algorithm. In particular, the filtered reference LMS is integrated inside the controller with a single reference input and four error signals. Moreover, four output signals can be used for driving different type of actuators.

FIGURE A.5: TigerANC Lite II.

Pameter	**Value**	**Pameter**	**Value**
DSP Processor	ADSP TS101S	Resolution	16 bits
ADC/Resolution	2 ADC @ 16bit	Input range	± 10 V
ADC conversion time	5 μs	CAN	high & low speed
Multiplexer	2	PWM	6 outputs @ 50MHz
MUX settling time	5 μs	External memory	FIFO
Output channels	2/8	Ethernet	100 Mbit/s
No. of DAC	2/8	Supply voltage	9 to 28 V

TABLE A.3: Technical specifications of the TigerANC Lite II by Antysound.

References

Adachi, S. (2003). Modeling, control and experiment of a feedback active noise control system for free sound fields. *Control and Modeling of Complex Systems*, 303–322.

Adachi, S., M. Ogawa, A. Takahashi, and H. Sano (2001). Feedback active noise control system based on H_∞ control. *Acoustical Science and Technology 22*(6), 437–438.

Adachi, S. and H. Sano (1996). Application of two-degree-of-freedom type active noise control using imc to road noise inside automobiles. In *Decision and Control, 1996., Proceedings of the 35th IEEE Conference on*, Volume 3, pp. 2794–2795. IEEE.

Adachi, S. and H. Sano (1998). Active noise control system for automobiles based on adaptive and robust control. In *Control Applications, 1998. Proceedings of the 1998 IEEE International Conference on*, Volume 2, pp. 1125–1129. IEEE.

Ahrens, D.-I. F. S. and I. J. Feng (2014). Active methods for unrestricted sound design. *Auto Tech Review 3*(5), 44–47.

Akiho, M. (1995). Virtual reference signals for active road noise cancellation in a vehicle cabin. Technical report, SAE Technical Paper.

AMS (2015). Austrian microsystems Active Noise Cancellation. http://www.amd.com/eng/Audio/Active-Noise-Cancellation. Accessed: 2015-04-03.

Aubert, A. and A. Howle (2007). Design issues in the use of elastomers in automotive tuned mass dampers. *SAE International 7*, 217.

Bai, M. R. and S. Elliott (2004). Preconditioning multichannel adaptive filtering algorithms using evd-and svd-based signal prewhitening and system decoupling. *Journal of sound and vibration 270*(4), 639–655.

Belgacem, W., A. Berry, and P. Masson (2012). Active vibration control on a quarter-car for cancellation of road noise disturbance. *Journal of Sound and Vibration 331*(14), 3240–3254.

Beranek, L. L. and I. L. Vér (1992). *Noise and vibration control engineering*. John Wiley & Sons.

Bernhard, R. (2000). The characterization of vibration sources and measurement of forces using multiple operating conditions and matrix decomposition methods. *Proceedings of Intemoise 2000*.

Bernhard, R. J. (1995). Active control of road noise inside automobiles. In *INTER-NOISE and NOISE-CON Congress and Conference Proceedings*, Volume 1995, pp. 21–32. Institute of Noise Control Engineering.

Bose (2014). Bose Active Sound Management Technology. http://www.bose.co.uk/GB/en/Images/Bose%20Active%20Sound%20Management%20-%20Technical%20Information_tcm6-80159.pdf. Accessed: 2014-03-03.

Bose and NXP (2014). Bose Active Sound Management software for noise cancellation in cars now available on chip from NXP semiconductors. http://www.businesswire.com/news/home/20131217005237/en/BoseC2%AE-Active-Sound-Management-Software-Noise-Cancellation#.UxRjkxDczIY. Accessed: 2014-03-03.

Bräunig, D.-I. J., D.-I. H. Kunze, I. S. Sentpali, I. J. Hübelt, and M. Klemm (2013). Coupling of tyre/road excitations into the vehicle structure. *ATZ worldwide 115*(1), 18–21.

Brown, S. W. (1995). *A feasibility analysis of single-sensor active noise cancellation in the interior of an automobile*. Ph. D. thesis, Massachusetts Institute of Technology.

Cerrato, G. (2009). Automotive sound quality–powertrain, road and wind noise. *Sound & vibration 43*(4), 16–24.

Cheer, J. and S. Elliott (2013). Mutlichannel feedback control of interior road noise. In *Proceedings of Meetings on Acoustics*, Volume 19, pp. 030118. Acoustical Society of America.

Cheer, J. and S. J. Elliott (2012). Spatial and temporal filtering for feedback control of road noise in cars.

Cheer, J. and S. J. Elliott (2014). The design and performance of feedback controllers for the attenuation of road noise in vehicles. *International Journal of Acoustics and Vibration*.

Cheer, J. and S. J. Elliott (2015). Multichannel control systems for the attenuation of interior road noise in vehicles. *Mechanical Systems and Signal Processing* (0), –.

Costin, M. H. and D. R. Elzinga (1989). Active reduction of low-frequency tire impact noise using digital feedback control. *Control Systems Magazine, IEEE 9*(5), 3–6.

Couche, J. (1999). *Active control of automobile cabin noise with conventional and advanced speakers*. Ph. D. thesis, Virginia Polytechnic Institute and State University.

Dehandschutter, Wouter, V. H. J. S. J. and P. Sas (1998). Real-time enhancement of reference signals for feedforward control of random noise due to multiple unccorrelated sources. *IEEE Transactions on Signal Processing 2*(1), 58–69.

Dehandschutter, W., R. Van Cauter, and P. Sas (1995). Active control of simulated structure borne road noise using force actuators.

Dohm, M., F. Angermaier, G. Eisele, S.-Y. Park, and J.-W. Lee (2013). Road noise optimization by use of the tpa-tool "chassis vins". In *Lecture, Aachen Acoustic Colloquium*, pp. 99–107.

Douglas, S. C. (1999). Fast implementations of the filtered-x lms and lms algorithms for multichannel active noise control. *Speech and Audio Processing, IEEE Transactions on 7*(4), 454–465.

Douville, H., P. Masson, and A. Berry (2006). On-resonance transmissibility methodology for quantifying the structure-borne road noise of an automotive suspension assembly. *Applied acoustics 67*(4), 358–382.

Doyle, S. (2014, July). Application of active noise cancellation technologies to a lotus evora. In *IPQC Automotive NVH*.

Duncan, A., G. Goetchius, K. Govindswamy, and J. Guan (2011). Structure borne nvh workshop. In *SAE International 2011 Noise and Vibration Conference and Exhibition*.

Durand, J.-F., L. Gagliardini, and C. Soize (2005). Nonparametric modeling of the variability of vehicle vibroacoustic behavior. Technical report, SAE Technical Paper.

Durand, J.-F., C. Soize, and L. Gagliardini (2008). Structural-acoustic modeling of automotive vehicles in presence of uncertainties and experimental identification and validation. *The Journal of the Acoustical Society of America 124*(3), 1513–1525.

Elliott, A., A. Moorhouse, T. Huntley, and S. Tate (2013). In-situ source path contribution analysis of structure borne road noise. *Journal of Sound and Vibration 332*(24), 6276–6295.

Elliott, S. (1998). Filtered reference and filtered error lms algorithms for adaptive feedforward control. *Mechanical systems and signal processing 12*(6), 769–781.

Elliott, S. (2000a). *Signal processing for active control*. Academic press.

Elliott, S. and J. Cook (2000). A preconditioned lms algorithm for rapid adaptation of feedforward controllers. In *Acoustics, Speech, and Signal Processing, 2000. ICASSP'00. Proceedings. 2000 IEEE International Conference on*, Volume 2, pp. II845–II848. IEEE.

Elliott, S. and P. Nelson (1988). Multichannel active sound control using adaptive filtering. In *Acoustics, Speech, and Signal Processing, 1988. ICASSP-88., 1988 International Conference on*, pp. 2590–2593. IEEE.

Elliott, S. and I. Stothers (1986). A multichannel adaptive algorithm for the active control of start-up transients. In *Proceedings of the 213rd Euromech Colloquium, Marseille, 8-11 September*.

Elliott, S., I. Stothers, P. Nelson, A. McDonald, D. Quinn, and T. Saunders (1988). The active control of engine noise inside cars. In *INTER-NOISE and NOISE-CON Congress and Conference Proceedings*, Volume 1988, pp. 987–990. Institute of Noise Control Engineering.

Elliott, S. J. (2000b). Optimal controllers and adaptive controllers for multichannel feedforward control of stochastic disturbances. *Signal Processing, IEEE Transactions on 48*(4), 1053–1060.

Elliott, S. J., I. Stothers, and P. A. Nelson (1987). A multiple error lms algorithm and its application to the active control of sound and vibration. *Acoustics, Speech and Signal Processing, IEEE Transactions on 35*(10), 1423–1434.

Elliott, S. J. and T. J. Sutton (1996). Performance of feedforward and feedback systems for active control. *Speech and Audio Processing, IEEE Transactions on 4*(3), 214–223.

Fahy, F. J. and P. Gardonio (2007). *Sound and structural vibration: radiation, transmission and response*. Academic press.

Ferren, W. B. and R. J. Bernhard (1991). Active control of simulated road noise. Technical report, SAE Technical Paper.

Gade, S., N. Møller, J. Hald, and L. Alkestrup (2004). The use of volume velocity source in transfer measurements. In *Proceedings of the 2004 International Conference on Modal Analysis Noise and Vibration Engineering (ISMA)*, pp. 2641–2648.

Gauterin, F. (1994a). Angewandte psychoakustik als bindeglied zwischen subjektiver reifengeräuschbeurteilung und klassischer meßtechnik. *Soundengineering: kundenbezogene Akustikentwicklung in der Fahrzeugtechnik*, 126.

Gauterin, F. (1994b). *Objektivierung der subjektiven Beurteilung zeitlich schwankender tieffrequenter Reifengeräusche*. Ph. D. thesis.

Halosonic (2014). Halosonic: Noise management solution. http://www.halosonic.co.uk/. Accessed: 2014-03-03.

Hansen, C. H. (2001). *Understanding active noise cancellation*, Volume 1. Taylor Francis.

Hansen, C. H. (2013). *Active control of noise and vibration*, Volume 1. CRC Press.

Harman (2014a). Harman cancels out road noise, without headphones. http://spectrum.ieee.org/cars-that-think/transportation/systems/harman-cancels-road-noise. Accessed: 2014-03-03.

Harman (2014b). Quieting the car. http://harmaninnovation.com/blog/pt-ru/quieting-the-car/. Accessed: 2014-05-25.

Hasegawa, S., T. Tabata, A. Kinoshita, and H. Hyodo (1992). The development of an active noise control system for automobiles. Technical report, SAE Technical Paper.

Heatwole, C. M. and R. J. Bernhard (1994). Prediction of multiple-input active control of road noise in automobile interiors. In *INTER-NOISE and NOISE-CON Congress and Conference Proceedings*, Volume 1994, pp. 367–372. Institute of Noise Control Engineering.

Heatwole, C. M., X. Dian, and R. J. Bernhard (1993). Determination of the number of input transducers required for active control of road noise inside automobiles. *INTER-NOISE and NOISE-CON Congress and Conference Proceedings 1993*(1), 207–212.

Howard, C. Q. and D. J. J. Leclercq (2006). Feedback noise control of low frequency noise in a station-wagon using a field programmable analog array (fpaa). In *International Symposium on Active Noise and Vibration Control (6th: 2006: Adelaide, Australia) Active 2006*.

Inoue, T., A. Takahashi, S. Minowa, and H. Sano (2003). Development of active noise control system for engine booming noise. *HONDA R&D TECHNICAL REVIEW 15*(2), 201–208.

Jacobsen, F. (2007). The sound field in a reverberation room. *Lecture note* (31261).

Kim, H., S. Oh, K.-C. Kim, J. Y. Lee, J. Cheong, and J. Her (2014). Optimization of body structure for road noise performance. Technical report, SAE Technical Paper.

Kim, H.-S., Y. Park, and K.-H. Sur (1996). Active noise control of road booming noise with constraint multiple filtered-x lms algorithm. In *International congress on noise control engineering*, pp. 1155–1158.

Kinoshita, A, T. T. D. K. and Y. Nakaji (1994). Active booming noise control system for automobiles. *Japanese Society of Automotive Engineers 14*(1), 67–71.

Kompella, M. S. and R. J. Bernhard (1993). Measurement of the statistical variation of structural-acoustic characteristics of automotive vehicles. Technical report, SAE Technical Paper.

Kompella, M. S., P. Davies, R. J. Bernhard, and D. A. Ufford (1994). A technique to determine the number of incoherent sources contributing to the response of a system. *Mechanical systems and signal processing 8*(4), 363–380.

KUL, L. International, M. G. AG, M. E. N.V., U. of Manchester, U. of Patras, and V. AG (1996). Anrava-advanced noise reduction by active vibration actuators. Technical report, KUL and LMS, International and Metzeler, Gimetall, AG and Monroe, Europe, N.V. and University of Manchester and University of Patras and VW, AG.

Laugesen, S. and S. J. Elliott (1993). Multichannel active control of random noise in a small reverberant room. *Speech and Audio Processing, IEEE Transactions on 1*(2), 241–249.

Letens, U., G. Koners, and T. J. Saunders (1999). Adaptive road noise cancellation for a midclass estate car. *The Journal of the Acoustical Society of America 105*(2), 1243–1243.

LMS and Siemens (2014). Lms qsources structural and acoustic exciters. http://www.plm.automation.siemens.com/en_gb/products/lms/testing/qsources. Accessed: 2014-14-12.

Lueg, P. (1936, June 9). Process of silencing sound oscillations. US Patent 2,043,416.

Lyon, R. H. (1987). *Machinery noise and diagnostics*. Butterworths Boston etc.

Mackay, A. and S. Kenchington (2004). Active control of noise and vibration-a review of automotive applications. In *INTER-NOISE and NOISE-CON Congress and Conference Proceedings*, Volume 2004, pp. 247–258. Institute of Noise Control Engineering.

Magrans, F. (1981). Method of measuring transmission paths. *Journal of Sound and Vibration 74*(3), 321–330.

Maia, N., J. Silva, and A. Ribeiro (2001). The transmissibility concept in multi-degree-of-freedom systems. *Mechanical Systems and Signal Processing 15*(1), 129 – 137.

Malkoun, A., J. Sapena, K. Arcas, and F. X. Magrans (2014). Vehicle and rail noise separation method proposal based in transfer path analysis techniques. In *Proceedings of the 21st International Congress on Sound and Vibration [CDROM]. Beijing, China: International Institute of Acoustics and Vibration (IIAV).*

Meillier, J.-L. and P. Mairesse (1996). Transfer path analysis in a multisource environment, application for road noise analysis. In *Proceedings of the 14th International Modal Analysis Conference*, pp. 314–319. Society of Experimental Mechanics.

Melton, D. E. and R. Greiner (1992). Adaptive feedforward multiple-input, multiple-output active noise control. In *Acoustics, Speech, and Signal Processing, 1992. ICASSP-92., 1992 IEEE International Conference on*, Volume 2, pp. 229–232. IEEE.

Milani, A. A., I. M. Panahi, and P. C. Loizou (2009). A new delayless subband adaptive filtering algorithm for active noise control systems. *Audio, Speech, and Language Processing, IEEE Transactions on 17*(5), 1038–1045.

Mohammad, J. I. and S. J. Elliott (2006). The performance of active control of sound and vibration in a fully-coupled structural-acoustic system using different reference sensors. In *Proceedings of the 13th International Congress on Sound and Vibration [CDROM]. Vienna, Austria: Vienna University of Technology/International Institute of Acoustics and Vibration (IIAV).*

Mohammad, J. I., S. J. Elliott, and A. Mackay (2008). The performance of active control of random noise in cars. *The Journal of the Acoustical Society of America 123*(4), 1838–1841.

Mohanty, A. R., B. D. St Pierre, and P. Suruli-Narayanasami (2000). Structure-borne noise reduction in a truck cab interior using numerical techniques. *Applied Acoustics 59*(1), 1–17.

Moorhouse, A., A. Elliott, and Y. H. Heo (2013). Intrinsic characterisation of structure-borne sound sources and isolators from in-situ methods. *The Journal of Acoustical Society of America 133*(5), 3462 – –3462.

Moorhouse, A. and B. Gibbs (1998). Simplified characterisation of multiple point excited structures using mobility matrix eigenvalues and eigenvectors. *Acta Acustica united with Acustica 84*(5), 843–853.

Müeller (2014). Müeller BBM Active Sound Technology. www.muellerbbm-ast.com/. Accessed: 2014-03-03.

Nelson, P. A. and S. J. Elliott (1991). *Active control of sound*. Academic press.

Neto, A. C. and P. R. d. O. de Oliveira, Leopoldo (2010). Tranfer path analysis of road noise: Overview and customised approaches for road rumble noise. Technical report, SAE Technical Paper.

Noll, S., J. Dreyer, and R. Singh (2013). Effect of local stiffness coupling on the modes of a subframe-bushing system. Technical report, SAE Technical Paper.

Oh, S.-H., H.-s. Kim, and Y. Park (2002). Active control of road booming noise in automotive interiors. *The Journal of the Acoustical Society of America 111*(1), 180–188.

Oh, S.-H. and Y. Park (2000). Active noise control algorithm using iir-based filter. *Journal of sound and vibration 231*(5), 1396–1412.

Oswald, L. J. (1984). Reduction of diesel engine noise inside passenger compartments using active, adaptive noise control. In *INTER-NOISE and NOISE-CON Congress and Conference Proceedings*, Volume 1984, pp. 483–488. Institute of Noise Control Engineering.

Otte, D., P. Sas, and P. Van de Ponseele (1988). Noise source identification by use of principal component analysis. In *Proceedings of inter-noise*, Volume 88.

Park, C., C. R. Fuller, and M. R. F. Kidner (2002). Evaluation and demonstration of advanced active noise control in a passenger automobile. In *International Symposium on Active Control of Sound and Vibration (2002: Southampton, UK) Active 2002*.

Park, C. G., C. R. Fuller, J. P. Carneal, V. Collin, J. T. Long, R. E. Powell, and J. L. Schmidt (2004). On-road demonstration of noise control in a passenger automobile-part 2. In *INTER-NOISE and NOISE-CON Congress and Conference Proceedings*, Volume 2004, pp. 184–195. Institute of Noise Control Engineering.

Plunt, J. (1999). Strategy for transfer path analysis (tpa) applied to vibro-acoustic systems at medium and high frequencies. In *PROCEEDINGS OF THE INTERNATIONAL SEMINAR ON MODAL ANALYSIS*, Volume 2, pp. 1025–1030. KATHOLIEKE UNIVERSITEIT LEUVEN.

Plunt, J. (2005). Finding and fixing vehicle nvh problems with transfer path analysis. *Sound and vibration 39*(11), 12–17.

Price, S. and R. Bernhard (1986). Virtual coherence: A digital signal processing technique for incoherent source identification. In *Proceedings of IMAC*, Volume 4.

Qiu, X. and C. Hansen (2007). Multidelay adaptive filters for active noise control. In *International Congress on Sound and Vibration (14th: 2007: Cairns, Australia)*.

Qiu, X., N. Li, G. Chen, and C. H. Hansen (2006). The implementation of delayless subband active noise control algorithms. In *Proceedings of the 2006 International Symposium on Active control of Sound and Vibration*.

QNX (2014). Qnx acoustics for active noise control. http://www.qnx.com/products/anc/. Accessed: 2014-03-03.

Rafaely, B. and S. J. Elliot (2000). A computationally efficient frequency-domain lms algorithm with constraints on the adaptive filter. *Signal Processing, IEEE Transactions on 48*(6), 1649–1655.

Ribeiro, A., J. Silva, and N. Maia (2000). On the generalisation of the transmissibility concept. *Mechanical Systems and Signal Processing 14*(1), 29–35.

Rustighi, E., S. Elliott, S. Finnveden, K. Gulyás, T. Mócsai, and M. Danti (2008). Linear stochastic evaluation of tyre vibration due to tyre/road excitation. *Journal of Sound and Vibration 310*(4), 1112–1127.

Sakamoto, K. and T. Inoue (2015). Development of feedback-based active road noise control technology for noise in multiple narrow-frequency bands and integration with booming noise active noise control system. *SAE International Journal of Passenger Cars-Mechanical Systems 8*(2015-01-0660), 1–7.

Sano, H., T. Inoue, A. Takahashi, D. Ishihara, T. Yamashita, and K. Terai (2000). Active control system for low frequency road noise combined with an audio system. *Honda R&D Tech. Rev 12*, 71.

Sano, H., T. Inoue, A. Takahashi, K. Terai, and Y. Nakamura (2001). Active control system for low-frequency road noise combined with an audio system. *Speech and Audio Processing, IEEE Transactions on 9*(7), 755–763.

Sapena, J., A. Tabbal, J. Jové, and F. Guerville (2012). Interior noise prediction in high-speed rolling stock driver's cab: Focus on structure-borne paths (mechanical and aero sources). In *Noise and Vibration Mitigation for Rail Transportation Systems*, pp. 445 – 452. Springer.

Sas, P. and W. Dehandschutter (1999). Active structural and acoustic control of structure-borne road noise in a passenger car. *Noise & Vibration Worldwide 30*(5), 17–27.

Schirmacher, R. (2010). Active noise control and active sound design-enabling factors for new powertrain technologies. Technical report, SAE Technical Paper.

Schirmacher, R., R. Kunkel, and M. Burghardt (2012). Active noise control for the 4.0 tfsi with cylinder on demand technology in audi's s-series. Technical report, SAE Technical Paper.

Silentium (2014). Silentium automotive. http://www.silentium.com. Accessed: 2014-03-03.

Stothers, I., A. McDonald, S. Hutchins, and C. Bowles (1998, June 16). Adaptive control system. US Patent 5,768,124.

Stothers, I. M. (1997, November 25). Adaptive control system. US Patent 5,691,893.

Stothers, I. M., D. C. Quinn, and T. J. Saunders (1995). Computationally efficient lms based hybrid algroithm applied to the cancellation of road noise. In *INTER-NOISE and NOISE-CON Congress and Conference Proceedings*, Volume 1995, pp. 727–734. Institute of Noise Control Engineering.

Subramanian, S., R. Surampudi, K. Thomson, and S. Vallurupalli (2003). Optimization of damping treatment for structure borne noise reduction. Technical report, SAE Technical Paper.

Sun, G., T. Feng, J. Xu, M. Li, and T. Lim (2015). Modified fxlms algorithm with equalized convergence speed for active control of powertrain noise. *SAE International Journal of Passenger Cars-Mechanical Systems 8*(2015-01-2217).

Sutton, T. J., S. J. Elliott, A. M. McDonald, and T. J. Saunders (1994). Active control of road noise inside vehicles. *Noise Control Engineering Journal 42*(4).

Thite, A. and D. Thompson (2003a). The quantification of structure-borne transmission paths by inverse methods. part 1: Improved singular value rejection methods. *Journal of Sound and Vibration 264*(2), 411–431.

Thite, A. and D. Thompson (2003b). The quantification of structure-borne transmission paths by inverse methods. part 2: Use of regularization techniques. *Journal of Sound and Vibration 264*(2), 433–451.

Thompson, J. (1995). Plane wave resonance in the tire air cavity as a vehicle interior noise source. *Tire Science and Technology 23*(1), 2–10.

Tu, Y. and C. Fuller (2000). Multiple reference feedforward active noise control part i: analysis and simulation of behavior. *Journal of sound and vibration 233*(5), 745–759.

Wan, E. A. (1996). Adjoint lms: An efficient alternative to the filtered-x lms and multiple error lms algorithms. In *Acoustics, Speech, and Signal Processing, 1996. ICASSP-96. Conference Proceedings., 1996 IEEE International Conference on*, Volume 3, pp. 1842–1845. IEEE.

Wang, X. (2010). *Vehicle noise and vibration refinement*. Elsevier.

Widrow, B., J. R. Glover Jr, J. M. McCool, J. Kaunitz, C. S. Williams, R. H. Hearn, J. R. Zeidler, E. Dong Jr, and R. C. Goodlin (1975). Adaptive noise cancelling: Principles and applications. *Proceedings of the IEEE 63*(12), 1692–1716.

Widrow, B. and S. D. Stearns (1985). Adaptive signal processing. *Englewood Cliffs, NJ, Prentice-Hall, Inc., 1985, 491 p. 1*.

Widrow, B. and E. Walach (2008). Adaptive inverse control. *A Signal Processing Approach, Wiley, Hoboken, NJ*.

Williams, R. (2014). An efficient process for the characterisation and evaluation of interior rolling noise. http://www.bksv.fr/~/media/France/EXHIBITION/FDM2013/CONFERENCES/1806_WILLIAMS.ashx. Accessed: 2015-08-22.

Wyckaert, K. and H. Van der Auweraer (1995). Road noise analysis of a passenger car: A compilation of results from operating data analysis, transmission path analysis and suspension and cavity modal analysis. In *Proceedings of the 13th International Modal Analysis Conference*, Volume 2460, pp. 1220.

Yoo, B. K. and K.-J. Chang (2005). Road noise reduction using a source decomposition and noise path analysis. Technical report, SAE Technical Paper.

Zafeiropoulos, N., A. Moorhouse, A. Mackay, and U. Senapati (2013). A comparison of two in-situ transfer path analysis methods. In *Recent Advances in Structural Dynamics*.